MUSCULOSKELETAL SHOULDER MODELLING FOR CLINICAL APPLICATIONS

Christian Klemt

Dissertation submitted in fulfilment of the requirements for the degree of:

Doctor of Philosophy

Department of Bioengineering, Imperial College London

July 2018

Declaration of originality

The work presented in this thesis is my own and all else is appropriately referenced.

Copyright Declaration

Acknowledgements

I would like to thank my supervisors, Prof Anthony MJ Bull and Mr Peter Reilly, for their invaluable guidance and constant support throughout my doctoral research. Their guidance was, and will continue to be, invaluable and I think it goes without saying that the concepts presented in this thesis would not have been possible without our discussions. I look forward to seeing our research progress through future projects, and I hope our collaboration continues for many years to come.

I would like to thank all members of the Biomechanics group (in no particular order: Ziyun, Erica, Suzy, Daniel, Lance, Marvin, Hassan and others) who were supportive throughout my doctoral research in many ways.

I am grateful to my sponsors, JRI Orthopaedics and the Engineering and Physical Sciences Research Council, who enabled me to pursue this PhD degree.

Finally, a special thanks to my family who have always been there for me. I would not be able to finish this thesis without them.

Abstract

The shoulder is the most commonly dislocated joint in the human body, with the vast majority of these dislocations being located anteriorly. Anterior shoulder dislocations are commonly associated with capsuloligamentous injuries and osseous defects. Recurrent anterior instability is a common clinical problem and understanding the influence of structural damage on joint stability is an important adjunct to surgical decision-making. Clinical practice is guided by experience, radiology, retrospective analyses and physical cadaver experiments. As the stability of the shoulder is load dependent, with higher joint forces increasing instability, the aim of this thesis was to develop and validate computational shoulder models to simulate the effect of structural damage on joint stability under *in-vivo* loading conditions to aid surgical decision-making for patients with anterior shoulder instability.

The UK National Shoulder Model, consisting of 21 upper limb muscles crossing 5 functional joints, was customised to accurately quantify shoulder loading during functional activities. Ten subject-specific shoulder models were developed from Magnetic Resonance Imaging and validated against electromyographic signals. These models were used to identify the best combination of anthropometric parameters that yield best model outcomes in shoulder loading through linear scaling of personalised shoulder models. These parameters were gender and the ratio of body height to shoulder width ($p<0.04$) and these model predictions are significantly improved ($p<0.02$) when compared to the generic model.

The forces derived from the modelling were used in two subject-specific finite element models with an anatomically accurate representation of the labrum, to assess shoulder stability through concavity compression under physiological joint loading for pathologies associated with anterior shoulder instability. The key results from these studies were that there is a high risk of shoulder dislocation under physiological joint loading for patients with a 2 mm anterior or 4 mm anteroinferior osseous defect. The loss in anterior shoulder stability in overhead throwing athletes with intact glenoid following biceps tenodesis is compensated by a non-significant increase in rotator cuff muscle force which maintain shoulder stability across all overhead throwing sports, except baseball pitching, where biceps tenodesis has significantly decreased ($p<0.02$) anterior shoulder stability.

The work in this thesis has advanced the technology of musculoskeletal modelling of the shoulder through the inclusion of concavity compression and has applied this to various relevant clinical questions through the further development of an anatomical atlas, and an atlas of tasks of daily living. The applications of such modelling are broader than those addressed here and therefore this work serves as the foundation for potential further studies, including the bespoke design of arthroplasty or other soft tissue procedures.

Table of Contents

List of Figures

List of Tables

Abbreviations

Acromioclavicular	AC
Activity of daily living	ADL
AnyBody Upper Extremity model	ABM
Body weight	BW
Coefficient of multiple correlation	CMC
Computed Tomography	CT
Degrees of freedom	DOF
Delft Shoulder and Elbow model	DSEM
Diffusion Tensor Imaging	DTI
Effective insertion	EI
Effective origin	EO
Electromyography	EMG
Finite element	FE
Forward dynamics	FD
Garner and Pandy model	GPM
Glenohumeral	GH
Glenohumeral contact force	GHCF
International Society of Biomechanics	ISB
Inverse dynamics	ID
Magnetic Resonance Imaging	MRI
Musculoskeletal	MSK
Physiological cross-sectional area	PCSA
Root mean square error	RMSE
Scapulpthoracic gliding plane	STPG
Scapula tracker	ST
Stability ratio	SR
Standard deviation	SD
Stanford-VA model	SVM
Sternoclavicular	SC
Swedish Shoulder Model	SSM
United Kingdom National Shoulder Model	UK NSM
Visible Human	VH
Waterloo model	WSM

Chapter 1

Thesis motivation and scope.

This chapter offers an overview of the subject matter of this thesis and provides the thesis aim, scope and structure.

1.1 Problem Statement and Motivation

The shoulder provides the largest range of motion of any joint in the human body, offering sufficient mobility and strength to facilitate high-speed athletic motions in addition to functional daily activities (Halder et al. 2000). The large degree of mobility at the shoulder is provided by the low congruency of the articulating structures (Hess 2000) and the additional motion provided by the scapula, with joint stability being achieved through active muscle activations as well as contributions from passive stabilisers including the capsuloligamentous complex and labrum (Bigliani et al. 1996). Therefore, the shoulder has been termed as the perfect compromise between joint mobility and stability (Veeger & van der Helm 2007).

However, the lack of articular constraint at the shoulder predisposes the joint to instability, with translational shear forces that exceed the stabilising potential of the shoulder leading to joint dislocation. Due to high *in-vivo* loading to the shoulder during traumatic incidents and contact sports as well as the loss in joint stabilising potential with age and pathology, the shoulder is the most commonly dislocated articulation in the human body (Shah et al. 2017; Zacchilli & Owens 2010). The incidence of traumatic shoulder instability has been reported to be as high as 1.7% in the general population (Liavaag et al. 2011), with more than 90% of these dislocations being located anteriorly (Pope et al. 2011).

Anterior shoulder dislocations are commonly associated with capsulolabral injuries and osseous defects (Shah et al. 2017). These structural defects may be treated with bone grafting rather than an arthroscopic soft tissue stabilisation procedure once the osseous defect reaches a critical size in order to restore joint stability (Itoi et al. 2000; Yamamoto et al. 2009a, 2010). Although surgical decision-making is guided by experience, radiology, retrospective analyses and cadaveric testing with non-physiological loading, recurrent anterior shoulder instability is a common clinical problem. The incidence rates of recurrent anterior shoulder instability are as high as 67% (Burkhart et al. 2007) in patients with high physical demands and large glenoid defects that were treated with an arthroscopic soft tissue stabilisation procedure.

As recurrent anterior shoulder instability is associated with a deprivation in social functioning and emotional well-being (Barber et al. 2003), alongside a loss in joint functionality, the precise knowledge of the influence of structural damage on joint stability is an important adjunct for surgical decision-making in order to ensure joint stability without exposing the patient to unnecessary surgical risks.

1.2 Aim and Scope

The aim of this thesis is to develop and validate computational models of the shoulder to simulate the effect of structural damage on joint stability under physiological joint loading in order to aid surgical decision-making for patients with anterior shoulder instabilities.

1.3 Thesis Objectives

The objectives of this thesis are as follows:

- develop and validate subject-specific finite element models of the shoulder with an anatomically accurate representation of the labrum in order to quantify the loss in joint stability for glenoid labral pathologies under physiological joint loading;
- develop and validate subject-specific musculoskeletal shoulder models to improve model reliability through anthropometric scaling in order to accurately assess shoulder loading during essential functional activities of daily life; and
- utilise these subject-specific computational shoulder models to evaluate joint stability during functional daily activities as well as overhead throwing sports under *in-vivo* joint loading for structural damage associated with recurrent anterior shoulder instability in order to aid surgical decision-making.

1.4 Thesis Outline

This thesis is subdivided into seven chapters.

Chapter 2 presents a literature review on the clinical situation of patients with anterior shoulder instabilities as well as computational modelling techniques to assess joint functionality.

Chapter 3 describes the development and validation of subject-specific finite element models of the shoulder with an anatomically accurate representation of the labrum in order to quantify the loss in joint stability with labral pathology under physiological joint loading to aid surgical decision-making.

Chapter 4 explains the development and validation of subject-specific musculoskeletal shoulder models through manual digitisation of model parameters from Magnetic Resonance Imaging in order to improve the accuracy of model predictions through the use of anthropometric parameters for model scaling.

Chapter 5 utilises the validated subject-specific MSK shoulder models from Chapter 4, with prior knowledge of the labral contribution to joint stability as quantified in Chapter 3, to evaluate shoulder loading during essential functional daily activities in order to aid rehabilitation planning for patients following Bankart repair.

Chapter 6 utilises the knowledge of shoulder loading during functional daily activities from Chapter 5 as well as the subject-specific finite element models from Chapter 3 to determine the risk of shoulder dislocation during daily activities for glenoid osseous defects of different magnitudes in order to aid surgical decision-making.

Chapter 7 utilises the validated subject-specific MSK shoulder models from Chapter 4, with prior knowledge of the labral contribution to joint stability as quantified in Chapter 3, to investigate the effect of biceps tenodesis on anterior shoulder stability in overhead throwing athletes in order to aid sport-specific surgical decision-making for athletes with type II SLAP tear.

Chapter 8 presents the overall discussion of this thesis and proposes future work.

Chapter 2

Literature review and background.

This chapter introduces the key clinical questions addressed with this thesis, specifically associated with anterior shoulder dislocation. The high rates of recurrent anterior instabilities in young patients are discussed in the light of injury mechanisms, treatment strategies and rehabilitation programmes, paving the way for computational shoulder modelling techniques to be introduced. These computational tools are discussed with respect to their functionality, clinical applications and future developments in order to highlight the potential of computational shoulder modelling as an aid to clinical decision-making in patients with anterior shoulder instability and thus to propose the work for the remainder of this thesis.

2.1 Functional Anatomy of the Shoulder

The functional anatomy of the shoulder is introduced in this section. The focus will be on the stabilising structures of the joint as relevant for patients will recurrent anterior shoulder instability.

2.1.1 Primary Function

The shoulder provides the largest range of motion of any joint in the human body, enabling not only activities of daily living but also high-speed athletic motions to be performed (Inman et al. 1996). The large degree of joint mobility is provided by the four articulating structures of the shoulder girdle (Figure 2.1; Hess 2000). These include the sternoclavicular (SC) joint, acromioclavicular (AC) joint, glenohumeral (GH) joint and the scapulothoracic gliding plane (STGP), where the greatest range of rotation occurs at the GH joint. As the focus of this thesis is on the GH joint, the following sections will only expand on this articulation.

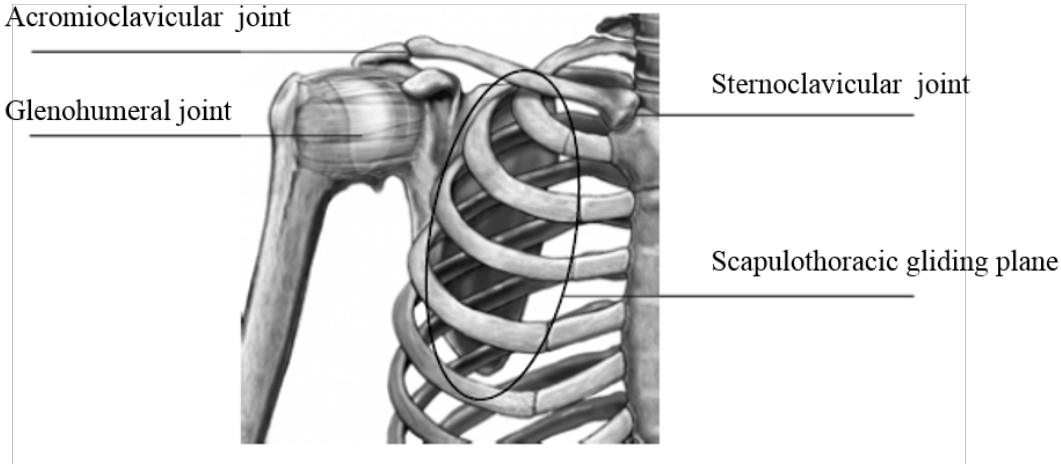

Figure 2.1: Articulations of the shoulder girdle, shown from an anterior view. The image was reproduced and modified with permission from Hess (2000).

The GH joint involves the articulation of the humeral head and the glenoid fossa of the scapula. This articulation achieves a great range of motion (ROM) based on two anatomical features. Firstly, the articulating surface of the shallow glenoid fossa is less than one third than that of the humeral head (Iannotti et al. 1992). Secondly, the articulating structures of the GH joint are incongruent (Soslowsky et al. 1992; Walch et al. 2002; Zumstein et al. 2014). The radius of the curvature of the glenoid fossa is approximately 3 mm larger than that of the humeral head (Iannotti et al. 1992). This mismatch allows the humeral head to rotate over a large range of motion without articular impingement; this also allows small translations of up to 3 mm during arm elevation (Bey et al. 2011; Dal Maso et al. 2015; Matsuki et al. 2012; Nishinaka et al. 2008).

2.1.2 Joint Stability

The large mobility of the GH joint comes at the expense of joint stability. The articulation of the shallow glenoid fossa and the large humeral head means that the joint is not stable from the articulating geometry. The stability of the GH joint is provided by an interplay of active and passive stabilisers.

2.1.2.1 Active Joint Stabilisers

The rotator cuff muscles are the primary stabiliser of the GH joint (Terry and Chopp 2000), and these muscles include the subscapularis, supraspinatus, infraspinatus and teres minor (Figure 2.2; Hess 2000). The rotator cuff muscle lines of action are near perpendicular to the glenoid plane (Ackland and Pandy 2009) and therefore these muscles are able to effectively apply compressive forces to the joint to provide joint stability. In addition, the rotator cuff muscles are also best positioned to co-contract in order to counteract destabilising shear forces (Veeger & van der Helm 2007) and direct the resultant GH joint force vector into the glenoid fossa to provide joint stability (Lippitt and Matsen 1993). This is illustrated in Figure 2.3, where the force couple in the transverse plane formed by the subscapularis and infraspinatus contraction counteracts the externally produced shear forces, predominantly the deltoid, in order to direct the resultant GH joint force vector into the glenoid fossa to stabilise the joint.

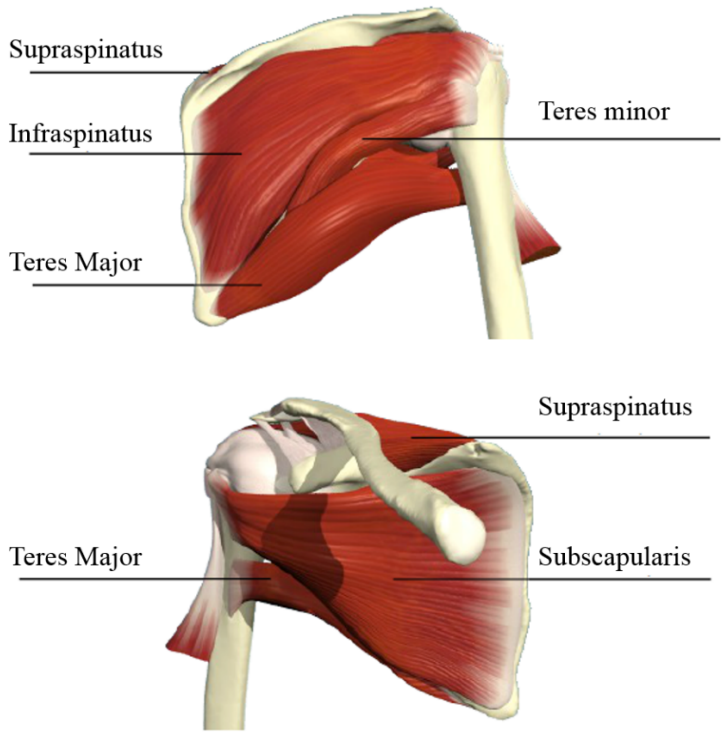

Figure 2.2: Top: Posterior view of the rotator cuff muscles and teres major. Bottom: Anterior view of the subscapularis, supraspinatus and teres major. The image was reproduced and modified with permission from Hess (2000).

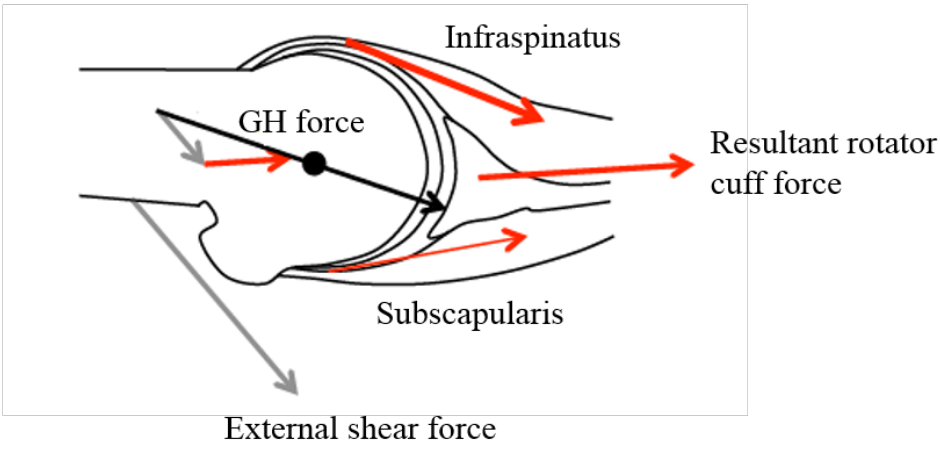

Figure 2.3: The stabilising action of the rotator cuff showing co-contraction of the subscapularis and infraspinatus in the transverse plane to counteract the externally produced shear force and direct the resultant GH joint force vector into the glenoid fossa. The image was reproduced and modified with permission from Terry and Chopp (2000).

2.1.2.2 Passive Joint Stabilisers

The passive stabilising structures of the GH joint include the joint capsule, the glenohumeral ligaments and the glenoid labrum (Hess 2000).

The GH joint capsule is a lax anatomical structure whose contribution to joint stability is very small (Steinbeck et al. 1998). The joint capsule is reinforced by the glenohumeral ligaments that provide joint stability when stretched beyond their resting length, which means that these soft tissues, similar to the joint capsule, stabilise the GH joint at high angles of arm elevation (Burkart and Debski 2002; Pizzari et al. 1999).

The glenoid labrum is a circumferential fibrocartilagenous structure that is attached to the rim of the glenoid fossa (Figure 2.4; Cooper et al. 1992; Alashkham et al. 2017). Cadaveric experiments have demonstrated that the labrum makes up half the glenoid socket depth (Howell & Galinat 1989), thereby contributing to GH stability through concavity compression. Concavity compression refers to the stability that is awarded to the convex humeral head when compressed into the concave glenoid-labral socket through contraction of muscles surrounding the shoulder. The degree of glenohumeral stability that is awarded through concavity compression is dependent on the magnitude of the joint compressive force as well as the concavity of the glenoid labral socket (Fukuda et al. 1988), with higher compressive joint loads and a deeper glenoid labral concavity both increasing the resistance to humeral head translation (Figure 2.5; Lazarus et al. 1996). The resection of the labrum during cadaveric testing has demonstrated a 10-20% loss in joint stability in the mid-range of motion, where the capsuloligamentous structures are lax (Lippitt et al. 1993; Halder et al. 2001).

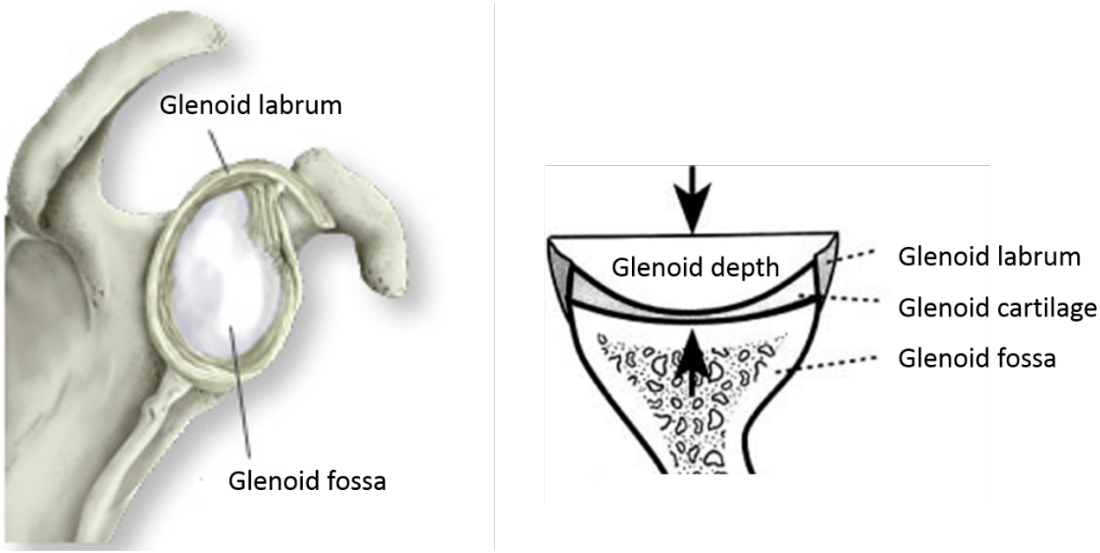

Figure 2.4: The glenoid labrum: Left: shown from a lateral view, Right: cross-sectional view. The image was reproduced and modified with permission from Bigliani et al. (1996).

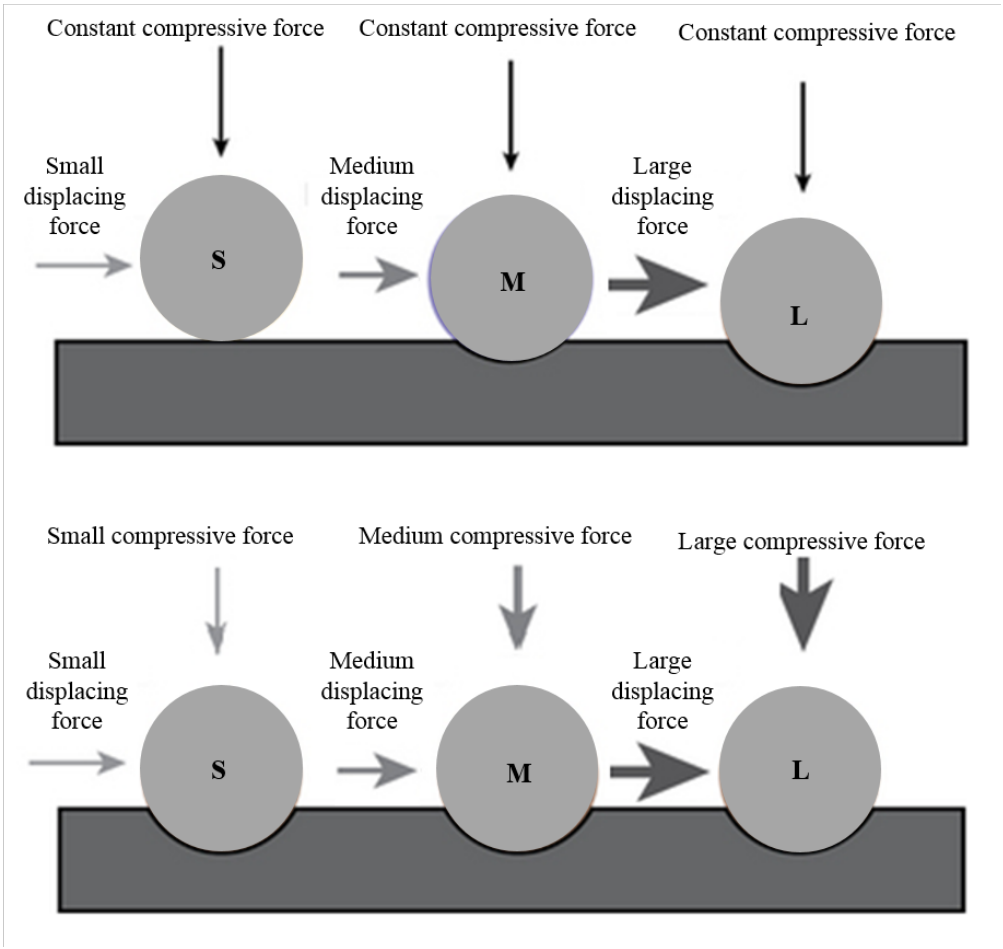

Figure 2.5: Schematic of stability through concavity compression. Top – GH joint stability increases from left to right due to an increasing concavity of the socket, while the joint compressive force is constant. Bottom – GH joint stability increases from left to right due to an increasing joint compressive force, while the concavity of socket is kept constant. The image was reproduced and modified with permission from Lippitt and Matsen (1993).

2.2 Anterior Shoulder Dislocation

This section will provide an overview of the clinical situation of patients with anterior shoulder dislocation. The focus will be on injuries, treatment strategies and rehabilitation programs as well as associated rates of recurrent anterior shoulder instability.

2.2.1 Clinical Situation

The articulation of the shallow glenoid fossa and the large humeral head makes the GH joint inherently unstable. The incidence of traumatic shoulder instability is reported to be as high as 1.7% in the general population (Liavaag et al. 2011). This makes the GH joint the most frequently dislocated articulation in the human body (Shah et al. 2017; Zacchilli & Owens 2010), with more than 90% of these dislocations being located anteriorly (Pope et al. 2011; Owens et al. 2009).

The predominant causes of an anterior shoulder dislocation include a fall on an outstretched arm, a forceful external rotation of the humerus in an abducted position as well as an anteriorly-directed blow against the shoulder (Rowe 1956; Robinson et al. 2006; Paterson et al. 2010; Crichton et al. 2012). Based on these injury mechanisms, the age range of patients with anterior shoulder dislocation demonstrates a bimodal distribution (Cutts et al. 2009; Shah et al. 2017). The largest patient group involves young adult men that have sustained high-energy injuries to the GH joint usually during contact sports as a result of one of the three injury mechanisms above (Liavaag et al. 2011; Owens et al. 2009). The second-largest group are elderly patients, who have sustained GH joint injuries with much lower energy levels, typically after a fall on an outstretched arm (Leroux et al. 2014).

Recurrent anterior shoulder instability is a common sequelae in young patients, with recurrence rates ranging between 47-92% in patients under the age of 20 years at the time of primary shoulder dislocation (Rowe 1956; Arciero et al. 1994; Hovelius et al. 1996; McLaughlin and MacLellan 1967; Flint et al. 2018). The majority of these recurrent instabilities occurs within the first two years of primary traumatic joint dislocation (Moseley and Overgaard 1962; Jobe et al. 1991). In contrast to young patients, the incidence rate for recurrent instabilities in patients over the age of 40 years is 10-20% (DeBerardino et al. 2001), and therefore anterior shoulder dislocation typically represents an isolated event in elderly patients (McLaughlin and Cavallaro 1950; McLaughlin and MacLellan 1967).

2.2.2 Injuries

Anterior shoulder dislocations are typically accompanied by structural injuries to the articulation, with the severity of this structural damage increasing with each episode of recurrent anterior shoulder instability (Atef et al. 2016). As the humeral head is levered out of the glenoid fossa, the anterior shoulder dislocation is commonly associated with the attenuation of capsuloligamentous restraints and the avulsion of the anteroinferior glenoid labrum (Figure 2.6; Bankart lesion), rotator cuff tears as well

as fractures of the anteroinferior glenoid rim (Figure 2.7; bony Bankart lesion). As the posterior part of the humeral head leaves the articulation, it frequently collides with the anterior rim of the glenoid fossa, creating an indentation fracture at the posterior part of the humeral head (Figure 2.7; Hill-Sachs lesion).

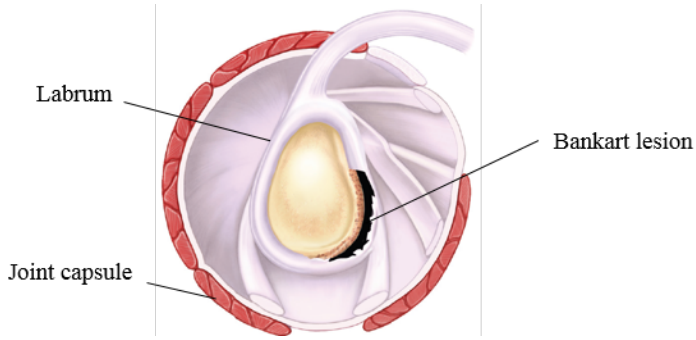

Figure 2.6: Avulsion of the anteroinferior glenoid labrum. The image was reproduced and modified with permission from Gaunt et al. (2010).

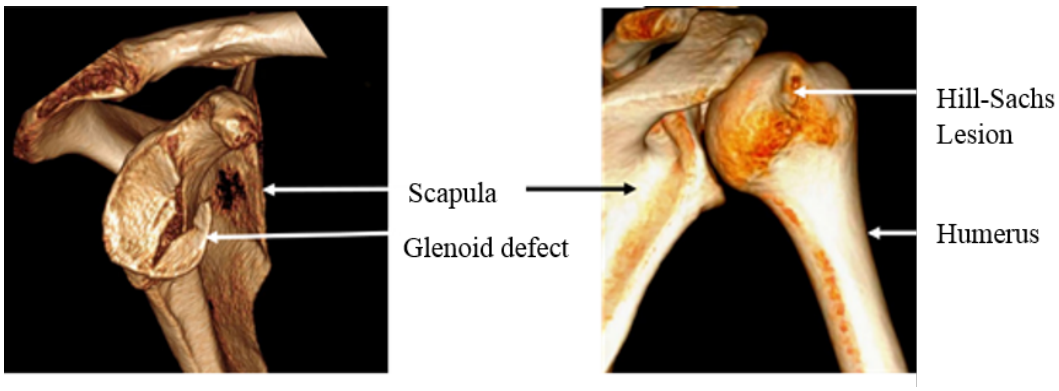

Figure 2.7: Left: Anteroinferior glenoid osseous defect. Right: Hill-Sachs lesion shown from a posterior view. The images were reproduced and modified with permission from Yamamoto and Itoi (2015).

2.2.2.1 Soft Tissue Injuries

The vast majority of patients following an anterior shoulder dislocation have structural soft tissue abnormalities, with the avulsion of the anteroinferior glenoid labrum being the most common injury (Gaunt et al. 2010). The incidence of anteroinferior labral avulsion was reported to range between 48-76% in young patients following first traumatic anterior shoulder dislocation (Taylor and Arciero 1997; Norlin 1993; Baker et al. 1990), with incidence rates increasing to 83-100% following recurrent instabilities (Kim et al. 2003; Hintermann and Gachter 1995; Coughlin et al. 1992). Similarly, the prevalence of Bankart lesions in patients over the age of 40 years has been reported to be as high as 66% following primary traumatic anterior shoulder dislocation, with incidence rates reaching 87% following recurrent instabilities (Araghi et al. 2005; Mizuno et al. 2016).

The occurrence of anteroinferior labral avulsions is commonly associated with an attenuation of the capsuloligamentous complex. Capsuloligamentous laxity is more commonly encountered than capsuloligamentous tears (Kim et al. 2010). The incidence of tears to the inferior glenohumeral ligament has been reported to range between 15-30% for patients with recurrent instabilities (Bokor et al. 1999; Bui-Mansfield et al. 2007), while capsular tears were found to be present in 32-54% of patients with recurrent episodes of anterior shoulder dislocation (Ogawa and Yoshida 1997; Bacilla et al. 1997; Grana et al. 1993). The incidence of these injuries has been reported to increase with age due to a loss in mechanical tissue strength (Lee et al. 1999; Reeves 1968).

The anteroinferior glenoid labral avulsion may extend to the superior labrum, with superior labrum anterior to posterior (SLAP) lesions being a rare complication following anterior shoulder instability (Thomas & Matsen 1989). The incidence of SLAP tears has been reported to range between 10-17% for patients with recurrent instabilities (Kim et al. 2010; Antonio et al. 2007).

Anterior shoulder dislocations may be accompanied by rotator cuff tears. These injuries are increasingly common sequelae of dislocation in patients older than 40 years of age, with an incidence rate of 40% in patients older than 40 years of age, an incidence rate of 50% in patients older than 60 years of age and an incidence rate of 80% in patients older than 80 years of age (Itoi & Tabata 1992; Milgrom et al. 1995; Rapariz et al. 2010; Neviaser et al. 1993). In contrast, rotator cuff tears are less commonly encountered in young patients, with incidence rates of below 13% (Walch 1997; Rumian et al. 2011). This discrepancy has been attributed to the decreased tensile strength of the rotator cuff tendons in the elderly (Reeves 1968).

The supraspinatus is predominantly involved in rotator cuff tears following an anterior shoulder dislocation (Itoi and Tabata 1992; Pevny et al. 1998). Supraspinatus tears commonly occur as an isolated rupture (Neviaser et al. 1988), with combined rotator cuff tears of supraspinatus and subscapularis being reported in about 25% of the cases (Neviaser et al. 1993; Itoi and Tabata 1992). Isolated subscapularis tears are uncommon, but these have been reported in young male patients post anterior shoulder dislocation (Seppel et al. 2017).

2.2.2.2 Bone Injuries

The prevalence of fracture or erosion of the anteroinferior glenoid rim among shoulders with primary dislocation has been reported to as high as 56% (Boileau et al. 2006; Edelson 1996), with prevalence rates for glenoid osseous defects reaching up to 83% in patients with recurrent instabilities (Kummel 1970; Sugaya et al. 2003; Warner et al. 2006). As the size of the glenoid osseous defect is related to the number of recurrent shoulder dislocations as well as physical activity (Griffith et al. 2008; Milano et al. 2011), these bone lesions represent a larger complication in younger patients (Kim et al. 2010; Yiannakopoulos et al. 2007). Glenoid osseous defects may extend to the anterior glenoid rim, with

recent imaging studies demonstrating that these lesions can be located anteriorly, at approximately the three o'clock position on a right shoulder (Griffith et al. 2003; Saito et al. 2005).

The presence of indentation fractures at the back of the humeral head following first traumatic anterior shoulder dislocation has been reported in 47% of patients (Widjaja et al. 2006; Rowe et al. 1984), with incidence rates raising to 86% in these patients following recurrent instabilities (Edwards et al. 2003; Hovelius et al. 1983). The location of the Hill-Sachs defect was described as oriented towards the eight o'clock position on a right shoulder, with the most anterior and posterior points of a sphere fit to the humeral head in the hanging arm position representing the three and nine o'clock positions respectively (Saito et al. 2009).

The incidence of combined glenoid osseous defect and Hill-Sachs lesion has been reported to be as high as 57% in patients with recurrent anterior shoulder instabilities (Calandra et al. 1989; Edwards et al. 2003).

In conclusion, anterior shoulder instabilities are commonly associated with bone and soft tissue injuries, with Bankart lesions and glenoid osseous defects being the most commonly observed structural defects. Anterior shoulder dislocations may be accompanied by rotator cuff tears, which represent a more commonly observed clinical complication in elderly patients.

2.2.3 Treatment

The majority of patients (>90%) following anterior shoulder instability is treated non-operatively (Ma et al. 2017). Physiotherapy aims to strengthen the rotator cuff muscles to restore joint stability through concavity compression, without exposing the patient to the unnecessary risk of surgery. However, the number of patients being treated surgically rather than through physiotherapy has increased over the past years (Dickens et al. 2017; Marshall et al. 2017; Rugg et al. 2018). This is due to retrospective analyses demonstrating recurrence rates of anterior shoulder instability of 60-80% in young, athletic patients following conservative treatment (Gigis et al. 2014; Khan et al. 2014).

The Bankart repair is the first choice treatment for patients with failed conservative management, high physical demands and small bone defects following anterior shoulder dislocation (Berendes et al. 2015; Boileau et al. 2009). The surgical stabilisation of an anteroinferior glenoid labral defect involves the anatomical reattachment of the torn labrum to the glenoid rim with suture anchors in order to restore joint stability through concavity compression (Figure 2.8; Bankart 1923). The Bankart repair may be performed as open surgery or arthroscopically, with capsular plication and rotator cuff repair being added to the surgical procedure as necessary to repair soft tissue defects (Higgins & Warner 2000; Soslowsky et al. 1992). Good clinical outcomes have been reported for open and arthroscopic Bankart repairs, with instability recurrence rates ranging between 9-23% in patients with high physical demands and limited bone loss (Hobby et al. 2007; Petrera et al. 2010; Speer et al. 1996). Furthermore,

improvements in physical symptoms, emotional wellbeing and quality of life (Kirkley et al. 2005) have been reported in patients following surgical repair of Bankart lesions. However, the incidence rates of recurrent anterior instability may be as high as 67% (Burkhart et al. 2007) following Bankart repair in patients with large glenoid osseous defects as well as large Hill-Sachs lesions that engage with the anterior glenoid rim. Therefore, the effectiveness of the Bankart repair in restoring joint stability may be limited by the size of the bone defect in combination with large ranges of shoulder motion and high joint loading (Randelli et al. 2012; Lo et al. 2004; Saliken et al. 2015).

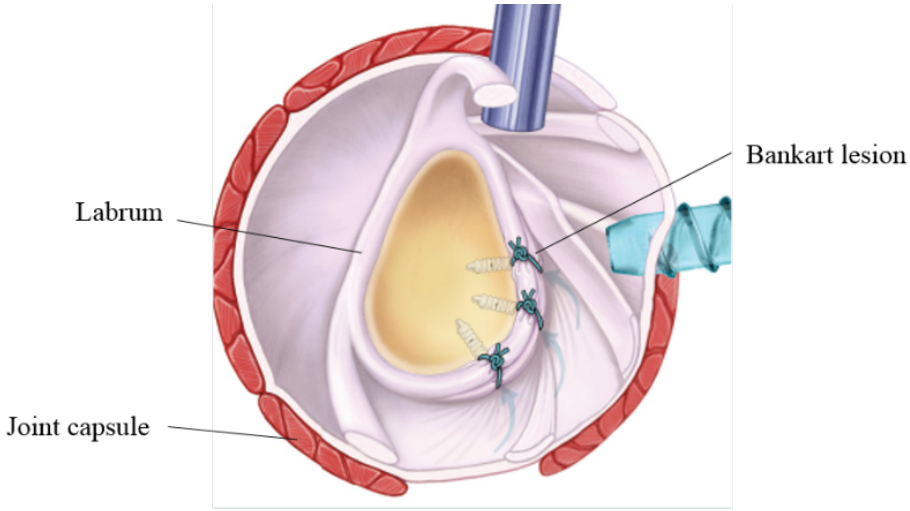

Figure 2.8: Repair of a Bankart lesion with three suture anchors. The image was reproduced and modified with permission from Gaunt et al. (2010).

As the selection of patients for Bankart repair was based on clinical experiences, several research studies involving cadaveric testing, medical imaging and retrospective analyses have been performed to aid clinical decision-making by identifying quantifiable measures and risk factors that predispose patients to recurrent anterior shoulder instability following Bankart repair (Flinkkila et al. 2010; Imhoff et al. 2010; Porcellini et al. 2009; van der Linde et al. 2011).

Several risk factors associated with a high risk of recurrent anterior shoulder instability following Bankart repair have been identified through retrospective analyses (Wasserstein et al. 2013; Abouali et al. 2013; Waterman et al. 2014; Neviaser et al. 2015). These clinical observations served to establish the shoulder instability severity index score (Balg & Boileau 2007) that identifies patients for whom a Bankart repair is relatively contraindicated, and bone-grafting is suggested to restore joint stability. These risk factors include patient age, glenoid defect size, type of sport and degree of sport participation.

Biomechanical studies have been performed to quantify the critical size of a glenoid osseous defect that bone-grafting, rather than a soft tissue repair, is required to restore joint stability (Itoi et al. 2000; Yamamoto et al. 2009a, 2010). These studies illustrate an inverse relationship between the size of the glenoid defect and the stability of the shoulder: the larger the defect, the less stable the shoulder. In the absence of Hill-Sachs lesions, these studies demonstrated a statistical significant decrease in joint

stability following the creation of glenoid osseous defects with a width of 6 mm, representing 20% of the glenoid length. These values have clinically been used as a contraindication for Bankart repairs (Warner et al. 2006).

Biomedical imaging studies have been performed to evaluate the risk of Hill-Sachs lesions engaging with the anterior glenoid rim (Omori et al. 2014; Yamamoto et al. 2007). These studies investigated the contact area of the humeral head on the glenoid fossa in the shoulder dislocation position, quantifying the 'glenoid track' as the distance from the medial margin of the rotator cuff footprint to the medial margin of the contact area. The size of the glenoid track is equivalent to 84% of the glenoid width, with only Hill-Sachs lesions that extend over the glenoid track, termed as Off-track lesions, being at risk of engagement. As the contact area of the humeral head on the glenoid fossa was investigated in the absence of glenoid osseous defects, the size of the glenoid track decreases in the presence of bony glenoid lesions (Figure 2.9). Off-track Hill-Sachs lesions have clinically been used as a contraindication for Bankart repairs (Di Giacomo et al. 2014).

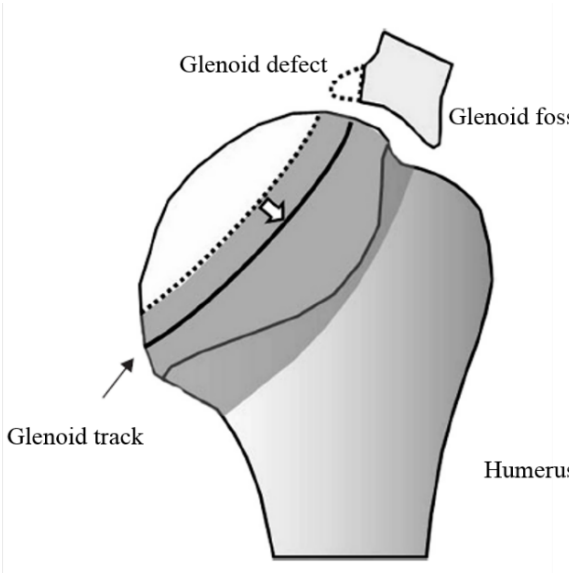

Figure 2.9: Glenoid track in case with glenoid osseous defect. The width of true glenoid track, approximately 84% of the glenoid width (gray shaded area), decreases due to the glenoid osseous defect (black line). The glenoid defect size should be deducted from the from the glenoid width. The image was reproduced and modified with permission from Yamamoto and Itoi (2015).

Based on these clinical recommendations, the Latarjet procedure has been performed most commonly to restore joint stability in patients with large glenoid osseous defects, and on-track Hill-Sachs lesions (Figure 2.10; Blonna et al. 2016; An et al. 2016). This surgical procedure involves the transfer of the coracoid process as well as the attached conjoint tendon to the anterior glenoid rim (Latarjet 1954) in order to stabilise the joint (Burkhart et al. 2007; Walch & Boileau 2000). Good clinical outcomes have been reported for Latarjet procedures (Hovelius et al. 2012; Lafosse et al. 2010; Maquieira et al. 2007), with instability recurrence rates of below 7% (Griesser et al. 2013). However, Latarjet procedures are

associated with surgical complication rates of up to 30% (Griesser et al. 2013) as well as a loss in external rotation ROM of 9° (Cowling et al. 2016).

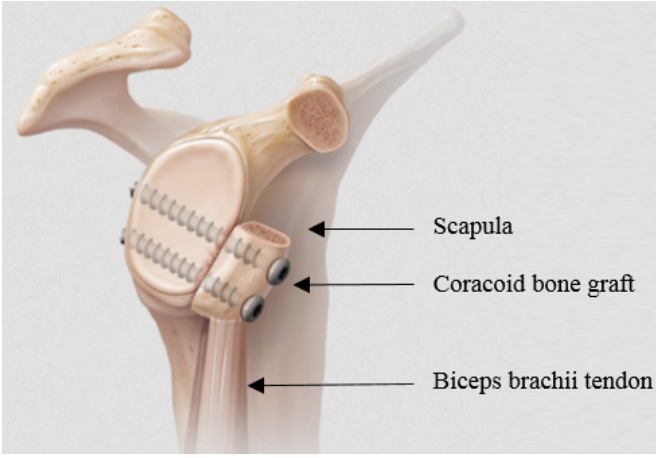

Figure 2.10: Repair of an anteroinferior glenoid osseous defect with a Latarjet procedure. The image was reproduced and modified with permission from Cowling et al. (2016).

In patients with engaging, off-track Hill-Sachs lesions following Latarjet procedure, the use of a Remplissage intervention has been recommended to restore joint stability (Di Giacomo et al. 2014). The Remplissage procedure involves the attachment of the infraspinatus tendon to the humeral defect to fill the Hill-Sachs lesion (Figure 2.11; Nourissat et al. 2014). While this surgical procedure has led to good clinical outcomes with instability recurrent rates of below 3% (Garcia et al. 2015), the Remplissage procedure is also associated with an average loss in external rotation ROM of 15° (Omi et al. 2014).

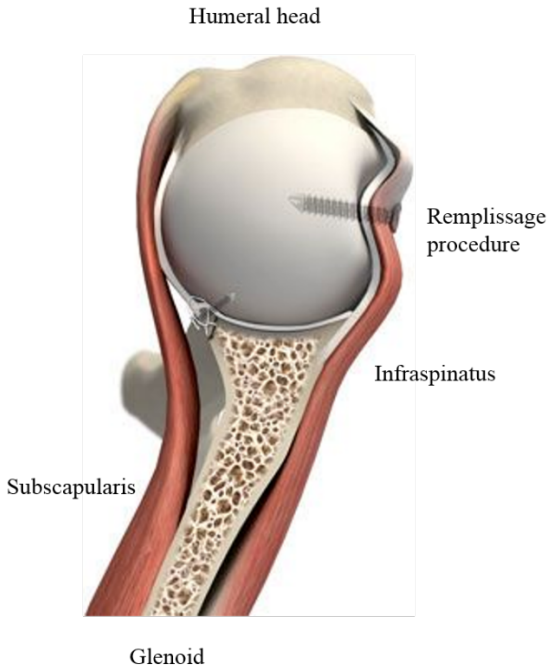

Figure 2.11: Remplissage procedure involves filling of the Hill-Sachs lesion with the infraspinatus tendon. The image was reproduced and modified with permission from Yang et al. (2018).

In conclusion, the rates of recurrent anterior shoulder instability following Bankart repair are higher than those of Latarjet procedures in patients with large osseous defects, but the surgical repair of Bankart lesions is less invasive and associated with lower surgical complication rates when compared to the Latarjet procedure. This makes the treatment selection of patients following anterior shoulder instability a balancing act between restoring joint stability without exposing patients to unnecessary surgical risks. Therefore, knowing critical bone lesion sizes under loading conditions expected by the patients during functional daily activities will assist clinical decision-making. Similarly, understanding the effect of SLAP II tears and rotator cuff pathology on anterior shoulder stability in overhead throwing athletes will aid surgical decision-making. These clinical questions will be addressed in Chapter 6 and 7.

2.2.4 Rehabilitation

The American Society of Shoulder and Elbow therapists has defined a successful outcome following an anterior shoulder instability treatment as a pain-free and stable shoulder that provides sufficient mobility and strength for the patient's targeted level of activity (Gaunt et al. 2010). Therefore, the rehabilitation of patients following anterior shoulder instability surgery plays an important role in the treatment process as physiotherapy is concerned with restoring joint mobility and enhancing joint stability through strengthening of the rotator cuff muscles (Speer et al. 1993).

The rehabilitation of patients following surgical intervention is guided by clinical observations and experiences. Rehabilitation guidelines do not represent standards of medical care, instead these should be used in combination with patient expectations, preferences and goals (Lervick 2013). Therefore, the greatest chance for successful rehabilitation is given through a cooperation of knowledgeable surgeons and rehabilitation specialists with educated patients (Gaunt et al. 2010).

The rehabilitation guidelines for patients following anterior shoulder instability surgery are tailored to the surgical intervention, with variations in surgical technique necessitating varied rehabilitation approaches for successful patient outcomes (Ma et al. 2017; Bacilla et al. 1997). Therefore, different rehabilitation protocols have been presented in the literature for the treatment of Bankart repairs, glenoid osseous defects as well as rotator cuff tears. As the Bankart repair is the most commonly performed surgical intervention for patients with anterior shoulder instability, the following sections will expand on the rehabilitation protocols of this surgical intervention only.

The rehabilitation of patients following Bankart repair aims to gradually restore the large ROM at the shoulder, while protecting the healing of the repaired capsulolabral tissues to prevent recurrent shoulder instabilities. The duration of the rehabilitation programs is typically 12 weeks (Gaunt et al. 2010; Wilk & Macrina 2013), with the progression of individual patients being dependent on patient and injury factors such as patient age, labral tear characteristics and tissue fixation strength (Ma et al. 2017).

The immediate phase (0-6 weeks post-surgical intervention) involves the maximal protection of surgically repaired Bankart lesions. The patient will guard the arm in a sling for 3-6 weeks (Levine et al. 1994; McDermott et al. 1999), typically in an internally rotated position based on clinical experiences (Wilk & Macrina 2013; Grana et al. 1993), in order to protect the shoulder from positions that place the repaired capsulolabral tissues at risk (McEleney et al. 1995). As excessive loading of the Bankart repair may disrupt the healing process between labrum and glenoid fossa, the rehabilitation guidelines advise patients to avoid performing normal day activities, with exceptions only being made for tasks involving personal hygiene and feeding (Dines & Levinson 1995). Due to the minimally invasive nature of the arthroscopic Bankart repair, patients may feel little pain and consequently be able to perform more daily activities potentially damaging to the repair without any symptoms. Therefore, the education of patients regarding the loading of the shoulder during daily activities is essential to avoid overloading of the Bankart repair.

While excessive loading of surgically repaired Bankart lesions in the immediate phase may disrupt the healing process between the labrum and glenoid fossa, the gradual application of controlled stresses to the repaired tissues has been demonstrated to promote tissue healing (Balestrini & Billiar 2009; Burk et al. 2016). Therefore, the passive ROM is initiated by the rehabilitation specialist in week three based on the patient's pain tolerance. The passive ROM is performed in diagonal, loose-packed positions (Ma et al. 2017) and slowly increased in all planes of arm elevation until the end of the immediate phase (Gaunt et al. 2010). The exposure of the shoulder to high angles of arm elevation is not recommended during this stage as joint positions particularly with external rotation and high abduction angles directly stress the repaired Bankart lesion (O'Connell et al. 1990; Kim et al. 2003).

The intermediate phase (7-12 weeks post-surgical intervention) involves restoring the full passive and active ROM, while controlling the load on the Bankart repair. The passive and active ROM is slowly progressed in all planes of arm elevation from week 7 onwards, with the shoulder being exposed to high angles of arm elevation at the end of this stage in order to restore full joint mobility as applicable to activities of daily living (Ma et al. 2017). While the rehabilitation guidelines permit patients at the end of this stage to perform essential functional daily activities associated with lifting of everyday objects and large ranges of motion, functional activities that heavily load the repaired tissues such as standing up and sitting down using arm rests as well as steering a car are still not recommended (Gaunt et al. 2010). Rotator cuff strengthening exercises may be initiated in the intermediate phase in order to prevent atrophy and weakness of the active joint stabilisers (Matheson et al. 2011). These involve planar movements with light weights and may be assisted by electrical stimulation to facilitate shoulder muscle contraction (Davies et al. 2017).

The final phase (13-20 weeks post-surgical intervention) involves restoring the full athletic ROM and improving muscular strength and power that is necessary for an individual to return to pre-injury sport-

related performance levels (Wilk et al. 2002). Therefore, the final phase of the physiotherapy is only applicable to patients with high physical demands following anterior shoulder instability treatment. Plyometric exercises are commonly performed at medium and high velocity to restore full athletic motion (Rubin & Kibler 2002), with overhead athletes not being able to return to full competition for at least 6 months following Bankart repair (Gibson et al. 2016).

The rehabilitation of patients following Bankart repair is a balancing act that involves restoring joint mobility, while protecting the healing of the repaired capsulolabral tissues. As the loading of the Bankart repair during functional daily activities is largely unknown, the education of patients regarding safe functional daily activities is challenging and based on clinical experiences. Therefore, Chapter 5 will investigate the loading of the Bankart repair during functional daily activities in order to aid rehabilitation planning.

2.3 Computational Shoulder Modelling

The stability at the shoulder is achieved through a complex interplay of active and passive joint stabilisers, with injuries to these soft tissues increasing the risk of joint instability (van der Heijden et al. 2009). As the direct measurement of parameters to assess shoulder functionality is inherently challenging (Prinold et al. 2013), the interplay of individual joint structures to the mobility-stability relationship at the shoulder remains not fully understood (Bolsterlee et al. 2013).

Traditional biomechanical measurements are restricted by existing experimental techniques and ethical issues, with existing measurement techniques commonly utilising *in-vitro* loading conditions to investigate joint loading for clinical recommendations (Apreleva et al. 2000; Ellis et al. 2006; Itoi et al. 2000; Parsons et al. 2002). As the stability of the shoulder is load dependent, with increasing joint forces leading to a loss in joint stability (Halder et al. 2001; Lippitt et al. 1993), these experimental findings may not be representative for *in-vivo* joint loading during functional daily activities. Some recent cadaver studies have addressed this and replicated *in-vivo* loading conditions by applying physiological loads to muscles or *in-vivo* contact forces or pressure to the joint (Eichinger et al. 2016; Giles et al. 2014; McMahon et al. 2013; Henninger et al. 2012).

Computational modelling of the shoulder represents a great opportunity to overcome these limitations and to assess joint functionality for a broad spectrum of loading conditions, in a large number of joint positions, with a variety of pathological conditions. Two computational modelling techniques have been advanced over the past three decades as an adjunct to clinical decision-making for patients with a variety of shoulder pathology. These modelling techniques include musculoskeletal (MSK) shoulder modelling as well as finite element (FE) analysis of the shoulder (Zheng et al. 2017).

2.3.1 Musculoskeletal Shoulder Modelling

This section will introduce existing MSK shoulder models and describe their clinical applications. The focus will be on the functionality and limitations of the United Kingdom National Shoulder Model (UK NSM) as this computational model is used in this thesis for shoulder modelling.

2.3.1.1 Musculoskeletal Shoulder Models & Clinical Applications

There are two different methods to analyse the biomechanics of the shoulder: Inverse Dynamics (ID) and Forward Dynamics (FD). ID simulations are conceptually and computationally simple, requiring only joint kinematics, external loading, and inertial properties as input in order to quantify articular and soft tissue loading during shoulder motion (Veeger et al. 2002). In contrast, FD models predict shoulder movement based on joint torques or muscle activation data, necessitating the implementation of muscle contraction mechanics (Hill 1938) as well as knowledge of the mechanical properties of tendons (Winters & Stark 1985). This makes FD simulations, unless highly constrained, complex and computationally-expensive problems to solve (Otten 2003). Therefore, the majority of MSK shoulder models in the literature uses an ID approach to analyse the biomechanics of the shoulder (van der Helm 1994).

The accurate prediction of musculoskeletal loading requires ID MSK shoulder models to include all joints spanned by biarticular muscles present in the upper limb and to divide these muscles into a number of force elements (van der Helm and Veenbaas 1991). There are several ID MSK shoulder models presented in the literature. These include the Delft Shoulder and Elbow model (DSEM; Nikooyan et al. 2011; van der Helm 1994), the United Kingdom National Shoulder Model (UK NSM; Charlton and Johnson 2006), the Swedish Shoulder Model (SSM; Hogfors et al. 1995), the Waterloo model (WSM; Dickerson et al. 2007), the Garner and Pandy model (GPM; Garner and Pandy 2001), the Stanford-VA model that is implemented in the OpenSim software (SVM; Delp et al. 2007), and the commercially available AnyBody Upper Extremity model (ABM; Lemieux et al. 2012).

The SSM includes most shoulder muscles but importantly neglects the elbow, which has muscles that cross the elbow joint as well as the shoulder (Hogfors et al. 1995). Similarly, the GPM as well as the Stanford-VA model lack muscles that are important scapula stabilisers such as the trapezius, serratus anterior and levator scapulae (Holzbaur et al. 2005, 2007). The DSEM as well as the WSM represent anatomically complete shoulder models, but the WSM, alongside the SSM, GPM, SVM and ABM, do not allow for measured scapula kinematics as model input. This is despite the fact that MSK shoulder model predictions are sensitive to scapula kinematics (Raikova & Aladjov 2002) and that methods for scapular tracking have been validated and implemented into the UK NSM (Prinold et al. 2011). Based on that as well as the development and clinical use of UK NSM at Imperial College London over the

last decade (Prinold 2012; Pandis 2015; Persad 2016; Ismail 2016), this computational model of the shoulder will be used within this thesis to model joint functionality.

MSK shoulder models apply basic mechanical laws to the human musculoskeletal system of the upper limb in order to predict articular and soft tissue loading from measurable motion data and external forces. The precise knowledge of MSK shoulder loading is of great clinical relevance and therefore MSK shoulder models have been used to answer a variety of clinical questions.

MSK shoulder models have been utilised to investigate the loading of the GH joint during functional activities. There are several studies reported in the literature researching joint loading during planar movements (Inman et al. 1996; Karlsson and Peterson 1992; Dul 1988; Bergmann et al. 2007) as well as wheelchair propulsion (van Drongelen et al. 2005; Veeger et al. 2002) and hand cycling (Arnet et al. 2012). The loading of the glenohumeral joint has also been studied during functional activities of daily life (Anglin et al. 2000; van Drongelen et al. 2006; Charlton and Johnson 2006; van Andel et al. 2008; Nikooyan et al. 2010), with these study findings being important for the description of normal joint loading, which is essential when aiming to quantify abnormal joint loading.

MSK shoulder models have also been used to investigate shoulder stability in association with tendon transfer surgeries (Jastifer et al. 2012; Magermans et al. 2004; Saul et al. 2003; Steenbrink et al. 2009), shoulder arthroplasties (Kontaxis & Johnson 2009; Masjedi & Johnson 2010; Suarez et al. 2009; van der Helm 1994), rotator cuff tears (Lemieux et al. 2012; Saul et al. 2011; Hughes et al. 1997; Masjedi et al. 2008) and tetraplegia (van Drongelen et al. 2005, 2006). These study findings are clinically important as they predict changes in shoulder functionality with alterations in shoulder anatomy due to pathology or surgery.

Over the past three decades, MSK shoulder models have been used to answer a variety of clinical questions, with bone and labral pathologies receiving little attention (Bolsterlee et al. 2013). This is despite these injuries being frequently associated with recurrent anterior shoulder instability, the most commonly encountered pathological condition at the shoulder as described in Section 2.2.2.

2.3.1.2 The United Kingdom National Shoulder Model

The UK National Shoulder (UK NSM) model is a 3D ID model of the upper limb consisting of six rigid bone segments, 87 muscle lines of action as well as three glenohumeral ligaments (Figure 2.12). The shoulder model was established using the bony geometry of the male Visible Human (VH) dataset (Spitzer & Whitlock 1998), while muscle morphology data were obtained from three cadaveric studies (van der Helm et al. 1992; Johnson et al. 1996; Veeger et al. 1997). Body segment parameters of mass, centre of mass and moment of inertia were obtained from regression equations (De Leva 1996). Model validation was performed through comparison with alternative models (Charlton & Johnson 2006) which include MSK shoulder models that directly have been validated against measurements from

instrumented shoulder implants (Nikooyan et al. 2010; comparison by Prinold 2012). Further model verification was performed through comparison of model predicted muscle moment arms with cadaveric measurements (Gatti et al. 2007) as well as through comparison of predicted muscle activations with electromyographic measurements (EMG; Johnson and Pandyan 2005; Pandis et al. 2015). Recent published work utilising the UK NSM includes the analysis of muscle and joint contact forces during driving (Pandis et al. 2015), cricket bowling (Persad 2016), pull-ups (Prinold 2012) and brick laying (Ismail 2016).

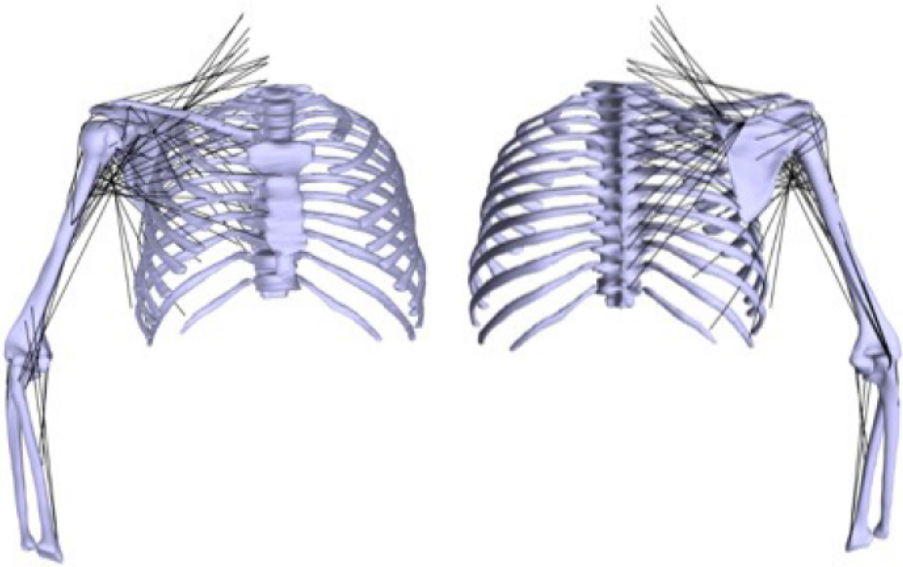

Figure 2.12: Anterior (left) and posterior (right) view of the muscle lines of action in the UK NSM.

The UK NSM model utilises measured human movement and subject-specific anthropometrics as model input to predict muscle and joint loading during shoulder motion. An overview of the processing steps is given below.

- Subject-specific model builder
  Input: Anatomical dataset, anthropometric measurements (height, weight), motion data
  Output: Body segment parameters, scaling factors

- Kinematic calculation
  Input: Scaling factors, local coordinate systems
  Output: Upper limb joint angles

- Inverse dynamics
  Input: Body segment parameters, scaling factors, joint angles, externally measured forces
  Output: Intersegmental forces and moments

- Muscle wrapping
  Input: Anatomical dataset, joint angles, scaling factors, body segment parameters
  Output: Muscle lines of action, muscle moment arms

- Loadsharing optimisation
  Input: Intersegmental forces and moments, muscle lines of action, muscle moment arms, muscle force boundaries, ligament boundaries
  Output: Joint contact forces, muscle forces, muscle activations

2.3.1.2.1 Subject-Specific Model Builder

The body segments of the UK NSM are scaled to an experimental subject to ensure that intersegmental distances of the computational model match the corresponding intersegmental distances of the subject. The accurate representation of the upper limb anatomy for an experimental subject is important as scapular scaling has been shown to greatly affect model predictions (Karduna et al. 2001).

The scapula, clavicle, humerus, radius and ulna are scaled linearly in three dimensions by the distance between the joint centres along the long axis of the bone segment (Figure 2.13). The thorax is scaled non-homogenously with thorax height being defined as distance between Xiphoid Process and the midpoint of Jugular Notch and 7th cervical vertebra, thorax width as distance between Jugular Notch and right Acromioclavicular joint, thorax depth as distance between 7th cervical vertebra and the midpoint of Xiphoid Process and Jugular Notch. The muscle origin and insertion sites are scaled with the corresponding segment, while the physiological cross-sectional area of each upper limb muscle remains unscaled.

The body segment parameters of mass, centre of mass and moment of inertia are scaled based on regression equations (De Leva, 1996) using the experimental subject's height and weight.

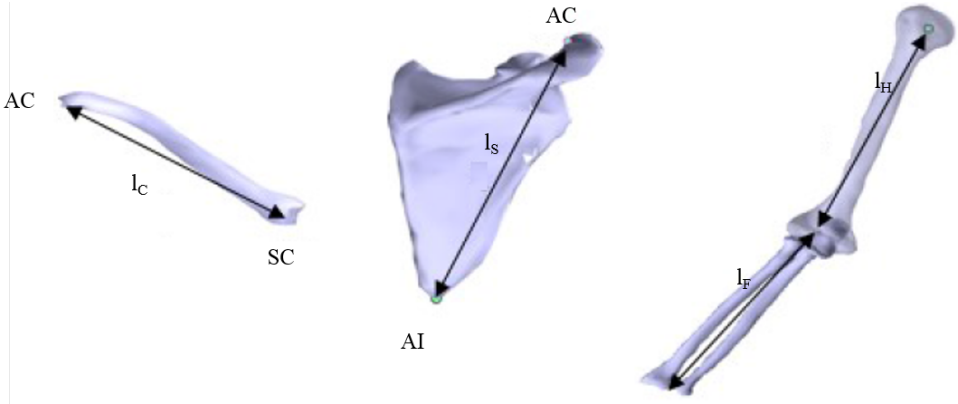

Figure 2.13: Segment lengths used for segment scaling, l_C – length of the clavicle, l_S – length of the scapula, l_H – length of the humerus, l_F – length of the forearm.

2.3.1.2.2 Kinematic Calculation

Once the UK NSM has been scaled to an experimental subject, local coordinate frames for each body segment can be defined based on anatomical landmarks (Wu et al. 2005). Detailed information on the local coordinate frames employed by the UK NSM can be found in Charlton and Johnson (2006). The joint angles between two body segments are calculated by extracting Euler angles from the transformation matrix between the two local coordinate frames.

The UK NSM models the articulations of the upper limb with 13 rotational degrees of freedom (DOF). There are 3 DOF at the sternoclavicular joint, 3 DOF at the acromioclavicular joint, 2 DOF at the scapulothoracic gliding plane, 3 DOF at the glenohumeral joint and 2 DOF at the elbow. The 3 DOF at the glenohumeral joint include joint rotations, meaning that the UK NSM does not model the translation of the humerus relative to the glenoid fossa. The glenohumeral joint rotation centre was computed using a least-square fitting method (Gamage & Lasenby 2002).

MSK shoulder models are very sensitive to kinematic input (Nikooyan et al. 2010), with scapular kinematics greatly affecting modelling outcomes (Masjedi & Johnson 2010). Therefore, in addition to the tracking of the scapula for an experimental subject during shoulder motion (Prinold et al. 2011), the modelling framework of the UK NSM employs a kinematic optimisation to minimise the least squares difference between modelled and measured scapular kinematics (Prinold & Bull 2014).

2.3.1.2.3 Inverse Dynamics

The Newtonian equations of motion serve to calculate the intersegmental joint forces and moments through derivations of joint angles, accelerations and externally applied forces. The Newton-Euler equations for forces F and moments M are as follows:

$$F = m \cdot \ddot{x} \qquad \text{Equation 2.1}$$

$$M = I \cdot \ddot{\theta} \qquad \text{Equation 2.2}$$

The equations are best illustrated with a free body diagram of a generic 2D body segment (Figure 2.14), where m·g represents the segment mass, $\ddot{x}$ represents the linear acceleration, $\ddot{\theta}$ represents the angular acceleration, R represents the reaction forces, I represents the moment of inertia, and M represents the moment acting in the x-y plane on a segment at the proximal (p) and distal (d) joint.

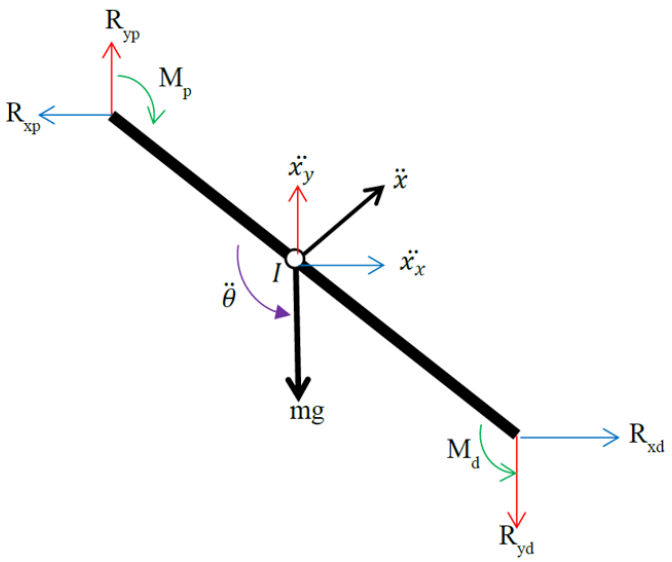

$$\sum F_x = m \cdot \ddot{x}$$

$$R_{xp} - R_{xd} = m \cdot \ddot{x}_x$$

$$\sum F_y = m \cdot \ddot{y}$$

$$R_{xp} - R_{xd} - m \cdot g = m \cdot \ddot{x}_y$$

$$\sum M = I \cdot \ddot{\theta}$$

Figure 2.14: Free-body diagram of a generic 2D body segment with Newton-Euler equations applied to the segment.

2.3.1.2.4 Muscle Wrapping

The scaled UK NSM as well as the calculated joint angles allow the calculation of the muscle path for each muscle of the upper limb. Most of these upper limb muscles are positioned around bones which are represented in the modelling framework of the UK NSM by geometric wrapping objects. The muscle wrapping algorithm computes the muscle path for each upper limb muscle as the shortest distance between muscle origin and insertion around the geometric wrapping objects. From the muscle origin, the tangential point at which the muscle meets the wrapping object has been termed as effective origin (EO), while the tangential point at which the muscle leaves the wrapping object has been termed as effective insertion (EI, Figure 2.15). The wrapping path is described by the straight line from muscle origin to EO, where it wraps around the geometric wrapping object, leaving the surface of the wrapping object at EI to the muscle insertion (I), forming a straight line segment. Muscle wrapping is only required if a direct line between muscle origin and insertion is obstructed by the wrapping object.

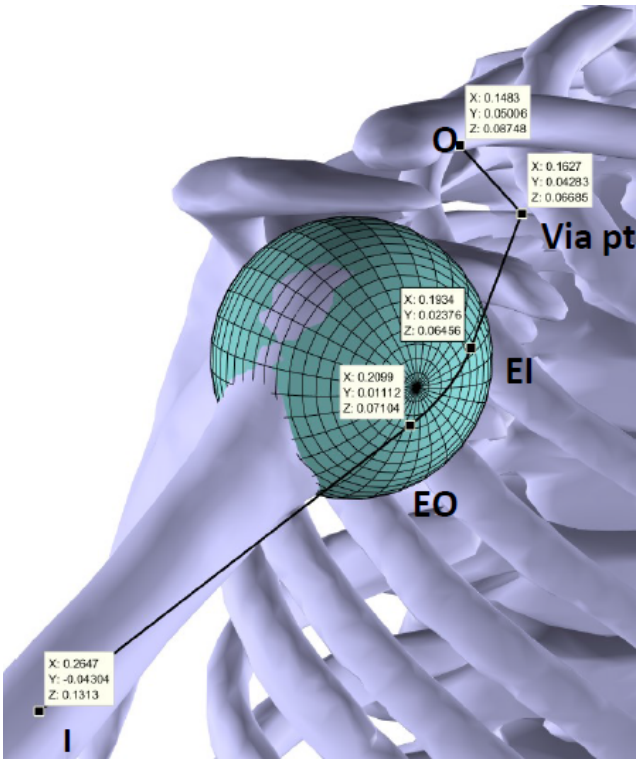

Figure 2.15: Muscle path of the anterior deltoid around the spherical wrapping object of the humeral head using a via point. O – muscle origin, EO – effective origin, EI – effective insertion, I – muscle insertion.

There are 13 wrapping objects in the UK NSM to represent the bony geometry of the upper limb. These wrapping objects include the geometric shapes of ellipsoids, spheres and cylinders, and these geometrical objects are also scaled to an individual during the model builder. The thorax as well as the STGP are modelled with two ellipsoids, while two spheres are fitted to the humeral head to serve as wrapping objects for the rotator cuff muscles as well as the long head of the biceps. The long axes of the humerus, radius, ulna and elbow are fitted with nine cylinders for the wrapping of all shoulder muscles (Table 2.1; Charlton & Johnson 2006).

The limitation of wrapping objects is that these may lead to non-physiological muscle path predictions at high ranges of motion. This is due to 'flipping' of upper limb muscles through a wrong muscle path around the geometric wrapping object (Figure 2.16). In part 1 of Figure 2.16, the muscle path of the deltoid is correctly calculated as the shortest distance between muscle origin and insertion while wrapping around a sphere that was fitted to resemble the humeral head. Equally, in part 2 of Figure 2.16, the muscle path of the deltoid is correctly computed in a joint position with high abduction angles. Part 3 of Figure 2.16 illustrates an example, where the muscle path calculation went wrong. In this case, the muscle path is given as shortest distance between muscle origin and insertion, while wrapping around the humeral head in an anticlockwise and non-physiological fashion. Those muscle path estimations may occur at large ranges of motion due to flipping of the muscle as a result of a miscalculation within the MSK shoulder model.

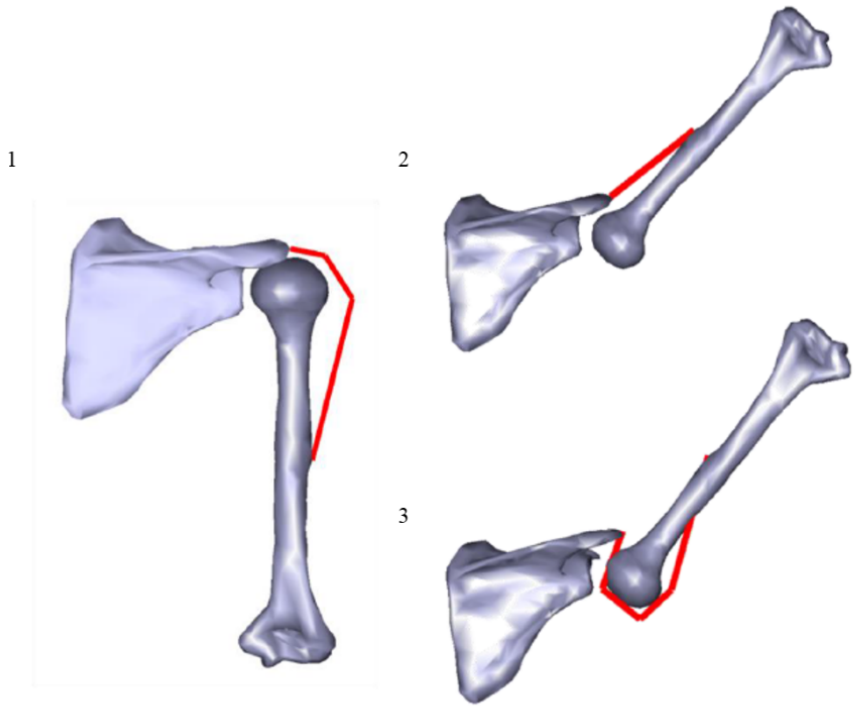

Figure 2.16: Muscle flipping of the deltoid. 1 – The hanging arm position, with the red line indicating the deltoid muscle line of action, 2- Humerus at 150°, with the deltoid muscle line of action following the correct path after muscle contraction, 3 – flipped deltoid muscle line of action to a non-physiological state due to an error in the muscle wrapping computation.

The use of via points (Klein Horsman et al. 2007; Persad 2016) as well as energy minimisation techniques (Marsden et al. 2008) have been suggested in the literature to solve problems associated with muscle wrapping at large ranges of shoulder motion. The UK NSM utilises via points for the anterior and posterior deltoid (Figure 2.15), while energy minimisation is not used.

Table 2.8: Bone segments, muscle elements and wrapping objects of the UK NSM. E – ellipsoid, S – sphere, C – cylinder, 0 – no wrapping.

Muscle	Origin	Insertion	Number of divisions	PCSA [cm^2]	Wrapping object	Wrapping object segment
Trapezius clavicle	Thorax	Clavicle	3	3.30	0	-
Trapezius scapula	Thorax	Scapula	13	9.70	E	Scapula
Levator Scapulae	Thorax	Scapula	4	2.30	E	Scapula
Rhomboid minor	Thorax	Scapula	2	1.30	0	-
Rhomboid major	Thorax	Scapula	5	4.40	0	-
Serratus Anterior	Thorax	Scapula	9	10.50	E	Scapula
Pectoralis minor	Thorax	Scapula	3	3.30	0	-
Latissimus Dorsi	Thorax	Humerus	5	6.60	E	Thorax
Pectoralis major	Thorax	Humerus	10	19.00	E	Thorax
Deltoid	Scapula	Humerus	5	12.20	S	Humerus
Supraspinatus	Scapula	Humerus	1	3.00	S	Humerus
Infraspinatus	Scapula	Humerus	3	6.00	S	Humerus
Subscapularis	Scapula	Humerus	3	7.80	S	Humerus
Teres minor	Scapula	Humerus	1	2.10	S	Humerus
Teres major	Scapula	Humerus	1	4.10	S	Humerus
Coracobrachialis	Scapula	Humerus	2	2.04	0	-
Biceps short	Scapula	Radius	1	2.83	C	Ulna
Biceps long	Scapula	Radius	1	2.97	S	Humerus
Triceps	Humerus	Ulna	6	13.42	C	Radius
Brachialis	Humerus	Ulna	2	5.24	C	Radius
Anconeus	Humerus	Ulna	2	1.60	0	-
Brachioradialis	Humerus	Radius	2	2.14	C	Ulna
Supinator humerus	Ulna	Radius	1	1.51	C	Ulna
Pronator humerus	Humerus	Radius	2	1.04	0	-
Costoclavicular ligament	Thorax	Clavicle	1	0.20	0	-
Conoid ligament	Clavicle	Scapula	1	0.49	0	-
Trapezoid ligament	Clavicle	Scapula	1	1.70	0	-

2.3.1.2.5 Loadsharing Optimisation

The last processing step in the modelling framework of the UK NSM involves the distribution of muscle forces across upper limb muscles to ensure that the torques exerted by the muscles around the joint centres are in equilibrium with calculated intersegmental joint moments. On the basis of the indeterminacy, the number of solutions for muscle force contributions exceeds the number of equations coming from the biomechanical analysis of the shoulder. Therefore, an optimisation algorithm is used as a loadsharing solution, which aims to find a physiologically meaningful solution for muscle force contributions by minimising the sum of squared muscle stresses (Charlton & Johnson 2006). Additionally, the force contribution of each muscle is constrained by lower and upper bound, with the lower bound being set to 0 N/cm^2, while the upper bound is represented by the product of physiological cross-sectional area (PCSA) of each muscle with maximum muscle stress of 100 N/cm^2 (Charlton & Johnson 2006).

$$\sum_{i=1}^{i=87} \left(\frac{F_i}{PCSA_i}\right)^2 \qquad \text{Equation 2.3}$$

where i = muscle element, F_i = estimated muscle element force, $PCSA_i$ = physiological cross-sectional area for each muscle element.

In addition to these muscle force boundary constraints, the modelling framework of the UK NSM constrains the glenohumeral joint reaction force vector to be within an ellipse that is fitted to the glenoid articulating surface in order to model joint stability (Figure 2.17).

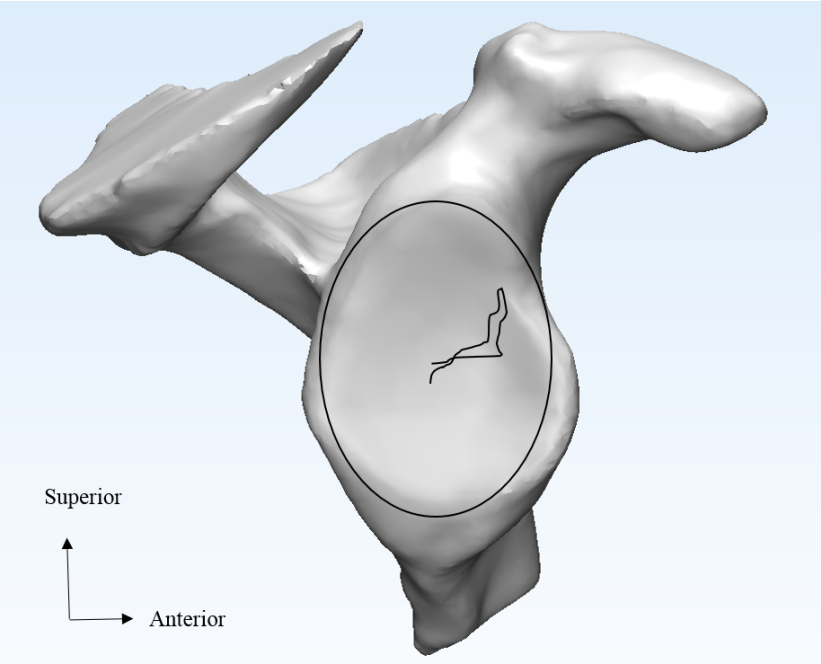

Figure 2.17: GH joint locus in the ellipse fitted to the glenoid plane. The black line within the ellipse represents the anterosuperior loading of the joint during an eating with a spoon activity.

2.3.1.3 Future Developments of the United Kingdom National Shoulder Model

The validation of the UK NSM has demonstrated small differences between predicted shoulder forces and instrumented implant measurements. These differences may be based on the absence of subject-specific modelling approaches, passive GH joint stabilisers, translations of the humeral head relative to the glenoid fossa and muscle dynamics for the physiological representation of shoulder muscles.

2.3.1.3.1 Customisation of Shoulder Modelling

The expression 'subject-specific' is commonly utilised to refer to MSK models that have modified the morphological structure of a generic MSK model in order to more closely match the anatomy of an experimental subject (Bolsterlee et al. 2013). Personalised MSK models have been created with varying levels of detail, ranging from scaling methods to complete 3D reconstructions from medical imaging.

Several mathematical scaling approaches have been proposed in the literature to transform muscle attachment sites from a generic MSK model to an experimental subject. These techniques involve linear scaling (Lew & Lewis 1977; Matias et al. 2009, 2011; Bolsterlee & Zadpoor 2014; Cleather & Bull 2010; Correa & Pandy 2011) and non-linear scaling based on bone geometries (Lewis et al. 1980; Sommer et al. 1982; Kaptein & van der Helm 2004; Murray et al. 2002; Pellikaan et al. 2014; Nolte et al. 2016; Nikooyan et al. 2011; Winby et al. 2008).

Kaptein and van der Helm (2004) demonstrated that non-linear scaling based on digitised bone geometries was capable of accurately transforming muscle attachment sites between different shoulder geometries, with an average error of less than 7 mm. Similarly, Bolsterlee and Zadpoor (2014) reported an average error of less than 10 mm for the linear scaling of scapular attachment sites between cadaveric geometries based on palpable landmarks. Although linear scaling methods overcome the need of medical images as required for non-homogenous scaling methods based on digitised bone geometries, both scaling methods introduce significant errors into MSK shoulder models due to the sensitivity of model predictions on muscle attachment sites (Bosmans et al. 2015; Carbone et al. 2012; Duda et al. 1996; Navacchia et al. 2016). Bolsterlee and Zadpoor (2014) demonstrated that a 10 mm variation in attachment site of a single muscle may change the force predictions of the perturbed muscle by 91%, while non-perturbed muscle force estimations may be altered by as much as 10%. This study also illustrated that the error associated with scaling of muscle attachment sites is dependent on the anatomical dataset that is used to establish the MSK shoulder model, suggesting that scaling from multiple anatomical datasets may help to improve model reliability.

Personalisation of MSK shoulder modelling through medical imaging has the potential to overcome these limitations of model scaling by providing accurate subject-specific information of the anatomy. The geometric properties of bones can be obtained accurately from Computed Tomography (CT), while muscle attachment sites and muscle volume can precisely be determined from Magnetic Resonance

Imaging (MRI). Despite recent advances in Diffusion Tensor Imaging (DTI), the estimation of muscle fibre length and pennation angles from medical imaging remains challenging (Galban et al. 2004). Therefore, several studies have performed sensitivity analyses to investigate the effect of these variables on musculoskeletal model parameters on model predictions (Pal et al. 2007; Lenaerts et al. 2008; Ackland et al. 2012; Valente et al. 2014; Ascani et al. 2015; Bolsterlee et al. 2015; Prinold et al. 2016). These studies demonstrate that model estimations are much less sensitive to muscle parameters such as optimum muscle length, tendon length and pennation angle, when compared to muscle attachment sites.

Subject-specific modelling techniques are becoming more widely developed and gaining greater credence (Scheys et al. 2008; Ascani et al. 2015; Bolsterlee et al. 2015; Prinold et al. 2016; Ding et al. 2016). Muscle moment arm predictions from a personalised musculoskeletal model constructed from magnetic resonance imaging (MRI) have been compared to those from a scaled-generic model of the lower limb (Delp et al. 1990), demonstrating significantly improved model estimations when compared to cadaveric measurements (Arnold et al. 2000; Scheys et al. 2008). The use of an EMG-driven neuromusculoskeletal lower limb model has shown improvements in joint contact force predictions through subject-specific digitisation of joint centres and muscle attachment sites from medical imaging (Gerus et al. 2013; Lenaerts et al. 2008). Similarly, a subject specific musculoskeletal modelling framework for the evaluation of shoulder muscle and joint function during activities of daily living demonstrated that generic models do not reproduce muscle loading obtained from subject-specific models (Wu et al. 2016).

In summary, subject-specific modelling techniques are becoming more widely developed and model predictions of personalised MSK models have been shown to be superior to those of a single generically scaled model. Therefore, there is a clear motivation and indication to implement subject-specific modelling in the UK NSM, to improve model reliability, which increases the relevance for clinical applications. This will be addressed in this thesis in Chapter 4.

2.3.1.3.2 Passive Joint Stability

Due to the lack of a comprehensive ligament model within a MSK shoulder model, there has been no musculoskeletal modelling study investigating the capsuloligamentous causes of shoulder instability. Despite the modelling of three glenohumeral ligaments within the UK NSM, further research is required to incorporate the entire capsuloligamentous complex into the UK NSM to accurately model shoulder function throughout the large range of motion. The first steps for this were made some years ago (Amadi et al. 2012), however further work is required to implement these research findings into the UK NSM.

Beside the absence of capsuloligamentous structures in the modelling framework of the UK NSM, this computational model does not simulate the contribution of the labrum to joint stability. The labral contribution to GH joint stability is commonly neglected in MSK shoulder models (Nikooyan et al.

2011; Garner and Pandy 2001), despite the labral contribution to joint stability of 10-20% as demonstrated during cadaveric experiments (Halder et al. 2001; Lippitt et al. 1993). Given that anteroinferior labral avulsion is the most commonly observed injury in patients with anterior shoulder instability, the inclusion of the labral contribution to joint stability into the modelling framework of the UK NSM is essential for an accurate evaluation of joint loading. This will be addressed in this thesis in Chapter 3.

2.3.1.3.3 Humeral Head Translation

The modelling of the GH joint with six DOF is essential to accurately simulate muscle stabilisation (Favre et al. 2009; Veeger and van der Helm 2007). As the UK NSM models the GH joint with 3 DOF, this computational modelling framework does not allow for translation of the humeral relative to the glenoid fossa.

The first departure from constraining the joint reaction force vector to the glenoid ellipse was made by Terrier et al. (2008), developing an algorithm to compute the GH joint reaction force with permitted humeral head translation. The results demonstrated good agreement with algebraic solutions for the 3D joint descriptions. Favre et al. (2012) was the first to develop a 3D model of the GH joint with six DOF, allowing for active muscle force driven control of humeral head translation. Despite this modelling advancement, the proposed framework was limited to the GH joint and also sensitive to muscle force inputs from computational shoulder models. Therefore, the GH joint is modelled with three DOF in existing MSK shoulder models (Nikooyan et al. 2011; van der Helm 1994; Hogfors et al. 1995; Dickerson et al. 2007; Garner and Pandy 2001; Delp et al. 2007).

The effect of modelling the GH joint with three DOF on MSK shoulder model predictions is assumed to be small during functional daily activities (Bolsterlee et al. 2013). This is based on fluoroscopic measurements demonstrating *in-vivo* humeral head translations of under 3 mm during arm elevation in healthy subjects (Bey et al. 2008; Dal Maso et al. 2015; Matsuki et al. 2012; Nishinaka et al. 2008). Therefore, in this thesis three DOF motion only is included at the GH joint.

2.3.2 Finite Element Modelling of the Shoulder

Finite element modelling provides a great opportunity to evaluate the internal loading of the shoulder through quantification of bone / soft tissue stresses and strains as well as articular dislocation forces. This is achieved through discretisation of complex anatomical structures into a finite number of elements with simple geometry (Huiskes & Hollister 1993). This enables very complex non-linear problems to be solved in a numerical fashion. The following sections will describe the clinical applications of FE modelling as well as the technical limitations of these computational tools.

2.3.2.1 Clinical Applications

FE modelling has been used over the past decades to solve a broad variety of problems in biomechanics that are associated with shoulder stability, rotator cuff tears, capsuloligamentous and labral defects as well as shoulder arthroplasty design.

2.3.2.1.1 FE Models of Shoulder Stability

The shoulder provides a large ROM facilitated by the low congruency of the articulating joint structures. This predisposes the shoulder to be the most commonly dislocated joint in the human body. Therefore, several studies using FE analysis have been conducted to model shoulder stability.

FE models of the shoulder have been used to investigate the stability of the joint. Terrier et al. (2007) developed a 3D FE model of the shoulder to investigate the effect of supraspinatus deficiency on joint stability. The study findings demonstrate a loss in joint stability for patients with supraspinatus deficiency due to increased humeral head migration. Walia et al. (2013) assessed joint stability for the presence of GH osseous defects, showing that joint stability may be reduced to a larger degree for combined lesions when compared to isolated osseous defects. The changes in joint contact stresses with alterations in the shape of the articulating geometries were investigated by Büchler et al. (2002; 2004). These studies demonstrate that the shape of the articulating geometries alters the GH joint contact area, which may affect joint stability.

2.3.2.1.2 FE Models of Rotator Cuff Tears

Rotator cuff disease is a commonly seen shoulder pathology. Rotator cuff tears may be associated with a loss in joint stability. The supraspinatus tendon is the most frequently ruptured tendon of the rotator cuff and the aetiology of a rotator cuff tear is multi-factorial including mechanical, biological and genetical factors (Chaudhury & Carr 2012; Dean & Carr 2016). However, the precise mechanism that initiates the rotator cuff disease remains unclear. Therefore, several studies using FE analysis have been conducted in order to investigate the underlying mechanical mechanism that may cause rotator cuff tears.

Luo et al. (1998) developed a 3D FE model of the glenohumeral joint to investigate the stress environment of the supraspinatus tendon during scapular plane abduction. The results demonstrate high stresses in the tendon during subacromial impingement that may initiate a tear. Seki et al. (2008) developed a 3D FE model to investigate the stress distribution throughout the supraspinatus tendon during arm elevation, demonstrating that maximum stresses occur at the anterior site. This correlates well with clinical findings that demonstrating a frequent occurrence of tendon ruptures at this site. The effect of morphological changes in the rotator cuff tendons following tendon division after tear was

investigated by Adams et al. (2007), with study findings demonstrating increased moment arms for the infraspinatus and teres minor.

2.3.2.1.3 FE Models of Capsuloligamentous and Labral Tears

The capsuloligamentous structures as well as the glenoid labrum are the passive stabilisers of the glenohumeral joint. These soft tissues are frequently injured following an anterior shoulder dislocation. Therefore, several studies have been conducted to understand the pathomechanics of the glenohumeral capsuloligamentous structures as well as the labrum.

A 3D FE model of the glenohumeral joint was developed to investigate the effect of humeral head translation on labral loading (Gatti et al. 2010; Hwang et al. 2014b). The study findings illustrate that superior humeral head migrations plays an important role in the development of superior labral pathology. The extension of this research by Hwang et al. (2015) demonstrated the effect of biceps tension on the torn superior glenoid labrum, suggesting that biceps tension influences the propagation of tears in the superior labrum. Debski et al. (2005) developed a 3D FE model of the glenohumeral joint to analyse the stress and strain distribution in the inferior glenohumeral ligament. The study findings demonstrate a strong dependency of soft tissue mechanical properties on model predictions. Similar results were reported by Ellis et al. (2006) and Moore et al. (2010). The deformation of the glenohumeral joint capsule was investigated by Drury et al. (2010), showing that the capsule undergoes the greatest deformation at the joint position of 60° abduction and at 20-40° of external rotation. These findings were of great clinical interest as this would propose the appropriate joint positions to examine anteroinferior capsule pathology.

2.3.2.2 Future Developments

FE modelling has been utilised over the past decades to solve a variety of problems in biomechanics. Despite the fact that the shoulder is the most commonly dislocated articulation in the human body, very little attention has been paid to FE modelling as an aid to surgical decision-making for patients with anterior shoulder instability (Zheng et al. 2017). In order to facilitate the translation of FE modelling of the shoulder into clinical practice, some challenges as listed below have to be overcome.

Most FE models of the shoulder presented in the literature consider only parts of the shoulder (Walia et al. 2013; Terrier et al. 2007; Luo et al. 1998; Sano et al. 2006), with major hard and soft tissues of the shoulder complex being neglected. Although this simplification significantly reduces the computational cost, it will lead to discrepancies between modelling results and *in-vivo* functioning of the joint. Therefore, the future development of FE models of the shoulder should consider modelling all major anatomical structures surrounding the shoulder as relevant for the clinical application of interest, with

the glenoid labrum being the most commonly neglected soft tissue in existing FE models (Debski et al. 2005; Inoue et al. 2013; Seki et al. 2008; Wakabayashi et al. 2003).

The existing FE models of the shoulder simulate joint functionality to aid clinical decision-making under non-physiological joint loading condition (Büchler et al. 2002a; Luo et al. 1998; Moore et al. 2010; Wakabayashi et al. 2003). As the stability of the shoulder is load dependent, with higher joint loads leading to a loss in stability (Lippitt et al. 1993; Halder et al. 2001), these simulations will limited in their ability to accurately predict *in-vivo* shoulder biomechanics. Therefore, future studies using FE analysis to aid clinical decision-making for patients with shoulder pathology should avoid the standard 50 N joint load, and instead should use physiological shoulder contact forces during functional daily activities as presented in the literature by Bergmann et al. (2007), Nikooyan et al. (2010), Anglin et al. (2000).

As introduced above, the majority of FE models of the shoulder simplify the representation of major hard and soft tissues in order to reduce the computational cost of the simulations. While the representation of soft tissues with viscoelastic properties is challenging due to limited data in the literature, the material properties of the labrum have been studied in detail (Smith et al. 2008; Smith et al. 2009). Therefore, the future development of FE models of the shoulder should consider the anatomically accurate representation of soft tissues as relevant for the clinical application of interest.

The validation of FE models of the shoulder is essential to facilitate the translation of research findings into clinical practice. While the majority of studies presented in the literature validate their FE models against cadaveric measurements (Inoue et al. 2013; Seki et al. 2008; Terrier et al. 2007), there is still a lack of validation for some studies (Büchler et al. 2002a; Debski et al. 2005; Luo et al. 1998; Yeh 2005). As the clinical translation of research findings is very important, the validation of future FE modelling studies should include a comprehensive comparison of model predictions with cadaveric measurements for a variety of different joint positions and loading conditions.

In this thesis, an FE model of the glenohumeral joint with an anatomically accurate representation of the labrum will be developed and validated in Chapter 3 in order to quantify the labral contribution to joint stability, thereby addressing the limitations mentioned above.

2.4 Concluding Remarks

The shoulder provides the largest range of motion of any joint in the human body, offering sufficient mobility and strength to facilitate high-speed athletic motions in addition to functional daily activities (Halder et al. 2000). The large degree of joint mobility is provided by the low congruency of the articulating structures, which makes the shoulder joint inherently unstable. As a consequence, the shoulder is the most commonly dislocated joint in the human body, with anterior shoulder instability

being frequently associated with bone and soft tissue injuries. The rates of recurrent anterior instability may be high, therefore precise knowledge of the influence of structural damage on joint stability is an important adjunct for surgical decision-making. Clinical practice is guided by experience, radiology, retrospective analyses and physical cadaver experiments with non-physiological loading. As the stability of the shoulder is load dependent, with higher joint forces leading to a proportional loss in stability, computational modelling offers great potential to simulate patterns of shoulder instability under *in-vivo* loading conditions. Although MSK shoulder models and FE models of the shoulder have been utilised over the past decades to aid clinical decision-making, these computational tools have several technical limitations that limit their success in clinical practice. If these can be addressed, then both computational modelling techniques offer a great opportunity to assess shoulder stability in patients with anterior shoulder instability with varying levels of structural damage as an aid surgical decision-making.

The following chapter takes this review to address the question of the loss in GH joint stability through labral pathology, with the avulsion of the anteroinferior labrum being the most commonly observed injury in patients with recurrent anterior shoulder instability as described in Section 2.2.2. This is achieved through development and validation of a computational finite element model of the glenohumeral joint with an anatomically accurate representation of the labrum that serves to quantify the labral contribution to joint stability under physiological joint loading.

Chapter 3

The contribution of the glenoid labrum to glenohumeral stability under physiological joint loading – a finite element analysis study.

The loss in joint stability with labral pathology has scarcely been investigated through experimental testing or computational modelling, despite the fact that the avulsion of the anteroinferior labrum is the most common injury in patients with anterior shoulder instability. Therefore, the aim of this chapter is to introduce the development and validation of subject-specific finite element models of the shoulder with an anatomically accurate representation of the labrum in order to quantify the labral contribution to joint stability under physiological joint loading. As the effect of glenohumeral concavity compression is commonly neglected in MSK shoulder models, the findings of this study may be incorporated into these computational models to improve model reliability. In addition, knowledge of the labral contribution to joint stability has the potential to aid surgical decision-making for patients with glenoid labral pathologies by allowing the assessment of joint stability in the presence of labral injuries.

This work was published in part as: 'The contribution of the glenoid labrum to glenohumeral stability under physiological joint loading using finite element analysis', with authors: Christian Klemt, Daniel Nolte, Grigorios Grigoriadis, Erica Di Federico, Peter Reilly, Anthony MJ Bull. Computer Methods in Biomechanics and Biomedical Engineering. 2017. 20(15):1613-1622.

3.1 Introduction

As described in Section 2.1, the glenohumeral joint is the most mobile articulation in the human body due to its relative lack of bony constraints. Despite its great mobility, the humeral head remains centred on the shallow glenoid fossa throughout the range of motion, exhibiting mainly ball-and-socket kinematics (Nishinaka et al. 2008). This centering of the humerus in the mid-range of motion is a function of glenohumeral stability that is achieved through compression of the humeral head into the glenoid labral concavity through rotator cuff muscle contraction (Lazarus et al. 1996) as well as through active control of translation through co-contraction of the rotator cuff muscles that act to resist shear forces (Itoi et al. 2000; Kawano et al. 2018). The degree of glenohumeral stability through concavity compression depends on the magnitude of the rotator cuff muscle force as well as the concavity of the glenoid labral socket, with a deeper glenoid labral concavity and higher compressive joint loads increasing the resistance to humeral head translation (Fukuda et al. 1988).

The labrum contributes to making up half the socket depth (Howell & Galinat 1989), yet its contribution to joint stability through concavity compression varies with joint position and applied compressive load. Lippitt et al. (1993) determined a labral contribution to joint stability of 20% with the glenohumeral joint tested in 45° of abduction and 35° of external rotation, while Halder et al. (2001) experimentally found a labral contribution of half that value, testing the joint in 0°, 30°, 60° and 90° of glenohumeral abduction. Both studies demonstrated a loss in glenohumeral stability ratio with increasing joint load.

These results are derived from physical cadaver experiments and suffer from limitations, including the low number of tested joint positions and the low loading conditions involving a maximum compressive load of 100 N, where directly-measured *in vivo* data has reported 151% body weight loading during activities of daily living (Bergmann et al. 2007). There is no current knowledge of the contribution of the glenoid labrum to joint stability through concavity compression under such high physiological loads.

Due to the lack of knowledge in the labral contribution to joint stability under *in-vivo* joint loading, the effect of glenohumeral concavity compression is commonly neglected in MSK shoulder models as presented in Section 2.3.1. There is only one MSK shoulder model simulating this effect, with the Waterloo Shoulder Model (Dickerson et al. 2007) utilising experimental measurements (Halder et al. 2001; Lippitt et al. 1993) to constrain the glenohumeral joint contact force vector. As MSK shoulder models have been used to answer a variety of clinical questions to improve surgical and rehabilitative treatment planning as well as joint arthroplasty design as described in Section 2.3.1, the precise knowledge of the labral contribution to joint stability and the integration of this into MSK modelling is important for an accurate evaluation of shoulder functionality.

Finite Element (FE) modelling represents a cost-efficient method to overcome the limitations of cadaveric studies and to simulate experimental testing under *in-vivo* loading conditions in order to study

glenohumeral concavity compression under physiological joint loading. FE models of the glenoid labrum have investigated labral pathomechanics (Gatti et al. 2010; Yeh 2005), the effect of rotator cuff tears (Hwang et al. 2014b) and the effect of biceps tendon loading (Hwang et al. 2014a; Hwang et al. 2015). No studies have represented the labrum with known regional variations in material properties (Smith et al. 2008, 2009) and, as such, these FE models cannot be employed to accurately assess glenohumeral stability through concavity compression.

Therefore, the aim of this study was to develop subject-specific FE models of the glenohumeral joint with an anatomically accurate representation of the glenoid labrum in order to quantify the contribution of the labrum to joint stability for any joint position under physiological loading conditions. This can then be incorporated into MSK shoulder models to simulate shoulder loading with consideration of glenohumeral concavity compression, and this can also be used as a tool to aid surgical decision-making for patients with glenoid labral pathologies, including those associated with anterior shoulder instabilities.

3.2 Materials and Methods

Two right shoulder geometries were obtained from high resolution physical slices of the male (spatial resolution: 0.33 mm x 0.33 mm x 1 mm) and female (spatial resolution: 0.33 mm x 0.33 mm x 0.33 mm) Visible Human datasets (U.S. National Library of Medicine). The glenoid fossa at the lateral angle of the scapula, the proximal humerus, the articulating cartilages as well as the glenoid labrum were manually segmented using Mimics (Mimics Research 17.0, Materialise, Leuven, Belgium). The segmented structures were converted to triangular surface meshes to form 3-dimensional models of the glenohumeral joint. In order to quantify the contribution of the labrum to joint stability two instances of each model were created: intact labrum and labral excision. These model instances did not include any musculotendinous structures or glenohumeral ligaments. Local coordinate systems as described in Wu et al. (2005) were assigned to the articulating structures in order to position and orient the humerus with respect to the glenoid fossa.

The surface meshes were imported into the FE analysis software (Marc Mentat 2015, MSC.Software, Palo Alto, USA). The articulating bones, the articular cartilages and the glenoid labrum were modelled as tetrahedral solid elements (Figure 3.1). The glenoid labrum was divided into eight sections in order to obtain an accurate representation of the material properties of the tissue as defined in Smith et al. (2008, 2009; Figure 3.2). Each labral section was assigned a coordinate frame to define the local fibre orientation as described in Gatti et al. (2010).

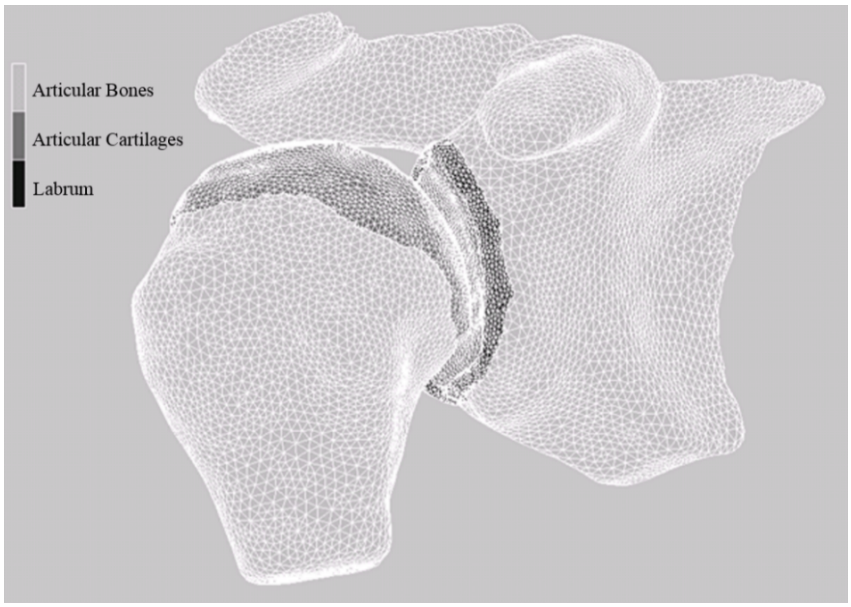

Figure 3.1: Three-dimensional finite element model of the visible human male glenohumeral joint.

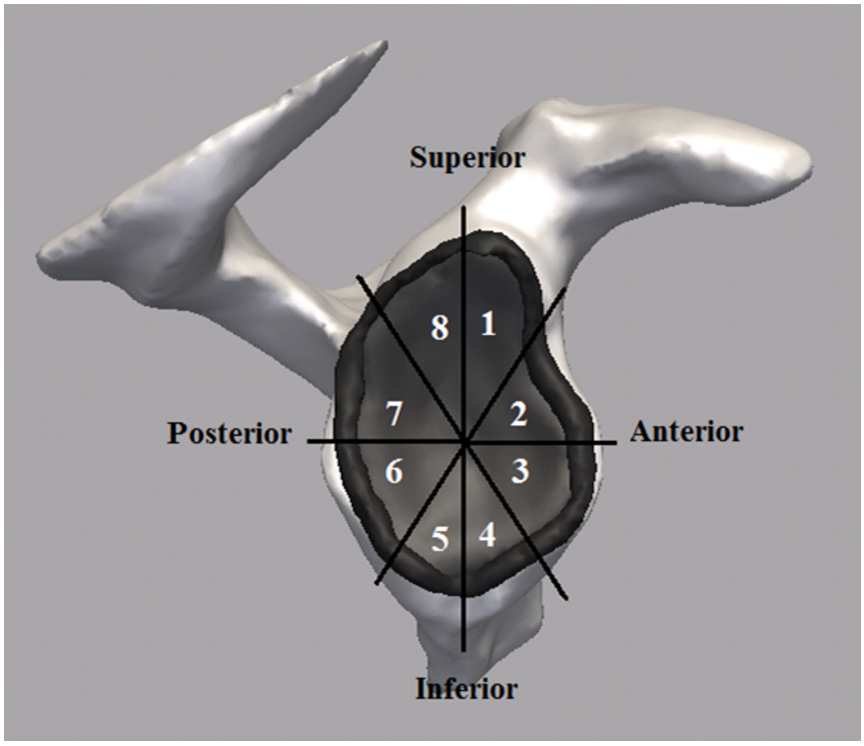

Figure 3.2: Anatomical representation of the glenoid labrum with eight sections that have been assigned local material properties.

The resulting FE mesh contained 16192 solid elements for the articulating bones, 17440 solid elements for the articular cartilages and 16592 solid elements for the glenoid labrum. A mesh convergence analysis for all components of the glenohumeral joint was performed by adjusting the mesh density to ensure the numerical stability of the results. Doubling the mesh density produced less than a one percent change in glenohumeral stability, but caused a 7-fold increase in solution time as shown in Table 3.1.

Table 3.1: Results of the mesh convergence analysis with the mean stability ratio being obtained for the glenohumeral joint with intact labrum, for a joint compressive load of 40 N in joint positions of 0°, 30°, 60°, 90° of glenohumeral abduction.

Number of Elements	Stability Ratio	Change in Stability Ratio [%]	Solution Time
6278	49.6	0	5
50224	45.8	7.6	13
401792	45.4	0.5	104

Baseline material properties for each structure of the glenohumeral joint were assigned based on the literature (Table 3.2). Due to relatively small deformations compared to other soft tissues, the articulating bones were modelled as rigid materials (Terrier et al. 2007). The articular cartilages were assigned linear elastic isotropic properties (Büchler et al. 2002a), while the labrum was modelled as a transversely isotropic material due to the modulus difference in the transverse plane and the circumferential direction (Smith et al. 2008, 2009). The labrum material coefficients for the hyperelastic model were obtained as shown in Equation 3.1, by applying the neo-Hookean constitutive equation (Quapp & Weiss 1998) to experimentally derived material properties for each labral section:

$$C_{1-8} = \frac{E_{1-8}}{4 \cdot (1 + \nu_{1-8})} \qquad \text{Equation 3.1}$$

where E = Young's modulus of each labral section, ν = Poisson's ratio of each labral section, $C_{1\text{-}8}$ = Hyperelastic labral coefficients of each labral section.

Table 3.2: Baseline material properties for the finite element model of the glenohumeral joint.

Anatomy	Material Type	Parameter	Value	Reference
Humerus	Rigid	-	-	Terrier et al. 2007
Humeral Cartilage	Isotropic Elastic	E υ	10 MPa 0.4	Büchler et al. 2002
Glenoid	Rigid	-	-	Terrier et al. 2007
Glenoid Cartilage	Isotropic Elastic	E υ	10 MPa 0.4	Büchler et al. 2002
Labrum	Transversely Isotropic Hyperelastic	C_1 C_2 C_3 C_4 C_5 C_6 C_7 C_8	3.4 5.4 7.0 5.9 5.2 4.8 5.7 4.3	Smith et al. 2008, 2009

For the validation study, the boundary conditions of the FE models were chosen to replicate the testing conditions employed by two cadaveric studies (Table 3.3). In the starting position, the humeral head was in contact with and centred on the glenoid socket. The interfaces between the articulating cartilages and between the humeral cartilage and the labrum were modelled using frictionless, surface-to-surface contact (Hwang et al. 2014a) due to the low coefficient of friction in synovial joints (Murakami et al. 1998). The interfaces between the articulating bones and the corresponding cartilages were modelled using tied contact. With the glenoid surface being fixed in all degrees of freedom during the simulation, the boundary conditions involved the application of a compressive force through the centre of the humeral head, perpendicular to the plane of the glenoid articulating surface, in order to simulate the joint loading. Under permanent joint compression, the humeral head was subsequently translated towards the circumference of the glenoid with a constant velocity of 2 mm/s. The humeral head was translated into eight anatomical directions: (1) superior, (2) anterosuperior, (3) anterior, (4) anteroinferior, (5) inferior, (6) posteroinferior, (7) posterior, and (8) posterosuperior. The stability of the glenohumeral joint was quantified through the stability ratio defined as the peak translational shear force divided by the applied compressive joint load, following the method of Fukuda et al. (1988).

Table 3.3: Finite element boundary conditions for the validation study.

Study	Joint Position	Joint Load	Reference
Study 1	0° of glenohumeral abduction 30° of glenohumeral abduction 60° of glenohumeral abduction 90° of glenohumeral abduction	20 N, 40 N, 60 N	Halder et al. 2001
Study 2	45° of glenohumeral abduction with 35° of external rotation	50 N, 100 N	Lippitt et al. 1993

The glenohumeral stability ratios obtained were compared to *in-vitro* measurements of joint stability at each direction of humeral head translation (averaged over compressive joint forces and glenohumeral abduction angles), at each compressive joint force (averaged over directions of humeral head translation and glenohumeral abduction angles) and at each glenohumeral abduction angle (averaged over directions of humeral head translation and compressive joint forces).

The labral contribution to glenohumeral stability ratio for each Visible Human dataset was determined by investigating the change in stability ratio (SR) between the models with intact labrum and those after labral excision as shown in Equation 3.2:

$$\text{Labrum contribution } (\%) = \frac{\text{SR labrum intact} - \text{SR labrum excised}}{\text{stability ratio labrum intact}} \qquad \text{Equation 3.2}$$

For the sensitivity analysis to investigate the influence of modelling parameters, FE models in 0° of glenohumeral abduction for all loading conditions and directions of humeral head translation were

made. The influence of the constitutive model and elastic moduli of both the glenoid labrum and articulating cartilage layers on the predictions of glenohumeral stability ratios was tested. The transversely isotropic hyperelastic constitutive model for the glenoid labrum was replaced with a transversely linear elastic isotropic model (Hwang et al. 2014a). Furthermore, the effect of labral fibre stiffness was tested over a range of ±1 published standard deviation (SD) using the hyperelastic model (Smith et al. 2008). The linear elastic isotropic constitutive model for the articular cartilages was replaced with a hyperelastic model. The effect of the articular cartilages material properties was tested by varying the Young's modulus over a range of ±1 published SD (Büchler et al. 2002b).

The stability ratios of the FE models at each direction of humeral head translation, compressive joint force and glenohumeral abduction angles were compared with a nonparametric Mann-Whitney test (Origin 2015, OriginLab Corporation, Northampton, USA) to assess differences in glenohumeral stability induced by changes in the loading regimen. Using the same statistical analysis, the influence of model parameters on the model output was determined.

The contribution of the labrum to joint stability ratio for any joint position under physiological loading conditions was quantified by developing mixed model regression equations which predict the stability ratios for the FE models with intact labrum and after labral excision. The regression equations estimate the joint stability ratio through concavity compression as a function of the direction of humeral head translation, glenohumeral abduction, glenohumeral rotation, glenohumeral flexion as well as the joint load. These equations were obtained by generating 200 stability ratios for each FE model and direction of humeral head translation. The generated stability ratios included maximum angles for glenohumeral abduction, glenohumeral rotation and glenohumeral flexion of 90°. The maximum joint load was set to 1000 N. These mixed model regression equations include data with equal weighting from both FE models in order to obtain an average representation of both joint shapes. The regression equations were obtained by determining the best fit between the stability ratio and each parameter of the equation using SPSS (Version 24, IBM Corporation, Armonk, USA). The fit with the highest R^2 value for each parameter was taken as input for the mixed model regression equations as described by Hurwitz et al. (2002). The coefficients for the mixed model regression equations were obtained by maximising the total R-squared value for each regression equation.

3.3 Results

The results of the validation study will be presented as comparison of model output against two different cadaveric studies as described in Table 3.3.

Comparison of model output against cadaver study 1

Both male and female FE models showed a decrease in glenohumeral stability ratios with increasing joint loads. This is in agreement with experimental data (Figure 3.3). With intact labrum and after labral excision, the stability ratios with 20 N joint load were significantly higher (p=0.039) than those with 60 N. The values of glenohumeral stability ratios derived by the FE models were all within ±1 standard deviation of the published experimental data.

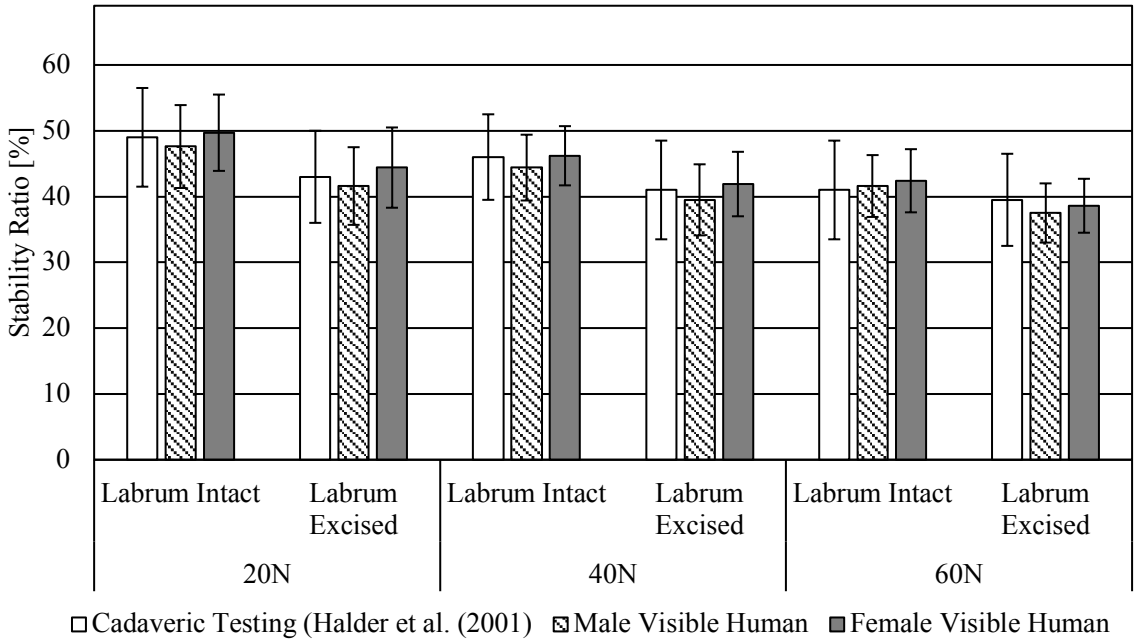

Figure 3.3: Mean stability ratios of the glenohumeral joint, with intact labrum and after labral excision, for joint compressive forces of 20, 40, and 60 N in joint positions with 0°, 30°, 60°, 90° of glenohumeral abduction.

The glenohumeral stability ratios for both male and female FE model demonstrated a decrease in joint stability with increasing abduction angle. This is in agreement with published experimental data (Figure 3.4). The stability of the glenohumeral joint was significantly higher (p=0.043) with intact labrum in the joint position with 0° of abduction, 0° of external rotation and 0° of flexion (male: 46.7% ± 4.8%; female: 47.9% ± 4.6%), than it was in 90° of glenohumeral abduction (male: 42.7% ± 3.9%; female: 43.6% ± 4.2%). After labral excision, the stability ratio in the joint position with 0° of abduction, 0° of external rotation and 0° of flexion was not significantly higher than that in 30°, 60° or 90°of abduction. The values of glenohumeral stability ratios from the FE models were all in agreement with corresponding experimental data.

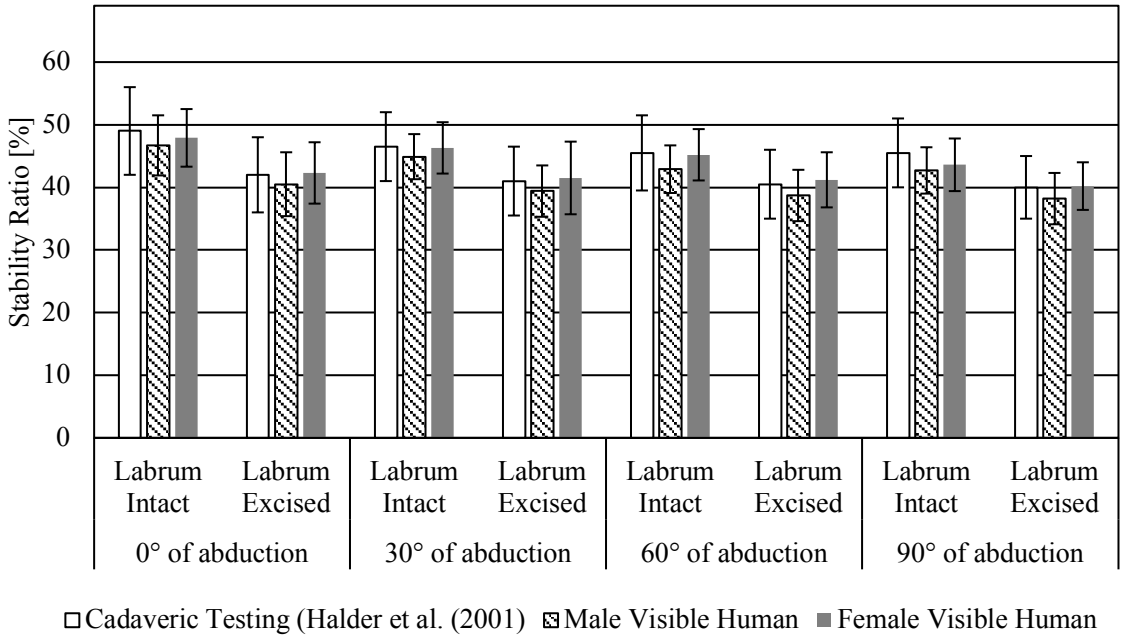

Figure 3.4: Mean stability ratios of the glenohumeral joint, with intact labrum and after labral excision, for joint positions in 0°, 30°, 60°, 90° of glenohumeral abduction with joint compressive forces of 20, 40, and 60 N.

The glenohumeral stability ratios for the male and female FE models varied considerably across the tested directions of humeral head translation; this is in agreement with published *in-vitro* measurements (Figure 3.5). The predictions for glenohumeral stability ratios were within ±1 SD of experimentally measured values in most cases. The FE model of the male subject with intact labrum estimated joint stability ratios that were 0.9% and 0.4% outside the confidence interval in the anterosuperior and posteroinferior direction respectively when compared to *in-vitro* measurements.

The contribution of the labrum to glenohumeral stability through concavity compression was quantified for the male and female FE model as 10.9% ± 3.0% and 9.4% ± 3.2%, respectively. These results are in agreement with values from the literature that describe an average decrease in joint stability after labral resection of 9.6% ± 1.7% (Halder et al. 2001). The loss in glenohumeral stability ratio after labral excision varied considerably across the tested directions with larger decreases in the anteroinferior (male 13.6% ± 4.2%; female 16.1 ± 4.6%) and inferior directions (male 13.5% ± 4.2%; female 12.1 ± 4.6%). In agreement with cadaveric testing, the stability ratio decreased the least in the superior (male 3.2% ± 2.3%; female 2.1% ± 1.9%) and posterosuperior direction (male 2.9% ± 2.2%; female 2.8% ± 2.4%).

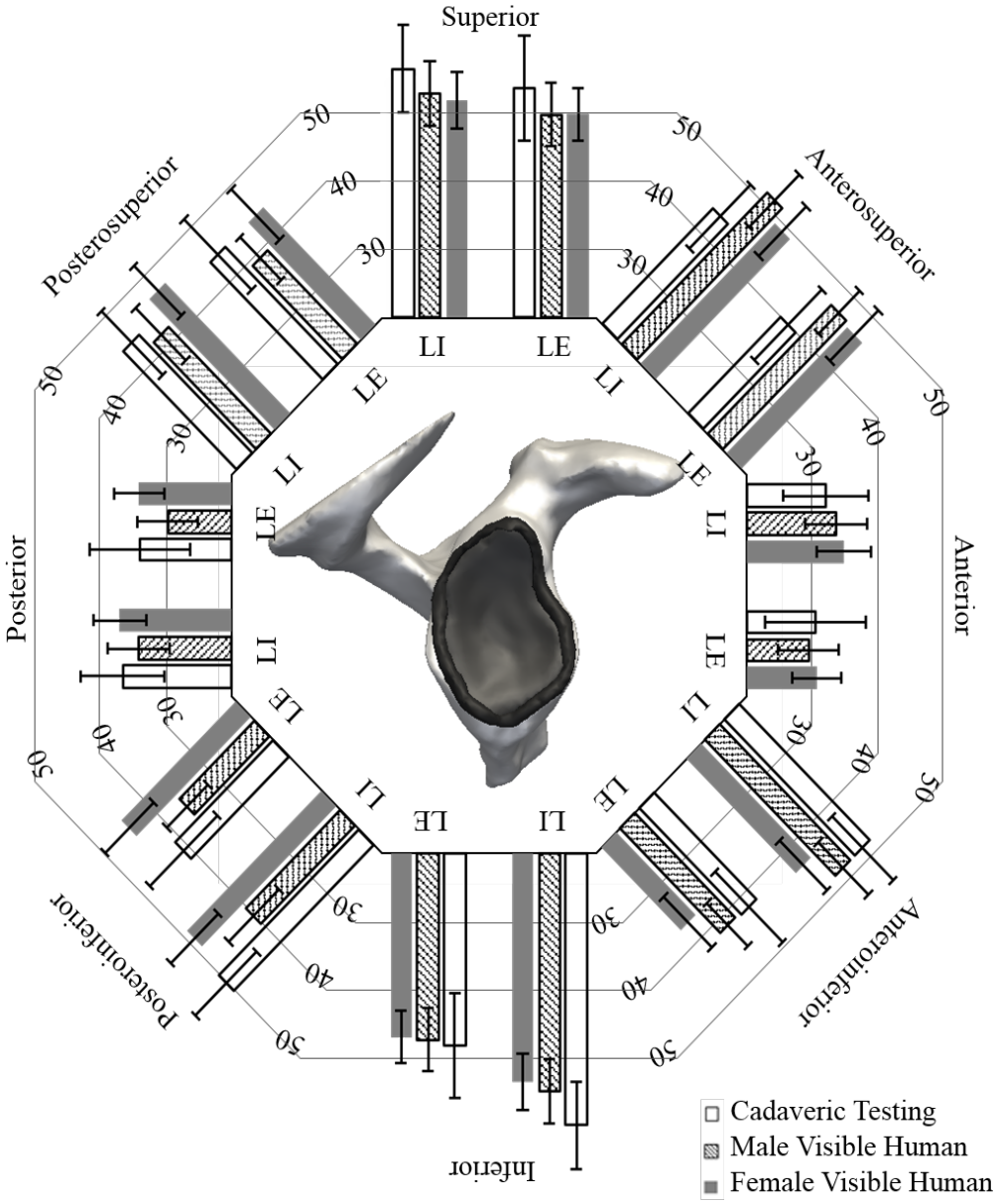

Figure 3.5: Mean stability ratios of the glenohumeral joint, with intact labrum (LI) and after labral excision (LE), for the eight anatomical directions of humeral head translation with joint compressive forces of 20, 40, and 60 N.

Comparison of model output against cadaver study 2

The glenohumeral stability ratios across the tested directions of humeral head translation with the joint in 45° of abduction and 35° of external rotation were within ±1 SD of published experimentally measured values in most cases (Table 3.4; Table 3.5). Minimal differences in stability ratios were observed for the FE model of the female subject with intact labrum when loaded under 50 N in the inferior and anteroinferior direction compared with experimental data with values being 2.5% and 1.3%, respectively, outside the confidence interval.

Table 3.4: Mean stability ratios of the glenohumeral joint, with intact labrum and after labral excision, for the joint in 45° of abduction and 35° of external rotation.

Anatomical Direction	50 N					
	Labrum Intact			Labrum Excised		
	Cadaver	Male	Female	Cadaver	Male	Female
Superior	59±13	55.1	53.7	47±8	49.8	47.7
Anterosuperior	38±11	47.8	48.0	30±10	38.9	39.8
Anterior	35±11	36.2	37.7	28±6	30.3	31.2
Anteroinferior	46±6	42.7	38.7	39±8	40.2	34.9
Inferior	64±8	57.1	53.5	41±13	42.8	41.4
Posteroinferior	50±19	38.6	52.1	30±10	27.5	39.9
Posterior	33±12	34.5	37.7	25±11	25.8	31.4
Posterosuperior	40±16	40.4	42.4	32±14	31.3	33.2

Table 3.5: Mean stability ratios of the glenohumeral joint, with intact labrum and after labral excision, for the joint in 45° of abduction and 35° of external rotation.

Anatomical Direction	100 N					
	Labrum Intact			Labrum Excised		
	Cadaver	Male	Female	Cadaver	Male	Female
Superior	51±9	49.2	48.4	45±7	44.8	44.3
Anterosuperior	not measured			not measured		
Anterior	29±5	32.1	33.5	26±5	26.7	27.9
Anteroinferior	not measured			not measured		
Inferior	56±12	51	45.3	40±13	37.8	34.1
Posteroinferior	not measured			not measured		
Posterior	30±12	30.2	33.7	23±9	21.9	25.2
Posterosuperior	not measured			not measured		

The contribution of the labrum to glenohumeral stability ratio was quantified as 19.3% ± 7.8% and 18.1% ± 5.9% for the male and female FE models, respectively. These results show high correspondence with published experimental values that describe an average decrease in joint stability after labral resection of 20.0% ± 8.5% (Lippitt et al. 1993). In agreement with cadaveric testing, the highest labral contributions to joint stability were found in the posteroinferior (male 28.7%; female 23.4%) and inferior directions (male 25.1%; female 20.7%).

The sensitivity analysis demonstrated that changing the constitutive model of the labrum from hyperelastic to linear elastic did not significantly alter the model output (p=0.45) with glenohumeral stability ratios increasing from 46.6% ± 6.8% to 49.3% ± 7.9% and from 47.9% ± 6.6% to 50.7% ± 7.4% for male and female subjects, respectively. Similarly, the change of constitutive model of the articular cartilages did not significantly change the model output (p=0.36) with glenohumeral stability ratios increasing from 46.6% ± 6.8% to 48.2% ± 8.3% and from 47.9% ± 6.6% to 49.6% ± 7.8% for the male and female FE model, respectively. Varying the labral fibre stiffness of the labrum over ±1

published SD using the hyperelastic model resulted in a change of less than ± 1.9% for the FE models. Likewise, varying the Young's modulus of the articular cartilages over a range of ±1 SD altered the model output by less than ± 1.5%. The changes in model output induced by varying the material properties over a range of ±1 SD were not significant (p=0.32).

The contribution of the labrum to the glenohumeral stability ratio is described by the mixed model regression equation as shown in Equation 3.3, which quantifies the stability ratios (SR) for any joint position under physiological loading conditions with intact labrum and after labral excision. The normalised coefficients for each parameter (Abd – glenohumeral abduction angle, Rot – glenohumeral rotation angle, Flex – glenohumeral flexion angle, Load – glenohumeral joint force) of the equation are shown in Tables 3.6 and 3.7.

$$SR = A_0 + A_1 \cdot Abd + A_2 \cdot Rot + A_3 \cdot Rot^2 + A_4 \cdot Flex + A_5 \cdot \log(Load) \qquad \text{Equation 3.3}$$

Table 3.6: Coefficients for each parameter of the regression equation to predict the stability ratio with intact labrum in each direction of humeral head translation.

	A_0	A_1	A_2	A_3	A_4	A_5	R^2
Superior	7.07E+01	-5.76E-02	8.93E-04	1.80E-04	3.67E-03	-8.66E+00	0.84
Anterosuperior	6.16E+01	-1.96E-02	-5.78E-05	-9.08E-04	-1.63E-02	-6.99E+00	0.92
Anterior	4.54E+01	-1.69E-02	7.79E-03	2.67E-03	1.52E-02	-7.12E+00	0.86
Anteroinferior	5.79E+01	-3.04E-02	-1.39E-04	-4.11E-03	-1.56E-02	-6.56E+00	0.88
Inferior	6.99E+01	-5.41E-02	2.32E-04	3.42E-04	1.06E-02	-8.64E+00	0.92
Posteroinferior	5.64E+01	-3.09E-02	4.63E-04	1.63E-03	7.79E-03	-6.52E+00	0.81
Posterior	4.51E+01	-3.11E-02	-9.26E-05	5.93E-04	8.52E-03	-5.80E+00	0.90
Posterosuperior	5.41E+01	-2.79E-02	-2.78E-04	-1.13E-03	-1.39E-02	-6.03E+00	0.91

Table 3.7: Coefficients for each parameter of the regression equation to predict the stability ratio with intact labrum in each direction of humeral head translation.

	A_0	A_1	A_2	A_3	A_4	A_5	R^2
Superior	6.46E+01	-4.81E-02	-7.16E-03	-3.14E-04	-5.94E-03	-8.49E+00	0.97
Anterosuperior	5.78E+01	-3.15E-02	-1.37E-03	-5.69E-03	-2.19E-02	-6.93E+00	0.96
Anterior	4.17E+01	-1.86E-02	5.17E-04	-1.29E-04	-1.51E-02	-6.32E+00	0.93
Anteroinferior	5.28E+01	-3.30E-02	-1.20E-06	-1.62E-03	-1.08E-02	-6.71E+00	0.87
Inferior	6.04E+01	-2.92E-02	-1.79E-04	-2.83E-03	-3.73E-03	-8.23E+00	0.93
Posteroinferior	5.29E+01	-2.56E-02	-4.63E-05	-3.88E-03	-1.60E-02	-7.62E+00	0.80
Posterior	4.37E+01	-2.67E-02	-1.40E-03	-2.12E-03	-3.36E-02	-7.41E+00	0.83
Posterosuperior	5.21E+01	-3.42E-02	-4.16E-03	-3.24E-03	-2.12E-02	-6.64E+00	0.85

The regression equations predict a loss in labral contribution to glenohumeral stability ratio with increasing joint forces. The loss in joint stability ratios ranges between 5-10% when tested under 1000 N joint load compared to the minimum of 20 N joint force as shown in Figure 3.6.

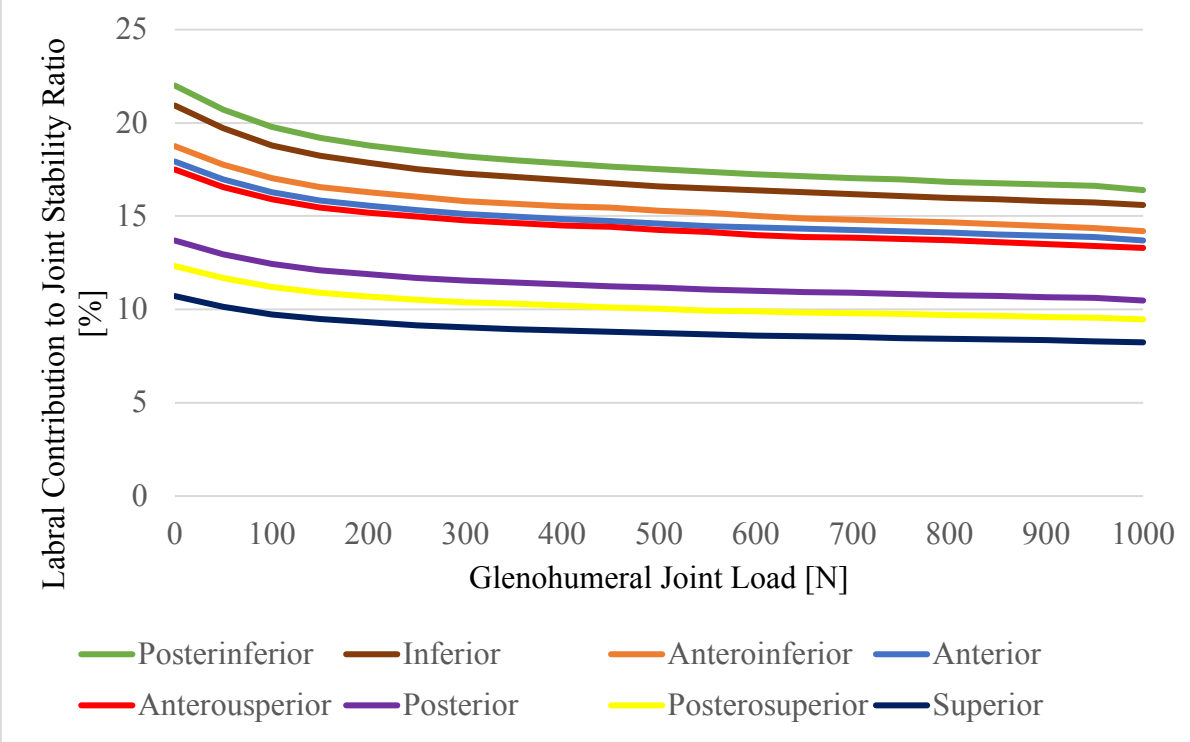

Figure 3.6: Labral contribution to glenohumeral stability for joint loads between 20 N and 1000 N for all eight anatomical directions of humeral head translation.

3.4 Discussion

In this study, two FE models of the glenohumeral joint with an anatomically accurate representation of the glenoid labrum were developed and validated against *in-vitro* measurements of glenohumeral stability as reported by two different cadaveric studies (Halder et al. 2001; Lippitt et al. 1993). The ratios of glenohumeral stability quantified by the FE models were found to correlate well to those experimentally measured with model predictions being within ±1 SD of the experimentally measured values in most cases.

The differences in glenohumeral stability ratios between the FE models and *in-vitro* measurements may be explained by anatomical variations of the labrum. Clinical investigations suggested that the morphology of the labrum differs considerably across individuals with additional variations seen in the anterosuperior labrum including a sub-labral foramen, a sub-labral recess and a Buford complex (Davidson & Rivenburgh 2004). These anterosuperior labral variations are associated with the detachment of the labrum from the underlying glenoid bone. Although labral detachments are more common in young people compared to the elderly (Neviaser et al. 1988), these variations in labral

appearance may have contributed to the small differences observed between the FE models and cadaveric measurements as the FE models assumed full contact between glenoid and labrum.

The small discrepancies in glenohumeral stability ratios between the FE models and experimental data may also be attributed to the segmentation of the labrum. The appearance of the labrum on high resolution physical slices is similar to the surrounding soft tissues, necessitating advice from medical experts to delineate the boundary of the labrum, and is thus potentially prone to error. Although the labral dimensions of the FE models are within the range of reported values in the literature (Cooper et al. 1992), there is still a potential impact of error in the manual segmentation. The lack of tissue contrast could be overcome with MR arthrography (Garwood et al. 2017) that showed better contours between the labrum and articular cartilages when performed under axial traction. Besides the appearance of the labrum on high resolution physical slices, the difference in sectioning between male (1 mm intervals) and female (0.33 mm intervals) Visible Human datasets may have contributed to the differences between model output and cadaveric measurements with larger sectioning intervals leading to a less accurate representation of the labrum. Therefore, the representation of the labrum in the FE model of the female dataset is anatomically more accurate than the FE model of the male dataset.

The differences in glenohumeral stability ratios between FE model and *in-vitro* measurements may potentially be based on the limited repeatability of experimental testing when compared to computational models. The alignment of the humerus relative to the glenoid during cadaveric testing was based on visual perceptions rather than local coordinate frames that were utilised for the FE models. Similarly, the friction coefficient may have increased in the course of *in-vitro* experiments due to cadaveric tissues drying out (Lippitt et al. 1993), while the FE models assumed constant frictionless conditions.

The subject-specific comparison of model output and experimental data was not possible as the *in-vitro* data were reported as average values of 10 cadaveric specimens. Therefore, it is difficult to allocate differences in model output and experimental testing to variations in labral dimensions, segmentation inaccuracies or the limited repeatability of cadaveric testing. Despite the lack of a subject-specific comparison of model and experimental output, the proposed FE models accurately estimate glenohumeral stability ratios that correspond to stability ratios reported in the literature.

The robustness of the FE model was verified with a sensitivity analysis involving the material properties of the labrum as well as the articular cartilages. The stability ratios of the glenohumeral joint were not significantly altered by changes in the constitutive model for either labrum or the articular cartilages. Similarly, the ratios of glenohumeral joint stability were not significantly altered by changes of one standard deviation in the moduli for either soft tissue. This demonstrates that the uncertainty associated with the selection of the material properties for the FE models due to variety of values reported in the literature did not significantly alter the model output.

The validation of the FE models against *in-vitro* measurements of glenohumeral stability ratios enabled regression equations to be developed to quantify the contribution of the labrum to joint stability for any joint position under *in-vivo* loading conditions. Although the validation of the FE models only involved a maximum joint load of 100 N, the utilisation of these models to physiological loading conditions is representative as the bones will not significantly deform under the chosen *in-vivo* loading conditions. Furthermore, the articular cartilages as well as the labrum are loaded in the linear region with the loading rates remaining the same in the FE models when testing glenohumeral stability under physiological loads (Woo et al. 1976). These regression equations can now be used to improve the reliability of MSK shoulder model predictions, which will be demonstrated in Chapter 5.

This study has several limitations. Firstly, the FE models do not include any musculotendinous structures. The labrum is a passive glenohumeral stabiliser that makes up half the depth of the glenoid-labral socket, thereby constraining translations of the humeral head. The superior labrum serves as attachment for the long head of biceps tendon that also has the ability to constrain superior humeral head translation. Due to the absence of any musculotendinous structures in the FE models with labral excision, the presented stability ratios do not consider any effect on joint stability by the long head of biceps tendon. Secondly, segmentation of the labrum could be improved by using MR arthrography with axial traction that has been developed to better delineate the contours between the labrum and articular cartilages (Garwood et al. 2017). Finally, we acknowledge that the regression equations are only based on the geometries of the Male and Female Visible human dataset and that the coefficients for these equations would be more robust if more datasets would have been used for this. However, this would require high resolution physical slices or MRI scans with a slice thickness of a third of a millimetre in order to accurately delineate the structures of the glenohumeral joint. Non-fat-supressed high-resolution T1-weighted MR images of the glenohumeral joint have been used in a few musculoskeletal shoulder FE models (Engelhardt et al. 2016, 2017), however, these were not available for this study. Therefore, the FE models are based on only two geometries of the glenohumeral joint. Despite these limitations, the mixed model regression equations represent the first approach to assess glenohumeral concavity compression under physiological loads. As this effect is commonly neglected in MSK shoulder models, the findings of this study may be incorporated into these computational models to improve model reliability through simulation of shoulder loading with consideration of glenohumeral concavity compression. In addition, knowledge of the labral contribution to joint stability has the potential to aid surgical decision-making for patients with glenoid labral pathologies by allowing the assessment of joint stability in the presence of labral injuries. In fact, simulating an avulsion of the anteroinferior labrum, the most commonly observed injury in patients with anterior shoulder dislocation, through excision of the anteroinferior labrum in the mixed model regression equations demonstrates a loss of 15% in joint stability ratio under physiological joint loading.

3.5 Conclusion

This chapter presented the development and validation of subject-specific FE models of the shoulder with an anatomically accurate representation of the labrum in order to quantify the labral contribution to joint stability under physiological joint loading. As the effect of glenohumeral concavity compression is commonly neglected in MSK shoulder models, the findings of this study may be incorporated into these computational models to improve model reliability. In addition, knowledge of the labral contribution to joint stability has the potential to aid surgical decision-making for patients with glenoid labral pathologies by allowing the assessment of joint stability in the presence of labral injuries, including those associated with anterior shoulder instability.

This chapter has addressed a limitation of the UK NSM as described in Section 2.3.2 through the development of regression equations to model glenohumeral concavity compression under physiological joint loading. Chapter 4 will utilise this knowledge and further address technical limitations of the UK NSM by presenting the development and validation of 10 subject-specific shoulder models from MRI in order to improve model reliability. This is of particular importance for the clinical applications of MSK shoulder modelling that will be presented in Chapters 5, 6, and 7.

Chapter 4

Anthropometric scaling of anatomical datasets for subject-specific musculoskeletal modelling of the shoulder.

The predictions of subject-specific MSK models have been demonstrated to be superior to those of a single generically scaled model. As the number of complete anatomical datasets for shoulder modelling in the literature is small, this chapter aims to develop and validate 10 MRI-based shoulder models, demonstrate the dependency of modelling results on anatomical geometry, identify the best combination of anthropometric parameters that yields most accurate model estimations of glenohumeral joint contact force and muscle forces through scaling of personalised shoulder models, and quantify the improvement in model reliability through anthropometric scaling of anatomical datasets when compared to a single scaled-generic model. This latter aspect is of particular importance for the translation of MSK shoulder modelling into clinical practice in order to address key clinical questions, including those associated with anterior shoulder instability.

This work was submitted in part for peer review publication, entitled 'Anthropometric scaling of anatomical datasets for subject-specific musculoskeletal modelling of the shoulder', with authors: Christian Klemt, Daniel Nolte, Ziyun Ding, Lance Rane, Rebecca A Quest, Mary E Finnegan, Miny Walker, Peter Reilly and Anthony MJ Bull.

4.1 Introduction

Validated computational models of the musculoskeletal (MSK) system can be used to understand normal and pathological human movement by predicting articular and tissue loading, parameters that cannot currently be measured directly. The precise knowledge of musculoskeletal loading is essential for clinical applications in order to improve surgical and rehabilitative treatment planning, assistive device design and analysis of joint arthroplasty design.

Although MSK models have been used for a variety of clinical applications over the past three decades as described in Section 2.3.1, the dependency of modelling results on model input, in particular the anatomical geometry (Bolsterlee & Zadpoor 2014; Carbone et al. 2012; Bosmans et al. 2015), has hampered the wider use of these computational models in clinical practice. Scaled-generic models, derived from the dissection of one or more cadaveric specimens, are widely used to represent a subject's anatomical geometry (Carbone et al. 2015; Charlton & Johnson 2006; Delp et al. 2007; Garner and Pandy 2001; Hogfors et al. 1995; Nikooyan et al. 2011). These models accommodate geometric variation across subjects through linear scaling, based on three-dimensional positions of anatomical landmarks (Kaptein & van der Helm 2004; Matias et al. 2009, 2011; Correa & Pandy 2011), commonly obtained from a static motion capture trial. As scaled-generic models do not account for individual variations in anthropometry, they lead to errors in muscle path estimations that will result in substantial inaccuracies in calculated muscle and joint forces (Kaptein & van der Helm 2004; Bolsterlee & Zadpoor 2014; Scheys et al. 2008a, 2008b).

Driven by the need for more accurate model predictions in clinical settings and facilitated by advances in medical imaging technology, subject-specific modelling techniques are becoming more widely developed. These range from simple scaling (Bolsterlee et al. 2015; Modenese et al. 2015; Praagman et al. 2010; Zhang & Besier 2017) to three-dimensional reconstructions of *in-vivo* anatomy from medical imaging (Gerus et al. 2013; Kia et al. 2014; Krekel et al. 2009; Prinold et al. 2016). Optimisation algorithms for the estimation of subject-specific musculotendon parameters have been proposed in the literature (Winby et al. 2008; Modenese et al. 2015), showing good agreement with cadaveric measurements (Ward et al. 2009). Muscle moment arm predictions from a personalised musculoskeletal model constructed from magnetic resonance imaging (MRI) have been compared to those from a scaled-generic model of the lower limb (Delp et al. 1990), demonstrating significantly improved model estimations when compared to cadaveric measurements (Scheys et al. 2008a, 2008b). The use of an EMG-driven neuromusculoskeletal lower limb model has shown improvements in joint contact force predictions through subject-specific digitisation of joint centres and muscle attachment sites from medical imaging (Gerus et al. 2013; Jung et al. 2016; Manal & Buchanan 2013). Similarly, a subject-specific musculoskeletal modelling framework for the evaluation of shoulder muscle and joint function during activities of daily living by Wu et al. (2016) demonstrated that generic models do not reproduce

muscle loading obtained from subject-specific models. The uncertainty of musculoskeletal model predictions by scaled-generic models may be as high as 20% when compared to highly-detailed, subject-specific musculoskeletal models (Lerner et al. 2015; Marra et al. 2015), with modelling errors being dependent on anthropometric differences between scaled-generic and subject-specific models (Bolsterlee et *al.* 2014).

Customisation of musculoskeletal modelling through medical imaging significantly improves model reliability, when compared to an individual linearly scaled-generic model (Scheys et al. 2008a, 2008b; Gerus et al. 2013). However, the development of subject-specific computational models is time, labour and technology intensive. In order to overcome the drawbacks of generating a personalised dataset for each subject, linear scaling of musculoskeletal shoulder models with high anthropometric similarity from a model database, or *atlas*, has the potential to yield modelling results that are close to predictions of subject-specific models and more accurate than a single, scaled-generic model. As the number of complete anatomical datasets for shoulder modelling in the literature is estimated to be 4 (from: Charlton and Johnson 2006; Hogfors et al. 1995; Holzbaur et al. 2005; Nikooyan et al. 2011) – and these are not all openly available, this study aims to develop and validate 10 MRI-based shoulder models, demonstrate the dependency of modelling results on anatomical geometry, identify the best combinations of anthropometric parameters that yield best model estimations in glenohumeral joint contact force and muscle forces through scaling of personalised musculoskeletal shoulder models, and quantify the improvement in model reliability through anthropometric scaling of anatomical datasets when compared to a single, scaled-generic model. The MRI-based musculoskeletal models as well as anatomical datasets developed in this study are available at www.msksoftware.org.uk.

4.2 Materials and Methods

Experimental Data

Ten healthy volunteers (five male, five female) with a wide variation in height participated in this study (Table 4.1). Subjects were classified as tall (height > 90^{th} percentile), medium (height 50^{th} – 90^{th} percentile) and short (height < 50^{th} percentile) according to anthropometric estimates for British adults (Pheasant and Haslegrave 2006). The study was granted ethical approval by the Health Research Authority (HRA) following attendance at the London Queen Square Research Ethics Committee and confirmation from Imperial College Healthcare NHS Trust to host this study.

Table 4.1: Anthropometric data of study participants. The subjects were classified as tall (height > 90th percentile), medium (height 50th – 90th percentile) and short (height < 50th percentile).

Subject	Sex	Age (years)	Height (m)	Height Percentiles	Height Classification	Body Mass (kg)
1	Female	30	1.57	46th	Short	59.7
2	Female	25	1.62	60th	Medium	57.5
3	Female	26	1.64	67th	Medium	59.4
4	Female	26	1.73	89th	Medium	64.4
5	Female	36	1.79	95th	Tall	76.4
6	Male	31	1.63	27th	Short	61.2
7	Male	28	1.72	48th	Short	63.7
8	Male	29	1.77	64th	Medium	70.2
9	Male	26	1.88	87th	Medium	98.1
10	Male	37	1.93	99th	Tall	80.6

All subjects were instructed to perform sixteen functional activities of daily living with three sets per activity (Table 4.2). Kinematic data collection was performed using a 10-camera optical motion tracking system (Vicon Motion Tracking System, Oxford, UK), sampled at 100 Hz. The hand forces for the sit to stand activity and the opening jam jar task were measured with a tension/compression load cell (Omega, model LMC703) and a torque load cell (Vishay, model 1048-0051-G508R) respectively. The load cell data were sampled at 1000 Hz and then synchronised with the motion data.

Table 4.9: Functional activities of daily living.

Activity	External Loading
Eat with spoon	none
Drink from mug	none
Reach back of head	none
Brush left side of head	none
Perineal care	none
Clean back	none
Reach opposite axilla	none
Reach across the body	none
Abduction	none
Flexion	none
Pick and place object	Constant 3 kg
Lift block to shoulder height	Constant 3 kg
Lift block to head height	Constant 3 kg
Lift shopping bag from floor	Constant 3 kg
Open jam jar	Measured - Load Cell
Sit to stand	Measured - Load Cell

The marker set comprised anatomical landmarks of the upper limb including markers on the second/fifth metacarpal (MCP2/MCP5), radial/ulna styloid (RS/US), medial/lateral epicondyles (ME/LE), right/left Acromioclavicular joint (RAC/LAC), right/left Sternoclavicular joint (RSC/LSC), Xiphoid Process

(PX), Manubrium (MA), Jugular Notch (IJ) and 7th cervical vertebra (C7) as well as clusters of three markers on the forearm (FA), upper arm (UA) and hand (H) (Figure 4.1; Shaheen et al. 2011). A scapula tracker (ST) was placed along the scapula spine to measure scapula kinematics (Prinold et al. 2011).

Figure 4.1: Positions of reflective markers and EMG electrodes. Only the right body half was tracked.

Surface electromyography (EMG; Myon 320, Myon AG, Switzerland) was recorded at 1000Hz from five muscles during the activities as well as for the maximum voluntary contraction tests: deltoid (DELT), pectoralis (PEC), trapezius (TRAP), biceps (BIC) and triceps (TRI). The electrodes were placed according to SENIAM recommendations (Hermens et al. 2000), with an orientation parallel to the muscle fibres, on the DELT (electrodes were placed on the muscle belly halfway along the line between the acromion and lateral epicondyle), PEC (electrodes were placed on the muscle belly halfway along the line between anterior sternum surface and the bicipital humeral groove), TRAP (electrodes were placed on the muscle belly halfway along the line between acromion and 7th vertebra), BIC (electrodes were placed on the muscle belly halfway along the line between medial acromion and cubit fossa) and TRI (electrodes were placed on the muscle belly halfway along the line between posterior crista of the acromion and the olecranon). Maximum voluntary contraction tests were performed according to recommendations in the literature (Krol et al. 2007; De Groot et al. 2004; Meskers et al. 2004; Boettcher et al. 2008; Ginn et al. 2011) as follows: DELT (shoulder abducted at 45° and elbow fully extended as shoulder is abducted against maximum resistance), PEC (palm press – shoulder flexed at 90° bilaterally with hands together and elbows flexed at 20° as arms are maximally horizontally abducted), TRAP (scapula lateral rotation accompanied by shoulder abduction at 90° abduction against maximum resistance), BIC (biceps curl – shoulder abducted less than 20° and elbow flexed at 90° as

forearm is flexed against maximum resistance) and TRI (shoulder abducted less than 20° and elbow flexed at 90° as forearm is extended against maximum resistance).

Following completion of the maximum voluntary contraction tests, calibration trials were performed prior to motion data collection. This involved the participants to be stood in front of a chair in the anatomical position, with fully extended elbows and forward facing palms, in order to take a static recording of the upper limb for cluster calibration in the local segment coordinate frames. Once seated, calibrations of scapula movement and position were performed using the scapula tracker as well as locator (Prinold et al. 2011). The scapula locator was utilised to identify the positions of scapula landmarks (acromion angle, inferior angle and trigonum spinae) in three different functional positions (Figure 4.2) in order to calibrate the scapula tracker to the scapula motion of the subject. The glenohumeral joint rotation centre was obtained using the scapula tracker during a 30 second movement trial, where study participants performed shoulder abduction and flexion, both with 90° of elbow flexion, and movements imitating the stirring of a pot (Prinold 2011).

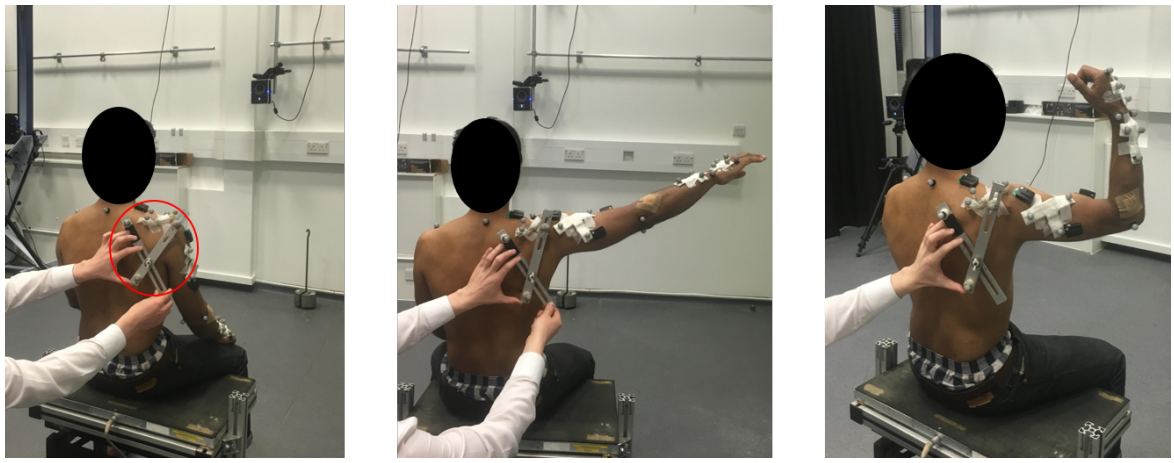

Figure 4.2: The three static positions for the calibration of the scapula. Left – resting position with hands resting on the knees; centre – scaption: shoulder at 90° abduction and elbow at 90° flexion with arm positioned at approximately 30° to the coronal plane; right – shoulder at approximately 150° abduction. The scapula locator, as indicated by the red circle, was used to determine the scapula orientation.

The calibration trials were followed by the motion data collection, with study participants being instructed to perform sixteen functional activities of daily living with three sets per activity and a thirty seconds rest break between the sets. These activities were selected based on recommendations for the most commonly performed tasks throughout a normal day (Charlton & Johnson 2006; Bergmann et al. 2007; Westerhoff et al. 2009; Coffey & McCarthy 2013; Murray & Johnson 2004). The study participants were provided with instructions to define the start and end point of each activity. No other instructions were given to ensure a natural execution of these functional activities.

MRI data of the upper limb were collected from study participants within two months of motion analysis. A 3D T1-weighted VIBE (volumetric interpolated breath-hold examination) sequence was

used to acquire axial images of the subjects in the supine position using a 3T Siemens Verio MRI scanner (Siemens AG, Erlangen, Germany). The signal was received through a spine coil and two body matrix coils, with MRI protocol settings as follows: imaging field of view 450 x 450 mm^2, matrix = 384 x 384, axial plane resolution 1.17 x 1.17 mm, slice thickness 1 mm. The field of view (FOV) included the right half of the upper limb, scanning from skull to finger tips in axial blocks of length 22.4 cm, with 2.5 cm overlap between adjacent sections. The MRI scan consisted of 5 sections for the tallest participant and 3 sections for the shortest subject, with 5 minutes, 43 seconds acquisition time per section.

Musculoskeletal Geometry

For each volunteer, the anatomical geometry of the upper limb was described with two models: a scaled-generic model and an MRI-based model.

As described in Section 2.3.1, the skeletal geometry of the generic UK National Shoulder Model was obtained from the male visible human dataset (Spitzer & Whitlock 1998), while muscle properties were taken from three different cadaveric studies (van der Helm et al. 1992; Johnson et al. 1996; Veeger et al. 1997). The segments (thorax, scapula, clavicle, humerus, radius, ulna) of the generic model were scaled to ensure that intersegmental distances of the model match the corresponding distances of the experimental subjects, that were measured based on anatomical landmarks during a static calibration trial. The segment scaling utilises linear scaling for all segments except the thorax, which involves scaling of thorax height as the distance between PX and the midpoint of IJ and C7, thorax width as the distance between IJ and RAC, and thorax depth as the distance between C7 and the midpoint of PX and IJ.

The MRI-based models were developed following the topology of the generic dataset (Charlton & Johnson 2006). The customised models include 87 muscle elements, representing 20 muscles of the upper limb. The upper limb muscles were manually segmented and the segmentations served to compute subject-specific physiological cross-sectional areas (PCSA; Holzbaur et al. 2007; Langenderfer et al. 2004; Peterson and Rayan 2011; Ruggiero et al. 2016) for each muscle as shown in Equation 4.1:

$$PCSA = \frac{V_m \cdot cos\theta}{L_m \cdot \frac{L_f}{L_m} \cdot \frac{L_o}{L_s}} \qquad \text{Equation 4.1}$$

where V_m represents the volume of each muscle, θ represents the pennation angle of each muscle, L_m represents the length of each muscle, L_f/L_m represents the ratio of fibre to muscle length of each muscle, L_o represents the optimal sarcomere length of human muscles, and L_s represents the sarcomere length for each muscles. These muscle morphology parameters were chosen from different cadaveric studies in the literature (Langenderfer et al. 2004; Veeger et al. 1997; Murray et al. 2000; Ruggiero et al. 2016),

while muscle length was obtained from the paths of axial centroids in the 3D muscle space (Handsfield et al. 2014).

Muscle origins, via points and insertion points were obtained through manual digitisation from MRI following the description of the UK NSM in Section 2.3.1, with full details of the development of the shoulder model being given in Charlton (2003). The muscles were simulated to wrap around bony segments of the upper limb that were described with geometric wrapping objects between muscle origins and insertions (Figure 4.3). The thorax and the scapulathoracic gliding plane were modelled with two wrapping ellipsoids, while humerus, radius and ulna were described with wrapping cylinders. The glenohumeral joint centre of rotation was defined as the centre of the humeral head which was determined with a sphere fit (Figure 4.4; Charlton & Johnson 2006). The wrapping object parameters were determined in two steps: an initial estimation from the scaled-generic model and then a manual adjustment based on the segmented MRI to ensure that the muscles wrapped smoothly over the subject-specific bony contour. All image segmentations and processing steps were performed using Mimics (Mimics Research 17.0, Materialise NV, Leuven, Belgium). Subject-specific segmental parameters including centre of mass and moments of inertia were determined through regression equations as described by De Leva (1996).

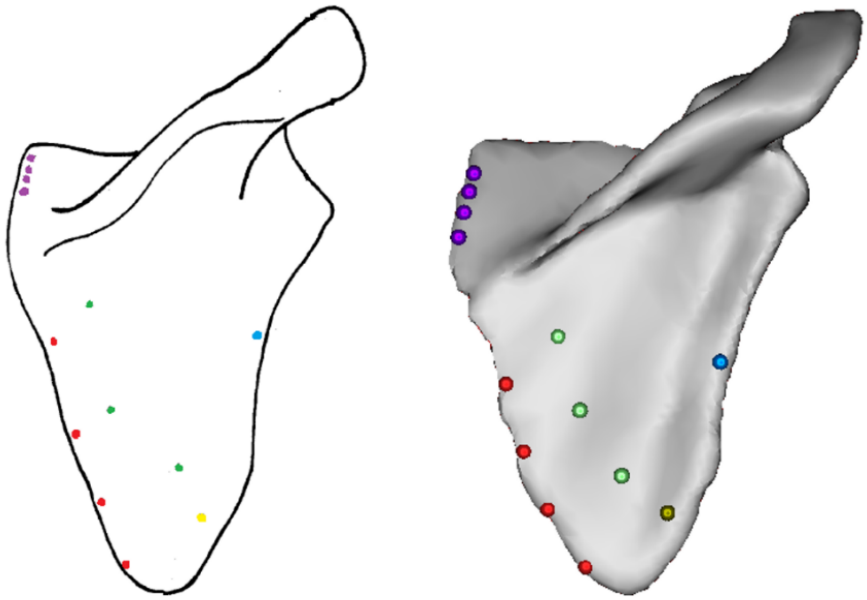

Figure 4.3: Posterior view of the scapula with attachment sites of the rhomboids (red), infraspinatus (green), teres major (yellow), teres minor (blue) and levator scapulae (purple). Left – digitisation by Johnson et al. (1996). Right – digitisation from MRI for a single subject.

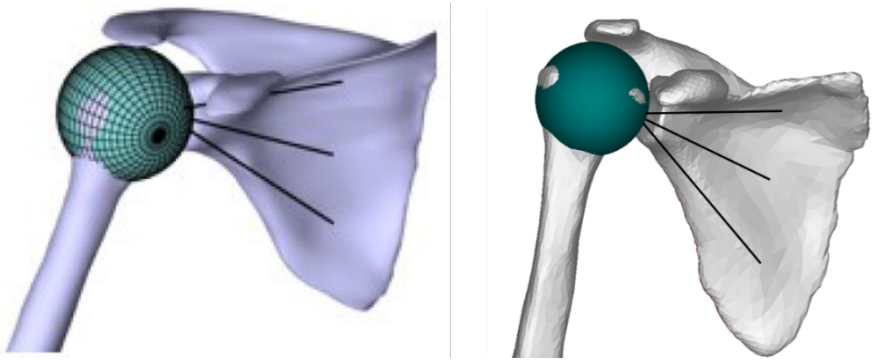

Figure 4.4: Anterior view of the GH joint for the wrapping object of the humeral head. Left – scaled-generic UK NSM. Right – subject-specific UK NSM.

Musculoskeletal Simulation

The motion data and external forces for each functional activity served as inputs into the UK National Shoulder Model (Charlton & Johnson 2006) which represents a 3D musculoskeletal modelling software written in Matlab (The Mathworks Inc., Cambridge, UK) that models forces at the glenohumeral joint. The version of the UK NSM used in this study is described in Section 2.3.1, and additionally incorporates the effect of glenohumeral concavity compression as detailed in Chapter 3. Each functional activity of daily living was simulated using the scaled-generic model version of the UK NSM as well as the subject-specific, MRI-based version of the UKNSM.

Data Analysis

Surface EMG signals of the upper limb were processed to evaluate muscle activations predicted by the MRI-based and scaled-generic model. The raw EMG signals were high-pass filtered at 30Hz, fourth order Butterworth filtered and rectified (Buchanan et al. 2004). The rectified signals were low-pass filtered at 10 Hz (Arnold et al. 2013). For each subject, data were normalised (Arnold et al. 2013) based on maximum EMG signals during the maximum voluntary contraction tests described above.

The muscle force predictions of the MRI-based and scaled-generic models were analysed by defining start and end point of each functional activity and interpolating the data between these points using a cubic spline function. The definitions of the start and end points are described in (Murray and Johnson 2004; Coffey and McCarthy 2013). The muscle force predictions were normalised by the maximum muscle force of each muscle.

Quantitative evaluation between EMG data and predicted muscle activations was conducted using Sprague and Geers metrics of magnitude (M), phase (P) and combined error (C; Schwer 2007). The Sprague and Geers metrics quantify the magnitude and phase error independently, while C combines the two errors and is computed as the root of the sum of squares of M and P. The interpretation of the Geers metric is as follows:

- 0 < Geers Metric < 0.15 excellent similarity
- 0.15 < Geers Metric < 0.30 very good similarity
- 0.30 < Geers Metric < 0.45 good similarity
- 0.45 < Geers Metric < 0.60 moderate similarity
- Geers Metric > 0.6 no similarity

The similarity of waveforms between EMG data and muscle activations was assessed using the coefficient of multiple correlation (CMC). The CMC quantifies waveform similarity between 0 and 1 (Ferrari et al. 2010), with the interpretation of results as follows (Garofalo et al. 2009):

- CMC < 0.65 no similarity
- 0.65 < CMC < 0.75 moderate similarity
- 0.75 < CMC < 0.85 good similarity
- 0.85 < CMC < 0.95 very good similarity
- 0.95 < CMC < 1 excellent similarity

The results comparing EMG data and predicted muscle activations are presented for each muscle and averaged over all trials, functional activities and study participants. Statistical significance was assessed using a non-parametric Mann-Whitney test.

The muscle moment arm predictions of the MRI-based model were normalised to allow comparison to literature data (Ackland et al. 2008, 2010; Gatti et al. 2007; Kuechle et al. 1997; Herrmann et al. 2011; Hughes et al. 1998; Holzbaur et al. 2005; Quental et al. 2015). The normalisation involved the multiplication of each moment arm with the ratio of average humeral head radius of all participants to the humeral head radius of a given participant. The humeral head radius for each study participant was obtained through a manual sphere fit.

The dependency of model predictions on the anatomical geometry was assessed in a 10-fold cross-validation. The anthropometric parameters selected for analysis were based on studies in the literature, demonstrating the effect of musculoskeletal geometry on modelling results (Bosmans et al. 2015; Carbone et al. 2012). These parameters include shoulder width (distance between LAC and RAC), humeral length (distance between midpoint of ME and LE and the humeral head center), humeral width (distance between the ME and LE), forearm length (distance between midpoint of ME and LE and midpoint of RS and US), forearm width (distance between RS and US), scapula length (distance between inferior scapula angle and superior scapula angle) and scapula width (distance of superior scapula angle and acromion angle). In the course of the cross-validation, each anatomical dataset served as input for each MRI-based shoulder model, with Pearson correlations and multiple linear regressions being used to test for relationships between anthropometric measurements and changes in a compound measure that took into account both the accuracy of the glenohumeral contact force as well as all

shoulder muscle forces (normalised root mean square error (RMSE, normalised by body mass [N/kg]). This was calculated by taking the average of all shoulder muscle force errors, summing this with the errors of the glenohumeral joint contact force and dividing those by two, so that both measures contributed an equal amount to the target value. Partial correlation coefficients were used to identify which variables contribute to significant changes in RMSE in the presence of all variables. Multiple regression models were identified when taking the significant predictors into account, with these models serving to determine anthropometric parameters or combinations of these that yield best modelling outcomes through scaling of personalised shoulder models. The final multiple regression model was identified using stepwise forward regression, with a significance level of $p < 0.05$ being used throughout. The appropriateness of the stepwise forward regression models was evaluated by examining histograms of the residuals as well as plots of the residuals against the independent and predicted values.

The final multiple regression model was utilised to identify the anatomically closest dataset for each MRI-based model. The model predictions of the scaled-closest model were compared to the single, scaled-generic model in order to assess improvements in modelling outcomes of glenohumeral loading through the use of anthropometric measures anatomical dataset scaling, when compared to a single, scaled-generic model. These improvements in modelling outcomes were assessed for the glenohumeral joint contact force as well the shoulder muscles forces. Statistical significance was assessed using a non-parametric Mann-Whitney test.

4.3 Results

The quantitative evaluation of EMG data and predicted muscle activations using Sprague and Geers metric is shown in Table 4.3. The MRI-based model predictions demonstrate good agreement with EMG measurements for deltoid, biceps, triceps and pectoralis, while the trapezius shows moderate agreement with EMG measurements.

Table 4.3: Quantitative differences between measured EMG data and predicted muscle activations for the MRI-based models [deltoid (DELT), biceps (BIC), triceps (TRI), pectoralis (PEC), trapezius (TRAP)] for all subjects using the Geers metric. M = magnitude error, P = phase error, C = combined error.

	MRI-based model		
	M	P	C
DELT	-0.21	0.32	0.38
BIC	-0.18	0.38	0.42
TRI	-0.16	0.33	0.37
PEC	-0.19	0.37	0.42
TRAP	-0.23	0.42	0.48

The analysis of waveform similarity between EMG data and predicted muscle activations using the coefficient of multiple correlation is shown in Table 4.4. The MRI-based model predictions demonstrate

good to very good similarity with EMG measurements for deltoid, biceps and triceps, while trapezius and pectoralis show moderate similarity with EMG measurements.

Table 4.4: Quantitative differences between measured EMG data and predicted muscle activations for the MRI-based models [deltoid (DELT), biceps (BIC), triceps (TRI), pectoralis (PEC), trapezius (TRAP)] for all subjects using the coefficient of multiple correlation.

	Coefficient of Multiple Correlation
	MRI-based model
DELT	0.87 ± 0.28
BIC	0.76 ± 0.31
TRI	0.81 ± 0.27
PEC	0.73 ± 0.22
TRAP	0.69 ± 0.36

The comparison of muscle moment arms between MRI-based models and cadaveric measurements for functional daily activities is shown in Figures 4.5 and 4.6. The MRI-based muscle moment arms compare well with *in-vitro* measurements for shoulder muscle prime movers, with cadaveric measurements being largely within one standard deviation of model estimations.

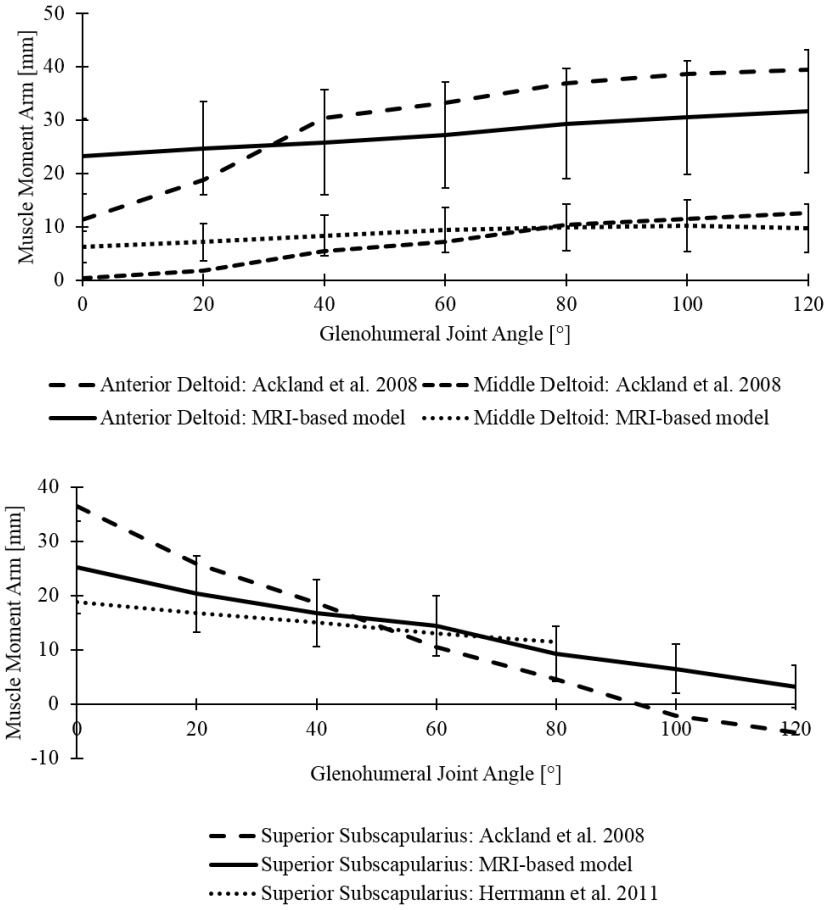

Figure 4.5: Comparison of muscle moment arm predictions of the MRI-based shoulder model with cadaveric measurements from the literature during sagittal plane flexion. Top – deltoid. Bottom – subscapularis.

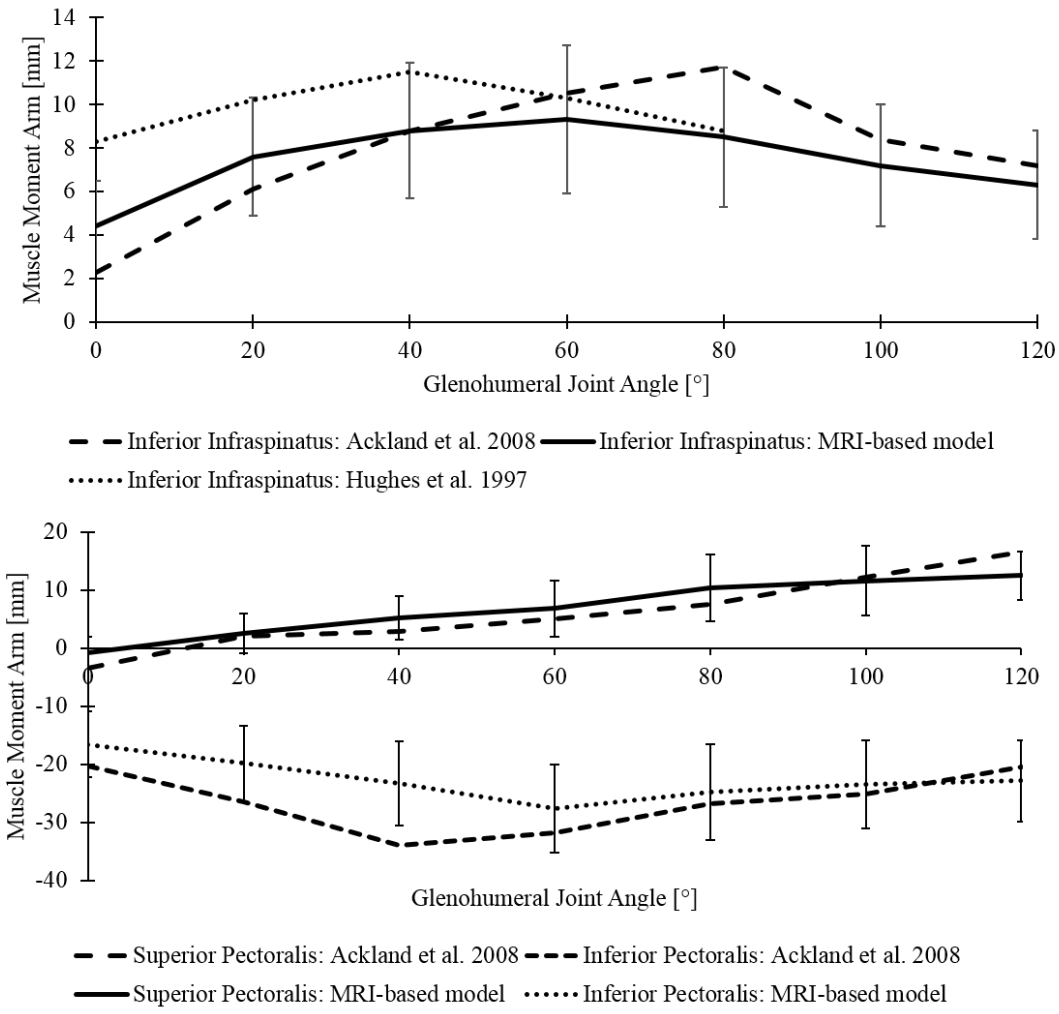

Figure 4.6: Comparison of muscle moment arm predictions of the MRI-based shoulder model with cadaveric measurements from the literature during coronal plane abduction. Top – infraspinatus. Bottom – pectoralis.

The dependency of model predictions of joint contact force and muscle forces on anatomical geometry is illustrated in Table 4.5, through correlation of anthropometric differences between subjects with the RMSE in in the compound measure that took equally into account both the accuracy of the glenohumeral contact force as well as all shoulder muscle forces. The best predictor for changes in RMSE is the ratio of body height to shoulder width (Pearson correlation coefficient; R=0.46, p=9.67E-5), followed by gender (R=0.42, p=1.44E-5; Figure 4.7). The next best predictors include the ratios of segment length to width (R=0.35, p=6.21E-3).

*Table 4.5: Partial correlation coefficients for anthropometric measurements on the root mean square error of the glenohumeral contact force and muscle forces. * Indicates correlation coefficients at the significance level of $p < 0.05$.*

Anthropometric Measure	Glenohumeral Contact Force
Ratio of body height to shoulder width	R = 0.46*
Gender	R = 0.42*
Ratio of scapula length to scapula width	R = 0.40*
Ratio of humeral length to humeral width	R = 0.37*
Ratio of forearm length to forearm width	R=0.29*
Shoulder width	R = 0.25*
Scapula width	R = 0.17
Humeral length	R = 0.16
Forearm length	R = 0.14
Body Mass Index	R = -0.06
Scapula length	R = 0.05
Humeral width	R = 0.05
Wrist width	R = 0.04
Body height	R = 0.03

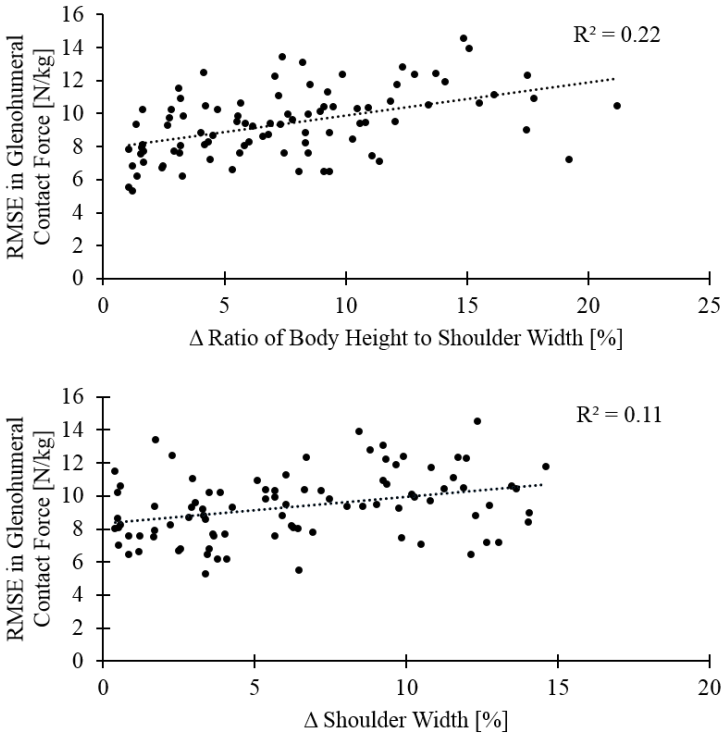

Figure 4.7: The root mean square error (RMSE) of the compound measure that took equally into account both the glenohumeral contact force and muscle forces, for anthropometric predictors. Top – ratio of body height to shoulder width. Bottom – shoulder width.

The final regression model was developed to take into account the significant predictors (Table 4.6). As identified by the forward multiple linear regression model, the ratio of body height to shoulder width as well as gender were in the final set of predictors for the RMSE in glenohumeral loading, with both variables combined explaining 45% of the variance (coefficient of determination; $R^2 = 0.45$, adjusted $R^2 = 0.43$). The inclusion of additional anthropometric variables such as the ratios of segment length to width only explained an additional 4% of the variation in RMSE. This is due to the significant correlation of the ratio of body height to shoulder width with the ratio of humeral length to humeral width (R=0.64, p=4.65E-11), the ratio of forearm length to forearm width (R=0.65, p=5.73E-12), the ratio of scapula length to scapula width (R=0.70, p=1.97E-15) as well as shoulder width (R=0.55, p=6.26E-8). The anatomically closest dataset, with the minimum error in joint contact force and muscle forces is derived from the multiple regression model as shown in Equation 4.2:

$$\min f(RMSE) = \min\,(7.11 + 0.24 \cdot \Delta\,\text{ratio of body height to shoulder width} + 3.85 \cdot \Delta\,\text{gender}) \qquad \text{Equation 4.2}$$

Table 4.6: The significance levels for the best anthropometric predictors of the root mean square error (RMSE) of the glenohumeral joint contact force and muscle forces as identified by the forward stepwise regression model.

Anthropometric Measures	p-value
Ratio of body height to shoulder width	0.01
Gender	0.04
Ratio of scapula length to scapula width	0.19
Ratio of humeral length to humeral width	0.36
Shoulder width	0.59
Ratio of forearm length to forearm width	0.81

The regression equation was utilised to identify the anatomically closest dataset for each MRI-based model, with the comparison of scaled-closest and scaled-generic model demonstrating a significant reduction in RMSE in glenohumeral joint contact force and muscle forces ($p < 0.02$) for the scaled-closest anatomical dataset (Table 4.7; Table 4.8).

Residual analysis of the forward stepwise regression models indicated that this linear model was an appropriate choice with the residuals being normally distributed and the residual plots indicating there was constant variance and no evidence of nonlinearity.

Table 4.7: Comparison of the root mean square error (RMSE) in glenohumeral joint contact force as modelled by the scaled-generic model and the scaled-closest model (identified through the multiple regression model).

** The scaled closest model was derived from the multiple linear regression model with the minimum RMSE of* $min\, f(RMSE) = min(7.11 + 0.24 \cdot \Delta ratio\ of\ body\ height\ to\ shoulder\ width + 3.85 \cdot \Delta gender)$*, where* Δ *ratio of body height to shoulder width represents the percentage difference in the ratio of body height to shoulder width between the subject and dataset, and* Δ *gender indicates the difference in gender, with* Δ *gender = 1 for different gender and* Δ *gender = 0 for the same gender.*

	Scaled-Generic Model	Scaled-Closest Model*
Subject	RMSE [N/kg]	RMSE [N/kg]
1	6.4	3.9
2	8.3	4.8
3	4.6	2.2
4	11.2	7.2
5	6.8	3.2
6	3.9	1.8
7	8.9	4.7
8	6.3	3.6
9	2.3	2.8
10	9.3	3.7
Mean	6.8	3.8
Standard deviation	2.7	1.6
p-value	0.007	

Table 4.8: Comparison of the root mean square error (RMSE) in mean shoulder muscle force as modelled by the scaled-generic model and the scaled-closest model (identified through the multiple regression model).

** The scaled closest model was derived from the multiple linear regression model with the minimum RMSE of* $min\,f(RMSE) = min(7.11 + 0.24 \cdot \Delta ratio\ of\ body\ height\ to\ shoulder\ width + 3.85 \cdot \Delta gender)$*, where* Δ *ratio of body height to shoulder width represents the percentage difference in the ratio of body height to shoulder width between the subject and dataset, and* Δ *gender indicates the difference in gender, with* Δ *gender = 1 for different gender and* Δ *gender = 0 for the same gender.*

	Scaled-Generic Model	Scaled-Closest Model*
Subject	RMSE [N/kg]	RMSE [N/kg]
1	1.8	1.4
2	2.3	1.7
3	1.7	0.8
4	2.9	2.2
5	1.9	1.3
6	1.6	0.7
7	2.4	1.7
8	1.8	1.2
9	0.8	1.0
10	2.5	1.4
Mean	2.0	1.4
Standard deviation	0.6	0.5
p-value	0.013	

4.4 Discussion

Customisation of musculoskeletal modelling through medical imaging has demonstrated significant improvements in model reliability when compared to scaled-generic models (Scheys et al. 2008a, 2008b; Gerus et al. 2013), but the model development is time, labour and technology intensive. Linear scaling of musculoskeletal shoulder models with high anthropometric similarity from an anatomical atlas has the potential to yield modelling results that are close to predictions of subject-specific models and more accurate than a single, scaled-generic model. This study has developed and validated 10 subject-specific shoulder models to demonstrate that linear scaling of MRI-based shoulder models with the closest ratio of body height to shoulder width and from the same gender yield best modelling outcomes in glenohumeral joint contact force and muscle forces. These model predictions are significantly improved when compared to an individual, scaled-generic dataset.

The validation of musculoskeletal shoulder models is essential for utility and clinical applicability, but the difficulty in measuring *in-vivo* muscle forces makes model validation a challenging task. The subject-specific models presented in this study were validated against measurements of muscle activations using EMG as well as measurements of muscle moment arms as reported in the literature.

Muscle forces are the main determinant for joint contact forces, making EMG measurements a justified comparator for model validation that has been widely used in the literature (Modenese et al. 2011; Moissenet et al. 2014; Cleather & Bull 2010). The predicted muscle activations of the MRI-based models yield coefficients of multiple correlation that show very good to moderate agreement with EMG measurements, with comparable coefficients for waveform similarity being reported in the literature (Tsai et al. 2012; McGinley et al. 2009). Similarly, the subject-specific models show combined errors of the Geers metric that are comparable to other validation results in the literature (ranking from 0.13 to 0.41, Cleather and Bull 2015), with a time lag being observed relative to measured EMG data, representing the neuromechanical delay between muscular activation and force production (Cavanagh & Komi 1979).

The comparison of muscle moment arm predictions with *in-vitro* measurements as reported in the literature demonstrates that experimental data are largely within one standard deviation of model estimations (Figures 4.5 and 4.6). The differences between computational simulation and experimental testing may be explained with the definition of muscle subregions that were chosen during cadaveric testing by Ackland et al. 2008; Hughes et al. 1997; Herrmann et al. 2011. While musculoskeletal shoulder models separate muscles into individual muscle lines of action, cadaveric studies divided shoulder muscles into functionally distinct muscle fiber bundles, making a direct comparison challenging. Nevertheless, MRI-based model estimations for shoulder muscle moment arms compare well to *in-vitro* measurements from different experimental studies (Ackland et al. 2008; Herrmann et al. 2011; Hughes et al. 1997), providing further evidence for physiological model estimations of the developed MRI-based shoulder models.

The 10 validated MRI-based shoulder models were utilised to identify the effect of anthropometrics on musculoskeletal modelling results and to provide an atlas for customisation of shoulder models in future applications. There are several studies assessing changes in model estimations with alterations in muscle physiology parameters (Bolsterlee et al. 2015; Bolsterlee & Zadpoor 2014; Bosmans et al. 2015; Carbone et al. 2012), with no study reported in the literature having investigated the effect of anthropometrics on musculoskeletal modelling outcomes. The precise understanding of this effect would be essential in order to evaluate the errors associated with scaling of generic cadaveric datasets to subjects with different anthropometry, particularly as some generic datasets in the literature (including: Charlton & Johnson 2006; Klein Breteler et al. 1999 and Carbone et al. 2015) may not necessarily be representative of an average person. The findings of this study demonstrate small correlation coefficients of body height, body mass as well as upper limb segment length with changes in root mean square error of the compound measure that took equally into account both the accuracy of the glenohumeral contact force as well as all shoulder muscle forces, while best model estimations of those measures tested are yielded for anatomical geometries with the closest ratio of body height to shoulder width and from the same gender as identified by the forward multiple regression model. The

significance of these two anthropometric parameters is supported by studies in the literature (Bosmans et al. 2015; Carbone et al. 2012), demonstrating significant alterations in model estimations with changes in moment arms through variations in muscle attachment sites. While the ratio of body height to shoulder width has a direct impact on moment arms due to the bony contours provided for muscle wrapping, there is evidence in the literature that muscle physiology parameters including muscle attachment sites are gender dependent (Edama et al. 2017; Clark et al. 2007).

The regression equation was utilised to identify the closest anatomical dataset for each MRI-based model, with the comparison of scaled-closest and scaled-generic model demonstrating a significant reduction in root mean square error in the compound measure that took equally into account both the accuracy of the glenohumeral contact force as well as all shoulder muscle forces ($p < 0.02$) for the scaled-closest anatomical dataset (Table 4.7, Table 4.8). This suggests that establishing a database of anatomical models for anthropometric scaling is essential to improve model reliability, when compared to linearly scaling a single, generic model that has demonstrated a maximum RMSE of 11 N/kg for the glenohumeral joint contact force and 3 N/kg for the shoulder muscle forces. Future research should aim to improve the number of anatomical datasets for scaling to see if a reduction in the mean (3.8 N/kg, 1.4 N/kg) and maximum (7.2 N/kg, 2.2 N/kg) joint contact forces and muscle forces, respectively, could be achieved. The additional anatomical geometries should be male and female volunteers with different ratios of body height to shoulder width as expressed by the multiple linear regression model.

This study has some limitations. Firstly, the identification of the anatomically closest dataset is only applicable for musculoskeletal shoulder models with the same scaling law and changes in scaling law are likely to alter the multiple linear regression model. Nevertheless, the scaling law as implemented in the UKNSM is widely used (Garner & Pandy 2001, Delp et al. 2007) and the data provided in this study provide the basis to adapt the regression model to musculoskeletal shoulder models with different scaling laws (Nikooyan et al. 2010). Secondly, the number of the MRI-based shoulder models developed in this study is limited. While a larger number of subject-specific models would increase statistical power of the findings, we believe that the 10 datasets are representative for a wide variety of subjects across the population and future work should aim to add MRI-based models to the atlas that will be towards the more extreme end of anthropometrics. Finally, the musculoskeletal model did not define an upper bound for each muscle to quantify the maximum force that each muscle can contribute to shoulder movement. While this is non-physiological, this approach has been widely used in the literature (Garner & Pandy 2001, Delp et al. 2007) to account for the inherent difficulty in measuring muscle stresses (van der Helm 1994, Crowninshield & Brand 1981, Challis & Kerwin 1993).

Despite these limitations, this is the first study to develop and validate 10 subject-specific shoulder models from MRI in order to demonstrate the effect of anthropometrics on modelling outcomes. The study findings show that linear scaling of subject-specific models with the closest ratio of body height

to shoulder width and from the same gender yield best modelling results in glenohumeral joint contact force and muscle forces, with significant improvements in model estimations when compared to a linearly-scaled generic model. This suggests that establishing an atlas with MRI-based models for scaling significantly improves model predictions. This should facilitate the translation of musculoskeletal models in clinical practice in order to aid clinical decision-making.

4.5 Conclusion

This chapter presented the development and validation of 10 subject-specific shoulder models from MRI in order to demonstrate the effect of anthropometrics on modelling outcomes. The study findings show that linear scaling of subject-specific models with the closest ratio of body height to shoulder width and from the same gender yield best modelling results in glenohumeral joint contact force and muscle forces, with significant improvements in model estimations when compared to a linearly-scaled generic model. The improvement in modelling accuracy is of particular importance for clinical applications, including those associated with anterior shoulder dislocation.

Chapter 5 will utilise the 10 MRI-based shoulder models as well as the effect of glenohumeral concavity compression as described in Chapter 3 in order to analyse glenohumeral contact forces during functional daily activities. These data have strong potential to aid rehabilitation planning for patients following Bankart repair, the most commonly performed surgical intervention in patients post anterior shoulder instability, as current rehabilitation guidelines are based on clinical experiences.

Chapter 5

Analysis of shoulder compressive and shear forces during functional activities of daily life.

The precise understanding of shoulder loading during functional daily activities is a prerequisite for aiding rehabilitation planning and improving implant design. As there is currently no detailed knowledge of glenohumeral contact forces during functional activities, with existing studies focusing on a small number of functional activities without always presenting the loading direction on the joint, the aim of this chapter is to analyse the compression and shear force components of the glenohumeral contact force during essential activities of daily living. This analysis is performed using anthropometric scaling of ten subject-specific versions of the UK NSM as described in Chapter 4, with the regression equations for the labral contribution to joint stability, as described in Chapter 3, being incorporated into the shoulder model in order to precisely model glenohumeral loading.

This work was published in part as: 'Analysis of shoulder compressive and shear forces during functional activities of daily life', with authors: Christian Klemt, Joe Prinold, Sharon Morgans, Samuel HL Smith, Daniel Nolte, Peter Reilly, Anthony MJ Bull. Clinical Biomechanics. 2018. 54(4):34-41.

5.1 Introduction

The forces at the glenohumeral joint are frequently dismissed as being small when compared to loads at the knee and hip joint (Poppen & Walker 1978). This is despite the fact that substantial loads through the joint have been demonstrated during activities of daily living (ADL) with either instrumented shoulder implants or musculoskeletal shoulder models (van Drongelen et al. 2006; Bergmann et al. 2007; van Andel et al. 2008; Westerhoff et al. 2009; Nikooyan et al. 2010). Anglin et al. (2000) have reported glenohumeral contact forces (GHCFs) of 240% of the body weight (BW) for lifting a 10kg suitcase laterally, 180% BW for holding a 5kg box ventrally and 170% BW on average for walking with a cane. Bergmann et al. (2007) found GHCFs of 70% BW for hammering a nail, 65% BW for hair combing and 40% BW for steering a car, while Charlton and Johnson (2006) reported GHCFs ranging from 23% to 75% BW for 10 functional activities including feeding, personal hygiene and lifting everyday objects.

The GHCFs are achieved through compression of the humeral head into the glenoid-labral concavity through contraction of muscles surrounding the shoulder, and the joint force can be decomposed into 3 components: compressive force, anterior-posterior shear force and superior-inferior shear force (Lee et al. 2000). The compressive force component is directed to the centre of the glenoid socket, while the shear force components destabilise the joint by translating the humeral head towards the glenoid rim, with the ratio of these force components determining the risk of joint luxation and the loading of the capsuloligamentous labral complex as well as the prosthesis-bone interface in shoulder arthroplasties (Lazarus et al. 1996; Nishinaka et al. 2008).

Therefore, the precise understanding of the magnitude of glenohumeral shear force component to compression force component during functional activities of daily life is essential to aid rehabilitation planning for patients post shoulder surgery, with these data enabling the assessment of existing rehabilitation strategies, the development of novel physiotherapy programmes as well as advice to be given to patients in order to avoid overloading of the joint following Bankart repair, the most commonly performed surgical intervention to treat patients with recurrent anterior shoulder instabilities (Arciero et al. 1994; Hayes et al. 2004). Furthermore, knowledge of glenohumeral compression and shear forces allows preclinical test procedures for shoulder arthroplasties to be designed to improve implant design as well as glenoid fixation, where off-centre loading is considered the major cause of loosening (Geraldes et al. 2017). These data also provide support for the design and testing of preclinical surgical procedures including tendon transfer surgeries (Ackland & Pandy 2009).

Despite several studies being reported in the literature, there is currently no detailed knowledge of glenohumeral contact forces during functional activities with existing studies focusing on a small number of functional activities without always presenting the loading direction on the joint. Therefore, the aim of this study is to analyse the compression and shear force components of the glenohumeral

contact force during essential activities of daily living which may aid shoulder rehabilitation and implant design.

5.2 Materials and Methods

Study Participants

Twenty-five healthy right-handed volunteers (20 males, 5 females) with no history of shoulder pathology participated in this study. Each activity was performed by a subset of volunteers (Table 5.1). Informed consent was obtained from each subject and ethical approval was granted by the Imperial College Research Ethics Committee.

Table 5.1: Participant information for each set of functional activities. Data are presented as mean and standard deviation (SD).

Dataset name	Participants	Age (years)	Height (m)	Body mass (kg)
ADL1	8	34.4 (SD 13.9)	1.73 (SD 0.08)	69.3 (SD 13.9)
ADL2	6	27.1 (SD 1.26)	1.77 (SD 0.09)	75.8 (SD 5.2)
Driving	4	26.0 (SD 1.41)	1.76 (SD 0.13)	67.5 (SD 13.9)
Planar tasks	7	25.4 (SD 1.13)	1.82 (SD 0.07)	75.0 (SD 6.1)

Functional Activities

The volunteers were instructed to perform 26 functional activities of daily life with three sets per activity (Table 5.2). These activities include basic functional activities of daily life such as feeding, personal hygiene, mobility and lifting everyday objects, alongside activities with larger range of motion such as planar movements. These activities were selected based on recommendations for the most commonly performed tasks during a standard day (Charlton & Johnson 2006; Bergmann et al. 2007; Westerhoff et al. 2009; Coffey & McCarthy 2013; Murray & Johnson 2004).

Table 5.2: Activities of daily living within each dataset.

Dataset name	Activity	Loading
ADL1	Reach back of head	-
	Lift block to head height	0.5kg
	Lift block to shoulder height	0.5kg
	Brush left side of head	-
	Clean back	-
	Drink from mug	-
	Eat with hand	-
	Eat with spoon	-
	Lift shopping bag from floor (standing)	2kg
	Lift shopping bag from floor (seated)	2kg
	Reach opposite axilla	-
	Perineal care (reach back pocket)	-
	Reach far ahead	0.5kg
	Sit to stand	Load cell
ADL2	Extreme (reach across body)	-
	Pick and place (short distance)	2kg
	Pull	-
	Push	-
Driving	Fast (right and left turn)	Load cell
	Slow (right and left turn)	Load cell
Planar tasks	Abduction (slow)	-
	Abduction (fast)	-
	Forward flexion (slow)	-
	Forward flexion (fast)	-

The ADL2 activity of 'Extreme' involves moving the hand to a point furthest from the shoulder, across the body and in the transverse plane, level with the glenohumeral joint (Figure 5.1 A). The 'Pick and place' activity involves moving an object approximately 30 cm away from the chest within the transverse plane, after an initial starting point close to the body (Figure 5.1 B). The 'Pull' activity involves the subject starting with outstretched arms, holding a thin wooden rod horizontally, and moving the arms in as far as possible. This is performed at chest height (Figure 5.1 C). The 'Push' activity is the opposing action (Figure 5.1 D). The 'Driving' activity involves moving a steering wheel with both hands until the wheel has rotated by 65° clockwise and anticlockwise for 'driving right' and 'driving left' respectively. The activity was performed at both low (12 mph) and high speeds (24 mph) in order to simulate different traffic situations, with the high speed simulating an emergency turn.. The torque resistance on the wheel was set to 4 Nm to simulate a driving torque under standard road conditions as described in Li and Xia (2014) and implemented by Pandis (2013).

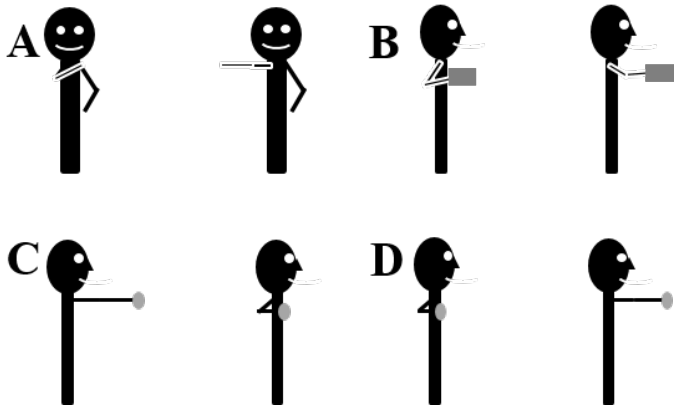

Figure 5.1: Representation of the activities of the ADL2 dataset. (A) Reach across the body, (B) Pick and place, (C) Pull, (D) Push.

Protocol

Kinematic data collection was performed using a 10-camera optical motion tracking system (Vicon Motion Tracking System, Oxford, UK) at 100 Hz and three force plates (Kistler Instrument Corp., Winterthur, Switzerland) at 1000 Hz. The 'Driving' activity was performed using the driving simulator as published in Pandis et al. (2015), while the 'Sit to stand' task was conducted using an instrumented chair as described in Duffell et al. (2013).

A scapula tracker (ST) was used to measure scapula kinematics (Prinold et al. 2011). The ST consists of a base attached to the mid-portion of the scapula spine and an adjustable foot positioned on the meeting-point between acromion process and scapula spine (Shaheen et al. 2011). The ST technical coordinate frame was calibrated with the anatomical coordinate frame of the scapula using the International Society of Biomechanics (ISB) recommended landmarks and measured directly using a scapula locator (Shaheen et al. 2011). Calibration was performed at 90° of humerothoracic elevation, 45° to the coronal plane. The calibration transformation was applied to each trial of that participant with errors from static palpation of landmarks being small (de Groot 1997). The scapula kinematics for the functional activity 'driving' was derived from regression equations based on the humerothoracic position (Charlton & Johnson 2006).

Twenty-one retro-reflective markers were used to track the thorax, scapula, clavicle, humerus, radius and ulna (Full details of the marker setup are provided in Chapter 4.2). The elbow epicondyles were defined as a rigid offset from the humerus technical frame with the arm at 90° of humerothoracic flexion, 45° from the coronal plane, 90° elbow flexion and a vertical forearm. Least-square fitting was used to calculate the glenohumeral head rotational centre during a functional task using the Locator to track the scapula (Gamage & Lasenby 2002).

A low-pass fourth-order Butterworth filter (cut-off 4.7 Hz) was used to remove noise from the kinematic data, whilst the force plate data were processed with a low-pass fourth-order Butterworth filter (cut-off 10 Hz) after spectral analysis of the signal (Prinold and Bull 2016).

The orientation of the upper limb joints in the 3D Euclidean space was calculated using Euler angles with z-x'-y'' Cardan Sequence (Prinold and Bull 2016). For the glenohumeral joint, the rotations about z, y, and x-axes are forward flexion/extension, external/internal rotation and abduction/adduction respectively (G. Wu et al., 2005).

Modelling and Analysis

The motion data and external forces served as inputs into the UK National Shoulder Model (UK NSM; as described in Section 2.3.1; Charlton & Johnson 2006) which was used to model glenohumeral contact forces in the right shoulder. The version of the UK NSM used in this study utilises anthropometric scaling of ten subject-specific anatomical datasets as described in Chapter 4, and additionally incorporates the labral contribution to joint stability as described in Chapter 3 into the modelling framework of the shoulder model. This latter aspect was implemented through modelling of the labral contribution to joint stability as a force in the equilibrium equations of the loadsharing optimisation.

The glenohumeral contact forces as predicted by the UK NSM are represented in the anatomical coordinate frame of the glenoid plane as described in Lee and Lee (2010), which allows the decomposition of the joint reaction force in 3 components: compressive force, anterior-posterior shear force and superior-inferior shear force (Figure 5.2).

The glenohumeral contact forces during functional daily activities were additionally analysed using the generic UK NSM as described in Section 2.3.1 (Charlton & Johnson 2006) as well as using the generic UK NSM with integration of passive glenohumeral concavity compression as described in Chapter 3, in order to demonstrate the changes in modelling outcomes through technical model improvements associated with glenohumeral concavity compression as described in Chapter 3 and customisation of shoulder modelling as detailed in Chapter 4.

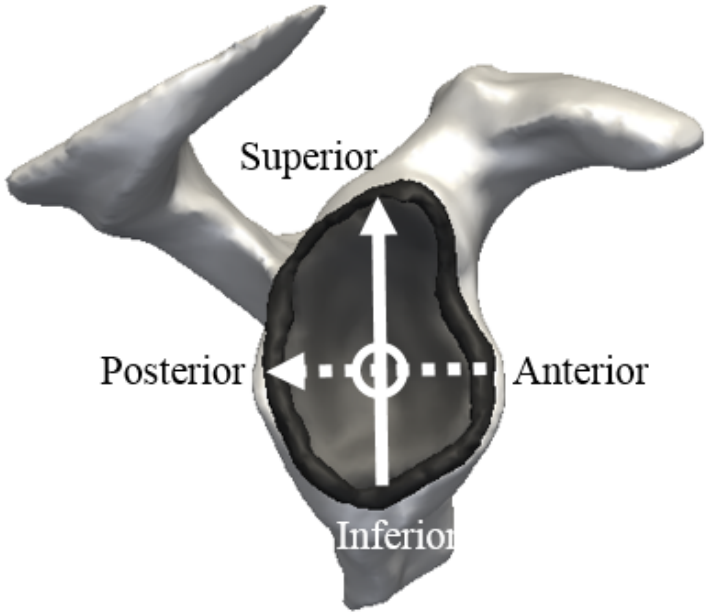

Figure 5.2: Components of the glenohumeral joint force in the glenoid coordinate frame. The superior-inferior shear force is represented by the solid arrow, the posterior-anterior shear force is represented by the dashed arrow, and the glenohumeral compression force is shown by the circle.

Data Normalisation

Each dataset was normalised to allow averaging and clear presentation of results. Once the 0%, 100%, and in some cases the 50% points of the activity were established the data was then interpolated between these points using a cubic spline function.

The activities in the ADL1 dataset were normalised according to the points described in Table 5.3. In some cases, the activities were split into two phases, where there was a clear distinction between the end of one phase (start point to functional position)and the start of the second phase (return from functional position to start point), resulting in two values being presented at 50% of the activity with a discontinuity in the results in some cases.

Table 5.3: Points used to normalise the activities in the ADL1 dataset.

Activity	Starting to functional position		Functional to starting position	
	0%	**50%**	**0%**	**50%**
Reach back of head	Initiation of movement	Wrist reaches furthest point	Initiation of return movement	Wrist returned to steady distance
Lift block to head height	Force exerted to lift block	Block released	Force exerted to lift block	Block released
Lift block to shoulder height	Force exerted to lift block	Block released	Force exerted to lift block	Block released
Brush left side of head	Initiation of movement	Wrist reaches furthest point	Initiation of return movement	Wrist returned to steady distance
Clean back	Initiation of movement	Wrist reaches furthest point	Initiation of return movement	Wrist returned to steady distance
Drink from mug	Force exerted to lift mug	Wrist reaches furthest point	Force exerted to lift mug	Wrist returned to steady distance
Eat with hand	Initiation of movement	Wrist reaches furthest point	Initiation of return movement	Wrist returned to steady distance
Lift shopping bag from floor	Force exerted to lift bag	Wrist reaches furthest point	Initiation of return movement	Wrist returned to steady distance
Reach opposite axilla	Initiation of movement	Wrist reaches furthest point	Initiation of return movement	Wrist returned to steady distance
Perineal care (reach back pocket)	Initiation of movement	Wrist reaches furthest point	Initiation of return movement	Wrist returned to steady distance
Reach far ahead	Force exerted to lift block	Block released	Force exerted to lift block	Block released
Sit to stand	Force applied to chair arms	Force returns to baseline	Force applied to chair arms	Force returns to baseline

To normalise the ADL2 dataset, the distance between the mid-point of the two wrist markers from their position in the first frame was calculated. The initiation of the movement in the desired direction, as judged from the distance time graph, was set as 0% and the furthest point at which the hand stopped appreciably moving in the desired direction as 100% (push, extreme), or vice versa as appropriate (pull, pick and place). This was defined visually per movement using the motion data.

The speed and angle of the wheel were used to normalise the 'Driving' data. An average vector between two markers on the appropriate side of the wheel's handle (right for a right turn and left for a left turn) was found over the first five frames. The angle from that vector was then found for each frame. The first frame in which the velocity of the angle went over 0.04 degrees/second was used as 0%. The point at which the angle went over 60° was set as the 100% point.

The 'Planar' data was normalised to humerothoracic elevation angle, using a y-z'-y'' Euler angle sequence. The largest value common to all subjects and trials at the bottom of the two phases of the motion (start of upward phase and end of downward phase) were used as the start and end points. The two 50% points were then defined as the smallest values common to all subjects and trials at the end of the upward motion phase and the start of the downward phase. These two phases were interpolated separately.

5.3 Results

The results presented in this section were obtained using the anthropometric scaling of ten subject-specific versions of the UK NSM as described in Chapter 4, with integration of passive glenohumeral concavity compression into the modelling framework of the UK NSM (Chapter 3). The results for the generic UK NSM as described in Section 2.3.1 (Charlton and Johnson 2006) as well as the generic UK NSM with integration of passive glenohumeral concavity compression can be found in Appendix 2.

The glenohumeral contact forces range from 24% (SD 10%) to 155% (SD 64%) of the body weight (BW) for the 26 functional activities of daily living (Table 5.4).

The ratio of glenohumeral shear force component to compression force component exceeds 0.5 in 6/26 functional activities (Table 5.4). The glenohumeral ratio ranges from 0.51 (SD 0.23) to 0.69 (SD 0.31) for activities such as reaching across the body, pushing and pulling, picking and placing an everyday object as well as sit to stand.

The glenohumeral contact force exceeds 155% BW (SD 64%) for the sit to stand task, with the ratio of anterior shear force component to compression force component being 0.42 (SD 0.17). The superior glenohumeral ratio exceeds 0.39 (SD 0.18), representing the second largest superior glenohumeral ratio of the entire dataset (Figure 5.3).

The glenohumeral contact force ranges from 45% (SD 13%) to 54% (SD 26%) BW for functional activities of lifting and placing everyday objects to shoulder/head height (Figure 5.4 A). The ratios of anterior shear force component to compression force component are the largest of the dataset, ranging from 0.36 (SD 0.15) to 0.50 (SD 0.24).

The glenohumeral contact force exceeds 49% BW (SD 25%) for the task ‘reaching across the body’. The ratio of anterior shear force component to compression force component is 0.44 (SD 0.19), while the inferior glenohumeral ratio exceeds 0.69 (SD 0.31), thereby representing the largest ratio of inferior shear force component to compression force component (Figure 5.4 B).

Table 5.4: Glenohumeral contact forces for 26 functional activities of daily living as predicted by the UK National Shoulder Model using anthropometric scaling of ten subject-specific shoulder models with consideration of passive glenohumeral concavity compression. Data are presented as mean and standard deviation (SD).

	Glenohumeral Contact Force [%BW]	Ratio of glenohumeral superior (+) – inferior (-) shear to compression force	Ratio of glenohumeral posterior (+) – anterior (-) shear to compression force
Reach back of head	36 (SD 9)	0.15 (SD 0.07)	-0.25 (SD 0.11)
Lift block to head height	49 (SD 16)	0.14 (SD 0.05)	-0.39 (SD 0.12)
Lift block to shoulder height	45 (SD 13)	0.12 (SD 0.04)	-0.36 (SD 0.15)
Brush left side of head	33 (SD 15)	0.13 (SD 0.07)	-0.38 (SD 0.16)
Clean back	39 (SD 13)	-0.54 (SD 0.27)	-0.15 (SD 0.06)
Drink from mug	30 (SD 10)	0.09 (SD 0.03)	-0.11 (SD 0.05)
Eat with hand	25 (SD 7)	0.12 (SD 0.05)	-0.13 (SD 0.06)
Eat with spoon	30 (SD 7)	0.08 (SD 0.02)	-0.14 (SD 0.07)
Lift shopping bag from floor	55 (SD 16)	-0.33 (SD 0.14)	-0.23 (SD 0.11)
Lift shopping bag on lap	62 (SD 19)	-0.26 (SD 0.12)	-0.22 (SD 0.12)
Reach opposite axilla	24 (SD 10)	0.17 (SD 0.09)	-0.40 (SD 0.24)
Perineal care	27 (SD 15)	-0.55 (SD 0.32)	-0.24 (SD 0.10)
Reach far ahead	53 (SD 24)	0.18 (SD 0.07)	-0.39 (SD 0.15)
Sit to stand	155 (SD 64)	0.39 (SD 0.18)	-0.42 (SD 0.17)
Driving slow right	34 (SD 11)	0.04 (SD 0.02)	-0.22 (SD 0.10)
Driving slow left	44 (SD 13)	0.05 (SD 0.03)	-0.20 (SD 0.07)
Driving fast right	32 (SD 8)	0.02 (SD 0.01)	-0.17 (SD 0.05)
Driving fast left	48 (SD 17)	0.08 (SD 0.04)	-0.24 (SD 0.09)
Extreme	49(SD 25)	-0.69 (SD 0.31)	-0.34 (SD 0.15)
Pick and place	54 (SD 26)	0.53 (SD 0.22)	-0.50 (SD 0.24)
Pull	58 (SD 17)	-0.51 (SD 0.23)	-0.16 (SD 0.07)
Push	55 (SD 21)	-0.53 (SD 0.20)	-0.17 (SD 0.07)
Abduction slow	56 (SD 15)	0.27 (SD 0.09)	-0.22 (SD 0.07)
Abduction fast	54 (SD 18)	0.28 (SD 0.14)	-0.19 (SD 0.08)
Flexion slow	53 (SD 16)	0.14 (SD 0.05)	-0.17 (SD 0.06)
Flexion fast	50 (SD 13)	0.14 (SD 0.06)	-0.13 (SD 0.05)

The glenohumeral contact forces for feeding tasks are below 30% BW (SD 10%). The glenohumeral ratios during these activities are small ranging between 0.11 (SD 0.05) and 0.14 (SD 0.07) for the anterior ratio, while the superior glenohumeral ratio ranges from 0.08 (SD 0.02) to 0.12 (SD 0.05). In contrast, the glenohumeral contact forces for tasks involving personal hygiene are below 36% BW (SD 13), with anterior glenohumeral ratios exceeding 0.24 (SD 0.10) (Figure 5.4 C).

The glenohumeral contact forces during the 'driving' activity range from 32% (SD 8%) to 48% BW (SD 17%). The ratio of anterior shear force component to compression force component does not exceed

0.24 (SD 0.09), while the superior glenohumeral ratio is below 0.08 (SD 0.04), thereby representing the lowest ratio from the 26 activities of daily living (Figure 5.4 D).

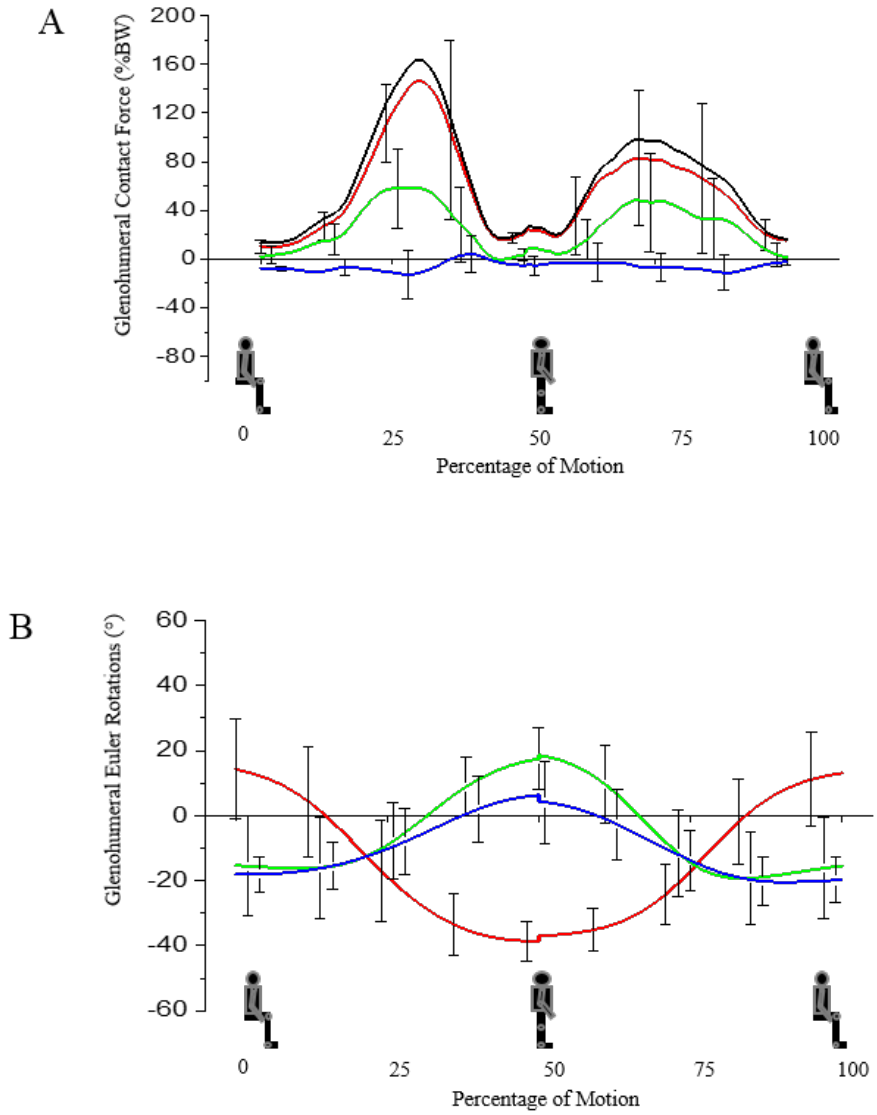

Figure 5.3: (A) Glenohumeral contact forces and (B) glenohumeral Euler rotations during 'sit to stand' activity. (A) The solid line represents the total joint contact force. The dotted line represents the joint compressive force, the dashed line represents superior (+) – inferior (-) shear, the dashed and dotted line represents posterior (+) – anterior (-) shear. (B) The dotted line represents (+) flexion, the dashed line represents (+) abduction and the dashed and dotted line represents (+) external rotation. Bars represent standard deviations.

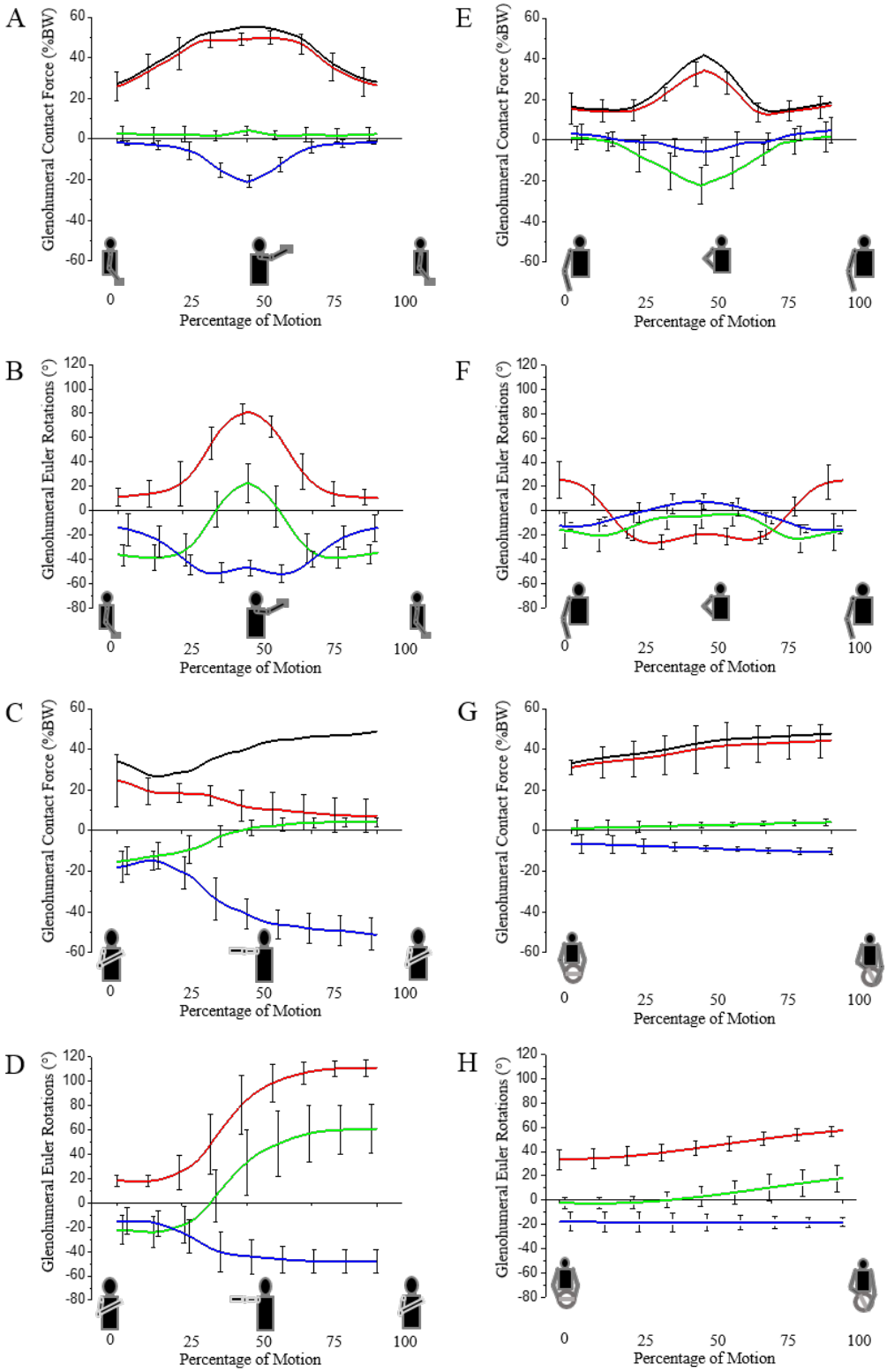

Figure 5.4: Glenohumeral contact forces during (A) 'Lifting block to head height', (C) 'Reaching across the body', (E) 'Cleaning back', (G) 'Drive fast left'. The solid line represents the total joint contact force. The red line represents the joint compressive force, the green line represents superior (+) – inferior (-) shear, the blue line represents posterior (+) – anterior (-) shear. Glenohumeral Euler rotations during (B) 'Lifting block to head height', (D) 'Reaching across the body', (F) 'Cleaning back', (H) 'Drive fast left'. The red line represents (+) flexion, the green line represents (+) abduction and the green line represents (+) external rotation. Bars represent standard deviations.

5.4 Discussion

This study has utilised anthropometric scaling of ten subject-specific versions of the UK National Shoulder Model with consideration of glenohumeral concavity compression in order to accurately quantify shoulder loading during essential functional daily activities. The summary of results in Table 5.4 demonstrates small, non-significant differences to those results in the appendix in Table A2.1 and Table A2.2, representing the results for the generic UK NSM as described in Section 2.3.1.2 (Charlton & Johnson 2006) as well as the generic UK NSM with integration of passive glenohumeral concavity compression as described in Chapter 3. The comparison of estimations for glenohumeral loading during functional daily activities shows that the inclusion of the labral contribution to joint stability has decreased the shear forces and thus the superior-inferior and posterior-anterior stability ratios in Table 5.4 and Table A2.2, when compared to Table A2.1. In addition, the customisation of shoulder modelling has by trend further decreased the predictions of glenohumeral loading during functional daily activities, which may reduce the differences between predictions from musculoskeletal shoulder models and instrumented shoulder implants, with estimations from computational shoulder models generally being overestimated (Nikooyan et al. 2010; Bergmann et al. 2007; Pandis et al. 2015). Therefore, the technical improvement of the UK NSM through subject-specific modelling with consideration of passive glenohumeral concavity compression has improved model reliability. Although this improvement in glenohumeral loading is non-significant as presented in this Chapter, these small alterations in glenohumeral loading due to technical modifications of the UK NSM may be essential for clinical applications, namely rehabilitation planning and shoulder arthroplasty design, as well as for surgical recommendations as described in Chapter 6 and 7.

Glenohumeral contact forces to aid implant design

In this chapter, glenohumeral compressive and shear forces during 26 functional activities of daily life were analysed to provide detailed insight into the loading of the joint. The results show that substantial loads are exerted across the joint even during basic activities of daily living (Table 5.4), with the joint force mainly being generated through contraction of shoulder muscles including the deltoid, pectoralis, latissimus dorsi, supraspinatus and infraspinatus. Although the findings of this study cannot be validated directly, they are in agreement with instrumented implant measurements as well as predictions from other musculoskeletal shoulder models that were validated against these measurements (van Drongelen et al. 2006; Bergmann et al. 2007; Westerhoff et al. 2009; Nikooyan et al. 2010). The peak glenohumeral contact forces for activities such as driving slow/fast as well as abduction (fast) and flexion (fast) were measured by Bergmann et al. (2007) as ranging between 40% BW and 57% BW, while our study computes joint forces between 33% BW (SD 9%) and 56% BW (SD 15%). Charlton and Johnson (2006) estimated peak glenohumeral forces to range from 23% to 75% BW for 10 functional activities including feeding, personal hygiene and lifting everyday objects, with results of this study predicting a

range of 24% BW (SD 9) to 62% BW (SD 24) for these functional daily activities. The small differences between data from this study (young healthy volunteers) and instrumented implant measurements (elderly participants) may be explained by kinematic differences.

The findings of this study demonstrate substantial shear forces on the glenoid plane during functional activities of daily life. The largest ratios of shear to glenohumeral compression force are computed for activities such as reaching across the body (0.53; SD 0.20), picking and placing everyday objects (0.53; SD 0.2), pulling and pushing (0.81; SD 0.33), sitting and standing (0.51; SD 0.21) as well as cleaning the back (0.54; SD 0.27). These results suggest that glenohumeral shear forces are substantial not only when high loads act at long lever arms but also at high angles of arm elevation (Figures 5.3 and 5.4).

The shear forces presented in this study are comparable to the study of Anglin et al. (2000) that presented shear forces of 15% to 40% BW for demanding, functional daily activities such as walking with a cane, lifting a 5 kg box with hands from the floor to shoulder height and lifting a 10 kg suitcase laterally. The direction of the contact force on the glenoid as quantified in this study corresponds to findings by Anglin et al. (2000), demonstrating loading of the antero-superior quadrant. Similarly, loading of the superior glenoid during arm elevation is consistent with Karlsson and Peterson 1992, Poppen and Walker 1978 and van der Helm 1994. Differences between individual studies may be based kinematic differences due to large variability in subject characteristics and joint angles.

The detailed understanding of glenohumeral contact forces and loading directions during essential functional activities of daily living as provided in this study will allow preclinical test procedures for shoulder arthroplasties to be improved in order to improve implant design and fixation with off-centre loading, where this is the major cause of glenoid loosening (Geraldes et al. 2017). The existing guidelines for preclinical testing are based on the study by Anglin et al. (2000), with findings from this study allowing improvements in testing protocols based on shear forces for essential functional activities of daily life that partly exceed the range of shear forces as presented by Anglin et al. (2000).

Glenohumeral contact forces to aid rehabilitation planning

The precise understanding of glenohumeral compressive and more importantly glenohumeral shear forces during essential functional activities of daily life will aid rehabilitation planning and allow advice to be given to patients about safe activities in order to avoid joint overloading post Bankart repair as described in Chapter 2.2.4. The existing rehabilitation guidelines following an anterior stabilisation aim to optimise the healing of the Bankart repair and capsuloligamentous structures while controlling pain and reducing immobilisation times to reduce muscle atrophy (McDermott et al. 1999; Bottoni et al. 2002; Kibler et al. 2001). Therefore, patients are advised to keep the arm in a sling for 6 weeks post-surgical intervention with exceptions being made for basic tasks such as feeding and personal hygiene (Dines & Levinson 1995). The data presented in this study demonstrate that the ratios of anterior shear

to glenohumeral compressive force are low, ranging between 0.11 (SD 0.05) and 0.15 (SD 0.06), while the inferior glenohumeral ratios range from 0.08 (SD 0.02) to 0.12 (SD 0.05). Consequently, the findings of this study provide scientific support for current rehabilitation guidelines regarding feeding tasks; this scientific evidence gives credence to clinical advice given, with the potential to reduce patients' fear and anxiety relating to re-injury and thereby improving confidence in performing activities of daily living.

In contrast to feeding tasks, the glenohumeral ratios for functional activities of daily life such as perineal care, cleaning back and reaching opposite axilla range between 0.15 (SD 0.06) and 0.24 (SD 0.10) and between 0.17 (SD 0.09) and 0.54 (SD 0.27) for anterior and superior ratios respectively. These data suggest that tasks of personal hygiene put a higher demand on a Bankart repair. In fact, clinically, after shoulder stabilisation procedures patients report difficulty reaching to the opposite axilla to clean with the operated arm (Dawson et al. 1996). The data in this study may help to explain why. The inferior and anterior shear forces experienced during this movement have the potential to produce patient "apprehension" via proprioceptive feedback mechanisms from the joint and soft tissues (Dean et al. 2013a, 2013b). In turn this may produce protective muscle activity reducing range of motion in the more cautious patient post repair (Ginn & Cohen 2005).

The current rehabilitation guidelines following an anterior stabilisation recommend avoiding using arm rests while standing up or sitting down on a chair in order to avoid overloading the labral repair within 12 weeks post-surgical intervention (Murphy et al. 2013; Rubin & Kibler 2002). The data presented in this study provide scientific support for those guidelines as the anterior glenohumeral ratio during the sit-to-stand task amounts to 0.42 (SD 0.17), with large shear forces impairing the recovery process due to high stresses exerted onto the Bankart repair.

The clinical guidelines for rehabilitation post Bankart repair also recommend not driving (and, therefore, not steering a car) within 12 weeks post-surgery for the same loading related reasons. The findings of this study demonstrate that the glenohumeral ratios are much less high for the driving activity, ranging between 0.02 (SD 0.01) and 0.05 (SD 0.03) as well as 0.17 (SD 0.05) and 0.24 (0.09) for superior and anterior ratios. In fact, the shear forces during the driving task are amongst the lowest of all 26 functional activities of daily living. Therefore, the data presented in this study suggest that the driving task is much less demanding for an anterior stabilisation from a mechanical point of view than previously assumed. We acknowledge that the repetitive nature of the driving task might increase the demand on the Bankart repair and reduce the load required for overloading the repaired structure (Uhl et al. 2010). However, the effect of repetitive motions on the load of the Bankart repair is challenging to evaluate and the peak shear forces were obtained at large rotation angles of the steering wheel of 60°. Therefore, the results of this study provide an indication that the driving task is less demanding for a Bankart repair than recommended in rehabilitation guidelines.

Limitations of this study

This study presented in this chapter has several modelling limitations. First of all, the scapula kinematics for the ADL1 dataset was derived from regression equations rather than measured kinematics. However, given the moderate joint angles for a large number of those activities, the effect should be relatively small (Pandis et al. 2015). Secondly, not all functional activities of daily living were performed by the same participants. Thirdly, the glenohumeral compressive force is directed towards the mid-glenoid as the UKNSM does not account for humeral head translation. As the humeral head exhibits a small degree of *in-vivo* translation during functional daily activities (Nishinaka et al. 2008), the loading is not applied through the centre of the glenoid, which produces a torque around the glenoid-labral socket. As the articulating surface of the glenoid is rather shallow and translational movements are small (Howell et al. 1988), this effect is expected to be small. Finally, the presented shoulder loads can only be partly transferred between different age groups due to kinematic changes (Nikooyan et al. 2010), and the presented data are only valid in the glenoid coordinate system and will have to be transformed into the humeral frame when assessing humeral loading during functional activities of daily living. Despite these limitations, this is the first study to have analysed shoulder loading with consideration of the labral contribution to joint stability as described in Chapter 3.

5.5 Conclusion

This chapter analyses shoulder compression and shear forces during 26 functional activities of daily life utilising the anthropometric scaling of ten subject-specific versions of the UK National Shoulder Model as introduced in Chapter 4, with consideration of glenohumeral concavity compression as described in Chapter 3. The results demonstrate substantial loads through the shoulder with the contact force exceeding 50% of the body weight in 11/26 activities of daily living, while the ratio of glenohumeral shear to compression forces exceeds 0.5 in 6/26 functional activities. The loading of the joint is considerable not only when high loads act at long lever arms but also at high angles of arm elevation.

Chapter 6 will utilise the knowledge of *in-vivo* shoulder loading during functional daily activities in order to quantify the critical size of a glenoid osseous defect that necessitates bone-grafting, rather than a soft tissue stabilisation, in order to restore joint stability. This will be achieved through comparison of *in-vivo* shoulder shear forces during functional daily activities with joint dislocation forces of the glenoid that will be obtained using the subject-specific FE models of the shoulder as presented in Chapter 3.

Chapter 6

Critical size of a glenoid defect causing anterior shoulder instability post Bankart repair under physiological joint loading.

The outcomes of surgical treatment of recurrent anterior shoulder instability with arthroscopic Bankart repair in patients with large glenoid osseous defects are inferior to those of patients undergoing treatment of osseous defects with bone-grafting. The rationale for not performing bone grafts on all patients with glenoid defects include concerns related to complication rates, long term sequelae and surgical learning curves. Therefore, the aim of this chapter is to determine the critical size of an anterior and anteroinferior glenoid osseous defect that leads to anterior shoulder instability post Bankart repair under physiological joint loading in order to assist clinical decision making.

This work was submitted in part for peer review publication, entitled 'Critical size of a glenoid defect causing anterior shoulder instability post Bankart repair under physiological joint loading', with authors: Christian Klemt, Daniel Nolte, Erica Di Federico, Peter Reilly and Anthony MJ Bull.

6.1 Introduction

As described in Section 2.2.2, glenoid osseous defects are commonly associated with recurrent anterior shoulder dislocation with the prevalence of fracture or erosion of the glenoid rim being reported to range from 8% (18 of 226) to 73% (116 of 158) of shoulders with recurrent anterior instability (Boileau et al. 2006; Hovelius et al. 1983; Norlin 1994). As osseous defects may result in a loss of glenoid concavity, the shoulder becomes unstable in the mid-range of motion where stability is achieved through compression of the humeral head into the glenoid labral socket through rotator cuff muscle co-contraction (Lazarus et al. 1996; Lee et al. 2000). Biomechanical studies have demonstrated an inverse relationship between the size of the defect and shoulder stability: the larger the osseous defect, the less stable the shoulder (Itoi et al. 2000; Yamamoto et al. 2009, 2010).

The outcomes of surgical treatment of recurrent anterior shoulder instability with arthroscopic Bankart repair in patients with large glenoid osseous defects are inferior to those of patients undergoing treatment of osseous defects with bone-grafting (Boileau et al. 2006; Chen et al. 2005; Lafosse et al. 2007; Min et al. 2018). The rationale for not performing bone grafts on all patients with glenoid defects include concerns related to complication rates, long term sequelae and surgical learning curves (Bonnevialle et al. 2018; Kim et al. 2002; Owens et al. 2011; Rollick et al. 2017). Therefore, defining the critical bone lesion size under loading conditions expected by the patient during functional daily activities will assist clinical decision making (Amirthanayagam & Emery 2014; Ohl et al. 2012).

From surgical findings, glenoid osseous defects have been described to be located at the anteroinferior glenoid rim (Lo et al. 2004; Lazarus et al. 1996; Gerber & Nyffeler 2002). However, recent imaging studies have demonstrated that these lesions may be located anteriorly, at approximately the three o'clock position on a right shoulder (Griffith et al. 2003; Saito et al. 2005). Currently, only three biomechanical studies from one group have quantified the critical size of an anterior and anteroinferior glenoid osseous defect that necessitates bone-grafting (Itoi et al. 2000; Yamamoto et al. 2009a, 2010). These studies found that for both an anterior and anteroinferior glenoid osseous defect of width 6 mm, corresponding to 19-21% of the glenoid length, a Bankart repair is insufficient to maintain shoulder stability and that joint stability through concavity compression is restored after reconstruction of the glenoid concavity by bone-grafting. Clinical guidelines have taken these data to recommend that glenoid osseous defects corresponding to 19-21% of the glenoid length are indicated for bone-grafting (Bigliani et al. 1996; Warner, 2006).

The results above are derived from physical cadaveric experiments and suffer from limitations, including non-physiological loading conditions involving a maximum joint load of 50 N, where *in-vivo* data from instrumented shoulder implant measurements have demonstrated 151% body weight loading during activities of daily living (Bergmann et al. 2007). As the stability of the shoulder is load dependent, with higher joint forces leading to a loss in stability, the use of physiological loading

conditions is an essential requirement for the assessment of joint stability (Halder et al. 2001; Lippitt et al. 1993).

Finite Element modelling represents an efficient method to overcome this limitation of cadaveric studies and to simulate experimental testing under *in-vivo* loading conditions. Therefore, the aim of this study was to determine the critical size of an anterior and anteroinferior glenoid osseous defect that leads to anterior shoulder instability post Bankart repair under physiological loading conditions in order to aid surgical decision-making for patients with recurrent anterior shoulder instabilities.

6.2 Materials and Methods

Development of an Intact Finite Element Model

Detailed information about the development and validation of two subject-specific finite element models of the shoulder is provided in Chapter 3. Briefly, two right shoulder geometries were obtained from high-resolution physical slices of the male and female Visible Human datasets (Ackerman 2017). The glenoid fossa at the lateral angle of the scapula, the proximal humerus, the articulating cartilage surfaces as well as the glenoid labrum were manually segmented using Mimics (Mimics Research 17.0, Materialise, Leuven, Belgium). The segmented structures were converted to triangular surface meshes to form a 3-dimensional model of the intact shoulder. Local coordinate systems were assigned to the articulating structures to position and orient the humerus with respect to the glenoid fossa (Wu et al. 2005). The surface meshes were imported into Finite Element (FE) analysis software (Marc Mentat 2015, MSC.Software, Palo Alto, USA). The articulating bones, the articular cartilage surfaces and the glenoid labrum were modelled as tetrahedral solid elements. The glenoid labrum was divided into eight sections in order to obtain an anatomically accurate representation of the tissue (Smith et al. 2008, 2009). Each labral section was assigned a coordinate frame to define the local fibre orientation (Gatti et al. 2010).

Baseline material properties for each structure of the shoulder were assigned based on literature values (Table 6.1; Büchler et al. 2002; Smith et al. 2008; Terrier et al. 2007). Due to relatively small deformations compared to other soft tissues, the articulating bones were modelled as rigid. The articular cartilage surfaces were assigned linear elastic isotropic properties (Büchler et al. 2002), while the labrum was modelled as a transversely isotropic hyperelastic material due to the modulus difference in the transverse plane and the circumferential direction (Smith et al. 2008, 2009). The material coefficients for the hyperelastic model were obtained by applying the neo-Hookean constitutive equation to experimentally derive material properties for each labral section (Quapp & Weiss 1998).

Table 6.1: Baseline material properties for the finite element model of the glenohumeral joint (as used in Chapter 3). E = Young's Modulus, υ = Poisson's Ratio, C_{1-8} = Hyperelastic Labral Coefficients.

Anatomy	Material Type	Parameter	Value	Reference
Humerus	Rigid	-	-	Terrier et al. 2007
Humeral Cartilage	Isotropic Elastic	E υ	10 MPa 0.4	Büchler et al. 2002
Glenoid	Rigid	-	-	Terrier et al. 2007
Glenoid Cartilage	Isotropic Elastic	E υ	10 MPa 0.4	Büchler et al. 2002
Labrum	Transversely Isotropic Hyperelastic	C_1 C_2 C_3 C_4 C_5 C_6 C_7 C_8	3.4 5.4 7.0 5.9 5.2 4.8 5.7 4.3	(C. D. Smith et al., 2008, 2009)

The interfaces between the articulating cartilage surfaces and between the humeral cartilage and the labrum were modelled using frictionless, surface-to-surface contact due to the low friction coefficient in synovial joints (Jones et al. 2015). The interfaces between the articulating bones and the corresponding cartilage surfaces were modelled using tied contact.

As presented in Chapter 3, the subject-specific FE models of the intact shoulder were validated against *in-vitro* measurements of glenohumeral stability as reported by two different cadaveric studies (Halder et al. 2001; Lippitt et al. 1993).

Development of Glenoid Osseous Defects

Glenoid osseous defects with a width of 2 mm, 4 mm, 6 mm and 8 mm were created separately at the anterior and anteroinferior glenoid rim, representing 8%, 14%, 20% and 26% of the glenoid length respectively, in order to replicate the testing employed by three cadaveric studies from the literature (Figure 6.1, Figure 6.2; Itoi et al. 2000; Yamamoto et al. 2009, 2010). The anterior osteotomy lines were drawn parallel to the line passing through superior and inferior contact points of the circumcircle that fits the superoinferior diameter of the glenoid, with the 0 mm osteotomy line being tangential to the anterior rim of the glenoid (Yamamoto et al. 2010). The anteroinferior osteotomy lines were simulated by lines that were inclined by 45° from the longitudinal axis of the glenoid which was obtained by fitting an outer circle to the superoinferior glenoid diameter (Itoi et al. 2000). The 0 mm anteroinferior osteotomy line was defined as being tangential to the anteroinferior glenoid rim. The glenoid osseous defects were introduced into the FE models by removing finite elements of the glenoid

fossa and the glenoid articular cartilage that correspond to each osteotomy line. The structural integrity of the glenoid labrum was preserved during the creation of the osseous defects.

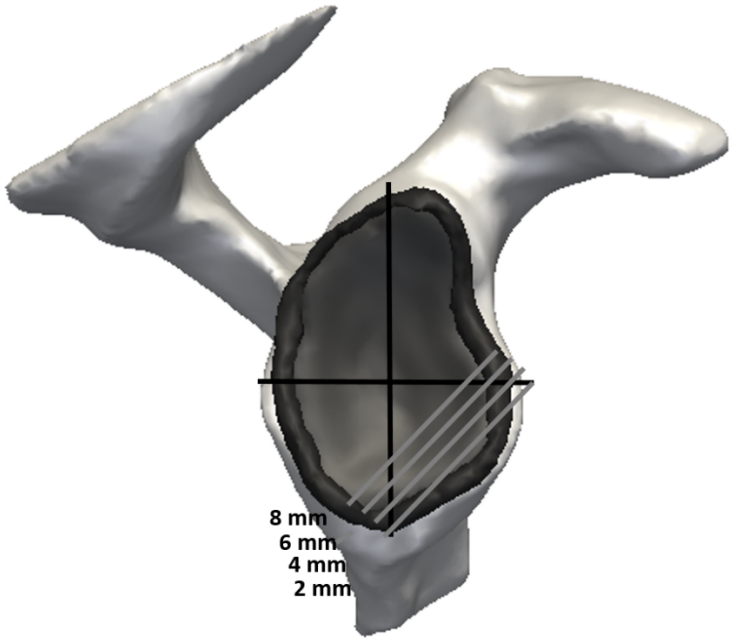

Figure 6.1: Simulated anteroinferior osteotomy lines, 2 mm through 8 mm, which were drawn at an inclination of 45° from the longitudinal axis of the glenoid. The glenoid defects with width of 2 mm, 4 mm, 6 mm and 8 mm correspond to 8%, 14%, 20% and 26% of the glenoid length respectively.

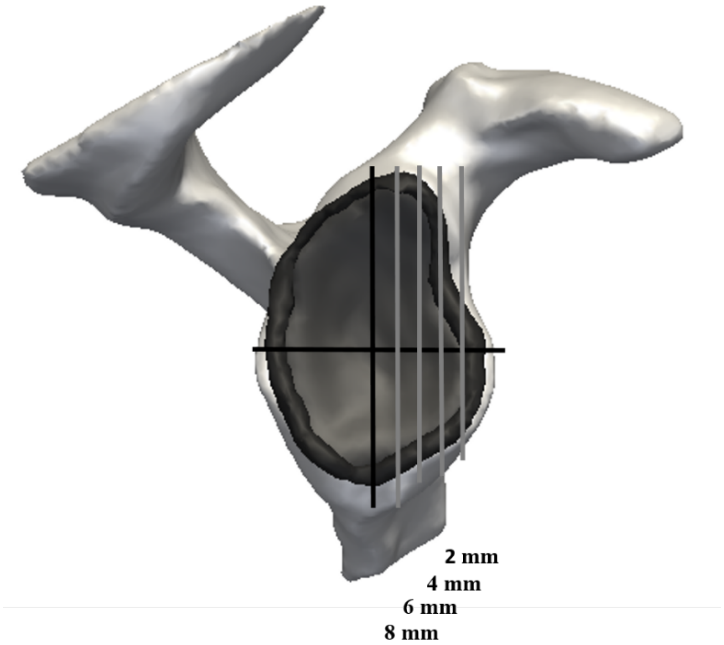

Figure 6.2: Simulated anterior osteotomy lines, 2 mm through 8 mm, which were drawn parallel to the longitudinal axis of the glenoid. The glenoid defects with width of 2 mm, 4 mm, 6 mm and 8 mm correspond to 8%, 14%, 20% and 26% of the glenoid length respectively.

A soft tissue Bankart repair was simulated through attachment of the labrum to the osteotomy line, re-establishing the level of glenoid concavity. This was achieved by displacing the medial surface nodes of the labrum towards the osteotomy line until the labrum was fully aligned and lifted to the level of the osteotomy line. The medial nodes of the glenoid labrum were fixed in that position during further simulations assessing joint stability, in order to model labral healing and reattachment of the labrum onto the glenoid rim. The labral reattachment onto the glenoid rim was modelled with tied contacts between glenoid and labrum.

The other parts of the intact FE models, including mesh density, material properties, contact definitions and loading conditions, were not changed.

Validation of a Finite Element Model with Glenoid Osseous Defect

The FE models of the shoulder with glenoid osseous defects were validated against *in-vitro* measurements of anterior shoulder stability (Yamamoto et al. 2009). For the validation study, the humerus was positioned in the shoulder dislocation position with 45° of abduction and 35° of external rotation. The boundary conditions of the FE models were chosen to replicate cadaveric experiments (Itoi et al. 2000; Yamamoto et al. 2009, 2010). In the starting position, the humeral head was in contact with and centred on the glenoid socket. With the glenoid surface being fixed in all degrees of freedom during the simulation, the boundary conditions involved the application of a 50 N compressive force through the centre of the humeral head, perpendicular to the plane of the glenoid articulating surface, in order to simulate the joint loading as applied in the cadaveric studies. Under permanent joint compression, the humeral head was subsequently translated towards the anteroinferior glenoid rim until dislocation occurred. The maximum force required to dislocate the shoulder was defined as the dislocation force. The dislocation forces were determined for the intact glenoid and after introducing both, anterior and anteroinferior glenoid osseous defects, with defects widths of 2 mm, 4 mm, 6 mm and 8 mm, corresponding to 8%, 14%, 20% and 26% of the glenoid length respectively.

Quantifying the Critical Size of a Glenoid Osseous Defect

The critical size of an anterior and anteroinferior glenoid osseous defect was investigated during 26 functional daily activities by determining the dislocation forces of the intact glenoid and after creating 2-8 mm anteroinferior osseous defects, corresponding to 8-26% of the glenoid length. For each functional activity that was simulated, the dislocation forces were determined in the joint position most susceptible to instability (see Table A3.1 in Appendix A3) where the ratio of shear to joint compression force was maximum, and under loading conditions that are representative of *in-vivo* shoulder. The shoulder dislocation forces were compared to *in-vivo* shoulder shear forces during functional daily activities (ADL) as quantified by the UK National Shoulder Model (UK NSM) in Chapter 5 using anthropometric scaling of 10 subject-specific shoulder models with consideration of glenohumeral

concavity compression. Each ADL was classified for each glenoid defect size as stable (dislocation force of the glenoid is larger than the *in-vivo* shear force of the ADL) or unstable (dislocation force of the glenoid is smaller than the *in-vivo* shear force of the ADL). The critical size of an osseous defect was quantified as the smallest osseous defect size that leads to shoulder dislocation across all functional daily activities (Figure 6.3). Statistical significance was tested through a non-parametric Mann-Whitney test using SPSS (SPSS 24.0, IBM Corporation, New York, United States of America).

The critical lesion size of an anterior and anteroinferior glenoid osseous defect that leads to anterior shoulder instability under physiological joint loading was additionally computed using the glenohumeral joint contact force predictions of the generic UK NSM (Charlton & Johnson 2006) as described in Section 2.3.1 as well as the generic UK NSM with integration of passive glenohumeral concavity compression, with those results from Chapter 5 being presented in Appendix A2 in Table A2.1 and Table A2.2. The comparison of these results will allow the assessment of the clinical importance of the modifications made to the UK NSM as described in Chapters 3 and 4.

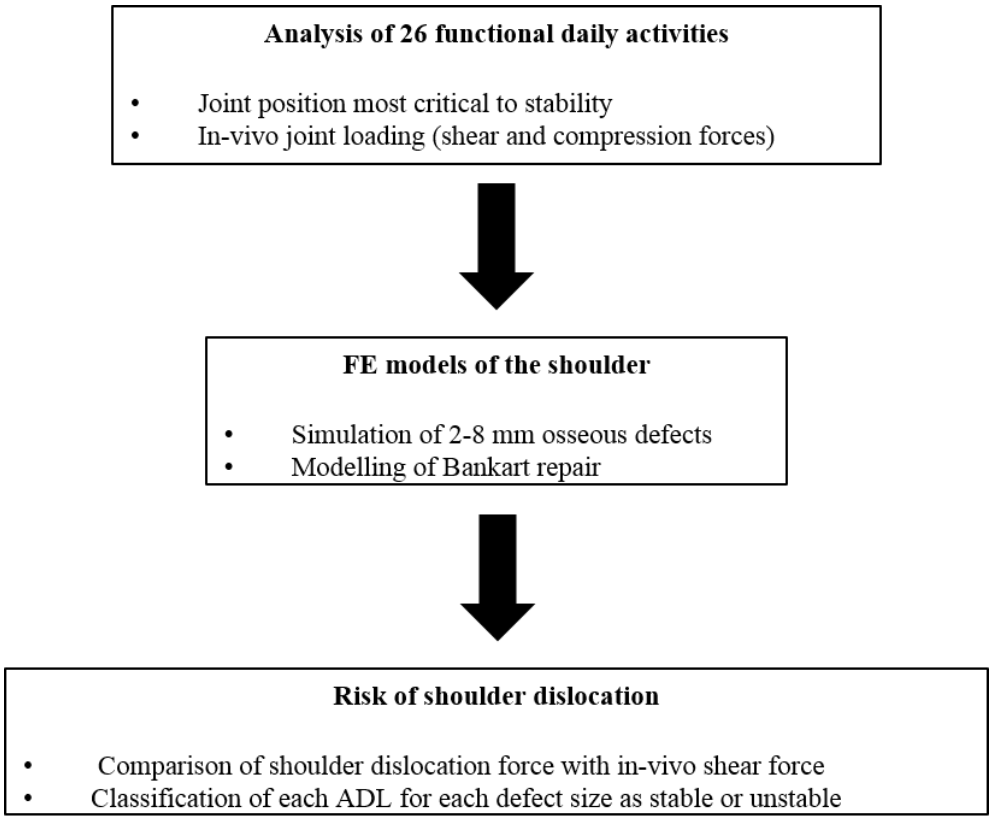

Figure 6.3: Overview of the study design.

6.3 Results

In agreement with cadaveric experiments, the dislocation forces determined by the male and female FE model demonstrate a decrease in shoulder stability with increasing size of the glenoid osseous defect. The dislocation forces quantified by the FE models compare well to those experimentally measured in the anterior direction, with model predictions being within one standard deviation of experimental values (Figure 6.4; Itoi et al. 2000; Yamamoto et al. 2009, 2010).

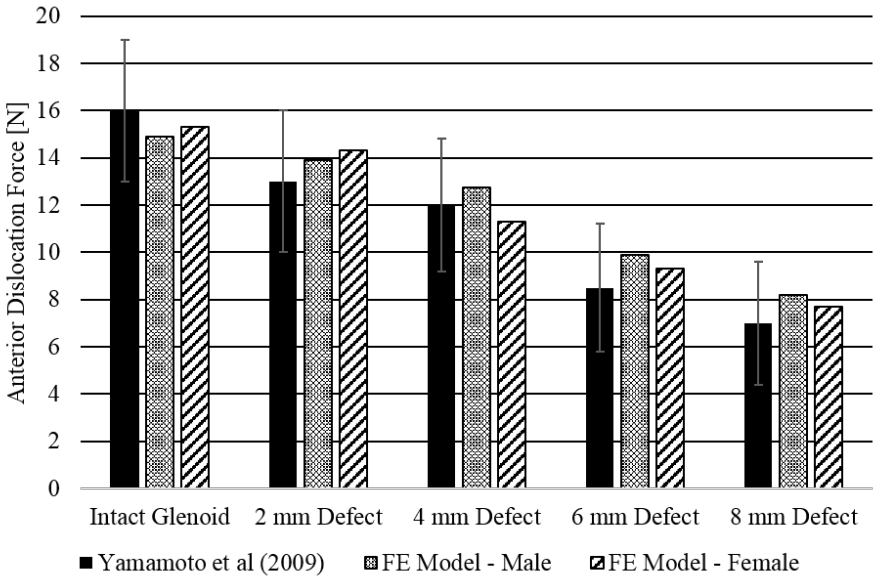

Figure 6.4: Anterior dislocation forces of the shoulder for the intact glenoid and with 2 mm, 4mm, 6 mm and 8 mm anterior glenoid osseous defects. The bars represent one standard deviation from in-vitro values. The glenoid defects with width of 2 mm, 4 mm, 6 mm and 8 mm correspond to 8%, 14%, 20% and 26% of the glenoid length respectively.

The classification of all ADLs with respect to joint stability for each glenoid osseous defect size is shown in Tables 6.2 and 6.3. These results are based on the UK NSM using anthropometric scaling of ten subject-specific shoulder anatomies with consideration of the glenohumeral concavity compression, while the corresponding classifications for the predictions of the generic UK NSM as described in Section 2.3.1 (Charlton and Johnson 2006) and the generic UK NSM with integration of passive glenohumeral concavity compression can be found in Appendix A3 in Table A3.2, A3.3, A3.4 and A3.5. This comparison is provided to demonstrate the effect of technical modifications to the UK NSM as described in Chapter 3 and 4, on clinical recommendations.

Table 6.2: Classification of each anterior glenoid osseous defect size for each ADL as unstable (dark grey) or stable (white), with the shear force predictions being obtained from the UK NSM using anthropometric scaling of ten subject-specific shoulder models with consideration of passive glenohumeral concavity compression. The glenoid defects with width of 2 mm, 4 mm, 6 mm and 8 mm correspond to 8%, 14%, 20% and 26% of the glenoid length respectively.

	Anterior Glenoid Osseous Defect				
	Intact	2 mm	4 mm	6 mm	8 mm
Lift Block to Head Height					
Lift Block to Shoulder Height					
Extreme (Reach Across Body)					
Pick and Place					
Reach far Ahead					
Reach Opposite Axilla					
Brush Left Side of Head					
Clean Back					
Reach Back of Head					
Drive Slow Right					
Drive Slow Left					
Drive Fast Left					
Slow Flexion					
Lift Shopping Bag on Lap					
Drive Fast Right					
Sit to stand					
Lift Shopping bag from Floor					
Fast Abduction					
Fast Flexion					
Slow Abduction					
Pull					
Push					
Perineal care					
Eat with Hand					
Drink from Mug					

Table 6.3: Classification of each anteroinferior glenoid osseous defect size for each ADL as unstable (dark grey) or stable (white), with the shear force predictions being obtained from the UK National Shoulder Model using anthropometric scaling of ten subject-specific shoulder models with consideration of passive glenohumeral concavity compression. The glenoid defects with width of 2 mm, 4 mm, 6 mm and 8 mm correspond to 8%, 14%, 20% and 26% of the glenoid length respectively.

	Anteroinferior Glenoid Osseous Defect				
	Intact	2 mm	4 mm	6 mm	8 mm
Pick and Place					
Clean Back					
Pull					
Push					
Sit to stand					
Reach Opposite Axilla					
Extreme (Reach Across Body)					
Lift Shopping bag from Floor					
Lift Block to Head Height					
Lift Block to Shoulder Height					
Lift Shopping Bag on Lap					
Perineal care					
Reach far Ahead					
Brush Left Side of Head					
Reach Back of Head					
Drive Slow Left					
Drive Slow Right					
Drive Fast Left					
Drive Fast Right					
Slow Flexion					
Slow Abduction					
Fast Flexion					
Fast Abduction					
Eat with Hand					
Drink from Mug					

There is a distinct difference in shoulder stability during ADLs between the anterior and anteroinferior direction, with the shoulder being less stable ($p = 0.01$) in the anterior direction when compared to the anteroinferior direction. The FE models estimate the critical size of an anterior glenoid osseous defect that leads to anterior shoulder instability post Bankart repair to be of width 2 mm, corresponding to 8% of the glenoid length. There are 3 loading conditions with high anterior shear forces such as lifting a block to head and shoulder height as well as reaching across the body that demonstrate a high likelihood of instability for the glenoid with a 2 mm anterior osseous defect (Table 6.2). Activities of daily living including picking and placing an everyday object, cleaning the lower back, lifting a shopping bag on the lap and driving show additionally a high risk of instability for the glenoid with an anterior osseous defect of width 4-6 mm, corresponding to 14-20% of the glenoid length. There are 10 ADLs such as eating, drinking and pulling/pushing that affect joint stability only for large anterior osseous defects with a width of greater than 8 mm.

The classification of all ADLs with respect to joint stability for each anteroinferior glenoid osseous defect size is shown in Table 6.3. The critical size of an anteroinferior glenoid defect that leads to anterior shoulder instability post Bankart repair under physiological joint loading was predicted by the FE models to be of width 4 mm, representing 14% of the glenoid length. There are 2 loading conditions with high anteroinferior shear forces such as picking and placing an object and cleaning the lower back body that demonstrate a high likelihood of instability for the glenoid with a 4 mm anteroinferior osseous defect (Table 6.3). Activities of daily living including pulling and pushing, lifting a shopping bag on the lap, reaching the opposite axilla and standing up and sitting down show additionally a great risk of instability for the glenoid with a 6-8 mm anteroinferior osseous defect, representing 20-26% of the glenoid length respectively. There are 14 ADLs including eating, drinking and driving that affect joint stability only for anteroinferior osseous defects of width greater than 8 mm.

6.4 Discussion

In this study, two FE models of the shoulder with glenoid osseous defects were validated against *in-vitro* measurements of shoulder stability, with these values being only reported in the direction (Yamamoto et al. 2009). The dislocation forces predicted by the FE models were within one standard deviation of experimentally measured values. The validated FE models quantified the critical size of an anterior and anteroinferior glenoid osseous defect that leads to anterior shoulder instability post Bankart repair under physiological loading conditions to be a width of 2 mm and 4 mm respectively, representing 8% and 14% of the glenoid length. This modelling study suggests that if there is an

osseous defect of such size, the glenoid concavity needs to be reconstructed to ensure joint stability through concavity compression.

Previous biomechanical studies showed that 6 mm glenoid osseous defects, corresponding to 19-21% of the glenoid length, were required to produce a significant loss in anterior shoulder stability; these results have clinically been used as an indication for bone-grafting to restore joint stability (Bigliani et al. 1998). However, these *in-vitro* experiments were conducted under non-physiological loading conditions (Itoi et al. 2000; Yamamoto et al. 2009, 2010). As the stability of the shoulder is load dependent, with higher joint forces leading to a loss in stability, the results of the FE models here strongly suggest that smaller, 2-4 mm glenoid osseous defects, corresponding to 8-14% of the glenoid length, should be considered as an indication for bone-grafting. Despite the difference between findings from this study and results from previous cadaveric testing as well as clinical observations that report good clinical outcomes for patients with small osseous defects following Bankart repair (Hobby et al. 2007; Petrera et al. 2010; Speer et al. 1996), there are other recent studies in the literature suggesting that smaller glenoid osseous defects corresponding to 7-15% of the glenoid length should be considered as an indication for bone-grafting (Shin et al. 2016a, 2016b; Shin et al. 2017; Ghodadra et al. 2010; Shaha et al. 2015). Shin et al. (2017) determined the dislocation forces for anterior osseous defects of different magnitudes, demonstrating that anterior bone lesions corresponding to 7.5% of the glenoid length lead to a statistical decrease in joint stability. In a different study, Ghodadra et al. (2010) demonstrated significant increases in glenohumeral contact pressure following the creation of an anterior glenoid osseous defect corresponding to 15% of the glenoid length. In addition, Shaha et al. (2015) reported that a subcritical bone loss of 13.5% of the glenoid length led to unacceptable clinical patient outcomes following Bankart repair. Similar clinical observations were made by Milano et al. (2011) and Griffith et al. (2008), suggesting that the critical amount of bone loss may be smaller than previously reported for activities involving high shoulder loading or large ranges of motion. This suggestion is supported by data presented in this study, with functional daily activities involving large shoulder forces and great ranges of motion, such as reaching across the body and lifting a block to head height, leading to instability for glenoid osseous defects corresponding to 8-14% of the glenoid length, while the majority of functional daily activities is less critical to stability (Table 6.2, Table 6.3). Therefore, the results of this study support the notion that the critical size of a glenoid osseous defect may be smaller than previously reported. This is despite the fact that shear force predictions by MSK shoulder models tend to be slightly overestimated (Bergmann et al. 2007).

A novel factor in this study is the use of joint loading in terms of *in-vivo* shoulder contact forces (compressive and shear) that have been quantified by musculoskeletal modelling for a wide range of activities of daily living as presented in Chapter 5. The comparison of shear forces with the predicted glenoid dislocation forces allows for mechanical assessment of joint stability through classification

of each ADL as stable or unstable for each for each glenoid defect size. This mechanical assessment of joint stability represents the first approach of its kind.

This study utilises finite element analysis to quantify the critical size of a glenoid osseous defect that necessitates bone-grafting. A Bankart repair was simulated after creation of the osseous defects in order to reestablish glenoid concavity by reattaching the labrum to the osteotomy line. The use of FE analysis allowed the labrum to be precisely aligned and lifted to the level of the osteotomy line during the Bankart repair. The medial nodes of the labrum were fixed to the osteotomy line while the dislocation forces of the shoulder were determined in order to simulate labral healing and reattachment of the labrum to the glenoid rim (Zimmermann et al. 2016). This is the first approach to assess shoulder stability after labral healing, an aspect that cannot be fully addressed during *in-vitro* experiments with suture anchors alone. The consideration of labral healing in the assessment of shoulder stability through concavity compression is critical as the labral contribution to joint stability is between 10-20% (Halder et al. 2001; Lippitt et al. 1993).

This study has utilised anthropometric scaling of ten subject-specific shoulder models with consideration of glenohumeral concavity compression. The comparison of estimated critical lesion sizes for this version of the UK NSM as shown in Table 6.2 and Table 6.3 with those estimations from the generic UK NSM as described in Section 2.3.1 (Charlton & Johnson 2006) as well as the generic UK NSM with integration of concavity compression as shown in Tables A3.2, A3.3, A3.4 and A3.5 demonstrates small differences between predicted lesion sizes for individual activities. While the critical lesion size that necessitates bone-grafting to restore joint stability through concavity compression does not change between the three versions of the UK NSM, the change in unstable lesion sizes for individual activities illustrates the need for the technical improvements as described in Chapters 3 and 4, and demonstrates the significance of these technical modelling improvements in order to accurately aid the clinical decision-making process.

This study has limitations in that the anatomy of the glenoid osseous defects were idealised to being either parallel to the glenoid longitudinal axis and at 45° to the longitudinal axis for anterior and anteroinferior osseous defects respectively in order to replicate *in-vitro* experiments. This does not represent all *in-vivo* defects, but it has been demonstrated that the margin of a glenoid defect is linear in most cases (Griffith et al. 2003). Also, the defects were created in 2 mm increments, thus representing a different proportion of loss for scapulae of different sizes (Ohl et al. 2012). This has been partially taken into account in this study through the use of one large and one small scapula. In addition, the dislocation forces for each functional daily activity were determined in the joint position most susceptible to instability, without considering movement of the humeral head during arm motion. As the humeral head remains mainly centred on the glenoid fossa with humeral head

translations of only a few millimetres during functional daily activities (Nishinaka et al. 2008), the effect of this simplification is assumed to be small.
The stability provided by the bony articulating structures is only one stabilising mechanism of the shoulder. Other mechanisms such as the capsuloligamentous structures need to be considered in future studies (Bigliani et al. 1998). Therefore, the results presented here are representative only for the mid-range of shoulder motion where the capsuloligamentous structures are lax (O'Brien et al. 1990).

The results presented here are only based on the geometries of the Male and Female Visible human dataset and these would be more representative if more datasets would have been used. However, this would require high resolution physical slices or Magnetic Resonance Imaging (MRI) scans with small slice thickness in order to accurately delineate the structures of the glenohumeral joint. These data were unavailable. Despite this limitation, this is the first study to determine the critical size of an anterior and anteroinferior glenoid osseous defect that leads to anterior shoulder instability under physiological loading conditions. This represents a potential adjunct to surgical decision making, particularly in identifying glenoid bone defects on preoperative CT scans that may require grafting.

6.5 Conclusion

This chapter has quantified the critical size of an anterior and anteroinferior glenoid osseous defect that leads to anterior shoulder instability post Bankart repair under physiological loading conditions. Two finite element (FE) models of the shoulder with glenoid osseous defects were developed and validated against physical *in-vitro* measurements. This findings of this chapter provide evidence to explain why shoulder instability persists in some patients who have had Bankart repair only, and proposes bone grafting for a 2 mm anterior and 4 mm anteroinferior glenoid osseous defect in order to optimise joint stability through concavity compression.

Chapter 7 will utilise the validated subject-specific MSK shoulder models from Chapter 4, with prior knowledge of the labral contribution to joint stability as quantified in Chapter 3, to investigate the effect of biceps tenodesis on anterior shoulder stability in overhead throwing athletes in order to aid surgical decision-making for patients with SLAP II labral tears, an injury that may occur in anterior shoulder instability as described in Section 2.2.2.

Chapter 7

The effect of biceps tenodesis on glenohumeral stability in overhead throwing athletes.

The outcomes of surgical treatment of type II SLAP tears with biceps tenodesis are superior to those of patients undergoing arthroscopic SLAP repair. However, surgeons remain hesitant to perform biceps tenodesis on these athletes due to the lack of reported clinical outcomes for individual overhead throwing sports and associated concerns that some of these throwing sports may predispose the joint to instability. Therefore, the aim of this study is to assess the effect of biceps tenodesis on shoulder stability for major overhead throwing sports in order to aid sport-specific surgical decision-making for athletes with type II SLAP tear.

This work will be submitted in part for peer review publication, entitled 'The effect of biceps tenodesis on glenohumeral stability in overhead throwing athletes, with authors: Christian Klemt, Diana Toderita, Peter Reilly and Anthony MJ Bull.

7.1 Introduction

The superior glenoid labrum including the insertion of the long head of the biceps brachii is a common site of injury in overhead activities (Rokito et al. 2014; Michener et al. 2018), and this site may also be torn during episodes of recurrent anterior shoulder instability as described in Section 2.2. Superior labrum anterior-to-posterior (SLAP) tears have been reported to be present in as many as 26% of shoulder arthroscopies (Kim et al. 2003; Waterman et al. 2015). Type II SLAP lesions, which are characterised by superior labral fraying and a detached biceps tendon (Snyder et al. 1990), account for the majority of these SLAP tears (Bey et al. 1998; Brockmeyer et al. 2016; Nam & Snyder 2003). Although the exact cause of type II SLAP tears is not known, these lesions are frequently related to large traction of the superior glenoid labrum-biceps complex during traumatic events or repeated overhead activity (Wilk & Macrina 2013; Welton et al. 2017; Mileski & Snyder 1998; McFarland et al. 2002). Surgical treatment options include SLAP repair as well as biceps tenodesis, biceps tenotomy and arthroscopic debridement (Hsu et al. 2008; Paoli et al. 2018).

The treatment of type II SLAP lesions with arthroscopic debridement has yielded poor clinical outcomes (Altchek et al. 1992; Pagnani et al. 1995; Kim et al. 2002), thus arthroscopic SLAP repair is nowadays considered as gold-standard treatment (Erickson et al. 2016; Patterson et al. 2014). Good clinical outcomes have been reported for arthroscopically repaired type II SLAP lesions in 75% to 97% of published studies (Musgrave & Rodosky 2001; Rhee et al. 2005; Samani et al. 2001; Snyder et al. 1995; Boileau et al. 2009). However, overhead throwing athletes have reported less consistent functional outcomes, with clinical studies demonstrating a return to preinjury level of sport participation ranging from 22% to 75% (Fedoriw et al. 2014; Sayde et al. 2012; Smith et al. 2016; Kim et al. 2003; Ide et al. 2005). In contrast, treating type II SLAP tears in overhead throwing athletes with arthroscopic biceps tenodesis using an interference screw fixation has yielded improved clinical outcomes (Denard et al. 2014), with return rates to preinjury level of sport participation exceeding 80% in all published studies (Boileau et al. 2009; Chalmers et al. 2014; Ek et al. 2014).

These superior outcomes of arthroscopic biceps tenodesis in terms of pain and function, when compared to arthroscopic SLAP repair, have been associated with the absence of traction in the superior glenoid labrum-biceps complex following the surgical transfer of the long head of the biceps brachii from its anatomical position at the superior glenoid to the bicipital groove of the humerus (Boileau et al. 2009; Strauss et al. 2014). However, this may lead to a loss in joint stability, with previous biomechanical studies indicating that the long head of the biceps brachii may restrict anterosuperior humeral head translation (Itoi et al. 1994; Su et al. 2010; Warner and McMahon 1995; Youm et al. 2009) and thus assist the rotator cuff muscles to center the humeral head on the glenoid fossa through concavity compression (Lazarus et al. 1996; Lippitt & Matsen 1993). Although the precise contribution of the long head of the biceps brachii to glenohumeral stability is not completely established, even a small

biomechanical role of the long head of the biceps brachii to glenohumeral stability is likely to be important for high-speed athletic motions such as overhead throwing (Chalmers et al. 2014). Therefore, surgeons are hesitant to perform biceps tenodesis on overhead throwing athletes (Hurley et al. 2018; Patterson et al. 2014) due to concerns that the surgical transfer of the long head of the biceps brachii tendon away from its anatomical position may predispose the joint to instability, particularly in overhead throwing athletes with concominant rotator cuff pathology (Neri et al. 2011; Merolla et al. 2018).

Despite several studies being reported in the literature (Denard et al. 2014, Chalmers et al. 2014; Ek et al. 2014), there is no current knowledge of the effect of biceps tenodesis on shoulder stability for specific overhead throwing sports, with existing clinical studies only presenting clinical outcomes involving pain and joint functionality, which are additionally presented only for a mixture of overhead throwing sports (Chalmers et al. 2014; Denard et al. 2014; Ek et al. 2014), despite known differences in shoulder loading for different overhead throwing motions (Usman et al. 2011; Ramappa et al. 2010). Therefore, the aim of this study is to assess the effect of biceps tenodesis on shoulder stability for major overhead throwing sports in order to aid sport-specific surgical decision-making for athletes with type II SLAP tears.

7.2 Materials and Methods

Study Participants

Thirteen healthy right-handed volunteers (10 males, 3 females; height 1.69 ± 0.10 m, body mass 68.5 ± 18.2 kg; age 26.4 ± 4.7 years) with no history of shoulder pathology participated in this study. Informed consent was obtained from each subject and ethical approval was granted by the Imperial College Research Ethics Committee.

Overhead Throwing Sports

The volunteers were instructed to perform five overhead throwing sports with three sets per activity (Table 7.1). These sports were selected based on Coleman et al. (2007), Cohen et al. (2006) and Brockmeier et al. (2009).

Table 7.1: Overhead throwing sports included in this study.

Athletic Activity	External Loading
Baseball pitching	0.14 kg ball
Quarterback throw	0.12 kg ball
Basketball free throw	0.62 kg ball
Volleyball serve	0.26 kg ball
Rugby lineout throw	0.62 kg ball

Protocol

Kinematic data collection was performed using a 10-camera optical motion tracking system (Vicon Motion Tracking System, Oxford, UK) at 240 Hz.

A scapula tracker (ST) was used to measure scapula kinematics (Prinold et al. 2011). The ST consists of a base attached to the mid-portion of the scapula spine and an adjustable foot positioned on the meeting-point between acromion process and scapula spine (Shaheen et al. 2011). The ST technical coordinate frame was calibrated with the anatomical coordinate frame of the scapula using the International Society of Biomechanics (ISB) recommended landmarks and measured directly using a scapula locator (Shaheen et al. 2011). Calibration was performed in three static positions: (1) shoulder at 90° humero-thoracic abduction and elbow at 90° flexion with arm positioned at approximately 30° to the coronal plane, (2) shoulder at approximately 150° humero-thoracic abduction and (3) shoulder at less than 10° of humero-thoracic abduction.

Twenty-one retro-reflective markers were used to track the thorax, scapula, clavicle, humerus, radius and ulna (Shaheen et al. 2011; Wu et al. 2005). The elbow epicondyles were defined as a rigid offset from the humerus technical frame with the arm at 90° of humerothoracic flexion, 45° from the coronal plane, 90° elbow flexion and a vertical forearm. Least-square fitting was used to calculate the glenohumeral head rotational centre during a functional task using the locator to track the scapula (Gamage & Lasenby 2002).

A low-pass fourth-order Butterworth filter (cut-off 4.7 Hz) was used to remove noise from the kinematic data after spectral analysis of the signal (Prinold and Bull 2016).

Modelling and Analysis

The motion data and external forces for each athletic activity served as inputs into the UK National Shoulder Model (UK NSM; as described in Section 2.3.1; Charlton and Johnson 2006) which represents a 3D musculoskeletal modelling software written in Matlab (The Mathworks Inc., Cambridge, UK) that models forces at the right shoulder. The version of the UK NSM used in this study additionally incorporates the effect of anthropometric scaling of ten subject-specific shoulder anatomies as described in Chapter 4, glenohumeral concavity compression as introduced in Chapter 3, as well as subject-specific scapula tracking (Prinold et al. 2011). The model outputs include glenohumeral contact forces as well as muscle forces including the long head of the biceps brachii as well as the rotator cuff muscles.

The athletic activities for each study participant were simulated with four different anatomical variants of the UKNSM in order to investigate the effect of biceps tenodesis on shoulder stability. These variants were: (1) intact anatomy (Charlton & Johnson 2006) with the long head of the biceps tendon being attached to its anatomical origin, (2) post biceps tenodesis without cuff tear whereby the attachment point of the long head of the biceps tendon was transferred from its anatomical origin to the top of the

bicipital groove (Boileau et al. 2009), (3) post biceps tenodesis with cuff tear, whereby the attachment point of the long head of the biceps tendon was transferred from its anatomical origin to the top of the bicipital groove, with combined presence of a full-thickness tear of the supraspinatus that was modelled by setting the muscle volume to zero, and (4) an isolated full-thickness supraspinatus tear that was modelled by setting the muscle volume to zero, in order to exclude significant losses in shoulder stability solely due to the presence of a full-thickness supraspinatus tear.

For each variant of the shoulder model, the peak forces in the long head of the biceps brachii as well as the rotator cuff muscles were analysed for each athletic activity in order to evaluate changes in shoulder muscle loading through biceps tenodesis for each overhead throwing sport. Similarly, the stability of the shoulder was assessed for all model instances and athletic activities using the stability ratio, defined by peak translational shear force divided by the joint stabilising compression force (Fukuda et al. 1988), in order to assess the effect of biceps tenodesis on joint stability for each overhead throwing sport. The stability ratios were obtained in two main anatomical directions of the glenoid as superior and anterior stability ratio respectively, with increasing stability ratios indicating a loss in joint stability.

Statistical differences in shoulder stability as well as shoulder muscle loading between the intact shoulder model and the other three model instances were assessed using a non-parametric Mann-Whitney test.

The effect of biceps tenodesis on shoulder stability for major overhead throwing sports was additionally computed using the generic UK NSM (Charlton and Johnson 2006) as described in Section 2.3.1 as well as the generic UK NSM with integration of passive glenohumeral concavity compression as introduced in Chapter 3, with these results being presented in Appendix A4. The comparison of these data to those using anthropometric scaling of 10 subject-specific shoulder models with consideration of glenohumeral concavity compression as presented in this Chapter will allow the assessment of the clinical importance of the modifications made to the UK NSM as described in Chapters 3 and 4.

7.3 Results

The muscle force of the long head of the biceps brachii decreases post biceps tenodesis across all five overhead sports (Figure 7.1), with significant reductions in long head of biceps brachii loading for a baseball pitch ($p<0.01$), quarterback throw ($p=0.02$) and volleyball serve ($p=0.04$).

The rotator cuff muscle forces increase post biceps tenodesis across all overhead sports (Figure 7.1), with none of these increases being statistically significant.

The rotator cuff muscle forces significantly increase ($p<0.04$) post biceps tenodesis with associated full-thickness supraspinatus tear across all overhead sports (Figure 7.1), with none of these increases in rotator cuff muscle force being induced by solely the presence of a full-thickness supraspinatus tear.

The stability ratios increase post biceps tenodesis in the superior and anterior anatomical direction of the glenoid across all overhead throwing sports (Figure 7.2). All of these losses in joint stability were non-significant, except baseball pitching, where biceps tenodesis led to a significant deterioration in anterior shoulder stability ($p=0.03$).

The stability of the shoulder further decreases post biceps tenodesis with combined presence of a full-thickness tear of the supraspinatus (Figure 7.2), with significant losses in anterior shoulder stability for a baseball pitch ($p<0.01$), quarterback throw ($p=0.01$) and volleyball serve ($p=0.02$), as well as significant losses in superior joint stability for a baseball pitch ($p<0.01$), quarterback throw ($p<0.01$), volleyball serve ($p=0.02$) and rugby lineout throw ($p=0.04$). None of these significant losses in joint stability was induced by solely the presence of a full-thickness tear of the supraspinatus.

The corresponding results of the generic UK NSM as described in Section 2.3.1 (Charlton and Johnson 2006) and the generic UK NSM with integration of passive glenohumeral concavity compression can be found in Appendix A4 in Table A4.1, A4.2, A4.3 and A4.4. This comparison is provided to demonstrate the effect of technical modifications to the UK NSM as described in Chapter 3 and 4, on clinical recommendations.

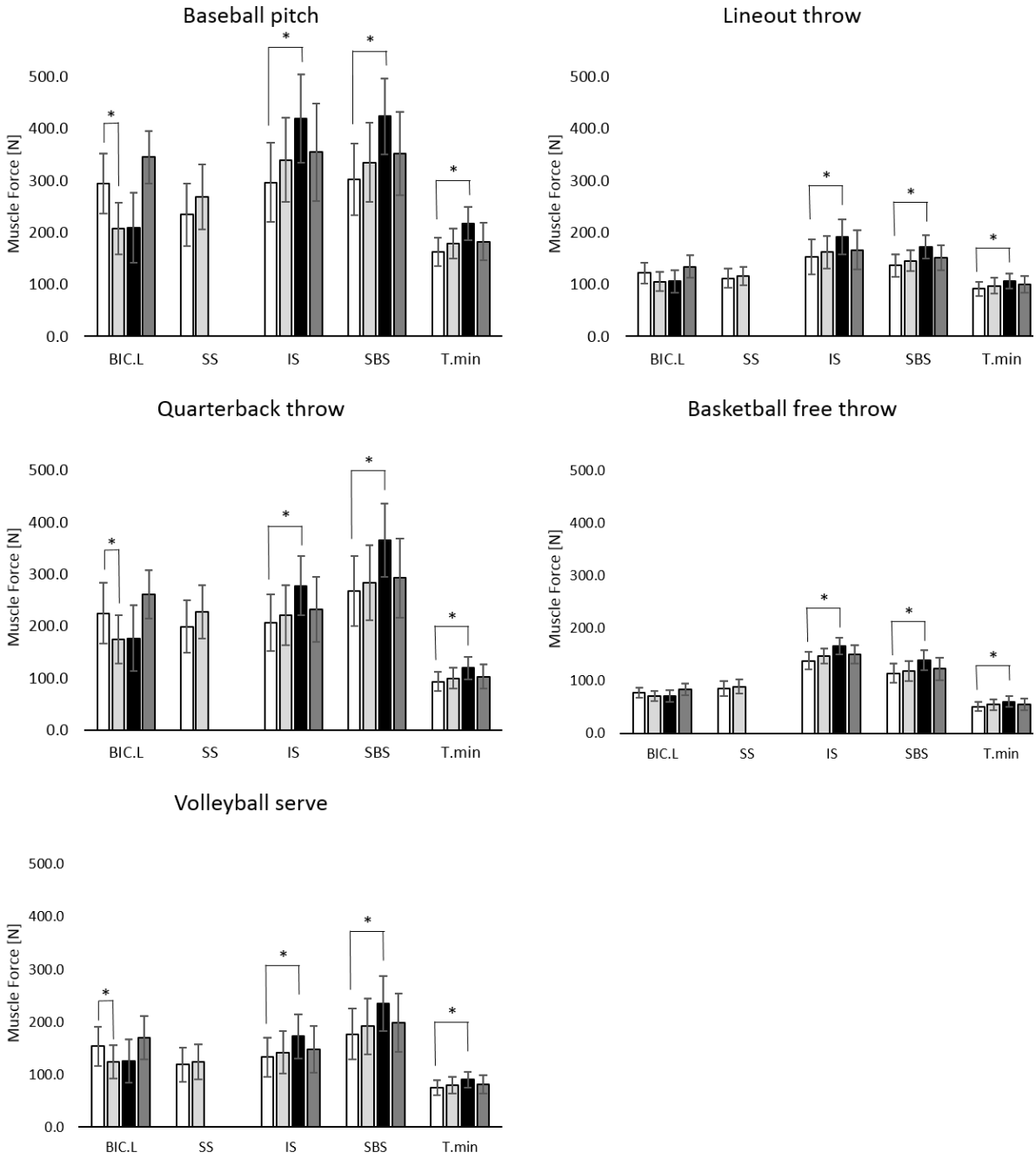

Figure 7.1: Mean (± SD) of the peak muscle forces of the long head of the biceps brachii (BIC.L), supraspinatus (SS), infraspinatus (IS), subscapularis (SBS) and teres minor (T.min), for the intact anatomy (model 1; white bars), post biceps tenodesis (model 2; light gray bars), post biceps tenodesis with combined presence of a full-thickness supraspinatus tear (model 3; black bars), and full-thickness supraspinatus tear (model 4; dark gray bars), for the five overhead throwing sports as predicted by the UK NSM using anthropometric scaling of ten subject-specific shoulder models with consideration of passive glenohumeral concavity compression.

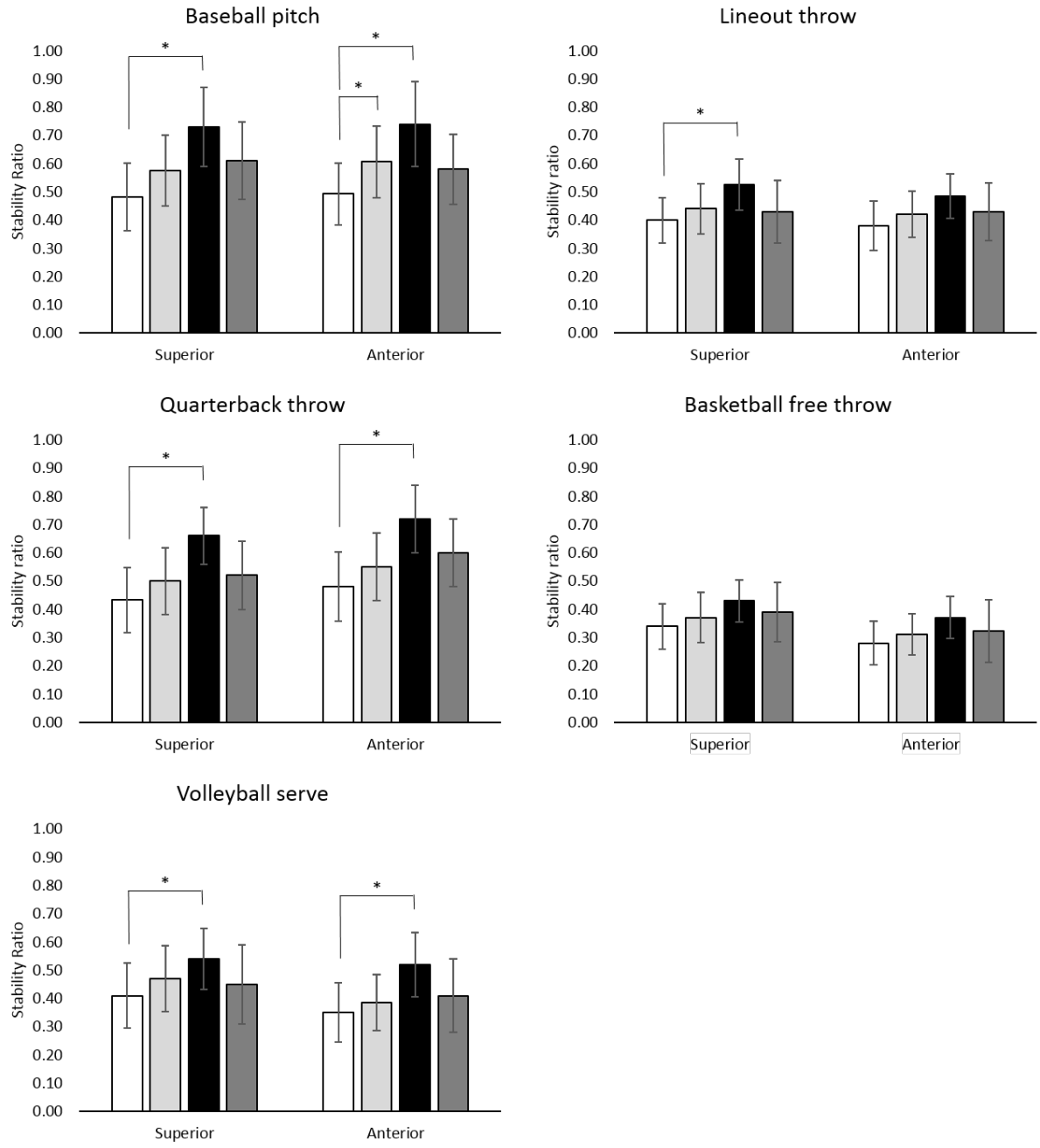

Figure 7.2: Mean stability ratios in the superior and anterior anatomical direction of the glenoid, for the intact anatomy (model 1; white bars), post biceps tenodesis (model 2; light gray bars), post biceps tenodesis with combined presence of a full-thickness supraspinatus tear (model 3; black bars), and full-thickness supraspinatus tear (model 4; dark gray bars), for the five overhead throwing sports as predicted by the UK NSM using anthropometric scaling of ten subject-specific shoulder models with consideration of passive glenohumeral concavity compression.

7.4 Discussion

This study has investigated the effect of biceps tenodesis on shoulder stability for major overhead throwing sports in order to aid sport-specific surgical decision-making for athletes with type II SLAP tears. The study findings demonstrate a decreased loading of the long head of the biceps following

biceps tenodesis, with statistically significant losses in muscle loading for three of the five overhead throwing sports, illustrating that the long head of the biceps significantly contributes to shoulder stability during overhead throwing activities. The loss in joint stability following the surgical transfer of the long head of the biceps brachii tendon away from its anatomical position is compensated by a non-significant increase in rotator cuff muscle force, with these muscles maintaining shoulder stability post biceps tenodesis across all overhead throwing sports, except baseball pitching. The presence of a full-thickness tear of the supraspinatus further decreases shoulder stability, with significant losses in joint stability for four of the five overhead throwing sports. The presence of a full-thickness supraspinatus tear leads to significant increases in rotator cuff muscle loading across all overhead throwing sports. As none of these significant losses in joint stability and significant increases in rotator cuff muscle loading was induced by solely the presence of a full-thickness tear of the supraspinatus, the study findings suggest that biceps tenodesis may be used as a primary treatment for overhead throwing athletes with intact rotator cuff muscles, except baseball pitchers, as shoulder stability is maintained post surgery and superior clinical outcomes for biceps tenodesis, when compared to arthroscopic SLAP repair (Boileau et al. 2009; Chalmers et al. 2014; Ek et al. 2014), have been reported in the literature.

A well-validated musculoskeletal shoulder model (Charlton & Johnson, 2006) was utilised in this study to investigate the effect of biceps tenodesis on joint stability for major overhead throwing sports. The novelty in this modelling approach is the use of anthropometric-scaling of subject-specific shoulder anatomies as described in Chapter 4, which has been demonstrated to accurately predict shoulder muscle and joint loading. Therefore, this is the first study to assess changes in shoulder joint loading and rotator cuff muscle forces following biceps tenodesis, with existing clinical studies only reporting short-term functional outcomes (Boileau et al. 2009; Chalmers et al. 2014; Ek et al. 2014), despite the increased long-term injury risk that has been associated with rotator cuff muscle overloading and increased shoulder joint shear forces (Orchard et al. 2015; Wang & Romeo 2015).

The use of a combined experimental and modelling approach allows the assessment of shoulder stability for individual overhead throwing sports. This is of particular importance as significant differences in shoulder loading have been demonstrated for different overhead throwing motions (Usman et al. 2011; Ramappa et al. 2010), with larger shoulder shear forces being associated with an increased likelihood of joint instability as illustrated in Chapter 6. As existing clinical studies are only reporting functional outcomes for a mixture of overhead throwing sports (Boileau et al. 2009; Chalmers et al. 2014; Ek et al. 2014), this study represents the first approach to investigate the effect of biceps tenodesis on shoulder stability for individual overhead throwing sports in order to aid sport-specific surgical decision-making for athletes with type II SLAP tear.

The study findings demonstrate a decreased loading of the long head of the biceps brachii following the surgical transfer of the long head of the biceps brachii from its anatomical position to the bicipital

groove of the humerus (Boileau et al. 2009; Strauss et al. 2014). In agreement with findings from cadaveric studies (Itoi et al. 1994; Su et al. 2010; Warner and McMahon 1995; Youm et al. 2009, this indicates that the long head of the biceps brachii assists the rotator cuff muscles to stabilise the shoulder through concavity compression (Lazarus et al. 1996; Lippitt & Matsen 1993). The reductions in loading of the long head biceps brachii were statistically significant in three of the five overhead throwing sports, demonstrating a higher contribution of the long head of the biceps brachii to joint stability for those overhead throwing sports that involve high speeds such as baseball pitching.

The loss in shoulder stability due to biceps tenodesis is compensated by an increased rotator cuff muscle force, with these muscles maintaining shoulder stability post biceps tenodesis. As the increase in rotator cuff muscle loading is non-significant, the surgical transfer of the long head of the biceps brachii to the bicipital groove is unlikely to increase the likelihood of rotator cuff muscle injury. These results are representative for all overhead throwing sports in this study, except baseball pitching, where biceps tenodesis has significantly reduced anterior shoulder stability. Therefore, the treatment of type II SLAP tears in baseball pitchers with biceps tenodesis may not be an effective treatment option. This is in agreement with clinical observations, demonstrating that MLB baseball pitchers have by far the lowest rate of return to preinjury level of sport participation across all overhead throwing sports (Chalmers et al. 2018). In fact, the treatment of professional baseball pitchers with arthroscopic SLAP repair has yielded higher rates of return to preinjury level of sport participation with 63%, when compared to 17% of those baseball pitchers that were treated with arthroscopic biceps tenodesis (Sayde et al. 2012). This may be explained through a loss in power and control of the pitch due to the loss in shoulder stability (Hurley et al. 2018). In addition, the decrease superior shoulder stability, although non-significant ($p=0.014$), represents the largest loss in superior stability across all overhead throwing sports, demonstrating the demand that is placed on the shoulder during baseball pitching. As tears of the supraspinatus as well as shoulder impingement are a common clinical problem in baseball pitchers (McHugh et al. 2016; Milgrom et al. 1995; Ouellette et al. 2008), the treatment of type II SLAP lesions in baseball pitchers with biceps tenodesis is not recommended as an increased superior shear force will worsen the clinical situation.

The stability of the shoulder post biceps tenodesis is further deteriorated in the presence of a full-thickness tear of the supraspinatus, with significant losses in shoulder stability for four of the five overhead throwing sports as well as significant increases in rotator cuff muscle loading across all overhead throwing sports. As none of these losses in joint stability and increases in rotator cuff muscle loading were induced by solely the supraspinatus tear, the findings of this study demonstrate that biceps tenodesis in the presence of a supraspinatus tear significantly reduces joint stability and causes rotator cuff muscle overloading. Therefore, the treatment of type II SLAP tears in overhead throwing athletes with full-thickness supraspinatus tear, which represents the most commonly torn rotator cuff muscle in these athletes, is not recommended as it predisposes the joint to instability. This study finding

corresponds well with clinical observations, demonstrating low rates of return to preinjury level of sport participation in overhead throwing athletes with concominant rotator cuff pathology (Neri et al. 2011; Merolla et al. 2018; Beyzadeoglu and Circi 2015).

The results presented in this study were obtained utilising anthropometric scaling of ten subject-specific shoulder models with consideration of glenohumeral concavity compression. The comparison of these results as shown in Figure 7.1 and Figure 7.2 to those estimations from the generic UK NSM as described in Section 2.3.1.2 (Charlton & Johnson 2006) as well as the generic UK NSM with integration of concavity compression as shown in Tables A4.1, A4.2, A4.3 and A4.4, demonstrates small, non-significant differences in predicted joint stability post biceps tenodesis. Although these model estimations are not significantly different from each other, the tables in the appendix demonstrate lack in significant loss in biceps loading for the volleyball serve, with a significant a significant loss in biceps loading for the volleyball serve being demonstrated in Figure 7.1 as predicted by the subject-specific UK NSM with consideration of glenohumeral concavity compression. Therefore, the technical improvement of the UK NSM as presented in Chapter 3 and 4 are essential to accurately assist clinical decision-making, especially in patients with SLAP II labral tear where biceps tenodesis was only performed based on clinical observations and without any assessment of shoulder loading for individual overhead throwing sports.

This study has several limitations. Firstly, the kinematic data were collected from healthy individuals with regular sport participation. Nevertheless, none of the study participants can be considered as a professional athlete in any of these overhead throwing sports. Secondly, the musculoskeletal shoulder model did not define an upper bound for each muscle to quantify the maximum muscle force that each muscle can contribute to shoulder movement. While this is non-physiological, this approach has been widely used in the literature (Delp et al. 2007; Garner & Pandy 2001) to account for the inherent difficulty in measuring muscle stresses (van der Helm 1994; Crowninshield & Brand 1981). Finally, the modelling of muscles in the musculoskeletal shoulder model without representation of muscle activation dynamics represents a non-physiological approach. Despite the lack of those data in the literature and thus in the computational shoulder model, the model predictions have been validated against electromyographic measurements for athletic motions (Prinold and Bull 2016) in addition to functional daily activities (Pandis et al. 2015).

7.5 Conclusion

This chapter investigates the effect of biceps tenodesis on shoulder stability for major overhead throwing sports in order to aid sport-specific surgical decision-making for athletes with type II SLAP tears. The study findings demonstrate a significant decrease in loading of the long head of the biceps brachii post biceps tenodesis in three overhead throwing sports. The loss in joint stability following

biceps tenodesis is compensated by a non-significant increase in rotator cuff muscle force which maintain shoulder stability across all overhead throwing sports, except baseball pitching, where biceps tenodesis has significantly decreased anterior shoulder stability. The presence of a full-thickness supraspinatus tear post biceps tenodesis further decreases shoulder stability, with significant losses in joint stability for four of the five overhead throwing sports, which is additionally accompanied by a significant increase in rotator cuff muscle overloading. Therefore, the study findings suggest that biceps tenodesis may be used as a primary treatment in overhead throwing athletes with intact rotator cuff muscles, except baseball pitchers, as shoulder stability is not comprised following biceps tenodesis.

The final chapter in this thesis will summarise the key findings of this thesis and place them into a broader context of other research in the field. Future work will be discussed to illustrate the potential of computational shoulder modelling for clinical decision-making.

Chapter 8

Concluding remarks and future work.

This chapter summarises the key findings of this thesis and places them into a broader context of other research in the field. Future work is proposed and discussed in order to illustrate the potential of computational shoulder models to aid clinical decision-making, specifically for patients with anterior shoulder instability.

8.1 Concluding Remarks

The shoulder is the most frequently dislocated joint in the human body (Shah et al. 2017; Zacchilli & Owens 2010), with the vast majority of these dislocations being located anteriorly (Pope et al. 2011). Anterior shoulder dislocations are commonly associated with capsulolabral injuries and osseous defects (Atef et al. 2016; Hintermann & Gachter 1995). Recurrent instability is a common clinical problem (Flint et al. 2018) and understanding of the influence of structural damage on joint stability is an important adjunct to surgical decision-making. Clinical practice is guided by experience, radiology, retrospective analyses and physical cadaver experiments with non-physiological loading. As the stability of the shoulder is load dependent, with higher joint forces increasing instability (Lippitt et al. 1993; Halder et al. 2001), the aim of this thesis was to simulate the effect of structural damage on joint stability under physiological joint loading in order to aid surgical decision-making, specifically for patients with anterior shoulder instability.

The loss in joint stability with labral pathology has scarcely been investigated through cadaveric testing (Halder et al. 2001; Lippitt et al. 1993), despite the fact that the avulsion of the anteroinferior labrum is the most common injury in patients with anterior shoulder instability (Atef et al. 2016). Therefore, two subject-specific finite element models of the shoulder with an anatomically accurate representation of the labrum were developed and validated in Chapter 3, in order to quantify the labral contribution to joint stability under physiological loading conditions and develop regression equations of these contributions. The developed regression equations could then be used in various other applications, including computational shoulder models to improve model reliability as the effect of glenohumeral concavity compression is commonly neglected in these types of shoulder models (Garner & Pandy 2001; Nikooyan et al. 2010), despite the fact that an anteroinferior labral avulsion leads to a loss in joint stability of 15% as demonstrated in Chapter 3.

The UK National Shoulder Model (Charlton & Johnson 2006), which represents a 3D musculoskeletal model of the upper limb, was customised in Chapter 4 in order to accurately model shoulder loading during functional daily activities. Ten subject-specific shoulder models were developed through manual digitisation of model parameters from MRI and validated against electromyographic signals as well as muscle moment arm data as presented in the literature. As the development of personalised shoulder models is time, labour and technology intensive, Chapter 4 additionally investigates the dependency of modelling results on anatomical geometry, identifies the best combination of anthropometric parameters that yields most accurate model estimations in glenohumeral joint loading through scaling of personalised shoulder models, and quantifies the improvement in model reliability through anthropometric scaling of anatomical datasets when compared to a single scaled-generic model. The results show that linear scaling of MRI-based shoulder models with the closest ratio of body height to shoulder width and from the same gender yield best modelling outcomes for a compound measure that

took equally into account both the accuracy of the glenohumeral contact force as well as all shoulder muscle forces, with model predictions being significantly improved when compared to an individual, scaled-generic dataset. This demonstrates that anthropometric scaling of shoulder models from a database of anatomical models improves model reliability in glenohumeral loading, which is essential for the translation of MSK shoulder modelling into clinical practice in order to address key clinical questions, including those associated with anterior shoulder dislocation.

In Chapter 5, anthropometric scaling of ten subject-specific shoulder models from a template database served to analyse shoulder contact forces during essential functional daily activities. Despite several studies being reported in the literature, there is currently no detailed knowledge of glenohumeral contact forces during functional activities with existing studies focussing on a small number of functional tasks without always presenting the loading direction (Anglin et al. 2000; Westerhoff et al. 2009; Charlton & Johnson 2006). Therefore, the aim of Chapter 5 was to precisely quantify shoulder compression and shear forces during essential functional daily activities which may ultimately serve implant design and rehabilitation planning for patients post Bankart repair. The study findings show that the ratio of glenohumeral shear to compression force exceeds 0.5 in 6/26 functional activities, demonstrating a considerable loading of the Bankart repair when high loads act at long lever arms as well as at high angles of arm elevation. Therefore, these data have the potential to aid rehabilitation planning by allowing advice to be given to patients in order to avoid overloading of the surgically repaired labrum (Gaunt et al. 2010).

The predicted shoulder forces during functional daily activities served as input into subject-specific finite element models of the shoulder with an anatomically accurate representation of the labrum, as described in Chapter 3, in order to determine the critical size of a glenoid osseous defect that leads to anterior shoulder instability under physiological joint loading. The study findings demonstrate a high risk of shoulder dislocation during functional daily activities post Bankart repair with a 2 mm anterior and 4 mm anteroinferior glenoid osseous defect. As rates of recurrent anterior shoulder instability in patients with large glenoid osseous defect that were treated with Bankart repair are higher than those patients that were treated with bone-grafting (Bliven & Parr 2018; Boileau et al. 2006), but bone-grafting is associated with concerns related to surgical complications and long term sequelae (Chen et al. 2005; Owens et al. 2011), this understanding of the critical amount of bone loss that leads to anterior shoulder instability post Bankart repair under physiological loading conditions will assist surgical decision-making.

In Chapter 7, the anthropometric scaling of subject-specific shoulder models from an anatomical template database served to assess shoulder stability in overhead throwing athletes post biceps tenodesis in order to aid surgical decision-making for patients with type II SLAP tears. As surgeons remain hesitant to perform biceps tenodesis on these athletes due to concerns that this surgical intervention

predisposes the joint to instability (Hurley et al. 2018; Patterson et al. 2014), the study findings may help to alleviate these concerns as shoulder stability post biceps tenodesis is only impaired in one of the throwing activities which is baseball pitching. Across all four other overhead throwing sports investigated in this study, an increase in rotator cuff muscle force is able to maintain anterior shoulder stability. As the presence of a full-thickness tear of the supraspinatus significantly reduces shoulder stability for the majority of overhead throwing sports, biceps tenodesis is an effective treatment in overhead throwing athletes with intact rotator cuff muscles, except baseball pitchers, as anterior shoulder stability is not impaired following biceps tenodesis.

In summary, the work presented in this thesis has developed and validated computational models of the shoulder to simulate the effect of structural damage on joint stability under physiological joint loading in order to aid surgical decision-making, specifically for patients with anterior shoulder instability.

One of the significant technical advances made is the incorporation of the effect of concavity compression in shoulder modelling. This is not normally taken into account in shoulder models, other than to restrain the joint reaction force to vector to be within the locus of the glenoid rim, and has had a small, but significant effect on modelling outputs.

8.2 Future Work

Musculoskeletal Shoulder Modelling

There are several studies in the literature demonstrating that customisation of musculoskeletal modelling through medical imaging significantly improves model reliability, when compared to an individual linearly scaled-generic model (Scheys et al. 2008a, 2008b; Gerus et al. 2013; Lerner et al. 2015; Marra et al. 2015). As the development of personalised shoulder models is time, labour and technology intensive, Chapter 4 presented the development of ten MRI-based shoulder models to demonstrate the effect of anthropometric parameters on modelling outcomes. The 10-fold cross-validation shows that linear scaling of anthropometric datasets with the most similar ratio of body height to shoulder width and from the same gender yield best modelling outcomes for glenohumeral contact force and muscle forces, with model predictions being significantly improved when compared to a single linearly-scaled generic model. This suggests that the establishment of an atlas with MRI-based models for scaling has strong potential to significantly improve model predictions for glenohumeral loading, which is essential for the translation of MSK shoulder modelling into clinical practice in order to address key clinical questions, including those associated with anterior shoulder instability.

Although anthropometric scaling of subject-specific shoulder models from an anatomical atlas with ten datasets has significantly reduced the mean root mean square error in glenohumeral joint loading, maximum errors associated with this approach are still as high as 10 N/kg and 3.0 N/kg for glenohumeral contact force and rotator cuff muscle forces respectively. Therefore, future research

should aim to improve the number of datasets in the anatomical atlas for model scaling. These additional geometries should be male and female volunteers with different ratios of body height to shoulder width as expressed by the multiple linear regression model in Section 4.3, in order to capture the diversity in dimensions of the musculoskeletal system that has been associated with individuals from different geographical origins (Gallagher et al. 1997; Gerace et al. 1994; Janssen et al. 2014). However, there is also a debate to be had about what level of accuracy is required for such models and this should consider the intended application, including, for example, if the application is for a subject-specific intervention, or if the application is more population-based.

A regression model was developed in order to estimate the number of subject-specific shoulder models in the anatomical atlas that are required to decrease the mean root mean square error in glenohumeral loading below a threshold value. Based on 10 subject-specific shoulder models in the anatomical atlas, the mean RMSE was computed for a 4-fold, 6-fold and 8-fold cross-validation, with each cross-validation being performed 10 times with random samples in order to obtain a representative mean RMSE in glenohumeral loading for each cross-validation, while overcoming the computational cost of 5040 possible combinations to analyse for a 4-fold cross-validation. These cross-validation results are shown in Table 8.1, while the regression model is given by equation 8.1.

Table 8.1: Root mean square error, in the compound measure that took equally into account the glenohumeral contact force and shoulder muscle forces, for the 4-fold, 6-fold, 8-fold and 10-fold cross-validations.

Cross-validation	RMSE in combined glenohumeral contact force and muscle forces [N/kg]
4-fold	9.2 ± 4.0
6-fold	5.7 ± 2.3
8-fold	4.2 ± 1.6
10-fold	2.7 ± 1.3

$$RMSE = 20.75 \cdot N^{-0.728} \qquad \text{Equation 8.1}$$

where N represents the number of subject-specific shoulder models in the anatomical atlas.

This regression model offers the opportunity to estimate the root mean square error in glenohumeral loading through scaling of subject-specific shoulder models from an anatomical atlas with a certain number of datasets. This mathematical model illustrates that improving the number of anatomical datasets for model scaling from 10 to 30 will decrease the root mean square error in glenohumeral contact force and muscle forces from 3.1 N/kg to 1.8 N/kg. Although changes in the composition of the anatomical atlas would alter the regression model, the selection of the ten shoulder anatomies in the current atlas makes this regression model a representative tool to estimate the number of subject-specific

shoulder anatomies that are required to decrease the mean root mean square error in glenohumeral loading below a threshold value.

Improving the number of subject-specific shoulder models in the anatomical atlas will increase the reliability of modelling predictions, which is essential for the translation of MSK shoulder modelling into clinical practice. Therefore, the anatomical atlas may serve to answer key clinical questions on a population-based approach by simulating shoulder functionality during essential functional daily activities for a large number of different anatomical datasets. This population based approach will represent the first computational attempt to provide clinical recommendations using a large number of subject-specific shoulder anatomies, with existing computational studies utilising a single anatomical dataset to aid surgical decision-making for patients with shoulder pathology (Jastifer et al. 2012; Magermans et al. 2004; Saul et al. 2011; van Drongelen et al. 2006). These clinical applications for future research may include tendon transfer surgeries such as the pectoralis major tendon transfer in subscapularis deficient patients (Nelson et al. 2014) or the latissimus dorsi tendon transfer in patients with severe rotator cuff muscle wastage (Henseler et al. 2014), in order to maximise the effectiveness of the surgical procedure on the ability to restore joint functionality. In addition to tendon transfer surgeries, future work may use the population-based modelling approach to analyse muscle forces during functional daily activities as this has barely been investigated in the literature (Pandis et al. 2015). This future clinical application has strong potential to aid rehabilitation planning, in particular for patients post rotator cuff repair, in order to avoid overloading of the surgically repaired soft tissues (Gaunt et al., 2010) and thus to ensure rotator cuff healing, which is essential as these muscles are the primary stabilisers of the shoulder. Based on the importance of the rotator cuff muscles to joint stability, future research may also aim to investigate the effect of rotator cuff muscle pathology on the critical lesion size of glenoid osseous defect. Although rotator cuff pathology is a common clinical finding (Yamamoto et al. 2010; Liem et al. 2014), especially amongst elderly patients, this effect has never been investigated.

Besides the use of subject-specific anatomical datasets to answer key clinical questions on a population-based approach, the pipeline to develop personalised shoulder models as presented in Chapter 4 offers the opportunity to create patient-specific shoulder models (Prinold et al. 2016). These have the potential to aid surgical planning on an individual patient-specific basis by allowing the prediction of joint functionality following surgical intervention for each patient. Therefore, patient-specific models may have great clinical impact on patients with severe muscle wastage or complex bone fractures. A possible future clinical application may include patients with brachial plexus palsy (Aktas et al. 2018; Philandrianos et al. 2013). In these patients, the nerves of the brachial plexus were damaged, predominantly during birth, leading to impaired functional patient outcomes due to muscle imbalance. These patients may be treated with tendon transfer surgery to restore joint functionality, with the

surgical intervention being dependent on the functional ability of patients prior to surgery (Noaman et al. 2004).

Therefore, patient-specific musculoskeletal shoulder modelling may help to simulate different surgical approaches for each patient in order to identify the surgical procedure that yields best functional outcomes, thus patient-specific musculoskeletal shoulder modelling and the use of an atlas of such models has strong potential to aid surgical decision-making and the design of surgical interventions.

Finite Element Analysis

The loss in joint stability with glenoid-labral pathology has scarcely been investigated through experimental testing or computational modelling (Halder et al. 2001; Lippitt et al. 1993), despite the fact that Bankart lesions and glenoid osseous defects are commonly associated with anterior shoulder instability (Atef et al. 2016; Hintermann & Gachter 1995). Therefore, two subject-specific finite element models of the shoulder with an anatomically accurate representation of the labrum were validated in Chapter 3 in order to quantify joint stability through concavity compression under physiological joint loading. These FE models were utilised in Chapter 6 to determine the critical size of a glenoid osseous defect that leads to anterior shoulder instability post Bankart repair under *in-vivo* loading conditions.

The stability of the shoulder provided by the bony articulating structures is only one stabilising mechanism (Lippitt and Matsen 1993), with other stabilising mechanisms involving passive structures such as the capsuloligamentous complex (Hess 2000). As the passive stabilisers are absent in the FE models as described in Chapter 3, the results of the critical lesion size of a glenoid osseous defect that leads to anterior shoulder instability post Bankart repair under physiological loading conditions as presented in Chapter 6 are only representative for the mid-range of shoulder motion, where the capsuloligamentous structures are lax (Steinbeck et al. 1998). As the inferior glenohumeral ligament is the primary restraint against anterior shoulder dislocation (Gelber et al. 2006), future work may aim to incorporate the capsuloligamentous complex into the FE models in order to improve model reliability. One approach of achieving this would be to follow the methodology of Amadi et al. (2012).

Besides the inclusion of the capsuloligamentous complex into the FE models, future work may aim to improve the number of these computational models to provide more representative results. Although two anatomically different joint shapes were utilised from the male and female visible human dataset (Ackerman 2017), the large variation in glenoid concavity across individuals (De Wilde et al. 2004; Howell & Galinat 1989; Huysmans et al. 2006) necessitates further shoulder anatomies to be modelled in order to robustly quantify the critical lesion size of a glenoid osseous defect. The anatomical datasets for this could be obtained from 7T MRI scans or physical sectioning of cadaveric tissues.

The improvement in the number of FE models as well as inclusion of the capsuloligamentous complex into these FE models may facilitate the application of these computational models to answer key clinical questions, including those associated with anterior shoulder instability. Future research may for instance utilise these computational tools to investigate the risk of Hill-Sachs lesions to engage with the anterior glenoid rim (Omori et al. 2014; Yamamoto et al. 2007). As described in Section 2.3, the contact area of the humeral head on the glenoid fossa was investigated during experimental testing, demonstrating that the width of the glenoid track is represented by 84% of the glenoid width (Omori et al. 2014; Yamamoto et al. 2007). However, these experiments were conducted in a limited number of joint positions (Yamamoto et al. 2017), although the glenoid track width is position dependent. Therefore, future work may aim to quantify the glenoid track for the whole range of functional shoulder positions including activities of daily living as well as overhead throwing sports in order to aid surgical decision-making for patients with different functional demands.

Beside the use of FE modelling for the native shoulder, these computational models may serve in future research to investigate the positioning and alignment of novel shoulder arthroplasties (Terrier et al. 2006). Based on the knowledge of shoulder loading during functional daily activities as presented in Chapter 5, this future research could evaluate the ability of novel shoulder implant designs to resist dislocating shear forces during functional daily activities in order to simulate implant performance. In addition to this, the use of FE modelling may also allow the assessment of implant fixation, which is essential as off-centre loading is considered to be the major cause of implant loosening (Geraldes et al. 2017).

Summary

In summary, the work presented in this thesis has developed and validated computational models of the shoulder to simulate the effect of structural damage on joint stability under physiological joint loading in order to aid surgical decision-making, specifically for patients with anterior shoulder instability. The application of these computational tools to key clinical questions has demonstrated strong clinical potential. Therefore, the use of these computational models may serve in the future to address a variety of other key clinical questions associated to bone or soft tissue pathology in order to assist clinical decision-making. Besides the native joint, the combined use of these tools may also serve to test for optimal alignment and position of novel shoulder arthroplasties.

Broader Context

The work presented in this thesis has utilised a computational modelling approach to simulate the effect of structural damage on joint stability under physiological joint loading in order to assist clinical decision-making, specifically for patients with anterior shoulder instability. Beside computational modelling studies, clinical practice is guided by retrospective analyses, physical cadaver experiments,

imaging studies as well as clinical experience. As recurrent anterior shoulder instability is a common clinical problem, the consideration of all these approaches is essential to restore joint stability as each of these approaches is associated with limitations.

The use of computational shoulder modelling has great potential to assist clinical decision-making as demonstrated in Chapter 5, 6 and 7, and may thus assist the treatment selection process for patients with shoulder pathology, especially those with anterior shoulder instability. As the treatment selection for these patients is a balancing act between restoring joint stability without exposing the patient to unnecessary surgical risks, the use of these computational shoulder models may ultimately contribute to reduce the high rates of recurrent anterior shoulder instabilities. This will not only impact on the healthcare system, with costs of 3000-4000£ per Bankart repair (Barber et al. 2016), but also benefit patients as recurrent anterior instabilities have been associated with a loss in quality of life as manifested in four domains: physical symptoms and pain, sport and sport function, lifestyle and social functioning as well as emotional well-being (Kirkley et al. 2005).

The computational technology developed in this thesis has demonstrated strong potential to assist clinical decision-making for patients, especially those with anterior shoulder instabilities. The motivation of this thesis may be taken as an example to motivate further research and collaborative studies worldwide in order to develop, validate and clinically apply these computational models of the musculoskeletal system in order to address key clinical questions associated with the development of osteoarthritis, wear of joint arthroplasties, planning of surgical and rehabilitative treatment as well as the design of assistive devices.

References

Abouali, J. A. K., Hatzantoni, K., Holtby, R., Veillette, C., & Theodoropoulos, J. (2013). Revision arthroscopic bankart repair. *Arthroscopy - Journal of Arthroscopic and Related Surgery*, *29*(9), 56-64.

Ackerman, M. J. (2017). The Visible Human Project: From Body to Bits. *IEEE Pulse*, *8*(4), 39–41.

Ackland, D. C., Lin, Y. C., & Pandy, M. G. (2012). Sensitivity of model predictions of muscle function to changes in moment arms and muscle-tendon properties: A Monte-Carlo analysis. *Journal of Biomechanics*, *45*(8), 1463–1471.

Ackland, D. C., Pak, P., Richardson, M., & Pandy, M. G. (2008). Moment arms of the muscles crossing the anatomical shoulder. *Journal of Anatomy*, *213*(4), 383–390.

Ackland, D. C., & Pandy, M. G. (2009). Lines of action and stabilizing potential of the shoulder musculature. *Journal of Anatomy*, *215*(2), 184–197.

Ackland, D. C., Roshan-Zamir, S., Richardson, M., & Pandy, M. G. (2010). Moment arms of the shoulder musculature after reverse total shoulder arthroplasty. *The Journal of Bone and Joint Surgery. American Volume*, *92*(5), 1221–1230.

Adams, C. R., Baldwin, M. A., Laz, P. J., Rullkoetter, P. J., & Langenderfer, J. E. (2007). Effects of rotator cuff tears on muscle moment arms: A computational study. *Journal of Biomechanics*, *40*(15), 3373–3380.

Aktas, D., Eren, B., Kenis-Coskun, O., & Karadag-Saygi, E. (2018). Function in unaffected arms of children with obstetric brachial plexus palsy. *European Journal of Paediatric Neurology : EJPN : Official Journal of the European Paediatric Neurology Society*, *22*(4), 610–614.

Alashkham, A., Alraddadi, A., Felts, P., & Soames, R. (2017). Blood supply and vascularity of the glenoid labrum: Its clinical implications. *Journal of Orthopaedic Surgery*, *25*(3), 512-519.

Alexander, S., Southgate, D. F. L., Bull, A. M. J., & Wallace, A. L. (2013). The role of negative intraarticular pressure and the long head of biceps tendon on passive stability of the glenohumeral joint. *Journal of Shoulder and Elbow Surgery*, *22*(1), 94–101.

Amadi, H. O., Bull, A. M. J., & Emery, R. J. H. (2012). Development and validation of a model for quantifying glenohumeral ligament strains during function. *Proceedings of the Institution of Mechanical Engineers, Part H: Journal of Engineering in Medicine*, *226*(6), 461–468.

Amirthanayagam, T. D., & Emery, R. J. H. (2014). Primum non nocere: risk assessment for new surgical procedures. *Journal of Shoulder and Elbow Surgery*, *26*(12), 1591–1597.

Anglin, C., Wyss, U. P., & Pichora, D. R. (2000). Glenohumeral contact forces. *Proceedings of the Institution of Mechanical Engineers, Part H: Journal of Engineering in Medicine*, *214*(6), 637–644.

Antonio, G. E., Griffith, J. F., Yu, A. B., Yung, P. S. H., Kai, M. C., & Ahuja, A. T. (2007). First-time shoulder dislocation: High prevalence of labral injury and age-related differences revealed by MR arthrography. *Journal of Magnetic Resonance Imaging*, *26*(4), 983–991.

Apreleva, M., Parsons, I. M., Warner, J. J. P., Fu, F. H., & Woo, S. L. Y. (2000). Experimental investigation of reaction forces at the glenohumeral joint during active abduction. *Journal of Shoulder and Elbow Surgery*, *9*(5), 409–417.

Araghi, A., Prasarn, M., St Clair, S., & Zuckerman, J. D. (2005). Recurrent anterior glenohumeral instability with onset after forty years of age: the role of the anterior mechanism. *Bulletin (Hospital for Joint Diseases (New York, N.Y.))*, *62*(3–4), 99–101.

Arciero, R. A., Wheeler, J. H., Ryan, J. B., & McBride, J. T. (1994). Arthroscopic Bankart Repair Versus Nonoperative Treatment for Acute, Initial Anterior Shoulder Dislocations. *The American Journal of Sports Medicine*, *22*(5), 589–594.

Arnold, A. S., Salinas, S., Asakawa, D. J., & Delp, S. L. (2000). Accuracy of muscle moment arms estimated from MRI-based musculoskeletal models of the lower extremity. *Computer Aided Surgery*, *5*(2), 108–119.

Arnold, E. M., Hamner, S. R., Seth, A., Millard, M., & Delp, S. L. (2013). How muscle fiber lengths and velocities affect muscle force generation as humans walk and run at different speeds. *Journal of Experimental Biology*, *216*(11), 2150–2160.

Ascani, D., Mazzà, C., De Lollis, A., Bernardoni, M., & Viceconti, M. (2015). A procedure to estimate the origins and the insertions of the knee ligaments from computed tomography images. *Journal of Biomechanics*, *48*(2), 233–237.

Aston, J. W. J., & Gregory, C. F. (1973). Dislocation of the shoulder with significant fracture of the glenoid. *The Journal of Bone & Joint Surgery. American Volume*, *55*(7), 1531–1533.

Atef, A., El-Tantawy, A., Gad, H., & Hefeda, M. (2016). Prevalence of associated injuries after anterior shoulder dislocation: a prospective study. *International Orthopaedics*, *40*(3), 519–524.

Bacilla, P., Field, L. D., & Savoie, F. H. (1997). Arthroscopic Bankart repair in a high demand patient population. *Arthroscopy*, *13*(1), 51–60.

Baker, C. L., Uribe, J. W., & Whitman, C. (1990). Arthroscopic evaluation of acute initial anterior shoulder dislocations. *American Journal of Sports Medicine*, *18*(1), 25–28.

Balestrini, J. L., & Billiar, K. L. (2009). Magnitude and Duration of Stretch Modulate Fibroblast. *The American Journal of Sports Medicine*, *22*(9), 14–22.

Bankart, A. S. (1923). Recurrent or habitual dislocation of the shoulder-joint. *British Medical Journal*, *2*(3285), 1132–1133.

Barber, F. A., Ryu, R. K. N., & Tauro, J. C. (2003). Should first time anterior shoulder dislocations be surgically stabilized? *Arthroscopy : The Journal of Arthroscopic & Related Surgery : Official Publication of the Arthroscopy Association of North America and the International Arthroscopy Association*, *19*(3), 305–309.

Bergmann, G., Graichen, F., Bender, A., & Ka, M. (2007). In vivo glenohumeral contact forces — Measurements in the first patient 7 months postoperatively. *Journal of Biomechanics*, *40*, 2139–2149.

Bergmann, G., Graichen, F., Bender, A., Kaab, M., Rohlmann, A., & Westerhoff, P. (2007). In vivo glenohumeral contact forces--measurements in the first patient 7 months postoperatively. *Journal of Biomechanics*, *40*(10), 2139–2149.

Bey, M. J., Elders, G. J., Huston, L. J., Kuhn, J. E., Blasier, R. B., & Soslowsky, L. J. (1998). The mechanism of creation of superior labrum, anterior, and posterior lesions in a dynamic biomechanical model of the shoulder: the role of inferior subluxation. *Journal of Shoulder and Elbow Surgery*, *7*(4), 397–401.

Bey, M. J., Peltz, C. D., Ciarelli, K., Kline, S. K., Divine, G. W., Holsbeeck, M. Van, Moutzouros, V. (2011). The American Journal of Sports Medicine In Vivo Shoulder Function After Surgical Repair of a Torn Rotator Cuff. *6*(4), 112–119.

Beyzadeoglu, T., & Circi, E. (2015). Superior labrum anterior posterior lesions and associated injuries: Return to play in elite athletes. *Orthopaedic Journal of Sports Medicine*, *3*(4), 1–5.

Bigliani, L. U., Kelkar, R., Flatow, E. L., Pollock, R. G., & Mow, V. C. (1996). Glenohumeral stability. Biomechanical properties of passive and active stabilizers. *Clin Orthop Relat Res*, (330), 13–30.

Bigliani, L. U., Newton, P. M., Steinmann, S. P., Connor, P. M., & Mcllveen, S. J. (1998). Glenoid rim lesions associated with recurrent anterior dislocation of the shoulder. *The American Journal of Sports Medicine*, *26*(1), 41–45.

Bliven, K. C. H., & Parr, G. P. (2018). Outcomes of the Latarjet Procedure Compared With Bankart Repair for Recurrent Traumatic Anterior Shoulder Instability. *Journal of Athletic Training*, *53*(2), 181–183.

Blonna, D., Bellato, E., Caranzano, F., Assom, M., Rossi, R., & Castoldi, F. (2016). Arthroscopic

Bankart Repair Versus Open Bristow-Latarjet for Shoulder Instability. *American Journal of Sports Medicine*, *44*(12), 3198–3205.

Boettcher, C. E., Ginn, K. A., & Cathers, I. (2008). Standard maximum isometric voluntary contraction tests for normalizing shoulder muscle EMG. *Journal of Orthopaedic Research : Official Publication of the Orthopaedic Research Society*, *26*(12), 1591–1597.

Boileau, P., Parratte, S., Chuinard, C., Roussanne, Y., Shia, D., & Bicknell, R. (2009). Arthroscopic treatment of isolated type II SLAP lesions: biceps tenodesis as an alternative to reinsertion. *The American Journal of Sports Medicine*, *37*(5), 929–936.

Boileau, P., Richou, J., Lisai, A., Chuinard, C., & Bicknell, R. T. (2009). The Role of Arthroscopy in Revision of Failed Open Anterior Stabilization of the Shoulder. *Arthroscopy - Journal of Arthroscopic and Related Surgery*, *25*(10), 1075–1084.

Boileau, P., Villalba, M., Héry, J. Y., Balg, F., Ahrens, P., & Neyton, L. (2006). Risk factors for recurrence of shoulder instability after arthroscopic Bankart repair. *The Journal of Bone and Joint Surgery. American Volume*, *88*(8), 1755–1763.

Bokor, D. J., Conboy, V. B., & Olson, C. (1999). Anterior instability of the glenohumeral joint with humeral avulsion of the glenohumeral ligament. A review of 41 cases. *The Journal of Bone and Joint Surgery. British Volume*, *81*(1), 93–96.

Bolsterlee, B., Vardy, A. N., van der Helm, F. C. T., & DirkJan Veeger, H. E. J. (2015). The effect of scaling physiological cross-sectional area on musculoskeletal model predictions. *Journal of Biomechanics*, *48*(10), 1760–1768.

Bolsterlee, B., Veeger, D. H. E. J., & Chadwick, E. K. (2013). Clinical applications of musculoskeletal modelling for the shoulder and upper limb. *Medical and Biological Engineering and Computing*, *51*(9), 953–963.

Bolsterlee, B., & Zadpoor, A. A. (2014). Transformation methods for estimation of subject-specific scapular muscle attachment sites. *Computer Methods in Biomechanics and Biomedical Engineering*, *17*(13), 1492–1501.

Bosmans, L., Valente, G., Wesseling, M., Van Campen, A., De Groote, F., De Schutter, J., & Jonkers, I. (2015). Sensitivity of predicted muscle forces during gait to anatomical variability in musculotendon geometry. *Journal of Biomechanics*, *48*(10), 2116–2123.

Bottoni, C. R., Wilckens, J. H., DeBerardino, T. M., D'Alleyrand, J.-C. G., Rooney, R. C., Harpstrite, J. K., & Arciero, R. A. (2002). A Prospective, Randomized Evaluation of Arthroscopic Stabilization versus Nonoperative Treatment in Patients with Acute, Traumatic, First-Time

Shoulder Dislocations. *The American Journal of Sports Medicine*, *30*(4), 576–580.

Brockmeier, S. F., Voos, J. E., Williams, R. J. 3rd, Altchek, D. W., Cordasco, F. A., & Allen, A. A. (2009). Outcomes after arthroscopic repair of type-II SLAP lesions. *The Journal of Bone and Joint Surgery. American Volume*, *91*(7), 1595–1603.

Brockmeyer, M., Tompkins, M., Kohn, D. M., & Lorbach, O. (2016). SLAP lesions: a treatment algorithm. *Knee Surgery, Sports Traumatology, Arthroscopy : Official Journal of the ESSKA*, *24*(2), 447–455.

Buchanan, T. S., Lloyd, D. G., Manal, K., & Besier, T. F. (2004). Neuromusculoskeletal modeling: estimation of muscle forces and joint moments and movements from measurements of neural command. *Journal of Applied Biomechanics*, *20*(4), 367–395.

Büchler, P., & Farron, A. (2004). Benefits of an anatomical reconstruction of the humeral head during shoulder arthroplasty: A finite element analysis. *Clinical Biomechanics*, *19*(1), 16–23.

Büchler, P., Ramaniraka, N. A., Rakotomanana, L. R., Iannotti, J. P., & Farron, A. (2002b). A finite element model of the shoulder: Application to the comparison of normal and osteoarthritic joints. *Clinical Biomechanics*, *17*(9–10), 630–639.

Bui-Mansfield, L. T., Banks, K. P., & Taylor, D. C. (2007). Humeral avulsion of the glenohumeral ligaments: The HAGL lesion. *American Journal of Sports Medicine*, *35*(11), 1960–1966.

Burk, J., Plenge, A., Brehm, W., Heller, S., Pfeiffer, B., & Kasper, C. (2016). Induction of Tenogenic Differentiation Mediated by Extracellular Tendon Matrix and Short-Term Cyclic Stretching. *Stem Cells International*, *43*(6), 251–259.

Burkart, A. C., & Debski, R. E. (2002). Anatomy and function of the glenohumeral ligaments in anterior shoulder instability. *Clinical Orthopaedics and Related Research*, (400), 32–39.

Burkhart, S. S., De Beer, J. F., Barth, J. R. H., Criswell, T., Roberts, C., & Richards, D. P. (2007). Results of Modified Latarjet Reconstruction in Patients With Anteroinferior Instability and Significant Bone Loss. *Arthroscopy - Journal of Arthroscopic and Related Surgery*, *23*(10), 1033–1041.

Calandra, J. J., Baker, C. L., & Uribe, J. (1989). The incidence of Hill-Sachs lesions in initial anterior shoulder dislocations. *Arthroscopy: The Journal of Arthroscopic and Related Surgery*, *5*(4), 254–257.

Carbone, V., Fluit, R., Pellikaan, P., van der Krogt, M. M., Janssen, D., Damsgaard, M., Verdonschot, N. (2015). TLEM 2.0 - A comprehensive musculoskeletal geometry dataset for subject-specific modeling of lower extremity. *Journal of Biomechanics*, *48*(5), 734–741.

Carbone, V., van der Krogt, M. M., Koopman, H. F. J. M., & Verdonschot, N. (2012). Sensitivity of subject-specific models to errors in musculo-skeletal geometry. *Journal of Biomechanics*, *45*(14), 2476–2480.

Cavanagh, P. R., & Komi, P. V. (1979). Electromechanical delay in human skeletal muscle under concentric and eccentric contractions. *European Journal of Applied Physiology and Occupational Physiology*, *42*(3), 159–163.

Chalmers, P. N., Erickson, B. J., Verma, N. N., D'Angelo, J., & Romeo, A. A. (2018). Incidence and Return to Play After Biceps Tenodesis in Professional Baseball Players. *Arthroscopy : The Journal of Arthroscopic & Related Surgery : Official Publication of the Arthroscopy Association of North America and the International Arthroscopy Association*, *34*(3), 747–751.

Chalmers, P. N., Trombley, R., Cip, J., Monson, B., Forsythe, B., Nicholson, G. P., Verma, N. N. (2014). Postoperative restoration of upper extremity motion and neuromuscular control during the overhand pitch: evaluation of tenodesis and repair for superior labral anterior-posterior tears. *The American Journal of Sports Medicine*, *42*(12), 2825–2836.

Charlton, I. W., & Johnson, G. R. (2006). A model for the prediction of the forces at the glenohumeral joint. *Proceedings of the Institution of Mechanical Engineers, Part H: Journal of Engineering in Medicine*, *220*(8), 801–812.

Chaudhury, S., & Carr, A. J. (2012). Lessons we can learn from gene expression patterns in rotator cuff tears and tendinopathies. *Journal of Shoulder and Elbow Surgery*, *21*(2), 191–199.

Chen, A. L., Hunt, S. A., Hawkins, R. J., & Zuckerman, J. D. (2005). Management of bone loss associated with recurrent anterior glenohumeral instability. *The American Journal of Sports Medicine*, *33*(6), 912–925.

Clark, E. M., Ness, A. R., & Tobias, J. H. (2007). Gender differences in the ratio between humerus width and length are established prior to puberty. *Osteoporosis International*, *18*(4), 463–470.

Cleather, D. J., & Bull, A. M. J. (2010). Lower-extremity musculoskeletal geometry affects the calculation of patellofemoral forces in vertical jumping and weightlifting. *Proceedings of the Institution of Mechanical Engineers, Part H: Journal of Engineering in Medicine*, *224*(9), 1073–1083.

Cleather, D. J., & Bull, A. M. J. (2015). The development of a segment-based musculoskeletal model of the lower limb: introducing FreeBody. *Royal Society Open Science*, *2*(6), 140449.

Coffey, A., & McCarthy, G. M. (2013). Older people's perception of their readiness for discharge and postdischarge use of community support and services. *International Journal of Older People*

Nursing, *8*(2), 104–115.

Cohen, D. B., Coleman, S., Drakos, M. C., Allen, A. A., O'Brien, S. J., Altchek, D. W., & Warren, R. F. (2006). Outcomes of isolated type II SLAP lesions treated with arthroscopic fixation using a bioabsorbable tack. *Arthroscopy : The Journal of Arthroscopic & Related Surgery : Official Publication of the Arthroscopy Association of North America and the International Arthroscopy Association*, *22*(2), 136–142.

Coughlin, L., Rubinovich, M., Johansson, J., White, B., & Greenspoon, J. (1992). Arthroscopic staple capsulorrhaphy for anterior shoulder instability. *The American Journal of Sports Medicine*, *20*(3), 253–256.

Cowling, P. D., Akhtar, M. A., & Liow, R. Y. L. (2016). What is a Bristow-Latarjet procedure?: A review of the described operative techniques and outcomes. *Bone and Joint Journal*, *98–B*(9), 1208–1214.

Crichton, J., Jones, D. R., & Funk, L. (2012). Mechanisms of traumatic shoulder injury in elite rugby players. *British Journal of Sports Medicine*, *46*(7), 538–542.

Crowninshield, R. D., & Brand, R. A. (1981). A physiologically based criterion of muscle force prediction in locomotion. *Journal of Biomechanics*, *14*(11), 793–801.

Cutts, S., Prempeh, M., & Drew, S. (2009). Anterior shoulder dislocation. *Ann R Coll Surg Engl*, *91*(4), 2–7.

Dal Maso, F., Raison, M., Lundberg, A., Arndt, A., Allard, P., & Begon, M. (2015). Glenohumeral translations during range-of-motion movements, activities of daily living, and sports activities in healthy participants. *Clinical Biomechanics*, *30*(9), 1002–1007.

Davidson, P. A., & Rivenburgh, D. W. (2004). Mobile superior glenoid labrum: a normal variant or pathologic condition? *The American Journal of Sports Medicine*, *32*(4), 962–966.

Davies, G. J., McCarty, E., Provencher, M., & Manske, R. C. (2017). ACL Return to Sport Guidelines and Criteria. *Current Reviews in Musculoskeletal Medicine*, *10*(3), 307–314.

Dawson, J., Fitzpatrick, R., & Carr, A. (1996). Questionnaire on the perceptions of patients about shoulder surgery. *The Journal of Bone and Joint Surgery. British Volume*, *78*(4), 593–600.

De Groot, J. H. (1997). The variability of shoulder motions recorded by means of palpation. *Clinical Biomechanics (Bristol, Avon)*, *12*(7–8), 461–472.

De Groot, J. H., Rozendaal, L. A., Meskers, C. G. M., & Arwert, H. J. (2004). Isometric shoulder muscle activation patterns for 3-D planar forces: A methodology for musculo-skeletal model validation. *Clinical Biomechanics*, *19*(8), 790–800.

De Leva, P. (1996). Adjustments to zatsiorsky-seluyanov's segment inertia parameters. *Journal of Biomechanics*, *29*(9), 1223–1230.

De Wilde, L. F., Berghs, B. M., Audenaert, E., Sys, G., Van Maele, G. O., & Barbaix, E. (2004). About the variability of the shape of the glenoid cavity. *Surgical and Radiologic Anatomy*, *26*(1), 54–59.

Dean, B. J. F., & Carr, A. J. (2016). The Effects of Glucocorticoid on Tendon and Tendon Derived Cells. *Advances in Experimental Medicine and Biology*, *920*, 239–246.

Dean, B. J. F., Gwilym, S. E., & Carr, A. J. (2013). Why does my shoulder hurt? A review of the neuroanatomical and biochemical basis of shoulder pain. *British Journal of Sports Medicine*, *47*(17), 1095–1104.

DeBerardino, T. M., Arciero, R. A., Taylor, D. C., & Uhorchak, J. M. (2001). Prospective evaluation of arthroscopic stabilization of acute, initial anterior shoulder dislocations in young athletes. Two- to five-year follow-up. *American Journal of Sports Medicine*, *29*(5), 586–592.

Delp, S. L., Anderson, F. C., Arnold, A. S., Loan, P., Habib, A., John, C. T., Thelen, D. G. (2007). OpenSim: Open-source software to create and analyze dynamic simulations of movement. *IEEE Transactions on Biomedical Engineering*, *54*(11), 1940–1950.

Delp, S. L., Loan, J. P., Hoy, M. G., Zajac, F. E., Topp, E. L., & Rosen, J. M. (1990). An Interactive Graphics-Based Model of the Lower Extremity to Study Orthopaedic Surgical Procedures. *IEEE Transactions on Biomedical Engineering*, *37*(8), 757–767.

Denard, P. J., Ladermann, A., Parsley, B. K., & Burkhart, S. S. (2014). Arthroscopic biceps tenodesis compared with repair of isolated type II SLAP lesions in patients older than 35 years. *Orthopedics*, *37*(3), 292-977.

Di Giacomo, G., De Vita, A., Costantini, A., De Gasperis, N., & Scarso, P. (2014). Management of humeral head deficiencies and glenoid track. *Current Reviews in Musculoskeletal Medicine*, *7*(1), 6–11.

Dickerson, C. R., Chaffin, D. B., & Hughes, R. E. (2007). A mathematical musculoskeletal shoulder model for proactive ergonomic analysis. *Computer Methods in Biomechanics and Biomedical Engineering*, *10*(6), 389–400.

Dines, D. M., & Levinson, M. (1995). The conservative management of the unstable shoulder including rehabilitation. *Clinics in Sports Medicine*, *14*(4), 797–816.

Ding, Z., Nolte, D., Kit Tsang, C., Cleather, D. J., Kedgley, A. E., & Bull, A. M. J. (2016). In Vivo Knee Contact Force Prediction Using Patient-Specific Musculoskeletal Geometry in a Segment-Based Computational Model. *Journal of Biomechanical Engineering*, *138*(2), 021018.

Drury, N. J., Ellis, B. J., Weiss, J. a, McMahon, P. J., & Debski, R. E. (2010). The impact of glenoid labrum thickness and modulus on labrum and glenohumeral capsule function. *Journal of Biomechanical Engineering*, *132*(12), 121003.

Duda, G. N., Brand, D., Freitag, S., Lierse, W., & Schneider, E. (1996). Variability of femoral muscle attachments. *Journal of Biomechanics*, *29*(9), 1185–1190.

Dul, J. (1988). A biomechanical model to quantify shoulder load at the work place. *Clinical Biomechanics (Bristol, Avon)*, *3*(3), 124–128.

Edama, M., Onishi, H., Kubo, M., Takabayashi, T., Yokoyama, E., Inai, T., Kageyama, I. (2017). Gender differences of muscle and crural fascia origins in relation to the occurrence of medial tibial stress syndrome. *Scandinavian Journal of Medicine & Science in Sports*, *27*(2), 203–208.

Edelson, J. G. (1996). Bony changes of the glenoid as a consequence of shoulder instability. *J Shoulder Elbow Surg*, *5*(4), 293–298.

Eichinger, J. K., Massimini, D. F., Kim, J., & Higgins, L. D. (2016). Biomechanical Evaluation of Glenoid Version and Dislocation Direction on the Influence of Anterior Shoulder Instability and Development of Hill-Sachs Lesions. *American Journal of Sports Medicine*, *44*(11), 2792–2799.

Ek, E. T. H., Shi, L. L., Tompson, J. D., Freehill, M. T., & Warner, J. J. P. (2014). Surgical treatment of isolated type II superior labrum anterior-posterior (SLAP) lesions: repair versus biceps tenodesis. *Journal of Shoulder and Elbow Surgery*, *23*(7), 1059–1065.

Engelhardt, C., Farron, A., Becce, F., Place, N., Pioletti, D. P., & Terrier, A. (2017). Effects of glenoid inclination and acromion index on humeral head translation and glenoid articular cartilage strain. *Journal of Shoulder and Elbow Surgery*, *26*(1), 157–164.

Engelhardt, C., Ingram, D., Mullhaupt, P., Farron, A., Becce, F., Pioletti, D., & Terrier, A. (2016). Effect of partial-thickness tear on loading capacities of the supraspinatus tendon: a finite element analysis. *Computer Methods in Biomechanics and Biomedical Engineering*, *19*(8), 875–882.

Favre, P., Senteler, M., Hipp, J., Scherrer, S., Gerber, C., & Snedeker, J. G. (2012). An integrated model of active glenohumeral stability. *Journal of Biomechanics*, *45*(13), 2248–2255.

Favre, P., Snedeker, J. G., & Gerber, C. (2009). Numerical modelling of the shoulder for clinical applications. *Philosophical Transactions. Series A, Mathematical, Physical, and Engineering Sciences*, *367*(1895), 2095–2118.

Fedoriw, W. W., Ramkumar, P., McCulloch, P. C., & Lintner, D. M. (2014). Return to play after treatment of superior labral tears in professional baseball players. *The American Journal of Sports Medicine*, *42*(5), 1155–1160.

Ferrari, A., Cutti, A. G., & Cappello, A. (2010). A new formulation of the coefficient of multiple correlation to assess the similarity of waveforms measured synchronously by different motion analysis protocols. *Gait & Posture*, *31*(4), 540–542.

Flinkkila, T., Hyvonen, P., Ohtonen, P., & Leppilahti, J. (2010). Arthroscopic Bankart repair: results and risk factors of recurrence of instability. *Knee Surgery, Sports Traumatology, Arthroscopy : Official Journal of the ESSKA*, *18*(12), 1752–1758.

Flint, J. H., Pickett, A., Owens, B. D., Svoboda, S. J., Peck, K. Y., Cameron, K. L., Rue, J.-P. (2018). Recurrent Shoulder Instability in a Young, Active, Military Population and Its Professional Implications. *Sports Health*, *10*(1), 54–59.

Fukuda, K., Chen, C. M., Cofield, R. H., & Chao, E. Y. (1988). Biomechanical analysis of stability and fixation strength of total shoulder prostheses. *Orthopedics*, *11*(1), 141–149.

Galban, C. J., Maderwald, S., Uffmann, K., de Greiff, A., & Ladd, M. E. (2004). Diffusive sensitivity to muscle architecture: a magnetic resonance diffusion tensor imaging study of the human calf. *European Journal of Applied Physiology*, *93*(3), 253–262.

Gamage, S. S. H. U., & Lasenby, J. (2002). New least squares solutions for estimating the average centre of rotation and the axis of rotation. *Journal of Biomechanics*, *35*(1), 87–93.

Garcia, G. H., Liu, J. N., Dines, D. M., & Dines, J. S. (2015). Effect of bone loss in anterior shoulder instability. *World Journal of Orthopedics*, *6*(5), 421–433.

Garner, B. A., & Pandy, M. G. (2001). Musculoskeletal model of the upper limb based on the visible human male dataset. *Computer Methods in Biomechanics and Biomedical Engineering*, *4*(2), 93–126.

Garofalo, P., Cutti, A. G., Filippi, M. V., Cavazza, S., Ferrari, A., Cappello, A., & Davalli, A. (2009). Inter-operator reliability and prediction bands of a novel protocol to measure the coordinated movements of shoulder-girdle and humerus in clinical settings. *Medical & Biological Engineering & Computing*, *47*(5), 475–486.

Garwood, E. R., Souza, R. B., Zhang, A., Zhang, A. L., Ma, C. B., Link, T. M., & Motamedi, D. (2017). Axial traction magnetic resonance imaging (MRI) of the glenohumeral joint in healthy volunteers: initial experience. *Clinical Imaging*, *42*, 178–182.

Gatti, C. J., Dickerson, C. R., Chadwick, E. K., Mell, A. G., & Hughes, R. E. (2007). Comparison of model-predicted and measured moment arms for the rotator cuff muscles. *Clinical Biomechanics (Bristol, Avon)*, *22*(6), 639–644.

Gatti, C. J., Maratt, J. D., Palmer, M. L., Hughes, R. E., & Carpenter, J. E. (2010). Development and

validation of a finite element model of the superior glenoid labrum. *Annals of Biomedical Engineering*, *38*(12), 3766–3776.

Gaunt, B. W., Shaffer, M. A., Sauers, E. L., Michener, L. A., McCluskey, G. M., & Thigpen, C. (2010). The American Society of Shoulder and Elbow Therapists' consensus rehabilitation guideline for arthroscopic anterior capsulolabral repair of the shoulder. *The Journal of Orthopaedic and Sports Physical Therapy*, *40*(3), 155–168.

Gelber, P. E., Reina, F., Monllau, J. C., Yema, P., Rodriguez, A., & Caceres, E. (2006). Innervation patterns of the inferior glenohumeral ligament: anatomical and biomechanical relevance. *Clinical Anatomy (New York, N.Y.)*, *19*(4), 304–311.

Gerace, L., Aliprantis, A., Russell, M., Allison, D. B., Buhl, K. M., Wang, J., Heymsfield, S. B. (1994). Skeletal differences between black and white men and their relevance to body composition estimates. *American Journal of Human Biology : The Official Journal of the Human Biology Council*, *6*(2), 255–262.

Geraldes, D. M., Hansen, U., Jeffers, J., & Amis, A. A. (2017). Stability of small pegs for cementless implant fixation. *Journal of Orthopaedic Research : Official Publication of the Orthopaedic Research Society*, *35*(12), 2765–2772.

Gerber, C., & Nyffeler, R. W. (2002). Classification of glenohumeral joint instability. *Clin Orthop Relat Res*, (400), 65–76.

Gerus, P., Sartori, M., Besier, T. F., Fregly, B. J., Delp, S. L., Banks, S. A., Lloyd, D. G. (2013). Subject-specific knee joint geometry improves predictions of medial tibiofemoral contact forces. *Journal of Biomechanics*, *46*(16), 2778–2786.

Ghodadra, N., Gupta, A., Romeo, A. A., Bach, B. R. J., Verma, N., Shewman, E., Provencher, M. T. (2010). Normalization of glenohumeral articular contact pressures after Latarjet or iliac crest bone-grafting. *The Journal of Bone and Joint Surgery. American Volume*, *92*(6), 1478–1489.

Gibson, J., Kerss, J., Morgan, C., & Brownson, P. (2016). Accelerated rehabilitation after arthroscopic Bankart repair in professional footballers. *Shoulder & Elbow*, *8*(4), 279–286.

Gigis, I., Heikenfeld, R., Kapinas, A., Listringhaus, R., & Godolias, G. (2014). Arthroscopic versus conservative treatment of first anterior dislocation of the shoulder in adolescents. *Journal of Pediatric Orthopedics*, *34*(4), 421–425.

Ginn, K. A., Halaki, M., & Cathers, I. (2011). Revision of the Shoulder Normalization Tests is required to include rhomboid major and teres major. *Journal of Orthopaedic Research : Official Publication of the Orthopaedic Research Society*, *29*(12), 1846–1849.

Grana, W. A., Buckley, P. D., & Yates, C. K. (1993). Arthroscopic Bankart suture repair. *The American Journal of Sports Medicine*, *21*(3), 348–353.

Griesser, M. J., Harris, J. D., McCoy, B. W., Hussain, W. M., Jones, M. H., Bishop, J. Y., & Miniaci, A. (2013). Complications and re-operations after Bristow-Latarjet shoulder stabilization: a systematic review. *Journal of Shoulder and Elbow Surgery*, *22*(2), 286–292.

Griffith, J. F., Antonio, G. E., Tong, C. W. C., & Ming, C. K. (2003). Anterior shoulder dislocation: quantification of glenoid bone loss with CT. *AJR. American Journal of Roentgenology*, *180*(5), 1423–1430.

Griffith, J. F., Antonio, G. E., Yung, P. S. H., Wong, E. M. C., Yu, A. B., Ahuja, A. T., & Chan, K. M. (2008). Prevalence, pattern, and spectrum of glenoid bone loss in anterior shoulder dislocation: CT analysis of 218 patients. *AJR. American Journal of Roentgenology*, *190*(5), 1247–1254.

Halder, A. M., Kuhl, S. G., Zobitz, M. E., Larson, D., & An, K. N. (2001). Effects of the glenoid labrum and glenohumeral abduction on stability of the shoulder joint through concavity-compression : an in vitro study. *The Journal of Bone and Joint Surgery. American Volume*, *83–A*, 1062–1069.

Halder, A. M., Itoi, E., & An, K. N. (2000). Anatomy and biomechanics of the shoulder. *The Orthopedic Clinics of North America*, *31*(2), 159–176.

Handsfield, G. G., Meyer, C. H., Hart, J. M., Abel, M. F., & Blemker, S. S. (2014). Relationships of 35 lower limb muscles to height and body mass quantified using MRI. *Journal of Biomechanics*, *47*(3), 631–638.

Hayes, K., Ginn, K. A., Walton, J. R., Szomor, Z. L., & Murrell, G. A. C. (2004). A randomised clinical trial evaluating the efficacy of physiotherapy after rotator cuff repair. *The Australian Journal of Physiotherapy*, *50*(2), 77–83.

Henseler, J. F., Nagels, J., Nelissen, R. G. H. H., & de Groot, J. H. (2014). Does the latissimus dorsi tendon transfer for massive rotator cuff tears remain active postoperatively and restore active external rotation? *Journal of Shoulder and Elbow Surgery*, *23*(4), 553–560.

Hermens, H. J., Freriks, B., Disselhorst-Klug, C., & Rau, G. (2000). Development of recommendations for SEMG sensors and sensor placement procedures. *Journal of Electromyography and Kinesiology*, *10*(5), 361–374.

Herrmann, S., Konig, C., Heller, M., Perka, C., & Greiner, S. (2011). Reverse shoulder arthroplasty leads to significant biomechanical changes in the remaining rotator cuff. *Journal of Orthopaedic Surgery and Research*, *6*, 42.

Hess, S. (2000). Functional stability of the glenohumeral joint. *Manual Therapy*, *5*(2), 63–71.

Higgins, L. D., & Warner, J. J. (2000). Arthroscopic Bankart repair. Operative technique and surgical pitfalls. *Clinics in Sports Medicine*, *19*(1), 49–62.

Hintermann, B., & Gachter, A. (1995). Arthroscopic findings after shoulder dislocation. *The American Journal of Sports Medicine*, *23*(5), 545–551.

Hobby, J., Griffin, D., Dunbar, M., & Boileau, P. (2007). Is arthroscopic surgery for stabilisation of chronic shoulder instability as effective as open surgery? A systematic review and meta-analysis of 62 studies including 3044 arthroscopic operations. *The Journal of Bone and Joint Surgery. British Volume*, *89*(9), 1188–1196.

Hogfors, C., Karlsson, D., & Peterson, B. (1995). Structure and internal consistency of a shoulder model. *Journal of Biomechanics*, *28*(7), 767–777.

Holzbaur, K. R. S., Murray, W. M., & Delp, S. L. (2005). A model of the upper extremity for simulating musculoskeletal surgery and analyzing neuromuscular control. *Annals of Biomedical Engineering*, *33*(6), 829–840.

Holzbaur, K. R. S., Murray, W. M., Gold, G. E., & Delp, S. L. (2007). Upper limb muscle volumes in adult subjects. *Journal of Biomechanics*, *40*(4), 742–749.

Hovelius L, Eriksson K, Fredin H, E. Al. (1983). Recurrences after initial dislocation of the shoulder. Results of a prospective study of treatment. *J Bone Joint Surg Am.*, *65*(3), 343–349.

Howell, S. M., & Galinat, B. J. (1989). The Glenoid-Labral Socket A constrained articular surface. *Clinical Orthopaedics and Related Research*, *NA;*(243), 122–125.

Howell, S. M., Galinat, B. J., Renzi, a J., & Marone, P. J. (1988). Normal and abnormal mechanics of the glenohumeral joint in the horizontal plane. *The Journal of Bone and Joint Surgery.American Volume*, *70*(2), 227–232.

Hsu, S. H., Miller, S. L., & Curtis, A. S. (2008). Long head of biceps tendon pathology: management alternatives. *Clinics in Sports Medicine*, *27*(4), 747–762.

Hughes, R. E., Niebur, G., Liu, J., & An, K. N. (1998). Comparison of two methods for computing abduction moment arms of the rotator cuff. *Journal of Biomechanics*, *31*(2), 157–160.

Hughes, R. E., Schneeberger, A. G., An, K. N., Morrey, B. F., & O'Driscoll, S. W. (1997). Reduction of triceps muscle force after shortening of the distal humerus: a computational model. *Journal of Shoulder and Elbow Surgery*, *6*(5), 444–448.

Huiskes, R., & Hollister, S. J. (1993). From structure to process, from organ to cell: recent developments of FE-analysis in orthopaedic biomechanics. *Journal of Biomechanical Engineering*, *115*(4B), 520–527.

Hurley, E. T., Fat, D. L., Duigenan, C. M., Miller, J. C., Mullett, H., & Moran, C. J. (2018). Biceps tenodesis versus labral repair for superior labrum anterior-to-posterior tears: a systematic review and meta-analysis. *Journal of Shoulder and Elbow Surgery*. *8*(7), 14–19.

Hurwitz, D. E., Ryals, A. B., Case, J. P., Block, J. A., & Andriacchi, T. P. (2002). The knee adduction moment during gait in subjects with knee osteoarthritis is more closely correlated with static alignment than radiographic disease severity, toe out angle and pain. *Journal of Orthopaedic Research*, *20*(1), 101–107.

Huysmans, P. E., Haen, P. S., Kidd, M., Dhert, W. J., & Willems, J. W. (2006). The shape of the inferior part of the glenoid: A cadaveric study. *Journal of Shoulder and Elbow Surgery*, *15*(6), 759–763.

Hwang, E., Carpenter, J. E., Hughes, R. E., & Palmer, M. L. (2014a). Effects of biceps tension and superior humeral head translation on the glenoid labrum. *Journal of Orthopaedic Research : Official Publication of the Orthopaedic Research Society*, *32*(11), 1424–1429.

Iannotti, J. P., Gabriel, J. P., Schneck, S. L., Evans, B. G., & Misra, S. (1992). The normal glenohumeral relationships. An anatomical study of one hundred and forty shoulders. *The Journal of Bone and Joint Surgery. American Volume*, *74*(4), 491–500.

Ide, J., Maeda, S., & Takagi, K. (2005). Sports activity after arthroscopic superior labral repair using suture anchors in overhead-throwing athletes. *The American Journal of Sports Medicine*, *33*(4), 507–514.

Imhoff, A. B., Ansah, P., Tischer, T., Reiter, C., Bartl, C., Hench, M., Vogt, S. (2010). Arthroscopic repair of anterior-inferior glenohumeral instability using a portal at the 5:30-o'clock position: analysis of the effects of age, fixation method, and concomitant shoulder injury on surgical outcomes. *The American Journal of Sports Medicine*, *38*(9), 1795–1803.

Inman, V. T., Saunders, J. B., & Abbott, L. C. (1996). Observations of the function of the shoulder joint. 1944. *Clinical Orthopaedics and Related Research*, (330), 3–12.

Inoue, A., Chosa, E., Goto, K., & Tajima, N. (2013). Nonlinear stress analysis of the supraspinatus tendon using three-dimensional finite element analysis. *Knee Surgery, Sports Traumatology, Arthroscopy : Official Journal of the ESSKA*, *21*(5), 1151–1157.

Itoi, E., Lee, S. B., Berglund, L. J., Berge, L. L., & An, K. N. (2000). The effect of a glenoid defect on anteroinferior stability of the shoulder after Bankart repair: a cadaveric study. *The Journal of Bone and Joint Surgery. American Volume*, *82*(1), 35–46.

Itoi, E., Newman, S. R., Kuechle, D. K., Morrey, B. F., & An, K. N. (1994). Dynamic anterior stabilisers of the shoulder with the arm in abduction. *The Journal of Bone and Joint Surgery. British Volume*,

76(5), 834–836.

Itoi, E., & Tabata, S. (1992). Rotator cuff tears in anterior dislocation of the shoulder. *International Orthopaedics*, *16*(3), 240–244.

Jastifer, J., Gustafson, P., Patel, B., & Uggen, C. (2012). Pectoralis Major Transfer for Subscapularis Deficiency: A Computational Study. *Shoulder & Elbow*, *4*(1), 25–29.

Jobe, F. W., Giangarra, C. E., Kvitne, R. S., & Glousman, R. E. (1991). Anterior capsulolabral reconstruction of the shoulder in athletes in overhand sports. *The American Journal of Sports Medicine*, *19*(5), 428–434.

Johnson, G. R., & Pandyan, A. D. (2005). The activity in the three regions of the trapezius under controlled loading conditions--an experimental and modelling study. *Clinical Biomechanics (Bristol, Avon)*, *20*(2), 155–161.

Jones, B. K., Durney, K. M., Hung, C. T., & Ateshian, G. A. (2015). The friction coefficient of shoulder joints remains remarkably low over 24 h of loading. *Journal of Biomechanics*, *48*(14), 3945–3949.

Jung, Y., Phan, C.-B., & Koo, S. (2016). Intra-Articular Knee Contact Force Estimation During Walking Using Force-Reaction Elements and Subject-Specific Joint Model. *Journal of Biomechanical Engineering*, *138*(2), 021016.

Kaptein, B. L., & van der Helm, F. C. T. (2004). Estimating muscle attachment contours by transforming geometrical bone models. *Journal of Biomechanics*, *37*(3), 263–273.

Karduna, A. R., McClure, P. W., Michener, L. A., & Sennett, B. (2001). Dynamic measurements of three-dimensional scapular kinematics: a validation study. *Journal of Biomechanical Engineering*, *123*(2), 184–190.

Karlsson, D., & Peterson, B. (1992). Towards a model for force predictions in the human shoulder. *Journal of Biomechanics*, *25*(2), 189–199.

Kawano, Y., Matsumura, N., Murai, A., Tada, M., Matsumoto, M., Nakamura, M., & Nagura, T. (2018). Evaluation of the Translation Distance of the Glenohumeral Joint and the Function of the Rotator Cuff on Its Translation: A Cadaveric Study. *Arthroscopy : The Journal of Arthroscopic & Related Surgery : Official Publication of the Arthroscopy Association of North America and the International Arthroscopy Association*.

Khan, A., Samba, A., Pereira, B., & Canavese, F. (2014). Anterior dislocation of the shoulder in skeletally immature patients: comparison between non-operative treatment versus open Latarjet's procedure. *The Bone & Joint Journal*, *96–B*(3), 354–359.

Kibler, W. B., McMullen, J., & Uhl, T. (2001). Shoulder rehabilitation strategies, guidelines, and

practice. *The Orthopedic Clinics of North America*, *32*(3), 527–538.

Kim, D.-S., Yoon, Y.-S., & Yi, C. H. (2010). Prevalence comparison of accompanying lesions between primary and recurrent anterior dislocation in the shoulder. *The American Journal of Sports Medicine*, *38*(10), 2071–2076.

Kim, T. K., Queale, W. S., Cosgarea, A. J., & McFarland, E. G. (2003). Clinical features of the different types of SLAP lesions: an analysis of one hundred and thirty-nine cases. *The Journal of Bone and Joint Surgery. American Volume*, *85–A*(1), 66–71.

Klein Breteler, M. D., Spoor, C. W., & Van der Helm, F. C. (1999). Measuring muscle and joint geometry parameters of a shoulder for modeling purposes. *Journal of Biomechanics*, *32*(11), 1191–1197.

Klein Horsman, M. D., Koopman, H. F. J. M., van der Helm, F. C. T., Prose, L. P., & Veeger, H. E. J. (2007). Morphological muscle and joint parameters for musculoskeletal modelling of the lower extremity. *Clinical Biomechanics (Bristol, Avon)*, *22*(2), 239–247.

Kontaxis, A., & Johnson, G. R. (2009). The biomechanics of reverse anatomy shoulder replacement – A modelling study. *Clinical Biomechanics*, *24*(3), 254–260.

Krekel, P. R., De Bruin, P. W., Valstar, E. R., Post, F. H., Rozing, P. M., & Botha, C. P. (2009). Evaluation of bone impingement prediction in Pre-operative planning for shoulder arthroplasty. *Proceedings of the Institution of Mechanical Engineers, Part H: Journal of Engineering in Medicine*, *223*(7), 813–822.

Kuechle, D. K., Newman, S. R., Itoi, E., Morrey, B. F., & An, K. N. (1997). Shoulder muscle moment arms during horizontal flexion and elevation. *Journal of Shoulder and Elbow Surgery*, *6*(5), 429–439.

Kummel, B. M. (1970). Fractures of the glenoid cusing chronic dislocation of the shoulder. *Clinical Orthopaedics and Related Research*, *69*, 189–191.

Lafosse, L., Boyle, S., Gutierrez-Aramberri, M., Shah, A., & Meller, R. (2010). Arthroscopic Latarjet Procedure. *Orthopedic Clinics*, *41*(3), 393–405.

Langenderfer, J., Jerabek, S. A., Thangamani, V. B., Kuhn, J. E., & Hughes, R. E. (2004). Musculoskeletal parameters of muscles crossing the shoulder and elbow and the effect of sarcomere length sample size on estimation of optimal muscle length. *Clinical Biomechanics (Bristol, Avon)*, *19*(7), 664–670.

Lee, S. B., Kim, K. J., O'Driscoll, S. W., Morrey, B. F., & An, K. N. (2000). Dynamic glenohumeral stability provided by the rotator cuff muscles in the mid-range and end-range of motion. A study

in cadavera. *The Journal of Bone and Joint Surgery. American Volume*, *82*(6), 849–857.

Lee, Y. S., & Lee, T. Q. (2010). Specimen-specific method for quantifying glenohumeral joint kinematics. *Annals of Biomedical Engineering*, *38*(10), 3226–3236.

Lemieux, P.-O., Nuno, N., Hagemeister, N., & Tetreault, P. (2012). Mechanical analysis of cuff tear arthropathy during multiplanar elevation with the AnyBody shoulder model. *Clinical Biomechanics (Bristol, Avon)*, *27*(8), 801–806.

Lenaerts, G., De Groote, F., Demeulenaere, B., Mulier, M., Van der Perre, G., Spaepen, A., & Jonkers, I. (2008). Subject-specific hip geometry affects predicted hip joint contact forces during gait. *Journal of Biomechanics*, *41*(6), 1243–1252.

Lerner, Z. F., DeMers, M. S., Delp, S. L., & Browning, R. C. (2015). How tibiofemoral alignment and contact locations affect predictions of medial and lateral tibiofemoral contact forces. *Journal of Biomechanics*, *48*(4), 644–650.

Leroux, T., Wasserstein, D., Veillette, C., Khoshbin, A., Henry, P., Chahal, J., Ogilvie-Harris, D. (2014). Epidemiology of primary anterior shoulder dislocation requiring closed reduction in Ontario, Canada. *The American Journal of Sports Medicine*, *42*(2), 442–450.

Levine, W. N., Richmond, J. C., & Donaldson, W. R. (1994). Use of the suture anchor in open Bankart reconstruction. A follow-up report. *The American Journal of Sports Medicine*, *22*(5), 723–726.

Lew, W. D., & Lewis, J. L. (1977). An anthropometric scaling method with application to the knee joint. *Journal of Biomechanics*, *10*(3), 171–181.

Lewis, J. L., Lew, W. D., & Zimmerman, J. R. (1980). A nonhomogeneous anthropometric scaling method based on finite element principles. *Journal of Biomechanics*, *13*(10), 815–824.

Li, Q., & Xia, C. (2014). Research of Electric Power Steering System Assistance Characteristic Based on The Identification of The Road. *Advanced Materials Research*, *756–759*.

Liavaag, S., Svenningsen, S., Reikeras, O., Enger, M., Fjalestad, T., Pripp, A. H., & Brox, J. I. (2011). The epidemiology of shoulder dislocations in Oslo. *Scandinavian Journal of Medicine & Science in Sports*, *21*(6), e334-40.

Liem, D., Buschmann, V. E., Schmidt, C., Gosheger, G., Vogler, T., Schulte, T. L., & Balke, M. (2014). The prevalence of rotator cuff tears: is the contralateral shoulder at risk? *The American Journal of Sports Medicine*, *42*(4), 826–830.

Lippitt, S. B., Vanderhooft, J. E., Harris, S. L., Sidles, J. A., Harryman, D. T. 2nd, & Matsen, F. A. 3rd. (1993). Glenohumeral stability from concavity-compression: A quantitative analysis. *Journal of Shoulder and Elbow Surgery*, *2*(1), 27–35.

Lippitt, S., & Matsen, F. (1993). Mechanisms of glenohumeral joint stability. *Clinical Orthopaedics and Related Research*. *291*(5), 20–28.

Lo, I. K. Y., Parten, P. M., & Burkhart, S. S. (2004). The Inverted Pear Glenoid: An Indicator of Significant Glenoid Bone Loss. *Arthroscopy - Journal of Arthroscopic and Related Surgery*, *20*(2), 169–174.

Ma, R., Brimmo, O. A., Li, X., & Colbert, L. (2017). Current Concepts in Rehabilitation for Traumatic Anterior Shoulder Instability. *Current Reviews in Musculoskeletal Medicine*, *10*(4), 499–506.

Magermans, D. J., Chadwick, E. K. J., Veeger, H. E. J., Rozing, P. M., & van der Helm, F. C. T. (2004). Effectiveness of tendon transfers for massive rotator cuff tears: a simulation study. *Clinical Biomechanics (Bristol, Avon)*, *19*(2), 116–122.

Manal, K., & Buchanan, T. S. (2013). An Electromyogram-Driven Musculoskeletal Model of the Knee to Predict *in Vivo* Joint Contact Forces During Normal and Novel Gait Patterns. *Journal of Biomechanical Engineering*, *135*(2), 021014.

Maquieira, G. J., Gerber, C., & Schneeberger, A. G. (2007). Suprascapular nerve palsy after the Latarjet procedure. *Journal of Shoulder and Elbow Surgery*, *16*(2), e13-5.

Marra, M. A., Vanheule, V., Fluit, R., Koopman, B. H. F. J. M., Rasmussen, J., Verdonschot, N., & Andersen, M. S. (2015). A Subject-Specific Musculoskeletal Modeling Framework to Predict In Vivo Mechanics of Total Knee Arthroplasty. *Journal of Biomechanical Engineering*, *137*(2), 20904–20912.

Marsden, S. P., Swailes, D. C., & Johnson, G. R. (2008). Algorithms for exact multi-object muscle wrapping and application to the deltoid muscle wrapping around the humerus. *Proceedings of the Institution of Mechanical Engineers. Part H, Journal of Engineering in Medicine*, *222*(7), 1081–1095.

Marshall, T., Vega, J., Siqueira, M., Cagle, R., Gelber, J. D., & Saluan, P. (2017). Outcomes After Arthroscopic Bankart Repair: Patients With First-Time Versus Recurrent Dislocations. *The American Journal of Sports Medicine*, *45*(8), 1776–1782.

Masjedi, M., & Johnson, G. R. (2010). Reverse anatomy shoulder replacement: comparison of two designs. *Proceedings of the Institution of Mechanical Engineers. Part H, Journal of Engineering in Medicine*, *224*(9), 1039–1049.

Matheson, G. O., Shultz, R., Bido, J., Mitten, M. J., Meeuwisse, W. H., & Shrier, I. (2011). Return-to-play decisions: are they the team physician's responsibility? *Clinical Journal of Sport Medicine : Official Journal of the Canadian Academy of Sport Medicine*, *21*(1), 25–30.

Matias, R., Andrade, C., & Veloso, A. P. (2009). A transformation method to estimate muscle attachments based on three bony landmarks. *Journal of Biomechanics*, *42*(3), 331–335.

Matias, R., Andrade, C., & Veloso, A. P. (2011). Accuracy of a transformation method to estimate muscle attachments based on three bony landmarks. *Computer Methods in Biomechanics and Biomedical Engineering*, *14*(1), 73–78.

Matsuki, K., Matsuki, K. O., Yamaguchi, S., Ochiai, N., Sasho, T., Sugaya, H., … Banks, S. a. (2012). Dynamic In Vivo Glenohumeral Kinematics During Scapular Plane Abduction in Healthy Shoulders. *Journal of Orthopaedic & Sports Physical Therapy*, *42*(2), 96–104.

McCullagh, P. J. J. (1995). Biomechanics and Design of Shoulder Arthroplasty. *Proceedings of the Institution of Mechanical Engineers, Part H: Journal of Engineering in Medicine*, *209*(4), 207–213.

McDermott, D. M., Neumann, L., Frostick, S. P., & Wallace, W. A. (1999). Early results of Bankart repair with a patient-controlled rehabilitation program. *Journal of Shoulder and Elbow Surgery*, *8*(2), 146–150.

McEleney, E. T., Donovan, M. J., Shea, K. P., & Nowak, M. D. (1995). Initial failure strength of open and arthroscopic Bankart repairs. *Arthroscopy : The Journal of Arthroscopic & Related Surgery : Official Publication of the Arthroscopy Association of North America and the International Arthroscopy Association*, *11*(4), 426–431.

McFarland, E. G., Kim, T. K., & Savino, R. M. (2002). Clinical assessment of three common tests for superior labral anterior-posterior lesions. *The American Journal of Sports Medicine*, *30*(6), 810–815.

McGinley, J. L., Baker, R., Wolfe, R., & Morris, M. E. (2009). The reliability of three-dimensional kinematic gait measurements: a systematic review. *Gait & Posture*, *29*(3), 360–369.

McHugh, M. P., Tyler, T. F., Mullaney, M. J., Mirabella, M. R., & Nicholas, S. J. (2016). The Effect of a High Pitch Volume on Musculoskeletal Adaptations in High School Baseball Pitchers. *The American Journal of Sports Medicine*, *44*(9), 2246–2254.

McLaughlin, H. L., & MacLellan, D. I. (1967). Recurrent anterior dislocation of the shoulder. II. A comparative study. *The Journal of Trauma*, *7*(2), 191–201.

McMahon, P. J., Yang, B. Y., Chow, S., & Lee, T. Q. (2013). Anterior shoulder dislocation increases the propensity for recurrence: A cadaveric study of the number of dislocations and type of capsulolabral lesion. *Journal of Shoulder and Elbow Surgery*, *22*(8), 1046–1052.

Merolla, G., Paladini, P., & Porcellini, G. (2018). Assessment of return to play in professional overhead

athletes subjected to arthroscopic repair of rotator cuff tears and associated labral injuries using the Italian version of the Kerlan-Jobe Orthopedic Clinic Shoulder and Elbow score. *Musculoskeletal Surgery*.

Meskers, C. G. M., de Groot, J. H., Arwert, H. J., Rozendaal, L. A., & Rozing, P. M. (2004). Reliability of force direction dependent EMG parameters of shoulder muscles for clinical measurements. *Clinical Biomechanics (Bristol, Avon)*, *19*(9), 913–920.

Mileski, R. A., & Snyder, S. J. (1998). Superior labral lesions in the shoulder: pathoanatomy and surgical management. *The Journal of the American Academy of Orthopaedic Surgeons*, *6*(2), 121–131.

Milgrom, C., Schaffler, M., Gilbert, S., & van Holsbeeck, M. (1995). Rotator-cuff changes in asymptomatic adults. The effect of age, hand dominance and gender. *The Journal of Bone and Joint Surgery. British Volume*, *77*(2), 296–298.

Min, K., Fedorka, C., Solberg, M. J., Shaha, S. H., & Higgins, L. D. (2018). The cost-effectiveness of the arthroscopic Bankart versus open Latarjet in the treatment of primary shoulder instability. *Journal of Shoulder and Elbow Surgery*.

Mizuno, N., Yoneda, M., Nakagawa, S., & Hayashida, K. (2016). The pathology of the anterior capsule in patients over forty years of age with recurrent shoulder dislocation. *International Orthopaedics*, *40*(1), 81–86.

Modenese, L., Ceseracciu, E., Reggiani, M., & Lloyd, D. (2015). Estimation of musculotendon parameters for scaled and subject specific musculoskeletal models using an optimization technique. *Journal of Biomechanics*, *49*.

Modenese, L., Phillips, A. T. M., & Bull, A. M. J. (2011). An open source lower limb model: Hip joint validation. *Journal of Biomechanics*, *44*(12), 2185–2193.

Moissenet, F., Cheze, L., & Dumas, R. (2014). A 3D lower limb musculoskeletal model for simultaneous estimation of musculo-tendon, joint contact, ligament and bone forces during gait. *Journal of Biomechanics*, *47*(1), 50–58.

Moore, S. M., Ellis, B., Weiss, J. A., McMahon, P. J., & Debski, R. E. (2010). The glenohumeral capsule should be evaluated as a sheet of fibrous tissue: a validated finite element model. *Annals of Biomedical Engineering*, *38*(1), 66–76.

Murakami, T., Higaki, H., Sawae, Y., Ohtsuki, N., Moriyama, S., & Nakanishi, Y. (1998). Adaptive multimode lubrication in natural synovial joints and artificial joints. *Proceedings of the Institution of Mechanical Engineers, Part H: Journal of Engineering in Medicine*, *212*(1), 23–35.

Murphy, C. A., McDermott, W. J., Petersen, R. K., Johnson, S. E., & Baxter, S. A. (2013). Electromyographic analysis of the rotator cuff in postoperative shoulder patients during passive rehabilitation exercises. *Journal of Shoulder and Elbow Surgery*, *22*(1), 102–107.

Murray, I. A., & Johnson, G. R. (2004). A study of the external forces and moments at the shoulder and elbow while performing every day tasks. *Clinical Biomechanics (Bristol, Avon)*, *19*(6), 586–594.

Murray, W. M., Buchanan, T. S., & Delp, S. L. (2000). The isometric functional capacity of muscles that cross the elbow. *Journal of Biomechanics*, *33*(8), 943–952.

Murray, W. M., Buchanan, T. S., & Delp, S. L. (2002). Scaling of peak moment arms of elbow muscles with upper extremity bone dimensions. *Journal of Biomechanics*, *35*(1), 19–26.

Musgrave, D. S., & Rodosky, M. W. (2001). SLAP lesions: current concepts. *American Journal of Orthopedics (Belle Mead, N.J.)*, *30*(1), 29–38.

Nam, E. K., & Snyder, S. J. (2003). The diagnosis and treatment of superior labrum, anterior and posterior (SLAP) lesions. *The American Journal of Sports Medicine*, *31*(5), 798–810.

Navacchia, A., Myers, C. A., Rullkoetter, P. J., & Shelburne, K. B. (2016). Prediction of In Vivo Knee Joint Loads Using a Global Probabilistic Analysis. *Journal of Biomechanical Engineering*, *138*(3), 4032379.

Nelson, G. N., Namdari, S., Galatz, L., & Keener, J. D. (2014). Pectoralis major tendon transfer for irreparable subscapularis tears. *Journal of Shoulder and Elbow Surgery*, *23*(6), 909–918.

Neri, B. R., Elattrache, N. S., Owsley, K. C., Mohr, K., & Yocum, L. A. (2011). Outcome of type II superior labral anterior posterior repairs in elite overhead athletes: Effect of concomitant partial-thickness rotator cuff tears. *American Journal of Sports Medicine*, *39*(1), 114–120.

Neviaser, A. S., Benke, M. T., & Neviaser, R. J. (2015). Open Bankart repair for revision of failed prior stabilization: outcome analysis at a mean of more than 10 years. *Journal of Shoulder and Elbow Surgery*, *24*(6), 897–901.

Neviaser, R. J., Neviaser, T. J., & Neviaser, J. S. (1993). Anterior dislocation of the shoulder and rotator cuff rupture. *Clinical Orthopaedics and Related Research*, (291), 103–106.

Nikooyan, A. A., Veeger, H. E. J., Westerhoff, P., Graichen, F., Bergmann, G., & van der Helm, F. C. T. (2010). Validation of the Delft Shoulder and Elbow Model using in-vivo glenohumeral joint contact forces. *Journal of Biomechanics*, *43*(15), 3007–3014.

Nolte, D., Tsang, C. K., Zhang, K. Y., Ding, Z., Kedgley, A. E., & Bull, A. M. J. (2016). Non-linear scaling of a musculoskeletal model of the lower limb using statistical shape models. *Journal of Biomechanics*, *49*(14), 3576–3581.

Nordqvist, A., & Petersson, C. J. (1995). Incidence and causes of shoulder girdle injuries in an urban population. *Journal of Shoulder and Elbow Surgery*, *4*(2), 107–112.

Norlin, R. (1993). Intraarticular pathology in acute, first-time anterior shoulder dislocation: an arthroscopic study. *Arthroscopy : The Journal of Arthroscopic & Related Surgery : Official Publication of the Arthroscopy Association of North America and the International Arthroscopy Association*, *9*(5), 546–549.

Norlin, R. (1994). Use of Mitek anchoring for Bankart repair: A comparative, randomized, prospective study with traditional bone sutures. *Journal of Shoulder and Elbow Surgery*, *3*(6), 381–385.

O'Brien, S. J., Neves, M. C., Arnoczky, S. P., Rozbruck, S. R., Dicarlo, E. F., Warren, R. F., Wickiewicz, T. L. (1990). The anatomy and histology of the inferior glenohumeral ligament complex of the shoulder. *The American Journal of Sports Medicine*, *18*(5), 449–456.

O'Connell, P. W., Nuber, G. W., Mileski, R. A., & Lautenschlager, E. (1990). The contribution of the glenohumeral ligaments to anterior stability of the shoulder joint. *The American Journal of Sports Medicine*, *18*(6), 579–584.

Ogawa, K., & Yoshida, A. (1997). Extensive shoulder capsule tearing as a main cause of recurrent anterior shoulder dislocation. *Journal of Shoulder and Elbow Surgery*, *6*(1), 1–5.

Ohl, X., Billuart, F., Lagace, P.-Y., Gagey, O., Hagemeister, N., & Skalli, W. (2012). 3D morphometric analysis of 43 scapulae. *Surgical and Radiologic Anatomy : SRA*, *34*(5), 447–453.

Omori, Y., Yamamoto, N., Koishi, H., Futai, K., Goto, A., Sugamoto, K., & Itoi, E. (2014). Measurement of the Glenoid Track In Vivo as Investigated by 3-Dimensional Motion Analysis Using Open MRI. *The American Journal of Sports Medicine*, *42*(6), 1290–1295.

Orchard, J. W., Blanch, P., Paoloni, J., Kountouris, A., Sims, K., Orchard, J. J., & Brukner, P. (2015). Cricket fast bowling workload patterns as risk factors for tendon, muscle, bone and joint injuries. *British Journal of Sports Medicine*, *49*(16), 1064–1068.

Otten, E. (2003). Inverse and forward dynamics: models of multi-body systems. *Philosophical Transactions of the Royal Society of London. Series B, Biological Sciences*, *358*(1437), 1493–1500.

Ouellette, H., Labis, J., Bredella, M., Palmer, W. E., Sheah, K., & Torriani, M. (2008). Spectrum of shoulder injuries in the baseball pitcher. *Skeletal Radiology*, *37*(6), 491–498.

Owens, B. D., Dawson, L., Burks, R., & Cameron, K. L. (2009). Incidence of shoulder dislocation in the United States military: demographic considerations from a high-risk population. *The Journal of Bone and Joint Surgery. American Volume*, *91*(4), 791–796.

Owens, B. D., Harrast, J. J., Hurwitz, S. R., Thompson, T. L., & Wolf, J. M. (2011). Surgical trends in Bankart repair: an analysis of data from the American Board of Orthopaedic Surgery certification examination. *The American Journal of Sports Medicine*, *39*(9), 1865–1869.

Pagnani, M. J., Deng, X. H., Warren, R. F., Torzilli, P. a, & Altchek, D. W. (1995). Effect of lesions of the superior portion of the glenoid labrum on glenohumeral translation. *The Journal of Bone and Joint Surgery. American Volume*, *77*(7), 1003–1010. Retrieved from

Pal, S., Langenderfer, J. E., Stowe, J. Q., Laz, P. J., Petrella, A. J., & Rullkoetter, P. J. (2007). Probabilistic modeling of knee muscle moment arms: effects of methods, origin-insertion, and kinematic variability. *Annals of Biomedical Engineering*, *35*(9), 1632–1642.

Pandis, P. 2013. Musculoskeletal biomechanics of the shoulder in functional activities. PhD Thesis, Imperial College London.

Pandis, P., Prinold, J. A. I., & Bull, A. M. J. (2015). Shoulder muscle forces during driving: Sudden steering can load the rotator cuff beyond its repair limit. *Clinical Biomechanics*, *30*(8), 839–846.

Parsons, I. M., Apreleva, M., Fu, F. H., & Woo, S. L. Y. (2002). The effect of rotator cuff tears on reaction forces at the glenohumeral joint. *Journal of Orthopaedic Research : Official Publication of the Orthopaedic Research Society*, *20*(3), 439–446.

Patterson, B. M., Creighton, R. A., Spang, J. T., Roberson, J. R., & Kamath, G. V. (2014). Surgical Trends in the Treatment of Superior Labrum Anterior and Posterior Lesions of the Shoulder: Analysis of Data From the American Board of Orthopaedic Surgery Certification Examination Database. *The American Journal of Sports Medicine*, *42*(8), 1904–1910.

Pellikaan, P., van der Krogt, M. M., Carbone, V., Fluit, R., Vigneron, L. M., Van Deun, J., Koopman, H. F. J. M. (2014). Evaluation of a morphing based method to estimate muscle attachment sites of the lower extremity. *Journal of Biomechanics*, *47*(5), 1144–1150.

Peterson, S. L., & Rayan, G. M. (2011). Shoulder and upper arm muscle architecture. *Journal of Hand Surgery*, *36*(5), 881–889.

Petrera, M., Patella, V., Patella, S., & Theodoropoulos, J. (2010). A meta-analysis of open versus arthroscopic Bankart repair using suture anchors. *Knee Surgery, Sports Traumatology, Arthroscopy : Official Journal of the ESSKA*, *18*(12), 1742–1747.

Pevny, T., Hunter, R. E., & Freeman, J. R. (1998). Primary traumatic anterior shoulder dislocation in patients 40 years of age and older. *Arthroscopy : The Journal of Arthroscopic & Related Surgery : Official Publication of the Arthroscopy Association of North America and the International Arthroscopy Association*, *14*(3), 289–294.

Pizzari, T., Kolt, G. S., & Remedios, L. (1999). Measurement of anterior-to-posterior translation of the glenohumeral joint using the KT-1000. *The Journal of Orthopaedic and Sports Physical Therapy*, *29*(10), 602–608.

Pope, E. J., Ward, J. P., & Rokito, A. S. (2011). Anterior shoulder instability: A history of arthroscopic treatment. *Bulletin of the NYU Hospital for Joint Diseases*, *69*(1), 44–49.

Poppen, N. K., & Walker, P. S. (1978). Forces at the glenohumeral joint in abduction. *Clinical Orthopaedics and Related Research*, (135), 165–170.

Porcellini, G., Campi, F., Pegreffi, F., Castagna, A., & Paladini, P. (2009). Predisposing factors for recurrent shoulder dislocation after arthroscopic treatment. *The Journal of Bone and Joint Surgery. American Volume*, *91*(11), 2537–2542.

Praagman, M., Chadwick, E. K. J., van der Helm, F. C. T., & Veeger, H. E. J. (2010). The effect of elbow angle and external moment on load sharing of elbow muscles. *Journal of Electromyography and Kinesiology*, *20*(5), 912–922.

Prinold, J. A. I., & Bull, A. M. J. (2016). Scapula kinematics of pull-up techniques: Avoiding impingement risk with training. *Journal of Science and Medicine in Sport*, *19*(8), 629–635.

Prinold, J. A. I., Mazza, C., Di Marco, R., Hannah, I., Malattia, C., Magni-Manzoni, S., Viceconti, M. (2016). A Patient-Specific Foot Model for the Estimate of Ankle Joint Forces in Patients with Juvenile Idiopathic Arthritis. *Annals of Biomedical Engineering*, *44*(1), 247–257.

Prinold, J. A., Masjedi, M., Johnson, G. R., & Bull, a. M. (2013). Musculoskeletal shoulder models: A technical review and proposals for research foci. *Proceedings of the Institution of Mechanical Engineers, Part H: Journal of Engineering in Medicine*, *227*(10), 1041–1057.

Prinold, J. A I., & Bull, A. M. J. (2014). Scaling and kinematics optimisation of the scapula and thorax in upper limb musculoskeletal models. *Journal of Biomechanics*, *47*(11), 2813–2819.

Prinold, J. A I., Shaheen, A. F., & Bull, a. M. J. (2011). Skin-fixed scapula trackers: A comparison of two dynamic methods across a range of calibration positions. *Journal of Biomechanics*, *44*(10), 2004–2007.

Quapp, K. M., & Weiss, J. A. (1998). Material characterization of human medial collateral ligament. *Journal of Biomechanical Engineering*, *120*(6), 757–763.

Quental, C., Folgado, J., Ambrosio, J., & Monteiro, J. (2015). Critical analysis of musculoskeletal modelling complexity in multibody biomechanical models of the upper limb. *Computer Methods in Biomechanics and Biomedical Engineering*, *18*(7), 749–759.

Raikova, R. T., & Aladjov, H. T. (2002). Hierarchical genetic algorithm versus static optimization-

investigation of elbow flexion and extension movements. *Journal of Biomechanics*, *35*(8), 1123–1135.

Randelli, P., Ragone, V., Carminati, S., & Cabitza, P. (2012). Risk factors for recurrence after Bankart repair a systematic review. *Knee Surgery, Sports Traumatology, Arthroscopy : Official Journal of the ESSKA*, *20*(11), 2129–2138.

Rapariz, J. M., Martin-Martin, S., Pareja-Bezares, A., & Ortega-Klein, J. (2010). Shoulder dislocation in patients older than 60 years of age. *International Journal of Shoulder Surgery*, *4*(4), 88–92.

Reeves, B. (1968). Experiments on the tensile strength of the anterior capsular structures of the shoulder in man. *The Journal of Bone and Joint Surgery. British Volume*, *50*(4), 858–865.

Robinson, C. M., Howes, J., Murdoch, H., Will, E., & Graham, C. (2006). Functional outcome and risk of recurrent instability after primary traumatic anterior shoulder dislocation in young patients. *The Journal of Bone and Joint Surgery. American Volume*, *88*(11), 2326–2336.

Rokito, S. E., Myers, K. R., & Ryu, R. K. N. (2014). SLAP lesions in the overhead athlete. *Sports Medicine and Arthroscopy Review*, *22*(2), 110–116.

Rollick, N. C., Ono, Y., Kurji, H. M., Nelson, A. A., Boorman, R. S., Thornton, G. M., & Lo, I. K. (2017). Long-term outcomes of the Bankart and Latarjet repairs: a systematic review. *Open Access Journal of Sports Medicine*, *8*, 97–105.

Rowe, C. R., Zarins, B., & Ciullo, J. V. (1984). Recurrent anterior dislocation of the shoulder after surgical repair. Apparent causes of failure and treatment. *The Journal of Bone and Joint Surgery. American Volume*, *66*(2), 159–168.

Rugg, C. M., Hettrich, C. M., Ortiz, S., Wolf, B. R., & Zhang, A. L. (2018). Surgical stabilization for first-time shoulder dislocators: a multicenter analysis. *Journal of Shoulder and Elbow Surgery*, *27*(4), 674–685.

Ruggiero, M., Cless, D., & Infantolino, B. (2016). Upper and Lower Limb Muscle Architecture of a 104 Year-Old Cadaver. *PloS One*, *11*(12), e0162963.

Rumian, A., Coffey, D., Fogerty, S., & Hackney, R. (2011). Acute first-time shoulder dislocation. *Orthopaedics and Trauma*, *25*(5), 363–368.

Saito, H., Itoi, E., Minagawa, H., Yamamoto, N., Tuoheti, Y., & Seki, N. (2009). Location of the Hill-Sachs lesion in shoulders with recurrent anterior dislocation. *Archives of Orthopaedic and Trauma Surgery*, *129*(10), 1327–1334.

Saliken, D. J., Bornes, T. D., Bouliane, M. J., Sheps, D. M., & Beaupre, L. A. (2015). Imaging methods for quantifying glenoid and Hill-Sachs bone loss in traumatic instability of the shoulder: a scoping

review. *BMC Musculoskeletal Disorders*, *16(2)*, 164-168.

Samani, J. E., Marston, S. B., & Buss, D. D. (2001). Arthroscopic stabilization of type II SLAP lesions using an absorbable tack. *Arthroscopy : The Journal of Arthroscopic & Related Surgery : Official Publication of the Arthroscopy Association of North America and the International Arthroscopy Association*, *17*(1), 19–24.

Sano, H., Wakabayashi, I., & Itoi, E. (2006). Stress distribution in the supraspinatus tendon with partial-thickness tears: An analysis using two-dimensional finite element model. *Journal of Shoulder and Elbow Surgery*, *15*(1), 100–105.

Saul, K. R., Hayon, S., Smith, T. L., Tuohy, C. J., & Mannava, S. (2011). Postural dependence of passive tension in the supraspinatus following rotator cuff repair: a simulation analysis. *Clinical Biomechanics (Bristol, Avon)*, *26*(8), 804–810.

Saul, K. R., Murray, W. M., Hentz, V. R., & Delp, S. L. (2003). Biomechanics of the Steindler flexorplasty surgery: a computer simulation study. *The Journal of Hand Surgery*, *28*(6), 979–986.

Sayde, W. M., Cohen, S. B., Ciccotti, M. G., & Dodson, C. C. (2012a). Return to play after Type II superior labral anterior-posterior lesion repairs in athletes: a systematic review. *Clinical Orthopaedics and Related Research*, *470*(6), 1595–1600.

Sayde, W. M., Cohen, S. B., Ciccotti, M. G., & Dodson, C. C. (2012b). Return to play after type ii superior labral anterior-posterior lesion repairs in athletes: A systematic review. *Clinical Orthopaedics and Related Research*, *470*(6), 1595–1600.

Scheys, L., Van Campenhout, A., Spaepen, A., Suetens, P., & Jonkers, I. (2008a). Personalized MR-based musculoskeletal models compared to rescaled generic models in the presence of increased femoral anteversion: Effect on hip moment arm lengths. *Gait and Posture*, *28*(3), 358–365.

Schwer, L. E. (2007). Validation metrics for response histories: perspectives and case studies. *Engineering with Computers*, *23*(4), 295–309.

Seppel, G., Plath, J. E., Völk, C., Seiberl, W., Buchmann, S., Waldt, S., Braun, S. (2017). Long-term Results after Arthroscopic Repair of Isolated Subscapularis Tears. *American Journal of Sports Medicine*, *45*(4), 759–766.

Shah, A., Judge, A., Delmestri, A., Edwards, K., Arden, N. K., Prieto-Alhambra, D., Rees, J. L. (2017). Incidence of shoulder dislocations in the UK, 1995–2015: a population-based cohort study. *BMJ Open*, *7*(11), e016112.

Shaha, J. S., Cook, J. B., Song, D. J., Rowles, D. J., Bottoni, C. R., Shaha, S. H., & Tokish, J. M. (2015). Redefining “Critical” Bone Loss in Shoulder Instability: Functional Outcomes Worsen With

"Subcritical" Bone Loss. *The American Journal of Sports Medicine*, *43*(7), 1719–1725.

Shaheen, A. F., Alexander, C. M., & Bull, A. M. J. (2011). Effects of attachment position and shoulder orientation during calibration on the accuracy of the acromial tracker. *Journal of Biomechanics*, *44*(7), 1410–1413.

Shin, S.-J., Kim, R. G., Jeon, Y. S., & Kwon, T. H. (2017). Critical Value of Anterior Glenoid Bone Loss That Leads to Recurrent Glenohumeral Instability After Arthroscopic Bankart Repair. *The American Journal of Sports Medicine*, *45*(9), 1975–1981.

Shin, S.-J., Ko, Y. W., Scott, J., McGarry, M. H., & Lee, T. Q. (2016). The effect of defect orientation and size on glenohumeral instability: a biomechanical analysis. *Knee Surgery, Sports Traumatology, Arthroscopy : Official Journal of the ESSKA*, *24*(2), 533–539.

Shin, S.-J., Koh, Y. W., Bui, C., Jeong, W. K., Akeda, M., Cho, N. S., Lee, T. Q. (2016). What Is the Critical Value of Glenoid Bone Loss at Which Soft Tissue Bankart Repair Does Not Restore Glenohumeral Translation, Restricts Range of Motion, and Leads to Abnormal Humeral Head Position? *The American Journal of Sports Medicine*, *44*(11), 2784–2791.

Smith, C. D., Masouros, S. D., Hill, a M., Wallace, a L., Amis, a a, & Bull, a M. (2008). Tensile properties of the human glenoid labrum. *Journal of Anatomy*, *212*(1), 49–54.

Smith, C. D., Masouros, S., Hill, A. M., Amis, A. A., & Bull, A. M. J. (2009). A biomechanical basis for tears of the human acetabular labrum. *British Journal of Sports Medicine*, *43*, 574–578.

Smith, R., Lombardo, D. J., Petersen-Fitts, G. R., Frank, C., Tenbrunsel, T., Curtis, G., Sabesan, V. J. (2016). Return to Play and Prior Performance in Major League Baseball Pitchers After Repair of Superior Labral Anterior-Posterior Tears. *Orthopaedic Journal of Sports Medicine*, *4*(12), 2325967116675822.

Snyder, S. J., Banas, M. P., & Karzel, R. P. (1995). An analysis of 140 injuries to the superior glenoid labrum. *Journal of Shoulder and Elbow Surgery*, *4*(4), 243–248.

Snyder, S. J., Karzel, R. P., Del Pizzo, W., Ferkel, R. D., & Friedman, M. J. (1990). SLAP lesions of the shoulder. *Arthroscopy : The Journal of Arthroscopic & Related Surgery : Official Publication of the Arthroscopy Association of North America and the International Arthroscopy Association*, *6*(4), 274–279.

Sommer, H. J. 3rd, Miller, N. R., & Pijanowski, G. J. (1982). Three-dimensional osteometric scaling and normative modelling of skeletal segments. *Journal of Biomechanics*, *15*(3), 171–180.

Soslowsky, L. J., Flatow, E. L., Bigliani, L. U., Pawluk, R. J., Ateshian, G. a., & Mow, V. C. (1992). Quantitation of in situ contact areas at the glenohumeral joint: A biomechanical study. *Journal of*

Orthopaedic Research, *10*(4), 524–534.

Speer, K. P., Cavanaugh, J. T., Warren, R. F., Day, L., & Wickiewicz, T. L. (1993). A role for hydrotherapy in shoulder rehabilitation. *The American Journal of Sports Medicine*, *21*(6), 850–853.

Spitzer, V. M., & Whitlock, D. G. (1998). The Visible Human Dataset: the anatomical platform for human simulation. *The Anatomical Record*, *253*(2), 49–57.

Steenbrink, F., de Groot, J. H., Veeger, H. E. J., van der Helm, F. C. T., & Rozing, P. M. (2009). Glenohumeral stability in simulated rotator cuff tears. *Journal of Biomechanics*, *42*(11), 1740–1745.

Steinbeck, J., Liljenqvist, U., & Jerosch, J. (1998). The anatomy of the glenohumeral ligamentous complex and its contribution to anterior shoulder stability. *Journal of Shoulder and Elbow Surgery*, *7*(2), 122–126.

Strauss, E. J., Salata, M. J., Sershon, R. A., Garbis, N., Provencher, M. T., Wang, V. M., Verma, N. N. (2014). Role of the superior labrum after biceps tenodesis in glenohumeral stability. *Journal of Shoulder and Elbow Surgery*, *23*(4), 485–491.

Suarez, D. R., Valstar, E. R., van der Linden, J. C., van Keulen, F., & Rozing, P. M. (2009). Effect of rotator cuff dysfunction on the initial mechanical stability of cementless glenoid components. *Medical & Biological Engineering & Computing*, *47*(5), 507–514.

Sugaya, H., Moriishi, J., Dohi, M., Kon, Y., & Tsuchiya, A. (2003). Glenoid rim morphology in recurrent anterior glenohumeral instability. *The Journal of Bone and Joint Surgery. American Volume*, *85–A*(5), 878–884.

Taylor, D. C., & Arciero, R. A. (1997). Pathologic changes associated with shoulder dislocations. Arthroscopic and physical examination findings in first-time, traumatic anterior dislocations. *The American Journal of Sports Medicine*, *25*(3), 306–311.

Terrier, A., Buchler, P., & Farron, A. (2006). Influence of glenohumeral conformity on glenoid stresses after total shoulder arthroplasty. *Journal of Shoulder and Elbow Surgery*, *15*(4), 515–520.

Terrier, A., Reist, A., Vogel, A., & Farron, A. (2007). Effect of supraspinatus deficiency on humerus translation and glenohumeral contact force during abduction. *Clinical Biomechanics*, *22*(6), 645–651.

Terrier, A., Vogel, A., Capezzali, M., & Farron, A. (2008). An algorithm to allow humerus translation in the indeterminate problem of shoulder abduction. *Medical Engineering & Physics*, *30*(6), 710–716.

Terry, G. C., & Chopp, T. M. (2000). Functional Anatomy of the Shoulder. *Journal of Athletic Training*, *35*(3), 248–255.

Thomas, S. C., & Matsen, F. A. 3rd. (1989). An approach to the repair of avulsion of the glenohumeral ligaments in the management of traumatic anterior glenohumeral instability. *The Journal of Bone and Joint Surgery. American Volume*, *71*(4), 506–513.

Tsai, L.-C., Colletti, P. M., & Powers, C. M. (2012). Magnetic resonance imaging-measured muscle parameters improved knee moment prediction of an EMG-driven model. *Medicine and Science in Sports and Exercise*, *44*(2), 305–312.

Uhl, T. L., Muir, T. A., & Lawson, L. (2010). Electromyographical assessment of passive, active assistive, and active shoulder rehabilitation exercises. *PM & R : The Journal of Injury, Function, and Rehabilitation*, *2*(2), 132–141.

Usman, J., McIntosh, A. S., & Frechede, B. (2011). An investigation of shoulder forces in active shoulder tackles in rugby union football. *Journal of Science and Medicine in Sport*, *14*(6), 547–552.

Valente, G., Pitto, L., Testi, D., Seth, A., Delp, S. L., Stagni, R., Taddei, F. (2014). Are subject-specific musculoskeletal models robust to the uncertainties in parameter identification? *PloS One*, *9*(11), e112625. van Andel, C. J., Wolterbeek, N., Doorenbosch, C. A. M., Veeger, D. H. E. J., & Harlaar, J. (2008). Complete 3D kinematics of upper extremity functional tasks. *Gait & Posture*, *27*(1), 120–127.

Van der Heijden, M. M. P., Meijer, K., Willems, P. J. B., & Savelberg, H. H. C. M. (2009). Muscles limiting the sit-to-stand movement: an experimental simulation of muscle weakness. *Gait & Posture*, *30*(1), 110–114.

Van der Helm, F. C. T. (1994). A finite element musculoskeletal model of the shoulder mechanism. *Journal of Biomechanics*, *27*(5), 551–569.

Van der Helm, F. C., & Veenbaas, R. (1991). Modelling the mechanical effect of muscles with large attachment sites: application to the shoulder mechanism. *Journal of Biomechanics*, *24*(12), 1151–1163.

Van der Linde, J. A., van Kampen, D. A., Terwee, C. B., Dijksman, L. M., Kleinjan, G., & Willems, W. J. (2011). Long-term results after arthroscopic shoulder stabilization using suture anchors: an 8- to 10-year follow-up. *The American Journal of Sports Medicine*, *39*(11), 2396–2403.

Van Drongelen, S., Van der Woude, L. H., Janssen, T. W., Angenot, E. L., Chadwick, E. K., & Veeger, D. H. (2005). Mechanical load on the upper extremity during wheelchair activities. *Archives of*

Physical Medicine and Rehabilitation, *86*(6), 1214–1220.

van Drongelen, S., van der Woude, L. H. V, Janssen, T. W. J., Angenot, E. L. D., Chadwick, E. K. J., & Veeger, H. E. J. (2006). Glenohumeral joint loading in tetraplegia during weight relief lifting: a simulation study. *Clinical Biomechanics (Bristol, Avon)*, *21*(2), 128–137.

Veeger, H. E. J., Rozendaal, L. A., & van der Helm, F. C. T. (2002). Load on the shoulder in low intensity wheelchair propulsion. *Clinical Biomechanics (Bristol, Avon)*, *17*(3), 211–218.

Veeger, H. E. J., & van der Helm, F. C. T. (2007). Shoulder function: The perfect compromise between mobility and stability. *Journal of Biomechanics*, *40*(10), 2119–2129.

Veeger, H. E. J., Yu, B., An, K.-N., & Rozendal, R. H. (1997a). Parameters for modeling the upper extremity. *Journal of Biomechanics*, *30*(6), 647–652. Veeger, H. E. J., Yu, B., An, K. N., & Rozendal, R. H. (1997b). Parameters for modeling the upper extremity. *Journal of Biomechanics*, *30*(6), 647–652.

Wakabayashi, I., Itoi, E., Sano, H., Shibuya, Y., Sashi, R., Minagawa, H., & Kobayashi, M. (2003). Mechanical environment of the supraspinatus tendon: A two-dimensional finite element model analysis. *Journal of Shoulder and Elbow Surgery*, *12*(6), 612–617.

Walch, G., & Boileau, P. (2000). Latarjet-Bristow procedure for recurrent anterior instability. *Tech Shoulder Elbow Surg*, *1*(4), 256–261.

Walch, G., Edwards, T. B., Boulahia, A., Boileau, P., Mole, D., & Adeleine, P. (2002). The influence of glenohumeral prosthetic mismatch on glenoid radiolucent lines: results of a multicenter study. *The Journal of Bone and Joint Surgery. American Volume*, *84–A*(12), 2186–2191.

Walia, P., Miniaci, A., Jones, M. H., & Fening, S. D. (2013). Theoretical model of the effect of combined glenohumeral bone defects on anterior shoulder instability: A finite element approach. *Journal of Orthopaedic Research : Official Publication of the Orthopaedic Research Society*, *31*(4), 601–607.

Ward, S. R., Eng, C. M., Smallwood, L. H., & Lieber, R. L. (2009). Are current measurements of lower extremity muscle architecture accurate? *Clinical Orthopaedics and Related Research*, *467*(4), 1074–1082.

Warner, J. J., & McMahon, P. J. (1995). The role of the long head of the biceps brachii in superior stability of the glenohumeral joint. *The Journal of Bone and Joint Surgery. American Volume*, *77*(3), 366–372.

Warner, J. J. P. (2006). Anatomical Glenoid Reconstruction for Recurrent Anterior Glenohumeral Instability With Glenoid Deficiency Using an Autogenous Tricortical Iliac Crest Bone Graft.

American Journal of Sports Medicine, *34*(2), 205–212.

Wasserstein, D., Dwyer, T., Veillette, C., Gandhi, R., Chahal, J., Mahomed, N., & Ogilvie-Harris, D. (2013). Predictors of dislocation and revision after shoulder stabilization in Ontario, Canada, from 2003 to 2008. *The American Journal of Sports Medicine*, *41*(9), 2034–2040.

Waterman, B. R., Arroyo, W., Heida, K., Burks, R., & Pallis, M. (2015). SLAP Repairs With Combined Procedures Have Lower Failure Rate Than Isolated Repairs in a Military Population: Surgical Outcomes With Minimum 2-Year Follow-up. *Orthopaedic Journal of Sports Medicine*, *3*(8), 2325967115599154.

Waterman, B. R., Burns, T. C., McCriskin, B., Kilcoyne, K., Cameron, K. L., & Owens, B. D. (2014). Outcomes after bankart repair in a military population: predictors for surgical revision and long-term disability. *Arthroscopy : The Journal of Arthroscopic & Related Surgery : Official Publication of the Arthroscopy Association of North America and the International Arthroscopy Association*, *30*(2), 172–177.

Welton, K. L., Bartley, J. H., Major, N. M., & McCarty, E. C. (2017). MRI to Arthroscopy Correlations in SLAP Lesions and Long Head Biceps Pathology. *Sports Medicine and Arthroscopy Review*, *25*(4), 179–190.

Westerhoff, P., Graichen, F., Bender, a., Halder, a., Beier, a., Rohlmann, a., & Bergmann, G. (2009). In vivo measurement of shoulder joint loads during activities of daily living. *Journal of Biomechanics*, *42*(12), 1840–1849.

Widjaja, A. B., Tran, A., Bailey, M., & Proper, S. (2006). Correlation between Bankart and Hill-Sachs lesions in anterior shoulder dislocation. *ANZ Journal of Surgery*, *76*(6), 436–438.

Wilk, K. E., & Macrina, L. C. (2013). Nonoperative and postoperative rehabilitation for glenohumeral instability. *Clinics in Sports Medicine*, *32*(4), 865–914.

Wilk, K. E., Meister, K., & Andrews, J. R. (2002). Current concepts in the rehabilitation of the overhead throwing athlete. *The American Journal of Sports Medicine*, *30*(1), 136–151.

William Giles, J., Miguel Ferreira, L., Singh Athwal, G., & Andrew Johnson, J. (2014). Development and Performance Evaluation of a Multi-PID Muscle Loading Driven In Vitro Active-Motion Shoulder Simulator and Application to Assessing Reverse Total Shoulder Arthroplasty. *Journal of Biomechanical Engineering*, *136*(12), 121007.

Winby, C. R., Lloyd, D. G., & Kirk, T. B. (2008). Evaluation of different analytical methods for subject-specific scaling of musculotendon parameters. *Journal of Biomechanics*, *41*(8), 1682–1688.

Winters, J. M., & Stark, L. (1985). Analysis of fundamental human movement patterns through the use

of in-depth antagonistic muscle models. *IEEE Transactions on Bio-Medical Engineering*, *32*(10), 826–839.

Woo, S. L., Akeson, W. H., & Jemmott, G. F. (1976). Measurements of nonhomogeneous, directional mechanical properties of articular cartilage in tension. *Journal of Biomechanics*, *9*(12), 785–791.

Wu, G., Van Der Helm, F. C. T., Veeger, H. E. J., Makhsous, M., Van Roy, P., Anglin, C., Buchholz, B. (2005). ISB recommendation on definitions of joint coordinate systems of various joints for the reporting of human joint motion - Part II: Shoulder, elbow, wrist and hand. *Journal of Biomechanics*, *38*(5), 981–992.

Wu, W., Lee, P. V. S., Bryant, A. L., Galea, M., & Ackland, D. C. (2016). Subject-specific musculoskeletal modeling in the evaluation of shoulder muscle and joint function. *Journal of Biomechanics*, *49*(15), 3626–3634.

Yamamoto, A., Takagishi, K., Osawa, T., Yanagawa, T., Nakajima, D., Shitara, H., & Kobayashi, T. (2010). Prevalence and risk factors of a rotator cuff tear in the general population. *Journal of Shoulder and Elbow Surgery*, *19*(1), 116–120.

Yamamoto, N., & Itoi, E. (2015). Osseous Defects Seen in Patients with Anterior Shoulder Instability. *Clinics in Orthopedic Surgery*, *7*(4), 425–429.

Yamamoto, N., Itoi, E., Abe, H., Kikuchi, K., Seki, N., Minagawa, H., & Tuoheti, Y. (2009a). Effect of an anterior glenoid defect on anterior shoulder stability: a cadaveric study. *The American Journal of Sports Medicine*, *37*(5), 949–954.

Yamamoto, N., Itoi, E., Abe, H., Minagawa, H., Seki, N., Shimada, Y., & Okada, K. (2007). Contact between the glenoid and the humeral head in abduction, external rotation, and horizontal extension: a new concept of glenoid track. *Journal of Shoulder and Elbow Surgery*, *16*(5), 649–656.

Yamamoto, N., Kawakami, J., Nagamoto, H., Shiota, Y., & Itoi, E. (2017). The relationship between the glenoid track and the range of shoulder motion: A cadaver study. *Orthopaedics & Traumatology, Surgery & Research : OTSR*.

Yamamoto, N., Muraki, T., Sperling, J. W., Steinmann, S. P., Cofield, R. H., Itoi, E., & An, K. N. (2010). Stabilizing mechanism in bone-grafting of a large glenoid defect. *Journal of Bone and Joint Surgery - Series A*, *92*(11), 2059–2066.

Yang, J. S., Mehran, N., Mazzocca, A. D., Pearl, M. L., Chen, V. W., & Arciero, R. A. (2018). Remplissage Versus Modified Latarjet for Off-Track Hill-Sachs Lesions With Subcritical Glenoid Bone Loss. *The American Journal of Sports Medicine*, 363546518767850.

Yeh, M.-L. (2005). Stress Distribution in the Superior Labrum During Throwing Motion. *American Journal of Sports Medicine*, *33*(3), 395–401.

Zacchilli, M. A., & Owens, B. D. (2010). Epidemiology of Shoulder Dislocations Presenting to Emergency Departments in the United States. *The Journal of Bone and Joint Surgery-American Volume*, *92*(3), 542–549.

Zhang, J., & Besier, T. F. (2017). Accuracy of femur reconstruction from sparse geometric data using a statistical shape model. *Computer Methods in Biomechanics and Biomedical Engineering*, *20*(5), 566–576.

Zheng, M., Zou, Z., Bartolo, P. J. D. S., Peach, C., & Ren, L. (2017). Finite element models of the human shoulder complex: a review of their clinical implications and modelling techniques. *International Journal for Numerical Methods in Biomedical Engineering*, *33*(2).

Zimmermann, S. M., Scheyerer, M. J., Farshad, M., Catanzaro, S., Rahm, S., & Gerber, C. (2016). Long-Term Restoration of Anterior Shoulder Stability: A Retrospective Analysis of Arthroscopic Bankart Repair Versus Open Latarjet Procedure. *The Journal of Bone and Joint Surgery. American Volume*, *98*(23), 1954–1961.

Zumstein, V., Kraljevic, M., Hoechel, S., Conzen, A., Nowakowski, A. M., & Muller-Gerbl, M. (2014). The glenohumeral joint - a mismatching system? A morphological analysis of the cartilaginous and osseous curvature of the humeral head and the glenoid cavity. *Journal of Orthopaedic Surgery and Research*, *9*, 34.

Appendix A1 – Documentation for Ethical Approval

Imperial College
London

Imperial College Research Ethics Committee
Imperial College London
Room 221
Medical School Building
St Marys Campus
London
W2 1PG
Tel: +44 (0)207 594 9484

researchethicscommittee@imperial.ac.uk

Anthony M J Bull
Bioengineering Department
Royal School of Mines
Imperial College London
London, SW7 2AZ

Friday 2nd February 2018

Dear Professor Bull

Study Title:. Analysis of shoulder force distribution patterns during activities of daily living in order to aid surgical decision-making.

ICREC reference: 18IC4372

The above study was approved by your Head of Department on date and by the Joint Research Compliance Office on Friday 2nd Febraury 2018.

Under the Imperial College Research Ethics Committee process, a study that has been reviewed by the Joint Research Compliance Office and Head of Division/Department (or Principal), where no significant ethical issues have been identified in the protocol or ethics application, can be approved without requiring it to go to full committee.

Documents
The documents reviewed were:

- ICREC Application form
- Protocol (v2.2 2/01/18)
- Participant Information Sheet (v1 01/12/17)
- Consent Form (v1 01/12/17)
- Participant Data (v1 01/12/17)
- Email Advert (v1 01/12/17)
- Poster Advert (v1 01/12/17)
- JRCO Sponsorship and Insurance Request

Yours sincerely,

Ruth Nicholson,
Research Governance Manager,
Imperial College London

Appendix A2 – Additional results for Chapter 5

Table A2.1: Glenohumeral contact forces for 26 functional activities of daily living, predicted by the generic UK National Shoulder Model as described in Section 2.3.1.2 (Charlton and Johnson 2006). Data are presented as mean and standard deviation (SD).

	Glenohumeral Contact Force [%BW]	Ratio of glenohumeral superior (+) – inferior (-) shear to compression force	Ratio of glenohumeral posterior (+) – anterior (-) shear to compression force
Reach back of head	39 (SD 11)	0.17 (SD 0.08)	-0.28 (SD 0.13)
Lift block to head height	63 (SD 22)	0.12 (SD 0.04)	-0.47 (SD 0.16)
Lift block to shoulder height	55 (SD 17)	0.12 (SD 0.04)	-0.45 (SD 0.17)
Brush left side of head	38 (SD 17)	0.14 (SD 0.08)	-0.52 (SD 0.19)
Clean back	42 (SD 16)	-0.63 (SD 0.29)	-0.17 (SD 0.07)
Drink from mug	30 (SD 9)	0.09 (SD 0.03)	-0.10 (SD 0.04)
Eat with hand	28 (SD 9)	0.15 (SD 0.04)	-0.16 (SD 0.10)
Eat with spoon	34 (SD 9)	0.11 (SD 0.03)	-0.19 (SD 0.09)
Lift shopping bag from floor	59 (SD 15)	-0.36 (SD 0.16)	-0.25 (SD 0.12)
Lift shopping bag on lap	73 (SD 23)	-0.33 (SD 0.13)	-0.31 (SD 0.13)
Reach opposite axilla	28 (SD 13)	0.19 (SD 0.09)	-0.52 (SD 0.24)
Perineal care	31 (SD 17)	-0.61 (SD 0.38)	-0.28 (SD 0.11)
Reach far ahead	54 (SD 25)	0.22 (SD 0.08)	-0.37 (SD 0.16)
Sit to stand	174 (SD 73)	0.44 (SD 0.20)	-0.50 (SD 0.23)
Driving slow right	37 (SD 12)	0.06 (SD 0.02)	-0.25 (SD 0.11)
Driving slow left	47 (SD 14)	0.07 (SD 0.03)	-0.22 (SD 0.08)
Driving fast right	34 (SD 10)	0.02 (SD 0.01)	-0.21 (SD 0.06)
Driving fast left	49 (SD 17)	0.10 (SD 0.05)	-0.24 (SD 0.08)
Extreme	63 (SD 33)	-0.89 (SD 0.41)	-0.52 (SD 0.25)
Pick and place	67 (SD 34)	0.68 (SD 0.36)	-0.54 (SD 0.26)
Pull	68 (SD 23)	-0.57 (SD 0.30)	-0.16 (SD 0.07)
Push	66 (SD 21)	-0.51 (SD 0.28)	-0.22(SD 0.08)
Abduction slow	60 (SD 18)	0.30 (SD 0.11)	-0.25 (SD 0.08)
Abduction fast	57 (SD 17)	0.33 (SD 0.14)	-0.20 (SD 0.09)
Flexion slow	57 (SD 17)	0.15 (SD 0.05)	-0.21 (SD 0.08)
Flexion fast	53 (SD 14)	0.17 (SD 0.07)	-0.15 (SD 0.06)

Table A2.2: Glenohumeral contact forces for 26 functional activities of daily living, predicted by the generic UK National Shoulder Model as described in Section 2.3.1.2 (Charlton and Johnson 2006) with the addition of the effect of passive glenohumeral concavity compression as detailed in Chapter 3. Data are presented as mean and standard deviation (SD).

	Glenohumeral Contact Force [%BW]	Ratio of glenohumeral superior (+) – inferior (-) shear to compression force	Ratio of glenohumeral posterior (+) – anterior (-) shear to compression force
Reach back of head	33 (SD 8)	0.13 (SD 0.06)	-0.24 (SD 0.11)
Lift block to head height	55 (SD 18)	0.09 (SD 0.03)	-0.42 (SD 0.14)
Lift block to shoulder height	52 (SD 15)	0.10 (SD 0.04)	-0.40 (SD 0.16)
Brush left side of head	35 (SD 16)	0.12 (SD 0.07)	-0.46 (SD 0.17)
Clean back	39 (SD 14)	-0.57 (SD 0.27)	-0.16 (SD 0.07)
Drink from mug	29 (SD 9)	0.08 (SD 0.02)	-0.09 (SD 0.04)
Eat with hand	26 (SD 7)	0.13 (SD 0.03)	-0.14 (SD 0.09)
Eat with spoon	32 (SD 8)	0.09 (SD 0.02)	-0.16 (SD 0.08)
Lift shopping bag from floor	53 (SD 15)	-0.32 (SD 0.14)	-0.21 (SD 0.10)
Lift shopping bag on lap	69 (SD 22)	-0.30 (SD 0.13)	-0.27 (SD 0.12)
Reach opposite axilla	24 (SD 12)	0.17 (SD 0.09)	-0.47 (SD 0.22)
Perineal care	29 (SD 16)	-0.58 (SD 0.36)	-0.25 (SD 0.11)
Reach far ahead	52 (SD 24)	0.19 (SD 0.06)	-0.35 (SD 0.14)
Sit to stand	164 (SD 69)	0.41 (SD 0.20)	-0.44 (SD 0.19)
Driving slow right	35 (SD 11)	0.05 (SD 0.02)	-0.23 (SD 0.10)
Driving slow left	45 (SD 13)	0.06 (SD 0.03)	-0.20 (SD 0.07)
Driving fast right	33 (SD 9)	0.02 (SD 0.01)	-0.19 (SD 0.05)
Driving fast left	47 (SD 16)	0.09 (SD 0.04)	-0.23 (SD 0.08)
Extreme	58 (SD 29)	-0.82 (SD 0.41)	-0.45 (SD 0.21)
Pick and place	61(SD 31)	0.62 (SD 0.33)	-0.48 (SD 0.21)
Pull	63 (SD 19)	-0.52 (SD 0.25)	-0.14 (SD 0.06)
Push	62 (SD 19)	-0.47 (SD 0.27)	-0.19 (SD 0.07)
Abduction slow	58 (SD 15)	0.28 (SD 0.09)	-0.23 (SD 0.08)
Abduction fast	54 (SD 17)	0.30 (SD 0.14)	-0.18 (SD 0.08)
Flexion slow	54 (SD 13)	0.13 (SD 0.05)	-0.19 (SD 0.06)
Flexion fast	51 (SD 14)	0.14 (SD 0.06)	-0.14 (SD 0.05)

Table A3.1: The anteroinferior dislocation forces of the intact glenoid and after creating 2-8 mm osseous defects, with the joint being tested in the joint position most susceptible to instability. The shoulder angles represent forward flexion (Flex, positive sign indicates forward flexion), abduction (Abd, positive sign indicates abduction) and rotation (Rot, positive sign indicates internal rotation).

Functional Activity	Shoulder Position [°]			Anteroinferior Dislocation Forces [N]				
	Flex	Abd	Flex	Abd	Flex	Abd	Flex	Abd
Pick and Place	33	6	33	6	33	6	33	6
Extreme (Reach Across Body)	111	60	111	60	111	60	111	60
Clean Back	-38	16	-38	16	-38	16	-38	16
Pull	12	8	12	8	12	8	12	8
Push	21	3	21	3	21	3	21	3
Sit to stand	1	-6	1	-6	1	-6	1	-6
Lift Shopping Bag on Lap	39	-17	39	-17	39	-17	39	-17
Reach Opposite Axilla	60	27	60	27	60	27	60	27
Lift Shopping bag from Floor	-3	-24	-3	-24	-3	-24	-3	-24
Lift Block to Head Height	80	22	80	22	80	22	80	22
Lift Block to Shoulder Height	62	13	62	13	62	13	62	13
Perineal care	-19	-5	-19	-5	-19	-5	-19	-5
Reach far Ahead	76	24	76	24	76	24	76	24
Brush Left Side of Head	80	11	80	11	80	11	80	11
Reach Back of Head	67	-5	67	-5	67	-5	67	-5
Drive Slow Left	39	-2	39	-2	39	-2	39	-2
Drive Slow Right	27	2	27	2	27	2	27	2
Drive Fast Left	33	-3	33	-3	33	-3	33	-3
Drive Fast Right	20	-4	20	-4	20	-4	20	-4
Slow Flexion	114	69	114	69	114	69	114	69
Slow Abduction	120	83	120	83	120	83	120	83
Fast Flexion	98	61	98	61	98	61	98	61
Fast Abduction	102	70	102	70	102	70	102	70
Eat with Hand	34	-7	34	-7	34	-7	34	-7
Drink from Mug	24	-18	24	-18	24	-18	24	-18

Appendix A3 – Additional results for Chapter 6

Table A3.10: Classification of each anterior glenoid osseous defect size for each ADL as unstable (dark grey) or stable (white), with the shear force predictions being obtained from the generic UK National Shoulder Model as described in section 2.3.1.2 (Charlton and Johnson 2006). The glenoid defects with width of 2 mm, 4 mm, 6 mm and 8 mm correspond to 8%, 14%, 20% and 26% of the glenoid length respectively.

	Anterior Glenoid Osseous Defect				
	Intact	2 mm	4 mm	6 mm	8 mm
Lift Block to Head Height					
Lift Block to Shoulder Height					
Pick and Place					
Extreme (Reach Across Body)					
Reach far Ahead					
Reach Opposite Axilla					
Brush Left Side of Head					
Clean Back					
Lift Shopping Bag on Lap					
Reach Back of Head					
Drive Slow Right					
Drive Slow Left					
Drive Fast Left					
Slow Flexion					
Sit to stand					
Drive Fast Right					
Lift Shopping bag from Floor					
Fast Abduction					
Fast Flexion					
Slow Abduction					
Pull					
Push					
Perineal care					
Drink from Mug					

Table A3.3: Classification of each anterior glenoid osseous defect size for each ADL as unstable (dark grey) or stable (white), with the shear force predictions being obtained from the generic UK National Shoulder Model as described in section 2.3.1.2 (Charlton and Johnson 2006) with consideration of passive glenohumeral concavity compression as detailed in Chapter 3. The glenoid defects with width of 2 mm, 4 mm, 6 mm and 8 mm correspond to 8%, 14%, 20% and 26% of the glenoid length respectively.

	Anterior Glenoid Osseous Defect				
	Intact	2 mm	4 mm	6 mm	8 mm
Lift Block to Head Height					
Lift Block to Shoulder Height					
Pick and Place					
Extreme (Reach Across Body)					
Reach far Ahead					
Reach Opposite Axilla					
Brush Left Side of Head					
Clean Back					
Lift Shopping Bag on Lap					
Reach Back of Head					
Drive Slow Right					
Drive Slow Left					
Drive Fast Left					
Slow Flexion					
Sit to stand					
Drive Fast Right					
Lift Shopping bag from Floor					
Fast Abduction					
Fast Flexion					
Slow Abduction					
Pull					
Push					
Perineal care					
Eat with Hand					
Drink from Mug					

Table A3.4: Classification of each anteroinferior glenoid osseous defect size for each ADL as unstable (dark grey) or stable (white), with the shear force predictions being obtained from the generic UK National Shoulder Model as described in section 2.3.1.2 (Charlton and Johnson 2006). The glenoid defects with width of 2 mm, 4 mm, 6 mm and 8 mm correspond to 8%, 14%, 20% and 26% of the glenoid length respectively.

	Anteroinferior Glenoid Osseous Defect				
	Intact	2 mm	4 mm	6 mm	8 mm
Pick and Place					
Clean Back					
Pull					
Push					
Sit to stand					
Lift Shopping Bag on Lap					
Reach Opposite Axilla					
Lift Shopping bag from Floor					
Extreme (Reach Across Body)					
Lift Block to Head Height					
Lift Block to Shoulder Height					
Perineal care					
Reach far Ahead					
Brush Left Side of Head					
Reach Back of Head					
Drive Slow Left					
Drive Slow Right					
Drive Fast Left					
Drive Fast Right					
Slow Flexion					
Slow Abduction					
Fast Flexion					
Fast Abduction					
Drink from Mug					

Table A5: Classification of each anteroinferior glenoid osseous defect size for each ADL as unstable (dark grey) or stable (white), with the shear force predictions being obtained from the generic UK National Shoulder Model as described in section 2.3.1.2 (Charlton and Johnson 2006) with consideration of passive glenohumeral concavity compression as detailed in Chapter 3. The glenoid defects with width of 2 mm, 4 mm, 6 mm and 8 mm correspond to 8%, 14%, 20% and 26% of the glenoid length respectively.

	Anteroinferior Glenoid Osseous Defect				
	Intact	2 mm	4 mm	6 mm	8 mm
Pick and Place					
Clean Back					
Pull					
Push					
Sit to stand					
Lift Shopping Bag on Lap					
Reach Opposite Axilla					
Lift Shopping bag from Floor					
Extreme (Reach Across Body)					
Lift Block to Head Height					
Lift Block to Shoulder Height					
Perineal care					
Reach far Ahead					
Brush Left Side of Head					
Reach Back of Head					
Drive Slow Left					
Drive Slow Right					
Drive Fast Left					
Drive Fast Right					
Slow Flexion					
Slow Abduction					
Fast Flexion					
Fast Abduction					
Drink from Mug					

Appendix A4 – Additional results for Chapter 7

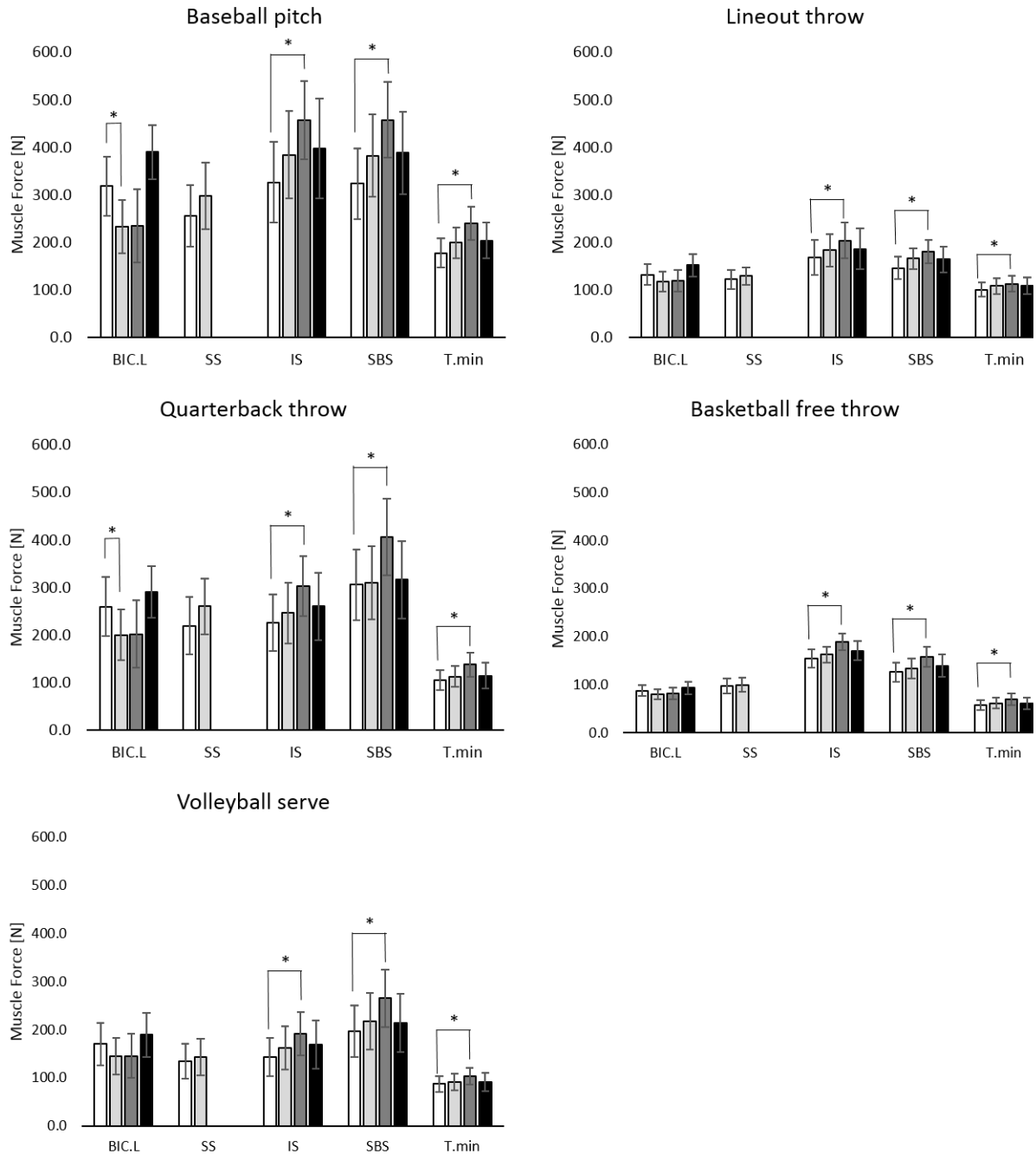

Figure A4.1: Mean (± SD) of the peak muscle forces of the long head of the biceps brachii (BIC.L), supraspinatus (SS), infraspinatus (IS), subscapularis (SBS) and teres minor (T.min), for the intact anatomy (model 1; white bars), post biceps tenodesis (model 2; light gray bars), post biceps tenodesis with combined presence of a full-thickness supraspinatus tear (model 3; black bars), and full-thickness supraspinatus tear (model 4; dark gray bars), for the five overhead throwing sports as predicted by the generic UK National Shoulder Model as described in section 2.3.1.2 (Charlton and Johnson 2006) with consideration of passive glenohumeral concavity compression as detailed in Chapter 3.

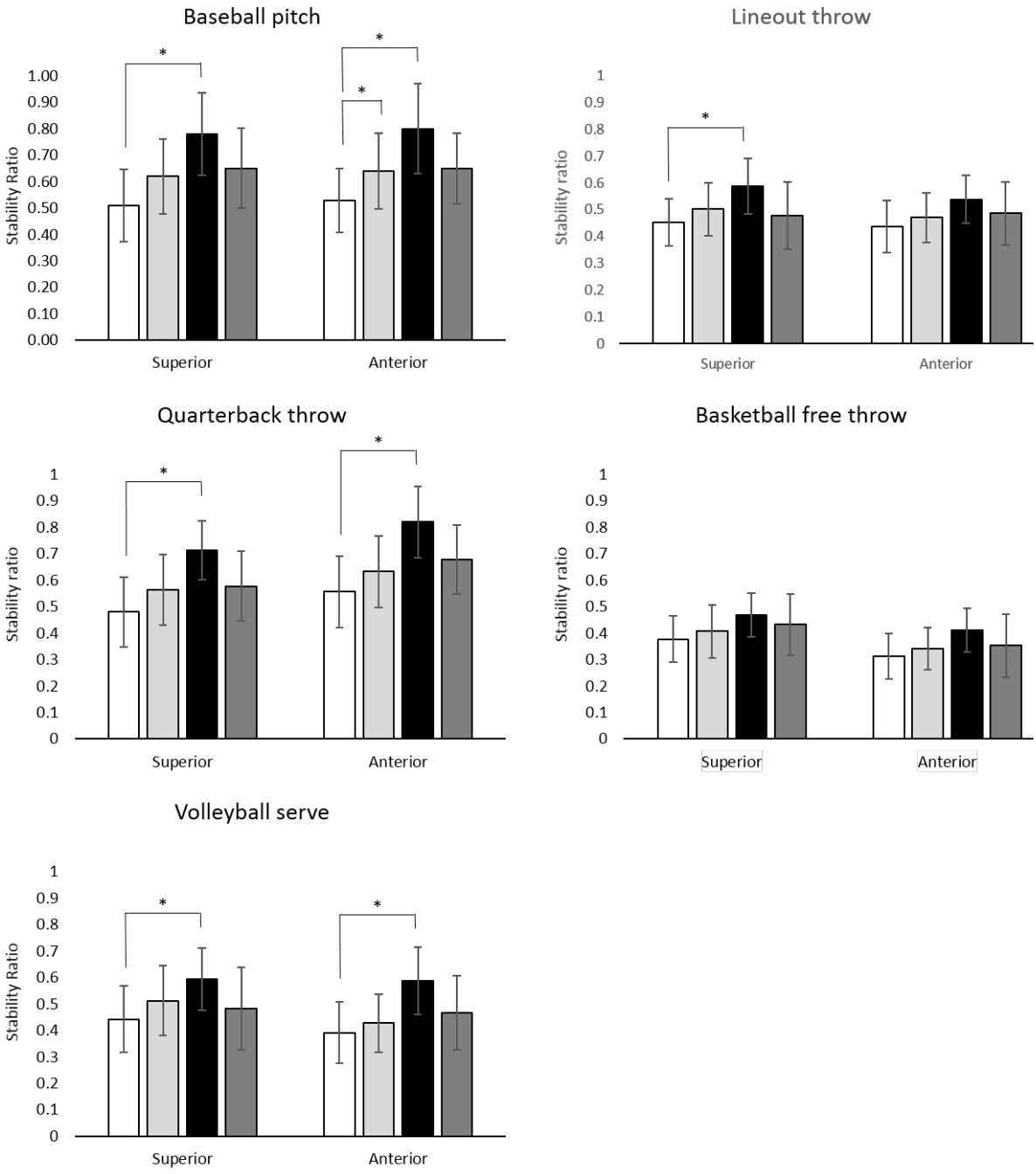

Figure A4.2: Mean stability ratios in the superior and anterior anatomical direction of the glenoid, for the intact anatomy (model 1; white bars), post biceps tenodesis (model 2; light gray bars), post biceps tenodesis with combined presence of a full-thickness supraspinatus tear (model 3; black bars), and full-thickness supraspinatus tear (model 4; dark gray bars), for the five overhead throwing sports as predicted by the generic UK National Shoulder Model as described in section 2.3.1.2 (Charlton and Johnson 2006) with consideration of passive glenohumeral concavity compression as detailed in Chapter 3.

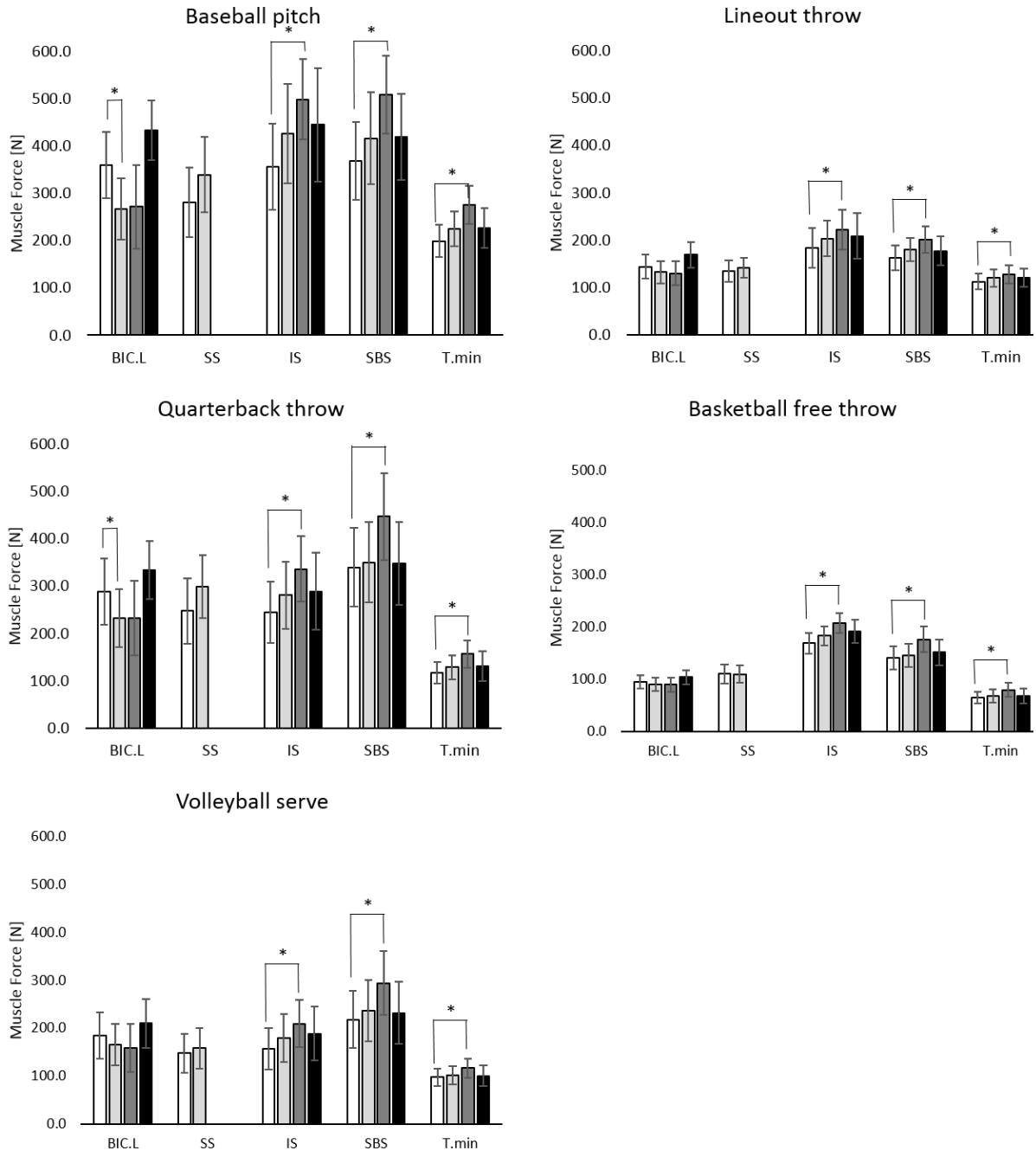

Figure A4.3: Mean (± SD) of the peak muscle forces of the long head of the biceps brachii (BIC.L), supraspinatus (SS), infraspinatus (IS), subscapularis (SBS) and teres minor (T.min), for the intact anatomy (model 1; white bars), post biceps tenodesis (model 2; light gray bars), post biceps tenodesis with combined presence of a full-thickness supraspinatus tear (model 3; black bars), and full-thickness supraspinatus tear (model 4; dark gray bars), for the five overhead throwing sports as predicted by the generic UK National Shoulder Model as described in section 2.3.1.2 (Charlton and Johnson 2006).

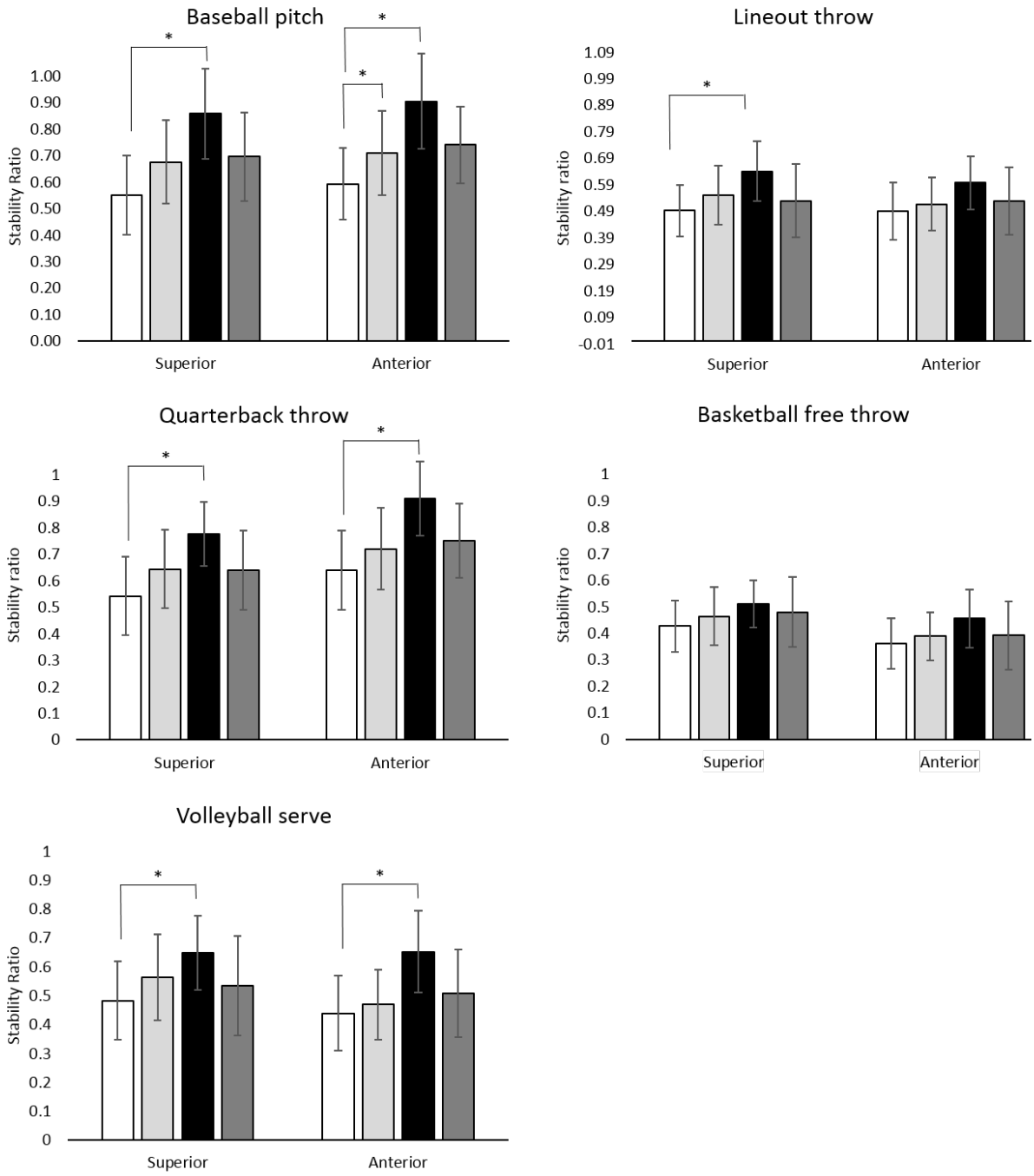

Figure A4.4: Mean stability ratios in the superior and anterior anatomical direction of the glenoid, for the intact anatomy (model 1; white bars), post biceps tenodesis (model 2; light gray bars), post biceps tenodesis with combined presence of a full-thickness supraspinatus tear (model 3; black bars), and full-thickness supraspinatus tear (model 4; dark gray bars), for the five overhead throwing sports as predicted by the generic UK National Shoulder Model as described in section 2.3.1.2 (Charlton and Johnson 2006).